IDENTIFICATION OF IMMUNOSUPPRESSIVE MECHANISMS IN GLIOBLASTOMA MULTIFORME BRAIN TUMOURS

OURANIA GKANATSIOU

DOCTOR OF PHILOSOPHY

ASTON UNIVERSITY

April 2022

ACKNOWLEDGMENTS

I would like to thank my supervisor, Dr. Kesley Attridge, for trusting me with this research project. His guidance and patience throughout my studies, the creativity and friendly approach are most appreciated. I would, also, like to express my gratitude to Prof Andrew Devitt for his support, mentoring and immediate response every time needed.

Additionally, I would like to thank the rest of the laboratory group and, especially, Dr. Ivana Milic, Dr. James Gavin and Rosemary Taylor for providing me with training on lab techniques and enthusiastically offering valuable assistance. Nonetheless, many thanks to our collaborators at the University of Wolverhampton, Prof Tracy Warr and Dr. Farjana Rowther, whose hard work helped me complete part of this research.

Lastly, special thanks to my family, boyfriend and flatmate, along with all the old and new friends I made. Irrespective of the distance, their tolerance, encouragement, continuous support, understanding and caring made this journey more pleasant and feasible to be completed and brought some sunshine in this cloudy country!

ABSTRACT

Glioblastoma Multiforme (GBM) is the most common form of brain tumours with poor prognosis. The current treatment failure is a result of high heterogeneity and tumour-driven immunosuppression. GBM tumours may suppress T cell responses by elevating the effect of the infiltrating regulatory T cells or through secreting soluble proteins and extracellular vesicles (EVs) in the tumour microenvironment. However, the key receptor-ligand interactions responsible are not yet known.

In this project, we hypothesised that GBM-derived soluble factors and EVs are immunosuppressive via the protein-protein interactions and regulate the CD4+ T cell function in the tumour microenvironment (TME). Mass Spectrometry-based Proteomic analysis was performed on tumour samples from GBM patients, after separation of the EVs from the soluble proteins, in order to scan the whole secretome. Optimisation protocols for sample preparation for Mass Spectrometry (MS) were developed using U251 glioblastoma cell-derived conditioned medium, in order to eliminate the model errors along the procedure steps. MS revealed the holistic protein profile in the GBM TME, and potential immunosuppressive candidates were identified following bioinformatics analysis. Furthermore, the data was stratified via molecular subtyping. Finally, the effects of EVs/soluble proteins and immunosuppressive candidates on CD4+ T cells were studied and the expression of cell surface markers and cytokine output was assessed.

Proteomic analysis in GBM secretome, identified more than 1300 proteins in both EVs and soluble protein fractions. THBS1, ICAM1, CD47 were the proteins selected as EV-related mediators of immunosuppression. The samples' grouping into molecular subtypes revealed

overlapping between them due to the high heterogeneity of GBM. For the first time, potential protein biomarkers, linked to each molecular subtype, were identified here, such as RPLP2, ATP2B1 or C9. Extracellular vesicles and soluble proteins contained in the secretome of GBM tumour samples inhibited T cell proliferation and viability, when added in high doses. The CD4+ T cell production of IFNγ , IL-21 and TNFα was impaired, especially as a response to GBM soluble proteins.

1.0.1 GRAPHICAL ABSTRACT

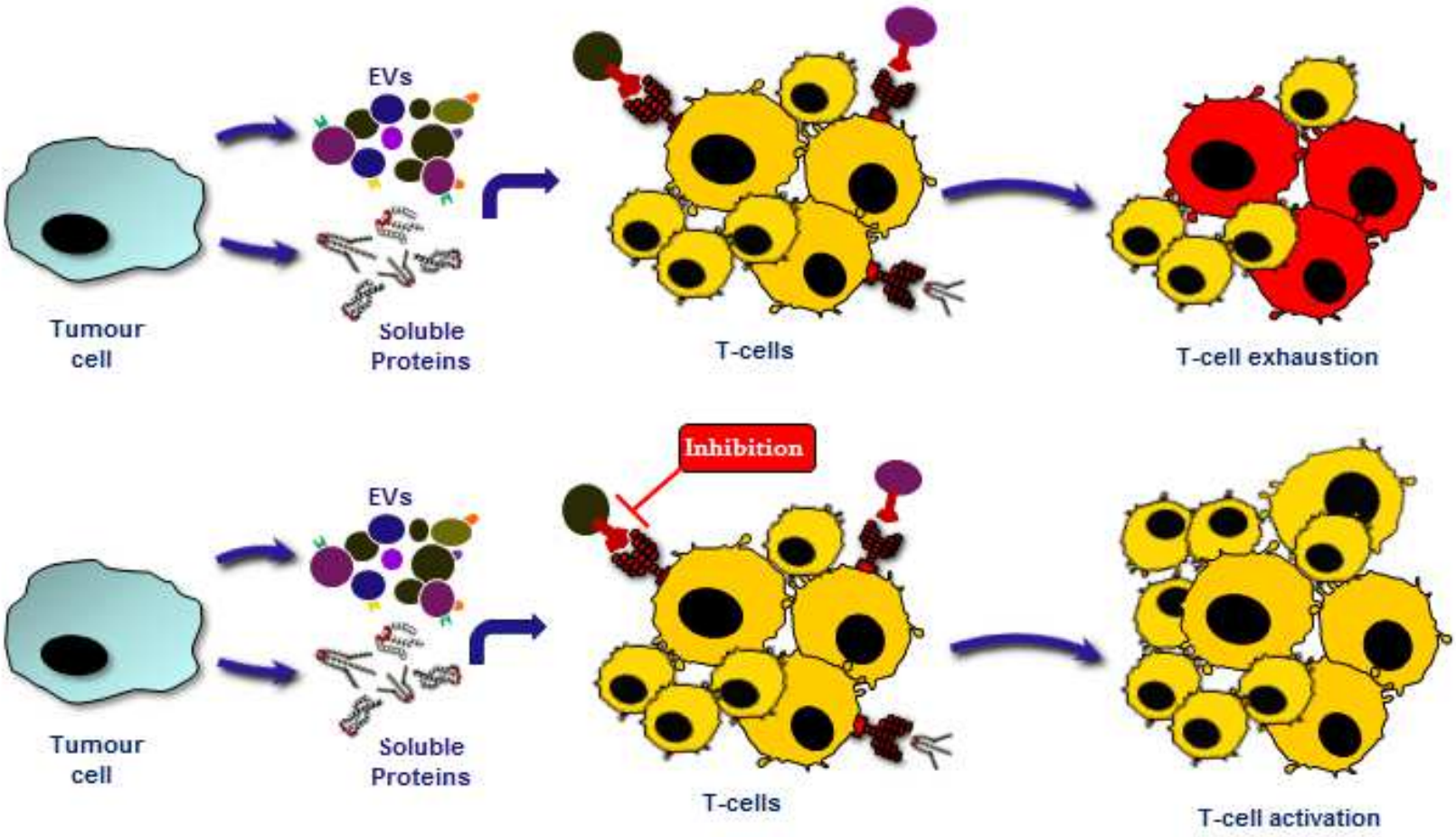

Schematic representation the research project hypothesis. EVs and soluble factors secreted by Glioblastoma cells in the tumour cause T cell exhaustion. Identifying and targeting of the immunosuppressive mechanisms restores T cell anti-tumour responses.

CONTENTS

LIST OF TABLES

LIST OF FIGURES

LIST OF ABBREVIATIONS

1433G.....14-3-3 protein gamma

mAb ..... Monoclonal Antibody

ABCA.....ATP-binding cassette sub-family A

AKT.....Protein kinase B

ABC .....Ammonium bicarbonate

APC.....Antigen presenting cell

APS..... Ammonium persulfate

ATP2B1..... ATPase plasma membrane Ca2+ transporting 1

BAX..... Bcl-2-associated X protein

BBB .....Blood-brain barrier

Bcl.....B cell lymphoma

BSA ..... Bovine serum albumin

C9.....Complement component 9

CATD.....Cathepsin D

CCL.....Chemokine C-C motif ligand

CD .....Cluster of differentiation

CDKN2A.....Cyclin-dependent kinase inhibitor 2A

CM ..... Conditioned medium

CNS.....Central Nervous System

CSC ..... Cancer stem cell

CSF-1 ..... Colony-stimulating factor-1

CTLA-4 ..... Cytotoxic T lymphocyte antigen-4

CXCR.....CXC chemokine receptor

CTL ..... Cytotoxic T lymphocyte

DAVID..... Database for annotation, visualization and integrated discovery

DC..... Dendritic cell

DHPR.....Dihydropyridine receptor

ECH1.....Delta(3,5)-Delta(2,4)-dienoyl-CoA isomerase

ECM .....Extracellular matrix

EGFR..... Epidermal growth factor receptor

EGFRvIII .....Epidermal growth factor receptor variant III

EIF3F.....Eukaryotic translation initiation factor 3 subunit F

ENOG.....2-phospho-D-glycerate hydro-lyase

EV .....Extracellular vesicle

FDA..... Food and Drug Administration

FCS..... Fetal Calf Serum

FoxP3 ..... Forkhead box P3

FunRich..... Functional Enrichment analysis tool

GATA-3..... Trans-acting T cell-specific transcription factor GATA-3

GBM.....Glioblastoma Multiforme

GM-CSF.....Granulocyte macrophage colony stimulating factor

GMDS.....GDP-mannose 4,6 dehydratase

GOF.....Gain of function

GSC.....Glioblastoma stem cell

IBP2..... Insulin-Like Growth Factor Binding Protein 2

ICAM1.....Intercellular Adhesion Molecule 1

ICOS.....Inducible co-stimulator

IDH1.....Isocitrate dehydrogenase 1

IFNγ ..... Interferon gamma

IL..... Interleukin

_iTreg..... induced regulatory T cell

IMS..... Industrial Methylated Sprits

KCPU.....Creatine kinase

KCC2A.....Calcium/calmodulin-dependent protein kinase

kDa..... Kilo Dalton

LAG-3..... Lymphocyte activation gene-3

LAP2A..... Leucine aminopeptidase

LC..... Liquid chromatography

LGALS9..... Galectin-9

LLT-1 ..... Lectin-like transcript-1

LYAG..... Lysosomal alpha-glucosidase

MAPK .....Mitogen-activated protein kinase

MDHC.....Malate dehydrogenase

MDSC.....Myeloid-derived suppressor cell

MeCN.....Acetonitrile

MFI.....Mean fluorescence intensity

MGMT O-6-methylotransferase

MHC .....Major histocompatibility complex

MIC-1 .....Macrophage inhibitory cytokine-1

MIF .....Macrophage migration inhibitory factor

mRNA .....messenger ribonucleic acid

MS..... .Mass spectrometry

MS/MS.....Tandem mass spectrometry

mTOR ..... mammalian target of rapamycin

MYC..... MYC proto-oncogene

NCAM..... Neural cell adhesion molecule

NEGR1.....Neuronal growth regulator 1

NF1 ..... Neurofibromatosis type 1

NK..... Natural killer

NSCs.....Neural stem cells

nTreg .....natural regulatory T cell

OSTP..... Osteopontin

PAGE..... Polyacrylamide gel electrophoresis

PAMP.....Pattern of pathogen-associated molecular pattern

PANTHER.....Protein ANalysis THrough Evolutionary Relationships

PBS..... Phosphate-buffered saline

PCA.....Principal component analysis

RQ-PCR.....Real-Time Quantitative Polymerase chain reaction

PD-1.....Programmed cell death protein 1

PDGFR ..... Platelet-derived growth factor receptor

PD-L1 ..... Programmed death ligand 1

PI3K ..... Phosphoinositide 3-kinase

PPLP.....Pyridoxal phosphate phosphatase

PTEN.....Phosphatase and tensin homolog

PTGDS.....Prostaglandin-H2 D-isomerase

QTOF..... Quadrupole Time of Flight

RAB..... Ras-related protein Rab

RAC1..... Ras-related C3 botulinum toxin substrate 1

RAF ..... Rapidly Accelerated Fibrosarcoma

RORγt.....retinoid-related orphan receptor γt

rpm .....Revolutions per minute

RPRP2.....60S acidic ribosomal protein P2

SD ..... Standard Deviation

SDS.....Sodium dodecyl sulphate

SEC.....Size exclusion chromatography

STAT3 .....Signal transducer and activator of transcription 3

STRING..... Search Tool for the Retrieval of Interacting Genes/Proteins

TAGL3.....Transgelin

TAMs ..... Tumour associated macrophages

T-bet.....T-box transcription factor 21

Tconv ..... Conventional T cell

TCR .....T cell receptor

TDEV.....Tumour derived extracellular vesicle

TEMED ..... Tetramethylethylenediamine

Tfh.....T follicular helper

THBS1.....Thrombospondin 1

TGFβ ..... Transforming growth factor β

Th.....T helper

TIL.....Tumour infiltrating lymphocyte

TLR ..... Toll like receptor

TME .....Tumour microenvironment

TMZ .....Temozolomide

TNF .....Tumour necrosis factor

TP53.....Tumour protein p53

Treg.....Regulatory T cell

Tris.....Trisaminomethane

TRPS.....Tunable resistive pulse sensing

TSG101.....Tumour susceptibility gene 101

VEGF.....Vascular endothelial growth factor

WHO.....World Health Organisation

YBOX.....Y-box-binding protein

CHAPTER 1 – INTRODUCTION

1.1. BACKGROUND

1.1.1.1 Brain tumours

Brain tumours, other CNS and intracranial tumours are the 9th most common type of cancer in the population in the United Kingdom comprising the 3% of the overall new cancer cases (Cancer Research UK, 2019). Approximately 11,000 people are diagnosed each year with brain cancer in the UK with only 14% of them surviving for over 10 years. The incidence rates are almost 34% more than in the early '90s, whilst it is predicted to increase in the next years. Brain tumours that start in the brain from abnormal cell division are called primary tumours. However, they can, also, be secondary tumours occurring as a result of metastasis from cancer that has started somewhere else in the body (Cancer Research UK, 2019).

There are different types of brain tumours. The majority of them are characterized as gliomas. Gliomas are arising from the glial cells in the brain or their precursor cells. Gliomas can be classified according to their histopathological criteria, the genotypic/molecular profile or the grades of malignancy (Louis et al., 2001). The main categories based on their cell type are astrocytomas, oligodendrogliomas and ependymomas. Astrocytomas constitute the 34% of all gliomas and can be graded from I to IV based on their malignancy and aggressiveness (Komori, 2015). Most often, astrocytomas are highly aggressive in terms of high cell division rates and invasiveness and they are classified as Grade III (anaplastic astrocytomas) or Grade IV astrocytomas- most known as Glioblastoma Multiforme (Cancer Research UK, 2019).

1.1.1.2 Glioblastoma Multiforme

Glioblastoma Multiforme (GBM) is the most frequent and malignant form of tumours occurring within the brain with associated universal poor prognosis (Wilson et al., 2014). More than 60% of the brain tumours in adults are considered to be Glioblastomas (Rock et al., 2012). The World Health Organisation (WHO, 2007) classifies GBM tumours as Grade IV gliomas. Studies have shown that almost 3.21 per 100,000 people develop GBM in their lifetime (data aged-adjusted), most possibly at the age of 64 years old (American Association of Neurological Surgeons; (Ostrom et al., 2014; Thakkar et al., 2014).

The GBM cell origin is controversial. Initially, GBM was considered to originate from glial cells. However, recent *in vivo* studies in mouse models suggest that Glioblastoma may arise from neural stem cells (NSCs), NSC-derived astrocytes and oligodendrocyte precursor cells (OPCs) (Yao et al., 2018). Small differences in GBM incidence rates according to sex, ethnicity and race are present, but not remarkable. Men are more likely to develop GBM than women in a ratio 1.6:1 (Thakkar et al., 2014). The risk factor is slightly higher for white people (Thakkar et al., 2014), Asians and Latinos compared to other ethnicities (Ohgaki & Kleihues, 2013; Ellor et al., 2014; Hanif et al., 2017). GBM tumours are in majority primary tumours arising *de novo* in the brain with no less aggressive tumour known as a precursor (Wilson et al., 2014). Nevertheless, fewer cases of secondary tumours initiating from a lower–grade glioma and turning into Grade IV GBM have been described. Approximately 90% of GBM patients have primary malignant tumours growing in older age and with worse prognosis than the secondary tumours (Ohgaki & Kleihues, 2013).

Glioblastoma Multiforme tumours are highly heterogeneous both inter-tumourily and intra-tumourily (Bergmann et al., 2020). A variety of studies identified multiple alterations in gene and mRNA expression and in DNA methylation status after conducting comprehensive genomic, transcriptomic, epigenetic and proteomic analyses (P. Zhang et al., 2020). Performing integrated multi-dimensional analysis in 200 GBM tumours and almost 600 genes, the Cancer Genome Atlas Consortium (TCGA) pilot project identified the most frequently occurring mutations or abnormal expression levels of a number of genes. The signature genes include phosphatase and tensin homolog (PTEN) and tumour protein 53 (TP53) mutations, epidermal growth factor receptor (EGFR) overexpression, which is present in almost 40% of GBM tumours (Verhaak et al., 2010; Hatanpaa et al., 2010) or the EGFR variant III (EGFRvIII), platelet-derived growth factor receptor alpha gene (PDGFRA) amplification, neurofibromatosis type 1 (NF1) mutants, somatic mutations in Phosphatidylinositol 3-kinase regulatory subunit alpha (PIK3R1), abnormalities in the p53, retinoblastoma (RB), and receptor tyrosine kinase pathways and methylation of the O6-methylguanine-DNA methyltransferase (MGMT) gene promoter (Cancer Genome Atlas Research Network, 2008; Verhaak et al., 2010). These alterations are typical for the primary GBM tumours. Mutated isocitrate dehydrogenase 1 (IDH1) protein though is considered as a valid marker for the secondary tumours diagnosis (Wilson et al., 2014).

Based on these, the most widely known and used Glioblastoma tumours classification into subtypes was proposed by Verhaak and his colleagues in 2010. Factor analysis revealed four robust clusters that consisted the four principal GBM subtypes; classical, mesenchymal, proneural, and neural (Verhaak et al., 2010; Wilson et al., 2014). After the original Verhaak classification, later studies refined GBM grouping into three main subtypes. No mRNA

enrichment was detected for the Neural subtype, leading to the conclusion that the particular subtype is non-tumour specific, but most likely derived after sample contamination with normal tissue cells (Teo et al., 2019; Q. Wang et al., 2017; Shen et al., 2012). Response to therapy may vary among the molecular subtypes. Proneural subtype is been reported to have a better response to treatment, while the mesenchymal type is linked to poorer prognosis (Wang et al., 2017). Classification can be a powerful tool in shortening the time between diagnosis and therapy and provide more effective and targeted treatment to the patients with Glioblastoma (Zhang et al., 2020).

1.1.1.3 Current treatment

Despite having a better insight into Glioblastoma Multiforme, this type of tumour is not yet curable. Several attempts have been done by scientists and clinicians to design effective drugs, and although they have promising results in animal models, they do not proceed in clinical trials. Therefore, the treatment approaches for GBM have not been improved dramatically for the past decades.

Most of the tumours are located in the supratentorial brain meaning the frontal, temporal, parietal, and occipital lobes and very rarely are found in the brainstem (<5%), the spinal cord (<5%) and in the cerebellum (<3%) (Ostrom et al., 2014)). Maximal surgical resection of the tumour is the first and most critical to survival step of the standard therapy, usually suggested to patients below 70 years old, because of its high risk. However, complete removal of the tumours is very challenging and not possible in most cases, due to the way these tumours invade brain tissue and spread rapidly to the normal brain tissue around.

The most recent additions to GBM's surgery were the Laser-Interstitial Thermal Therapy (LITT) that inserts an optical fibre to the tumour and causes thermal-initiated tumour necrosis (Kamath et al., 2019) and the DESI-MS, a mass-spectrometric approach, which can offer a better insight in the tumour burdens during the real-time surgery, based on the metabolic molecules produced by the tumour cells in the micro-environment (Pirro et al., 2017; Wójtowicz & Wietecha-Posłuszny, 2019). Surgery alone extends survival for only 6 months (Verhaak et al., 2010). Standard treatment combines surgical resection of the tumour with following adjuvant chemo-radiotherapy (Hanif et al., 2017). This includes external beam radiation therapy for a period lasting six weeks (total amount of 60 Gy is given in 30 fractions) and chemotherapeutic agent Temozolomide (TMZ) prescription to be provided daily as long as the RT lasts and for 5 days a month after that. The above-mentioned standardised treatment protocol enhances efficacy and prolongs patients' median survival to 14.6 months post-diagnosis. Despite this fact, some glioblastoma cells or cancer-stem cells still remain in the tumour microenvironment and constitute the leaders for the regular GBM recurrence (Stupp et al., 2005; Verhaak et al., 2010).

In detail, TMZ is the only alkylating agent approved by Food and Drug Administration (FDA) by now for primary GBM treatment and it is responsible for the methylation of three purine DNA bases in positions N-3, N-7 and O-6 leading to tumour cell apoptosis (J. Zhang et al., 2012). However, TMZ efficiency is impeded by O-6-methylotransferase (MGMT), an enzyme that reverses TMZ-caused damage by removing the recently added methyl group from the O-6 position of guanine (Wilson et al., 2014). This effect results in TMZ neutralization and resistance and complicates therapy. A number of GBM patients present low MGMT expression due to MGMT promoter gene silencing, resulting to increased

response to TMZ treatment (Esteller & Herman, 2004; J. Zhang et al., 2012). In recurrent GBM cases, another antiangiogenic agent can be used, named Bevacizumab, which interacts with Vascular endothelial growth factor (VEGF-A) and blocking its binding to the VEGF receptor. However, this agent's use is limited in Europe and it is not clearly linked with better survival outcomes, but it prevents progression of the tumour (Fernandes et al., 2017).

Certainly, a variety of therapies have been investigated for GBM cure, such as targeting of the signalling pathways that are implicated in Glioblastoma pathogenesis by inhibiting the mutated receptors or the downstream signalling components (Wilson et al., 2014). Monoclonal antibodies and small molecule inhibitors (single or multi-targeted) have been used mainly against growth factor receptors (EGFR, PDGFR, VEGF receptor), intracellular components of PI3K/Akt/mTOR and RAS/RAF/MAPK signalling pathways (Bai et al., 2011; Clarke et al., 2010). Unfortunately, any of them improved GBM prognosis further than the standard treatment (Wilson et al., 2014). Novel treatments that increase survival and overcome toxicity need to be developed.

1.1.2 Cancer immunology

1.1.2.1 The immune system

The immune responses are a rapid mechanism of defence produced by the immune system, in order to eliminate invaders in the body and offer protection against the disease. The immune system has a multi-layered defence, which consists of two main subclasses (Kennedy, 2010).

The innate immune system is a non-specific first-line response, which subdivides into the natural barriers and the inflammatory response. Natural killer cells (NKs), macrophages, dendritic cells (DCs), neutrophils and mast cells recognise a broad pattern of pathogen-associated molecular patterns (PAMPs) and activate phagocytosis, autophagy, cytokine secretion, cell lysis and immune cell recruitment to attack the pathogen (Rich et al., 2012; Mak et al., 2014).

The second class is the adaptive immune response, which is specific for the pathogen. It consists of different classes of lymphocytes, the B cells and T cells. B cells are generated into the bone marrow and they are responsible for the antibody formation and secretion, a function known as humoral response. T cells are produced in the bone marrow, but they mature in the thymus. T cells are the leaders of the cell-mediated response, but upon differentiation, a variety of subpopulations arise with quite distant functions. (Mak et al., 2014; Chaplin, 2010).

T cells differentiate in the thymus in discrete subtypes based on the receptors expressed on the cell membrane and their function. CD8+ cytotoxic T cells constitute 60-70% of the T effector cells (T cell responding to stimulus). They recognise antigens presented to the MHC

class molecule I and act cytolytically on the target cells upon activation. CD4+ cells recognise antigens presented by antigen presenting cells (APCs) on the MHC class molecule II and secrete a variety of molecules, such as chemokines and cytokines, which attract and/or activate more immune cells enhancing the macrophage-induced immune response. They are, also, implicated in the antibody formation by B cells. Due to their activity, they are known as T helper cells (Th) (Chaplin, 2010).

Another CD4+ T cell subset is the regulatory T cells (Tregs) subpopulation, whose role is critical for the immune homeostasis. Tregs are characterized from the IL-2 receptor alpha chain, CD25, and the FoxP3 transcription factor expression and the production of the immune-regulatory cytokines: transforming growth factor-β (TGFβ) and IL-10 (Chaplin, 2010). Tregs control the immune response by suppressing the activity of T effector cells, once its inflammatory role is completed. Furthermore, Tregs offer tolerance against self-antigens preventing from autoimmunity (Chaplin, 2010).

T cell activation takes place upon the engagement of the T cell receptor (TCR) with the MHC complex-presented antigen and the addition of a co-stimulatory signal provided by the interaction of the CD80/CD86 molecules on the APCs with the CD28 receptor on T cells (Nurieva et al., 2009).

1.1.2.2 From immune surveillance to immunoediting

The immune system plays a leading role in the battle against cancer development trying to retain cell homeostasis and offer protection (R. Kim et al., 2007). However, more recent studies have been arguing the fact that the immune system can only prevent or control the

tumour growth and have shown that it can also be implicated in tumour progression (Mittal et al., 2014).

In 1909, Paul Ehlrich stated that there is a mechanism of host defence that prevents neoplastic cells from turning into cancer cells. It took more than 50 years until this hypothesis was formed as the ''immune surveillance theory'' by the biologists Thomas and Burnet. Based on this, the immune cells recognise cancer-specific neo-antigens and initiate an immunological response (Ribatti, 2016). In more detail, the immune system scans the microenvironment for foreign pathogens or cells previously mutated and has the capacity of distinguishing between self and non-self-potential antigens (R. Kim et al., 2007; Chaplin, 2010). Not only elimination of infections, but also modulation and termination of the host inflammatory response is of high importance, since sustained/chronic inflammation favours tumourigenic microenvironment (Khatami, 2012). The fact that transplantation of normal tissue was accepted, whilst induced tumours were rejected in syngeneic mice models supported the idea of the immunological surveillance and the existence of antigen expression on the surface of tumour cells (R. Kim et al., 2007). Furthermore, in a variety of cancer types, survival rate was positively linked with a higher total number of lymphocytes and natural killer cells (Ribatti, 2016). However, athymic nude mice did not have a significantly higher amount of spontaneous or chemically-induced tumours than wild type mice (R. Kim et al., 2007) and low immunogenic tumours were still developing in immunocompetent hosts (Dunn et al., 2004).

Multiple laboratory-based findings the next years revealed that the immunological surveillance constitutes only one side of the events that take place and eventually it was replaced by the concept of ''immuno-editing'' (Mittal et al., 2014). Immuno-editing

describes better the dual interactions between immune and tumour cells, the dynamic balance between them and how sometimes the immune system fails to prevent tumours outgrowth or eliminate them.

Immunoediting process is divided in three stages, which are Elimination, Equilibrium and Escape, or otherwise the three E's (Dunn et al., 2004). Elimination is the process that corresponds to the original description of immune surveillance. Immune cells from both the innate and adaptive response are participating in recognising and confronting the transformed cells. Natural killer cells and T cells are activated by the tumour antigens or stress-induced molecules, such as inflammatory cytokines. Due to these, more immune cells including macrophages M1 are attracted to the microenvironment and release pro-inflammatory cytokines like IFNγ or IL-12 and TNFα with anti-tumour effects, in order to suppress cancer cell proliferation and vascularisation. CD8+ T cells mediate tumour cell death through interaction with Fas and TNF-related apoptosis-inducing ligand (TRAIL) molecules on cancer cell surface or through perforin release (Mittal et al., 2014; Mori et al., 1997; Swann & Smyth, 2007; Lowin et al., 1994). CD8+ T cells and Natural killer cells can also recognise and eliminate tumour cells expressing the NKG2D ligand (Gasser et al., 2005). Both cell types move to the tumour, where CD4+ cells produce IL-2 and IL-15 helping in functionality of the CD8+ cells and the latter ones attack the tumour-cells by IFNγ release mechanism (Dunn et al., 2004). During elimination the tumour cells are diminished in number, but they continue editing their genetic material.

In the equilibrium phase, the tumour cells that survived the elimination from the immune cells develop resistance to the immune surveillance by editing their genetic material. There are high numbers of CD8+ cytotoxic T cells, effector T cells and NK cells and low numbers,

regulatory T cells, macrophages and MDSCs, which can favour tumour progression (X. Wu et al., 2013). In presence of anti-tumour cytokines, such as IFNγ, IL-12 and TNFα, in the tumour microenvironment, T cells that recognise tumour antigens can eliminate the corresponding cells, whilst when the particular cytokines are low and the pro-tumoural IL-23 and IL-10 are present instead, they tend to promote angiogenesis and shift towards malignant phenotypes (Müller-Hermelink et al., 2008; Teng et al., 2012). Equilibrium is the longest of the three stages and it can last even years. Here, the immune defence and the cancer remain temporarily in balance. The cancer cells that were not eliminated in the previous phase undergo through consistent pressure of the anti-tumour responses, which try to eliminate them. However, they occur mutations, from which the ones that turn them into acquiring less immunogenic phenotypes are more favourable. This way, cancer cells proliferate and develop new clones of tumour cells with reduced immunogenicity, since can stay undetectable by the immune system and escape (Gonzalez et al., 2018).

This leads to the third stage of immunoediting, where tumour cells evade or suppress the immune response and act towards tumour outgrowth (R. Kim et al., 2007; Swann & Smyth, 2007; Ribatti, 2017). Multiple events happen in the microenvironment. The cancer cells adapt mechanisms that help them impede the anti-tumour responses, such as loss of MHC class I and NKG2D molecules, antigens or co-stimulatory signals, secretion of immunosuppressive cytokines like TGFβ, IL-10, IL-6 and VEGF that cause CD8+ cell inhibition and death, overexpression of anti-apoptotic molecules (Bcl2) or immune checkpoint proteins, such as PD-L1, T cell immunoglobulin and mucin domain-containing protein 3 (TIM3) and B7, which upon binding to their ligands on T cell surface can induce apoptosis, expression of immunosuppressive molecules, such as Indoleamine 2,3-

dioxygenase (IDO) and galectins (Dunn et al., 2004; Fourcade et al., 2012; Groh et al., 2002). Non tumour cells surrounding the tumour, like M2 macrophages, MDSCs and immature DCs derived from the bone marrow (or iDCs) can express immunosuppressive cytokines like TGFβ, IL-10 and favour the shift of T effector cells to Treg phenotype with increased expression of immune checkpoint proteins (Mittal et al., 2014; Ghiringhelli et al., 2005; R. Kim et al., 2007). At this point, the tumour has developed sufficient mechanisms to escape from the anti-tumour responses towards tumour progression.

1.1.2.3 Brain immune privilege

For several years, the brain was falsely considered as immune privileged. This term indicates that an antigen can be tolerated by the immune system without provoking inflammation and subsequently systemic immune response (Negi & Das, 2018a; Carson et al., 2006).

The CNS maintenance is of vital importance and requires exceptional care. The CNS privilege theory was built based on: the lack of evidence about any draining lymphatics in the brain, the decreased MHC complexes expression by the residual APCs known as microglia cells, the tolerance of transplants in the brain attempted by Medawar in 1948 and the presence of blood-brain barrier (BBB) (Carson et al., 2006; Louveau et al., 2015; Medawar, 1948)The BBB is a physical burden, which consists of specialised cells and prevents the brain from the immune cell invasion (Carson et al., 2006).

However, experiments in the last decades proved brain immune privilege theory wrong and the brain is now rather considered as a virtual secondary lymphoid organ with highly regulated immune surveillance (Negi & Das, 2018b). Loveau and colleagues showed that the presence of lymphatic vessels in the brain draining CSF and immune cells into the deep

cervical lymph nodes in the neck and that the lymphatic system in the brain is not isolated from the peripheral, but they are connected instead (Louveau et al., 2015). Moreover, the BBB is there to prevent the brain from toxins and pathogens circulating in the bloodstream, but it selectively allows lymphocytes to migrate into the brain in a controlled way, since the brain is surrounded by a non-elastic skull and, therefore, is not self-adjusted to an aberrant cell amount (Carson et al., 2006; Louveau et al., 2015; (I. Yang et al., 2010). The BBB also allows the migration of the cells out of the CNS, helping to remove antigens into the lower lymph nodes, in order to be destroyed. In comparison to what was found before, microglia in normal state express low levels of the MHC complexes, but when activated these cells act as phagocytic macrophages and upregulate the MHC and co-stimulatory molecules' (B7, CD40, CD80, CD86) expression, in order to activate in turn and stimulate CD4+ and CD8+ cell response. Microglia in activated state produce also cytokines, such as IL-1, IL-6, IL-23 and TNFα and chemokines, in order to recruit more lymphocytes (Negi & Das, 2017; Yang et al., 2010). The microglia – T cell interaction promotes the T cell responses. However, it is very important these responses to be controlled and the T cells not to be hyper-activated. Microglia cells are found to express the Fas ligand on their surface, but also Tregs play a main role in normal brain immune functionality and prevent autoimmunity (Tambuyzer et al., 2009; Cervantes-Barragan et al., 2012; Negi & Das, 2017).

Nevertheless, BBB makes the design of new treatment techniques for brain diseases, such as GBM, difficult and possible ways to overcome this should be taken into consideration in the new therapeutic

Since T cells are now known to pass through the BBB, immunotherapy is considered as the most promising treatment for GBM. Passive immunotherapy refers to adoptive CTLs cell

transfer into the body, after activating them ex vivo (Wilson et al., 2014). Active immunotherapy, on the other hand, including cancer vaccines, cytotoxic or immunostimulatory gene therapy and oncolytic virotherapy have been tested or are still under investigation. Some therapies were showing beneficial results in the preclinical trials, but not when proceeding into clinical trials (Wilson et al., 2014). Further studies may give valuable information about GBM immunology that is critical for the discovery of successful immunotherapies.

1.1.3 Immunosuppressive mechanisms in GBM

GBM was proved highly immunosuppressive. Glioblastoma tumours utilise several mechanisms for the formation of this immunosuppressive microenvironment, in order to escape the anti-tumour responses including amongst other factors expressed on their cell surface, soluble proteins secreted by glioblastoma cells or infiltration of immune cells with changed properties to favour tumour's growth (Buonfiglioli & Hambardzumyan, 2021; Nduom et al., 2015).

Except for the rapidly dividing tumour cells and cancer stem cells (CSCs), in the GBM tumour microenvironment (TME) there are also high levels of vascular endothelial cells, pericytes and a variety of immune cells, both residual and infiltrates. The cells communicate with each other forming niches in the extracellular matrix (ECM) (De Vleeschouwer & Bergers, 2017)

1.1.3.1 GBM vascularisation

High vascularisation is one of the Glioblastoma tumour's hallmarks (Hardee & Zagzag, 2012). Endothelial cell proliferation promotes expansion of the blood vessels in the hypoxic niche. The hypoxia-inducible factor (HIF) is implicated in the elevated levels of VEGF (Das & Marsden, 2013). Thus, VEGF abundant expression in the TME progressively results in interrupting the BBB consistency and triggers a cascade of events including recruitment of infiltrating macrophages and prevention of CTLs cells from approaching the TME. Overexpression of VEGF, also, inhibits DCs activity and enhances the immunosuppressive Tregs activity (De Vleeschouwer & Bergers, 2017; Motz & Coukos, 2013).

1.1.3.2 Tumour-associated macrophages (TAMs)

Approximately 50% of the tumour mass consists of residing and infiltrating immune cells (De Vleeschouwer & Bergers, 2017). Microglia and DCs, which are normally present in the brain, seem to be less than the infiltrating macrophages, whose properties are similar (Perng & Lim, 2015). Presence of TAMs in the TME is associated with poorer prognosis, since they regulate immunosuppression, promote GBM cell proliferation, survival, stemness, angiogenesis and resistance to chemo- and radiotherapy (Buonfiglioli & Hambardzumyan, 2021). TAMs are recruited chemoattractively mainly by colony-stimulating factor-1 (CSF-1). TAMs produce numerous factors, including stress-inducible protein 1 (STI1), growth factors, such as EGF and PDGFRA and participate in tumour invasion and migration (Wallmann et al., 2018). Proinflammatory M1 TAMs secrete TNF and IL-1β cytokines, whilst M2 polarised TAMs produce ARG1, IL-10, and IL-4 (Buonfiglioli & Hambardzumyan, 2021). Moreover, due to TGF-β1, macrophage inhibitory cytokine-1 (MIC-1) and IL-10, M1 TAMs, rapidly shift to M2 phenotype increasing the anti-inflammatory response and promoting tumour growth (Wu et al., 2010; Pyonteck et al., 2013). TAM-secreted cytokines, such as IL-10, IL-6, IL-1 and TGF-β1 inhibit the phagocytic properties and enhance the Treg effect, suppressing CD4 T helper cells. Interactions of S100B protein with the corresponding receptor on TAMs elevate STAT3 activity, which in turn increases further the anti-inflammatory effect and decreases IL-1 and TNF-α secretion (Razavi et al., 2016; Zhang et al., 2010).

1.1.3.3 Myeloid-derived suppressor cells (MDSCs)

Monocytes can differentiate into precursor MDSCs upon exposure to chemoattractive protein-1, IL-6, IL-8 and macrophage migration inhibitory factor (MIF) in the TME.

Monocytes exposed to glioblastoma cells shift to MDSC-like phenotype and they secrete high levels of IL-10, TGFβ, and PD-L1 expression (Rodrigues et al., 2010). MDSCs were assessed *in vitro* and found to significantly suppress T cell proliferation (Kumar et al., 2017) In GBM, infiltration and accumulation of MDSCs, leads to changes in metabolic activity of the TILs, since MDSCs deprive T cells from glucose. Issues with the glucose uptake result in inhibition of T cells and dysfunction, promoting tumour progression (Chang et al., 2013; Di Ianni et al., 2021).

1.1.3.4 Regulatory T cells (Tregs)

Tregs are recruited to the tumour microenvironment in high levels through secretion of CCL2 by glioblastoma cells (Jordan et al., 2008). It is not yet known if the actual cell counts have a direct effect on the disease prognosis, but the low CD8+ cells to Tregs ratio is reported to be related with worse prognosis (Fecci et al., 2006) and recurrence of the disease (Sayour et al., 2015; Kannappan et al., 2017). Fecci et al. (2006), reported that both CD4+ T cell and Treg compartments were lower in terms of absolute numbers in glioma patients, but regulatory T cells were still effective in forcing T helper cells towards Th2 phenotype or unresponsiveness (Fecci et al., 2006). The majority of them are natural Tregs (nTregs) derived from the thymus *de novo*, but they can also be induced (iTregs) in the TME after TGF-β1/IL-10 exposure (Ooi et al., 2014; Adeegbe & Nishikawa, 2013). High TGF-β expression is linked to elevated FoxP3 mRNA, which is a transcription factor expressed in Tregs, and subsequently to inhibition of CD8+ cytotoxic T cells activity (Kannappan et al, 2017). Hypoxia promotes Treg expansion through elevated the immunosuppressive STAT3 activation (Ooi et al., 2014). Depletion of regulatory T cells in *in vitro* and *in vivo* models in

glioma has been linked to better prognosis, restoration of T cell activation, shift from the Th2 to the pro-inflammatory Th1 phenotype and secretion of anti-tumoural TNFα and IFNγ (Humphries et al., 2010; Sonabend et al., 2008).

1.1.3.5 Natural killer cells (NK)

NK cells respond to the decreased MHC-I expression on tumour cells and eliminate them (Lu et al., 2019; Marcus et al., 2014). Innate lymphoid cells, such as NK cells, express the Th1 master regulator of transcription, T-bet, and increase IFNγ production when exposed to IL-12, IL-15 and IL-18 (Barrow & Colonna, 2019; Sedgwick et al., 2020). However, in CNS malignancies tumour cells, in order to evade immune surveillance, can constantly express or overexpress the MHC-I molecule, which acts as an inhibitory molecule for the NKs (Sedgwick et al., 2020). In another study, it was reported that activated NK cells are more in low gliomas in comparison to the high grade ones, like GBM (Lu et al., 2019). In GBM, the ligands expressed by glioma cells that stimulate the NK-mediated response are suppressed by TGFβ expression (Kozlowska et al., 2016; Roth et al., 2007) Glioma cells express an additional ligand with suppressive effect on T cells. Hence, tumour cells take advantage of the interaction between the Lectin-like transcript-1 (LLT1) ligand with the CD161 receptor on NK cells and manipulate them to inhibit the CD8+ cytotoxicity (Roth et al., 2007). NK cells are able of lysing GBM stem cells that have not been differentiated, but secreted IFNγ cytokine by them can promote the CSCs differentiation and attenuates NK cytotoxic response against them (Kozlowska et al., 2016; Sedwick et al., 2020).

1.1.3.6 Immune checkpoint molecules

T cell response depends on two signals, the major one arises from the antigen recognition and interaction of TCR with the MHC molecules and the secondary consists of co-stimulatory or inhibitory signals (Pardoll, 2012). Cancer cell evade the immune responses by expressing ligands for the T cell inhibitory molecules, which upon binding to them can suppress activation or induce apoptosis on T cells (Hosseinkhani et al., 2020; McBride et al., 2021).

GBM cells express several immune checkpoint molecules, such as the programmed death ligand (PD-L1) on their surface. Almost 90% of Glioblastoma tumours express PD-L1 (Zhu et al., 2012; Berghoff et al., 2015). Upon binding to the corresponding receptor, PD-1, on T cells, apoptosis is triggered. PD-L1 is, also, expressed on TAMs, MDSCs and microglia with the same effect on T cells (Perng & Lim, 2015; Bloch et al., 2013). Cytotoxic T-lymphocyte–associated antigen 4 (CTLA-4) is expressed in recruited Tregs and activated T conventional cells. It antagonizes CD28 at the interaction with CD80/CD86 on APCs. Upon binding, CTLA-4 inhibits T cell activation (J. E. Kim & Lim, 2015; Linsley et al., 1994). T cell immunoglobulin and mucin domain-containing molecule 3 (TIM-3) is another inhibitory molecule expressed on T cells and after binding to its receptor, Galectin-9 on cancer cells, negatively regulates the Th1 immune responses (Zhu et al., 2012). TIM-3/Gal9 were found to be overexpressed in glioma tumours (Liu et al., 2016 ; Ghouzlani et al., 2021). Lymphocyte activation gene-3 (LAG-3) is expressed on T cells, NK cells, DCs and B cells. Binding of LAG-3 to MHC class II molecule drives inhibition of the CD4+ T cell expansion and the cytokine production (He et al., 2016). LAG-3+ TIL were increased in chronic inflammatory

microenvironment, but the marker was not highly upregulated in TILs of IDH-wildtype gliomas (Mair et al., 2021).

1.1.3.7 Hypoxia

The hypoxic tumour microenvironment in GBM is an additional immunosuppressive factor. Brain tumours have high requirements in oxygen, from which they deprive the immune cells in the microenvironment. Conventional T cells are not affected in extensive degree, but γδ T cells activation is impaired, after suppression of the NKG2D marker (Park et al., 2021). Hypoxia directly modulates negatively the effector CD4+ T cells activity (Wei et al., 2011; Westendorf et al., 2017). Aberrant oxygen utilization by the GBM cells leads to activation of the immunosuppressive STAT3 signalling pathway that modulates HIF-1α expression, which in turn induces IL-10, TGF-β and VEGF infiltrates immunosuppressive cells in the TME (Noman et al., 2015; J. Wei et al., 2011). Overexpression of these molecules has known consequences already discussed above and leads to a vicious circle of immunosuppressive TME. STAT3-mediated immunosuppression inhibits phagocytosis, activation and expansion of T cells and increased number of Tregs in GBM (Wei et al., 2011).

1.1.4 Extracellular Vesicles

1.1.4.1 Role of Extracellular Vesicles

Extracellular vesicles are membrane-bound spherical cellular structures surrounded by a lipid bilayer that mediate the intercellular communication (Yáñez-Mó et al., 2015). They function as surrogates of biological material (proteins, lipids and RNAs) and mediate cargo exchange among the cells (Hellwinkel et al., 2015). EVs are produced by most cell types, health and apoptotic cells and are found in the majority of body fluids, including blood, urine and plasma (Yekula et al., 2020; Kalra et al., 2016). Despite having initially been discovered to solely expel waste disposal, they mediate inflammation, tissue homeostasis, cell survival and differentiation (Yuana et al., 2013; Ratajczak et al., 2006; Hopkin, 2016)

Extracellular vesicles are categorised to exosomes, microvesicles and apoptotic bodies based on their size and the way they are generated. Exosomes are the smallest extracellular vesicles with diameter of 30–100 nm generated from inward budding of the plasma membrane. Microvesicles' size is approximately 100-1000 nm and they originate from the outward budding of the plasma membrane. Apoptotic bodies have diameter over 1 μm and derive from apoptotic cells (Andreu & Yáñez-Mó, 2014).

1.1.4.2 Role of EVs in Glioblastoma

Under health conditions, EVs serve the physiological function of the normal cells in the brain. In the case of cancer though, EVs transfer tumourigenic material in the "neighbour" cells spreading the tumour further, by causing Fas ligand-mediated T cell apoptosis (Sagini et al., 2018).

Tumour-derived EVs can promote the tumour invasion, angiogenesis, metastasis and participate in metabolic reprogramming and in drug resistance (Yekula et al., 2020). VEGF, EGF and PDGF factors were found to be implicated in EV-mediated neo-angiogenesis and migration (Mondal et al., 2017; Treps et al., 2017). EVs can, also, mediate and be a source for the high metabolic requirements of the cancer cells, upregulating the glycolysis pathway, which is necessary for tumour cell growth, as already observed in prostate cells (Ronquist et al., 2016; Zhao et al., 2016).

Cancer cell-derived EVs contain DNA, mRNA, miRNA, various proteins and lipids that inherited from the parental cells. Skog and colleagues showed in 2008 that GBM cells secrete extracellular vesicles that enclose mRNA and miRNA. In the EVs, some mRNAs are in higher levels in comparison to cells (Skog et al., 2008). Internalized glioma cell-EVs are able of regulating the transcriptional repertoire in the recipient cells and form a more tumour-favourable microenvironment (Spinelli et al., 2018; C. C. Y. Li et al., 2013). Li et al. (2013), also, confirmed that vesicles-derived from GBM cell lines express proteins, which are specific biomarkers of the extracellular vesicles according to the ExoCarta database, such as TSG101, CD9, CD63, CD81 and proteins of the 14-3-3 pathway (C. C. Li et al., 2013; Rosa-Fernandes et al., 2017). Nonetheless, EVs derived from glioma cells of the aggressive Mesenchymal subtype were more enriched in marker proteins CD9, CD63 in comparison to the Proneural subtype, whilst the latter ones seem to have higher levels of CD81 and ANXA6 (Spinelli et al., 2018). GBM EVs reported to express the signature proteins of the tumour subtype they are purified from, but more details about the exact protein profile are not yet known (F. Ricklefs et al., 2016). Furthermore, GBM EVs have elevated levels of cytokines

and pro-angiogenic molecules, whilst EGFRvIII mRNA has, also, been described (Skog et al., 2008; Gabrusiewicz et al., 2018; Al-Nedawi et al., 2009).

1.1.4.3 The role of EVs in GBM Immunosuppression

Malignant cells release EVs in the TME, in order to manipulate the host immune response, escape the immune surveillance and favour tumour growth (Skog et al., 2008; Dörsam et al., 2018). This can take place due to ligand-receptor interactions between cancer-derived EVs and immune cells or through the EVs uptake from the recipient endothelial and immune cells (Mulcahy et al., 2014).

The transfer of miR-21 through EVs was linked with re-programming microglia to become functional and start proliferating and turning them into a more M2 macrophage-like phenotype (Abels et al., 2019). Gabrusiewicz and his colleagues (2018) showed that CD14+ cells in GBM tumours and monocytes that have been exposed to EVs from glioma stem cells have increased PD-L1 expression and STAT3 immunosuppressive pathway activity (Gabrusiewicz et al., 2018). Another study has shown that some EVs in glioblastoma express PD-L1 on their surface and impair T cell migration in the brain (Brown et al., 2018). Ricklefs and colleagues (2018) reported that blockade of the PD-1 can restore the T cell anti-tumour immunity at some extent, but not entirely (F. L. Ricklefs et al., 2018). In GBM, Glioblastoma stem cells (GSCs) can induce CD3+ T cell inhibition through EV-mediating monocyte shift to MDSCs (Domenis et al., 2017). Glioma EVs that contain TGFβ can also inhibit T cell activation and survival and suppress the CD8+ T cell response through downregulating granzymes and IFNγ secretion (Yekula et al., 2019).

EVs have been detected in blood circulation and are linked not only with enhanced tumourigenicity, but also with systemic immune responses (Noerholm et al., 2012; de Vrij

et al., 2015). Moreover, it has been reported that GBM EVs isolated by the patients' serum present a pro-tumoural profile with high levels of anti-inflammatory cytokines, pro-angiogenic and pro-permabilised agents (Harshyne et al., 2016) contain reactive antibodies promoting the Th2 responses and polarise monocytes towards an M2-like phenotype. Glioma EVs found in patients' serum were reported to release cytokines promoting a Th2-like phenotype, or molecules, such as Semaphorin 3A that disrupt the endothelial barrier integrity (Yekula et al., 2019). However, IFNγ-producing EVs were able of downregulating the anti-inflammatory phenotype in the tumour infiltrating microglia (Grimaldi et al., 2019).

Despite the implication in GBM tumour progression, EVs have, also, valuable information about the disease prognosis. More and more attempts are developing recently, in order to be targeted or manipulated for drug delivery, since they can overcome the BBB and they constitute natural cell components, causing low immunogenicity.

1.1.5 Soluble factors in GBM Immunosuppression

Numerous soluble proteins are secreted in the GBM tumour microenvironment and they can mediate the tumour growth, invasiveness, cell migration and suppress the anti-tumour immune responses.

Soluble factors, such as cytokines and chemokines are the main regulators of the immune responses, but the whole protein profile associated with glioblastoma has not been identified. Some of the known cytokines present in abundance in glioblastoma TME are IL-10, IL-1, IL-6, colony stimulating factor 1 (CSF-1), and the TGF-β that suppress effector cell activity (Nduom et al., 2015; Black et al., 1992). IL-6 is overexpressed in GBM (Xue et al.,

2016) and is linked with GBM growth, cell proliferation and Th2 responses (Tchirkov et al., 2001). IL-10 is an immunosuppressive cytokine, inhibiting the secretion of Th1 cytokines TNFα and IFNγ (Crane et al., 2012; Carlsson et al., 2014). TGFβ induces immunosuppression directly by inhibiting NK cells, CTLs, DCs or by elevating Treg proliferation and by infiltrating macrophages/microglia in the tumour microenvironment (Han et al., 2015; A. Wu et al., 2010). Soluble factors secreted by GBM cells have been found to preferentially promote Treg proliferation and expansion over conventional T cells (Crane et al., 2012). Additionally, T conventional cell (Tconv) can convert into Tregs after exposure to TGF-β (Crane et al., 2012). TAMs are recruited chemoattractively and constitute 30-50% of the tumour mass. One of the hallmarks of Glioblastoma is hypervascularisation. Upon exposure in the tumour milieu, TAMs can shift to a M2-polarised phenotype and secrete in turn more immunosuppressive factors, such as CSF-1, chemokine ligand 2 (CCL2), TGF-β, IL-4, IL-6, IL-10 promoting tumour progression and enhancing even more the Treg-mediated T cell suppression (Hambardzumyan et al., 2016; De Vleeschouwer & Bergers, 2017). IL-8 and CCL2- secreting GBM cells can induce the production of TNFα by glioma-associated macrophages, which in turn activates the expression of vascularisation, migration and adhesion markers VCAM-1, ICAM-1, CXCL5, and CXCL10 (Q. Wei et al., 2021). However, TNFα expression was elevated in leukocytes infiltrating the tumour microenvironment in comparison to areas of necrosis, representing a pathway of the host defence (Roessler et al., 1995). The pro-inflammatory cytokine receptor IFN-γRα, IFN-γRβ, TNFRI expression was found upregulated in tumours, but this was not followed by the same observation in the equivalent cytokine transcripts IFNγ, TNFα, LTα (Hao et al., 2002). IFNγ was produced by T helper cells to inhibit GBM proliferation through promoting the MHC class I, II molecules

and, subsequently, antigen presentation (Hao et al., 2002; Okada et al., 2009; Zhu et al., 2012). On the other hand, IFNγ was, also, reported to elevate the expression of the programmed death ligand B7-H1 (or PD-L1), which participates in T cell exhaustion (Okada et al., 2009). The pro-inflammatory IFNγ secretion by both cancer and T cells was reported to be reduced in the glioma microenvironment, whilst administration of it showed to downregulate the proliferative GBM cells (Kane & Yang, 2010). The IL-2 production, which is crucial for T cell activation was downregulated in glioma patients. Low IL-2 levels were combined with low IL-1β in GBM monocytes and low expression of the molecule MHC II (Curtin et al., 2005). Enhanced was the production of the macrophage migration inhibitory factor (MIF) by GBM cells, which promoted the escape of tumour cells from NK-mediated killing. Furthermore, binding of MIF to the CD74 receptor on microglia resulted in polarisation towards the M2-phenotype (Ghoochani et al., 2016; Mittelbronn et al., 2011).

Proteins in solution in the GBM microenvironment can change the properties of the immune cells, as it has been reported by several studies and favour the progression of tumour. Despite differences between normal and tumour tissue having been reported regarding the expression levels of specific proteins, the holistic protein profile of the secretome has not been investigated yet.

EVs and proteins can alter the fate of immune cells by changing the expression of exhaustion and activation markers, the master regulators of transcription and the cytokine output. Some markers are indicative for the immune cell subsets and their presence reveals their phenotype or indicates skewing towards a different cell phenotype. Previous publications have shown that EVs and soluble factors from GBM patients' blood have a suppressive effect on CD14+ monocytes, elevating the expression of CD163 and forcing them to polarise into

M2 phenotype by increasing the production of the Th2 cytokines IL-4, IL-13, IL-10 (Harshyne et al., 2016).

1.2 PROJECT RATIONALE

Glioblastoma Multiforme is the most common brain malignancy and has universally poor prognosis. Standard treatment prolongs survival for only approximately a year. New therapies have to overcome the blood-brain barrier obstacle. Since, immune cells are able to bypass the BBB, immunotherapy seems the most promising field for GBM treatment. However, GBM tumours are highly immunosuppressive for T cell anti-tumour immune responses. GBM tumours may mediate T cell inhibition through secreted soluble proteins or extracellular vesicles, but the key receptor-ligand interactions responsible are not yet known. Here, we hypothesised that soluble factors and extracellular vesicles in the secretome of GBM patient tissue biopsy suppress T cell activity in the tumour microenvironment and alter their cell surface, transcription factor and cytokine output, subsequently changing their properties. Identifying and targeting of the immunosuppressive mechanisms can reverse this phenomenon and restore the anti-tumour immunity in Glioblastoma *in vitro*.

In order to test the hypothesis, we aimed to optimise the protocol for successful separation of EVs and proteins in solution, which derive from the GBM patients' samples and the U251 cell line supernatant. Afterwards, we applied proteomic analysis using Mass Spectrometry to the tumour samples, in order to identify the potential mechanisms that interact with T cells in the TME and induce T cell anergy and exhaustion. Furthermore, we tested the effects of transport medium from fresh biopsy tissue of GBM patients and U251-derived

supernatant on T cell counts *in vitro*. Moreover, we applied bioinformatics analysis to the results obtained via Mass spectrometry and conducted a list with the most valuable candidates of immunosuppression. The proteins chosen as the best mediators of immunosuppression in GBM were added to the CD4+ T cells and their activity was assessed based on the expression levels of markers of exhaustion and activation and cytokine production to investigate shifting towards a more anti-inflammatory phenotype.

CHAPTER 2 – MATERIALS AND METHODS

2.1 TISSUE CULTURE

2.1.1 GBM Biopsies

Fresh GBM biopsy tissue was resected from patients and was transferred in transport medium lacking serum (The Walton Centre NHS Foundation Trust, Liverpool). Each tumour sample was distributed in three cryovials of approximately 1mL. All samples were stored in - 80°C.

2.1.2 Tissue Culture Media

Glioblastoma cancer cells U251 were grown in Roswell Park Memorial Institute (standard RPMI) 1640 (Sigma-Aldrich, USA) supplemented with 10% v/v Foetal Calf Serum (FCS, Sigma-Aldrich, USA), 2 mM L-Glutamine (Sigma-Aldrich, USA), 100 U/ml Penicillin and 100 µg/ml Streptomycin (Sigma-Aldrich, USA).

2.1.3 Cell culture conditions

Cultured cells were incubated under standard conditions (5% CO_2 and 95% air) in a fhumidified incubator at 37 °C. The cells were observed under the microscope and checked in terms of confluence or contamination. All solutions used were pre-warmed at 37°C in bead-bath.

2.1.4 Cancer cell line

Adherent Human U251 cell line was kindly granted by Prof. Tracy Warr, from University of Wolverhampton. The cells were cultured into T-75 (75 cm^2) flasks (Appleton Woods, UK) and passaged every 4-5 days. The cells were split when the flask was 80-90% confluent,

usually at a ratio of 1:5. In this procedure, first the media was poured and 10 ml Phosphate-buffered saline (PBS) buffer (Gibco, ThermoFisher Scientific, USA) was used to wash the cells and followed by a 4- minute incubation with 2 mL of 0.25% ETDA-Trypsin (Sigma, UK) solution at 37°C to help cell dissociation. Next, RPMI (5-10 ml) was added to neutralize trypsin. All cells were added to a falcon tube and centrifuged at 400 x g for 5 minutes. The supernatant was removed and the cells were re-suspended in fresh medium before being counted on the haemocytometer, in order to seed the desired cell density into a new flask in a total volume of 20 ml media.

2.1.5 Blood cone

Peripheral venous blood was obtained by healthy donors from the University Hospital Birmingham National Health Service Foundation Trust, United Kingdom.

2.2 SAMPLE PREPARATION FOR MS

2.2.1 Size-profiling and Concentration of EVs using Tunable Resistive Pulse Sensing

Tunable resistive pulse sensing (TRPS) by qNano system (Izon, Cambridge, MA, USA) was used to determine the size profile and concentration of particles. Nanopores NP200 (Izon Science, Oxford, U.K.) with target size range 100 - 400 nm were used at standard stretch 47 nm and the instrument was calibrated with calibration polystyrene beads CPC200 1000X (210 nm diameter) and concentration (1E+12 particles/ml). For each sample, 500 particles were recorded or alternatively the number of the particles within 10 minutes. The vesicles were detected as resistive pulses that caused alterations at the current blockade. The data

analysis was provided by the Izon Control Suite v.3.2 software. Applied Voltage: 0.40-0.70 V, Pressure: 0.7 kPa, Noise ≤0.063 RMS, Electrolyte: PBS.

2.2.2 EVs Isolation using qEV Size Exclusion Chromatography (SEC) columns

qEV columns (Izon Science, Oxford, UK) of ~70 nm pore diameter were used for EV purification. Separation of EVs from the proteins contained in a sample is based on Size Exclusion Chromatography. After rinsing the column with 10ml sterile ammonium bicarbonate (ABC), a sample volume up to 2ml was loaded on top of the filter and collected in fractions of 0.5 ml. The EV-enriched fraction was collected from fractions 6-12 (3.5 ml), followed by the protein-enriched fraction in fractions 13-30 (9 ml).

2.2.3 Bradford Protein Assay

Sample soluble protein concentration was determined by Bradford Assay (BioRad, UK). For the standard curve, bovine serum albumin (BSA, Sigma-Aldrich, UK) protein standard in stock solution (1 mg/mL) was used as a control. A volume of 25 µl of standard 5X BSA was diluted seven times serially in a 96-well plate. The samples were diluted in distilled water in a final volume of 25 µl and plated in triplicates. Next, 200 µl/well Bradford dye reagent was added to each sample. The plate was placed in the Multiscan Go Plate reader and the dye absorbance was measured at 595 nm. Finally, the protein concentration of the samples was quantified according to the BSA standard curve.

2.2.4 Nano Drop

Protein quantification was also tested using the NanoDrop® ND-1000 UV-Vis Spectrophotometer (ThermoFisher Scientific, UK). A microvolume of 1 µl is applied on the detection surface. A fiber optic connected to light source approaches the detection surface

and the light can pass through the sample. The spectrophotometer is connected to a PC running the Nanodrop 1000 v.3.8.1 software. The absorbance is measured at 280 nm. A blank sample of distilled water is pipetted on the detector prior to samples. The setting of 1 Abs=1 mg/mL is chosen for the protein quantification (Desjardins et al., 2009).

2.2.5 Sample Concentration

Amicon centrifugal filters (Merck Millipore, UK) were used to concentrate the samples. This step was added prior to SEC in order to obtain sample volumes suitable to be loaded on qEV columns (≤2 mL) and after qEV to obtain the right sample volumes for the next steps. Before qEV, 15-mL 3 kDa centrifugal filters were used for total sample concentration. The samples were centrifuged at 3240 x g at 4°C (maximum speed). After qEV, the collected EV-enriched and soluble proteins fractions were concentrated further under the same conditions. Amicon centrifugal filters of 10 kDa were used for EV concentration and 3 kDa filters for protein concentration to final volume of approximately 30 µl.

2.3 MASS SPECTROMETRY

After concentrating the samples to the desired volume, the protein concentration was estimated by NanoDrop and/or Bradford Assay.

2.3.1 Sodium Dodecyl Sulfate -Polyacrylamide Gel Electrophoresis (SDS-PAGE)

The protein concentration was quantified by Bradford protein assay. Using these values, the purified proteins were separated in a molecular-weight-based way on a 10% SDS-PAGE gel.

A stacking gel with large pores and a resolving gel with smaller pores were casted.

2.3.2 Gel preparation

The stacking gel and resolving gel were casted. In order to achieve this, the corresponding solutions were prepared. The recipe with the adjusted volumes required is following below.

Table 1. Recipe for casting SDS-PAGE gels

10% Resolving Gel	**1 Gel**
Distilled H2O	3.87 mL
40% Acrylamide/bis-acrylamide	2.12 mL
1.5 M Tris pH 8.8	2.16 mL
10% SDS	84 µL
10% (w/v) Ammonium Persulfate (APS)	84 µL
TEMED	8,4 µL
4% Stacking Gel	**1 Gel**
Distilled H2O	2,62 mL
40% Acrylamide	0,41 mL
0.5 M Tris pH 6.8	1,04 mL
10% SDS	41 µL
10% APS	41 µL
TEMED	4,16 µL

The resolving solution was added in between the casting glasses, which were placed in a casting frame. Isopropanol-2 was added on the top to avoid oxygen accumulation. After the

gel is polymerized, the isopropanol was removed and the stacking solution was added on the top of the separating gel and the plastic comb (10-well x 1.0 mm). After polymerization of the stacking gel, which lasts approximately 20 min on a room temperature, the comb was removed.

2.3.3 Gel electrophoresis

The gels were placed into the Mini-PROTEAN® Tetra Cell gel electrophoresis system and 1X Tris-Glycine-SDS (TGS) running buffer was added. Prior to that, the samples were reduced by using 5X Laemmli sample buffer (7 µl/sample), which then placed on the heater at 65°C for 15 minutes. The samples were loaded on the stacking gel and the PageRuler™ Plus Prestained Protein Ladder (ThermoScientific, UK) was also used, as a reference marker/standard for the determination of protein molecular weight. Constant voltage of 100V was applied for approximately 10 minutes. Then the voltage was increased up to 150V for ~45 min.

Next, the gels were stained with 100 ml Coomassie G250 blue (0.5% w/v in 40% aqueous methanol and 10% glacial acetic acid) overnight at 4°C. Then, Coomassie stain was removed and the gels were subsequently destained with de-staining solution at room temperature for approximately 2 hours.

2.3.4 In-gel digestion

Each sample on the gels was fractioned into five bands of the same size. Each band was, then, cut into smaller pieces and transferred into Eppendorf tubes. A volume of 150-200 µl of 50% acetonitrile (MeCN) in 50 mM ammonium bicarbonate (ABC) was added in the tubes to destain the gel pieces. The tubes were places in thermoshaker at 600 x g at 37°C for

approximately 10 minutes. The solution was then removed and the step was repeated. The samples left on the shaker for 1-2 hours. Afterwards, 200 µl of 100% of MeCN were added twice in the eppendorfs. The samples were left to dry for 30 minutes in the vacuum concentrator (Eppendorf, UK). For protein digestion, the gels were rehydrated with 40 µl Trypsin Gold (Promega Corporation, UK) in 3 mM ABC in a ratio 25:1 (protein: trypsin). Next, the samples were placed on the shaking table at 600 x g at 37 °C overnight with the addition of 200 µl 3 mM ammonium bicarbonate, in order to avoid gel dehydration. The next day, 100 µl of 100% MeCN were added to the eppendorfs and the samples were sonicated for 15 minutes, in order to extract the peptides. The extract was collected and transferred into fresh eppedorf tubes, whilst 200 µl of 50% MeCN in 50 mM ABC were added to previous ones with the gel pieces again and were left for a 15-min sonication. The extract was collected in the new tubes and the step was repeated. 200 µl of 100% MeCN was added on the gel pieces and the eppendorfs were vortexed. The extract was collected into new tubes, dried in the vacuum concentrator and stored at -20 °C until subsequent analysis was followed.

2.3.5 Mass spectrometer

The samples were prepared for LC-MS/MS. Samples were reconstituted in 3% MeCN in water with 0.1% formic acid. Tryptic peptides were separated using an nLC system (Dionex 3000, ThermoScientific, UK), online coupled to 5600 TripleTof (AB Sciex, UK), where peptides were analysed operating in information dependent mode. Sample (10 µL) was injected onto a trap column (PepMapTM, C18, 5 µm, 100 Å, 300 µm x 1 mm, ThermoScientific, UK) using 2% of eluent B (98% MeCN in aqueous 0.1 % formic acid) at a flow rate of 30 µL/min. Peptides were subsequently separated on an analytical column

(AcclaimTM, PepMapTM C18, 3 µm, 100 Å, 75 µm x 150 mm, ThermoScientific, UK) with the following gradient: 0-3 min 2% B, 3-48 min 2-45% B, 48-52 min 45-90% B, 52-55 min 90% B, 55-70 min 2% B). Electrospray was formed by spraying the nLC eluate at 2500V using a PicoTipTM emitter (New Objective, Germany). The 10 most intense ions from each MS survey scan were selected for MS/MS, while acquired ions were temporarily excluded from MS/MS acquisition for 30 seconds. The mass spectrometer was calibrated prior to acquisition to ensure a high mass accuracy (<10 ppm) on both MS and tandem mass spectrometry (MS/MS) levels. Where applicable, Progenesis QI for proteomics was used to compare different sample conditions. Using Mascot search engine, .wiff or .mgf files (MS and MS/MS) were searched against human proteome in SwissProt database, allowing for up to 2 trypsin miss cleavages.

2.4 REAL-TIME QUANTITATIVE POLYMERASE CHAIN REACTION (RQ-PCR)

Molecular subtyping of the Glioblastoma tissue biopsies by implementing RQ-PCR technique was undertaken by our collaborator, Dr. Farjana Rowther, at the University of Wolverhampton,

2.4.1 GBM Tumour Biopsies

Approximately 10 mg of brain tissue was cut down into smaller fragments. Collagenase was added to digest the samples in a concentration of 0.5 mg/ml and incubated for 25 minutes in culture media. Then, the samples passed through a 40 µm cell strainer and the cells were centrifuged at 400 x g for 10 mins. The pellet was checked for red blood cell (RBC)

contamination and in case there was, the RBCs were lysed using 10 ml RBC lysis buffer and centrifuged at 1000 g for 20 minutes. Afterwards, the pellet was processed for RQ-PCR.

2.4.2 DNA extraction

DNA extraction was performed from the GBM cell pellets described above using the QIAmp DNA Mini Kit (Qiagen, UK) on 10^6 cells according the manufacturer's recommendations NanoDrop ND-2000 was used to quantify DNA.

2.4.3 RQ-PCR

RQ-PCR was conducted on the biopsy-derived cell pellets (20 ng/well) using TaqMan™ Copy Number Assay and FAM reporter dye (Hs01364699_cn), (Life Technologies, UK). As a control, TaqMan assay for Telomerase Reverse Transcriptase (TERT) gene was used (VIC reporter) and copies of the target genes were normalised accordingly. Analysis of the copy number was performed by CopyCaller software. 2-DDCT method was applied establish the relative expression.

2.5 T CELL ASSAYS

2.5.1 CD4+ T cell isolation

Total cells were isolated from the peripheral blood of healthy human donors. The whole blood was transferred from the blood cone into a 50 ml falcon tube and topped up to 20ml with PBS. The CD4+ T cells were isolated from whole blood by negative selection. Two ml of blood were transferred into a 15 ml falcon tube. 100 µL of RosetteSep™ Human CD4+ T Cell Enrichment Cocktail (StemCell Technologies, Cambridge, UK) were added and the mix

was incubated at room temperature for 20 minutes and, then, 2ml of P2 (PBS + 2% FCS) were added and mixed together. In a new 15 ml falcon tube, 3 ml of Histopaque/Lymphoprep were added. The blood was added on top of the Histopaque/Lymphoprep. The solution was centrifuged at 1200 g for 20 minutes at room temperature with the brake off. After the centrifugation, the purified CD4+ T cells are present as an enriched layer between the plasma and the buoyant density gradient. The CD4+ T cells were transferred into a new tube, topped up to 5 ml with P2 and then centrifuged at 300 g for 10 minutes. This step was repeated. The cells were re-suspended in RPMI and counted.

2.5.2 CD4+ T cell stimulation

Cells were cultured in duplicates in round (U) bottom 96-well plates in a total volume of 200 µl C10 (RPMI). CD4+ T cells were plated at 2.5 x 10^4 cells/well (in 25 µl) and stimulated with Dynabeads Human T-Activator CD3/CD28 (Gibco, Thermo Fisher Scientific, UK) in 25 µl solution at a 1:2 T cells to Beads ratio. Then 100µL C10 was added [C10 RPMI 1640 (GIBCO), 100 U/ml penicillin (GIBCO), 100 µg/ml streptomycin (GIBCO), 50 µM 2-Mercaptoethanol (Sigma), 10% FCS (2% for C2) (Sigma)]. In order to assess the effect of the patient tumour-derived EVs and/or soluble proteins on T cells viability and markers, a titration of EVs or Soluble proteins was added on the top of CD4+ T cells (Fulll dose, 1;2, 1:4, 1:8 dose) in a total volume of 100µl. The cells were incubated at 37°C, 5% CO_2 for 5 days. After that, cells were harvested and stained for flow cytometry for multiple markers.

2.5.3 Re-stimulation for intracellular cytokine staining

To induce production of cytokines, the eBioscience™ Cell Stimulation Cocktail (500X) (Invitrogen, UK), which contains Phorbol 12-myristate 13- acetate (40.5 µM) and Ionomycin calcium salt (670 µM), was added to cells in a final concentration of 2 µg/ml per well (eBioscience Ltd.., Cheshire, UK). The cells were incubated at 37°C, 5% CO_2 for 2 hours. Then, Brefeldin A Solution (1000X) (Invitrogen, UK) was added in a concentration of 3 µg/ml before culturing for a further 2 hours.

2.5.4 Staining for Flow Cytometry

For staining transcription factors and cytokines, cells were first fixed and permeabilised. The cells were harvested into flow tubes and centrifuged at 400 x g for 5 minutes at room temperature. They were washed with PBS and centrifuged again at 400 x g for 5 minutes. Then, 500 µl/tube of the Fixation solution 1X (1:3 Fixation/Permeabilisation Concentrate: Fixation/Permeabilisation Diluent) was added from the FoxP3/Transcription Factor Staining Buffer Set (eBioscience) and the cells were incubated at 4°C for 30 mins. Next, cells were centrifuged at 400 x g for 5mins at room temperature, washed with PBS and centrifuged again at the same conditions. Permeabilisation solution (1X) 1.3 ml/tube was added followed by centrifugation at for 5 mins at room temperature. The step was repeated.

Afterwards, the cells were stained with the antibodies and incubated in the dark for 30 minutes at room temperature. 1.3 ml of Permeabilisation solution was added and the cells were centrifuged at 400 x g for 5 mins. The supernatant was removed and the samples were analysed by flow cytometry.

For detection of cell surface markers: All cells were harvested and centrifuged at 400 x g for 5 mins at room temperature. P2 (500 µl) were added and cells were centrifuged at the same conditions. Cell surface antigens were added and the cells incubated at 4°C for 30 mins. Next, 500 µl P2 were added and cells were centrifuged at 400 x g for 5 mins at room temperature. The supernatant was removed and the samples were analysed by flow cytometry. The cells were analysed by CytoFLEX S Flow Cytometer (Beckman Coulter, Germany) and FlowJo™ v10 software. Cell counts were determined by acquiring all cultured cells.

2.5.5 Candidate Proteins

For assessing the effect of the candidate proteins on T cells, CD4+ cells were cultured at 2.5 x 10^4 cells/well and Dynabeads Human T-Activator CD3/CD28 were added at 1:2 T cells to Beads ratio. Cells were cultured alone or with 1 µg/ml, 0.5 µg/ml ICAM-1 (Peprotech, London, UK), 10 µg/ml, 5 µg/ml, 2.5 µg/ml CD47 (R&D Systems, Bio-Techne Ltd, Abingdon, UK), 2 µg/ml, 1 µg/ml, 0.5 µg/ml THBS1 (Merck, Feltham, UK) or 500 ng/ml, 250 ng/ml, 125 ng/ml MIF (Peprotech).

Table 2. List of staining antibodies

Antibodies	**Clone**	**Conjugate**	**Supplier**	**Amount per tube (µL):**
CD4	RPA-T4	PE-Cy5	BD Biosciences	2

Cytokines:	**Clone**	**Conjugate**	**Supplier**	**Amount per tube (µL):**
IL-21	3A3-N2.1 (a.k.a 3A3-N2)	PE	BD Biosciences	8
TGFβ	TW4-9E7	Alexa Fluor 488	BD Biosciences	2
IL-17A	N49-653	BV510	BD Biosciences	2
IL-13	JES10-5A2	BV711	BD Biosciences	2
TNFα	MAb11	PE-Cy7	BD Biosciences	1
IFNγ	B27	V450	BD Biosciences	1

Cell Surface:	**Clone**	**Conjugate:**	**Supplier**	**Amount per tube (µL):**
ICOS (CD278)	DX29	BV421	BD Biosciences	1
TIM-3 (CD366)	7D3	PE	BD Biosciences	2
PD-1 (CD279)	EH12.1	PE-Cy7	BD Biosciences	4

Transcription Factor:	Clone	Conjugate	Supplier	Amount per tube (µL):
GATA-3	L50-823	Alexa Fluor 488	BD Biosciences	8
Bcl-6	K112-91	PE-Cy7	BD Biosciences	2
RoRγT	Q21-559	PE	BD Biosciences	2
T-Bet	O4-46	BV650	BD Biosciences	2
FoxP3	236A/E7	V450	BD Biosciences	1

2.6 STATISTICAL ANALYSIS

Statistical analysis of the research data was carried out using Microsoft Excel®. Data is shown as Mean ± SEM in most experiments. Pearson's correlation coefficient and Analysis of variance (ANOVA) was applied in the experiments in Chapter 3. The statistical significance was determined by the p-value. P-value<0.01 is highly significant. Statistical analysis is not available for experiments performed less than 3 times.

CHAPTER 3 – RESULTS

3.1 Optimisation Protocol for Preparation of Glioblastoma Tumour Samples for Proteomic Analysis

Glioblastoma Multiforme tumours use multiple mechanisms to eradicate immune responses. GBM extracellular vesicles play a pivotal role in cell-to-cell communication and are known to promote tumour invasion and progression (Maia et al., 2018). In the years since these experiments were performed, we and other groups have showed a linkage between Glioblastoma-derived EVs and immunosuppression (Ricklefs et al., 2018; Tankov & Walker, 2021), however little is yet known about specific culprits and the receptor-ligand interactions between EVs and immune cells. Our experiments aimed to address the capacity of EVs to suppress T cells responses within the tumour microenvironment and identify potential candidates. In order to identify the EV-bound immunosuppressive candidates for therapeutic reasons, work for this report has been focused on devising and optimising an EV isolation strategy suitable for downstream mass spectrometric analyses.

3.1.1 The GBM tumour cells secrete EVs in the transport media

Skog and colleagues (2008) reported EVs in GBM for the first time (Skog et al., 2008). EVs are released from glioblastoma cells in the microenvironment and have the capacity to transform the extracellular matrix due to their cellular constituents (Gonda et al., 2013). Moreover, EVs have been detected in the biofluids of GBM patients (Redzic et al., 2014; Santiago-Dieppa et al., 2014). In the current project, GBM tumours were transferred in transport medium. In order to assess whether the GBM patient transport medium can serve as liquid biopsy, the medium was examined by the qNano system for EVs secretion.

The qNano technology revealed the GBM tumour-derived EVs release in transport medium and allowed the particle sizing characterisation. The majority of EVs contained in the transport medium of GBM tumour tissue from 79 patients were between 70-300 nm (Figure 1). The average size from all patients was 147.1 nm and the mode EV size was 103 nm. The nanopore used (NP200) targets EV size ranging from 100 to 400 nm. The size characterisation was conducted against polysterene beads of known size.

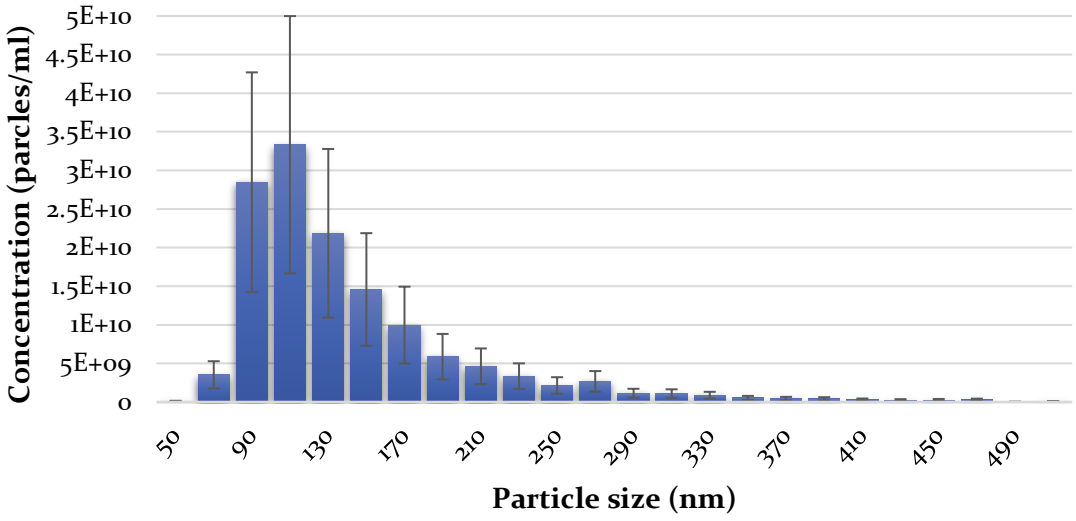

Figure 1. Average Tumour- derived EVs Sizing Profile.

The transport media that 79 GBM tumour tissue samples were contained was added on the qNano system at a volume of 35 µl. Extracellular vesicle sizing was carried out by TPRS. The EVs size was measured against polysterene calibration beads of known size. Modal beads CPC200 in concentration of 1 µl/ml (210 nm, 1E+12 particles/ml) were used to calibrate the qNano instrument. The nanopore used was NP200. The pressure was maintained at 0.7 kPa. Noise<0.063 RMS and the Voltage ~0.40-0.70V. The data analysis was performed by Izon Control Suite Software v.3.2 and is shown as Mean ± SEM.

3.1.2 Assessment of U251- derived EVs following particle size

As mentioned before, glioblastoma cells secrete extracellular vesicles in the tumour microenvironment and alter it towards cancer progression. Accordingly, U251 glioblastoma cells have been reported to secrete a number of EVs in culture media (Li et al., 2013). Here, the release of EVs in CM and their size was confirmed, in order to be assessed regarding their fit to serve as a representative experimental model for optimising the protocol by comparing them with the patient-derived EVs.

For this reason, U251-derived supernatant was tested for their content in extracellular vesicles using the qNano system. U251 supernatants in serum-free medium were collected. Most EVs were of the size of 50-450 nm (Figure 2). The average size was 180 nm, whilst the mode size was 110 nm. The EVs size isolated from the U251 supernatants is comparable to the EVs derived from the patients, as it was identified in the previous chapter (Chapter 3.1.1.) and with previous findings.

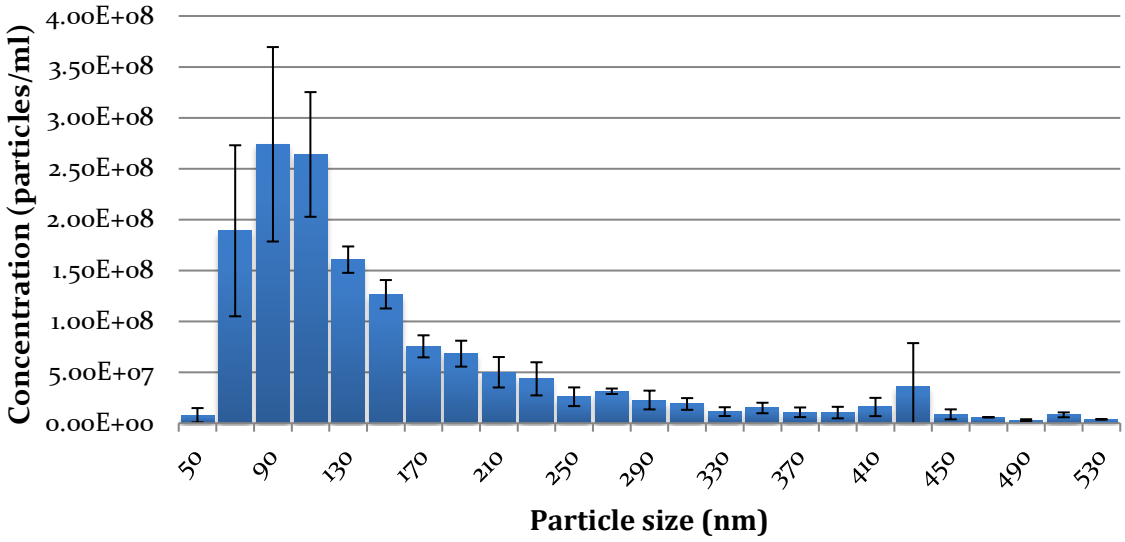

Figure 2. Average U251 supernatant-derived EV Particle Size Profile.

Three samples were tested by the Tunable Resistive Pulse Sensing technology (qNano System). U251 supernatant in serum free RPMI is used. A volume of 35 µl of sample was loaded on the instrument. 1 µl/ml of calibration beads CPC200 (210 nm, 1E+12 particles/ml) were used to calibrate the qNano instrument. The pressure was set up at 0.7 kPa. Noise < 0.063 RMS, Voltage ~ 0.40-0.70V. Data analysis was performed by Izon Control Suite Software v.3.2. The results are representative of three independent experiments (N=3) and are presented as Mean ± SEM.

3.1.3 Protein concentration profile correlates with EVs sample concentration

Soluble proteins derived from glioma cells mediate immunosuppression (Crane et al., 2012). The relationship between concentration of EVs and soluble proteins in the tumour samples has not been described by now. Potential correlation would be informative for the EV or protein content of a sample in case only one of them is known.

After identifying the EV concentration of the tumour samples by qNano (Data available from experiment in Chapter 3.1.1), the samples were assessed for their concentration in soluble proteins by Bradford assay. In the same sample, the relationship between EV and soluble protein concentration was statistically significant (**$p<0.001$) (Figure 3). A correlation of $r=0.83$ (Pearson's correlation coefficient) was proved, which means that the particular variables are strongly correlated and follow a linear relationship. A sample high in EV concentration has, also, high in-solution protein levels.

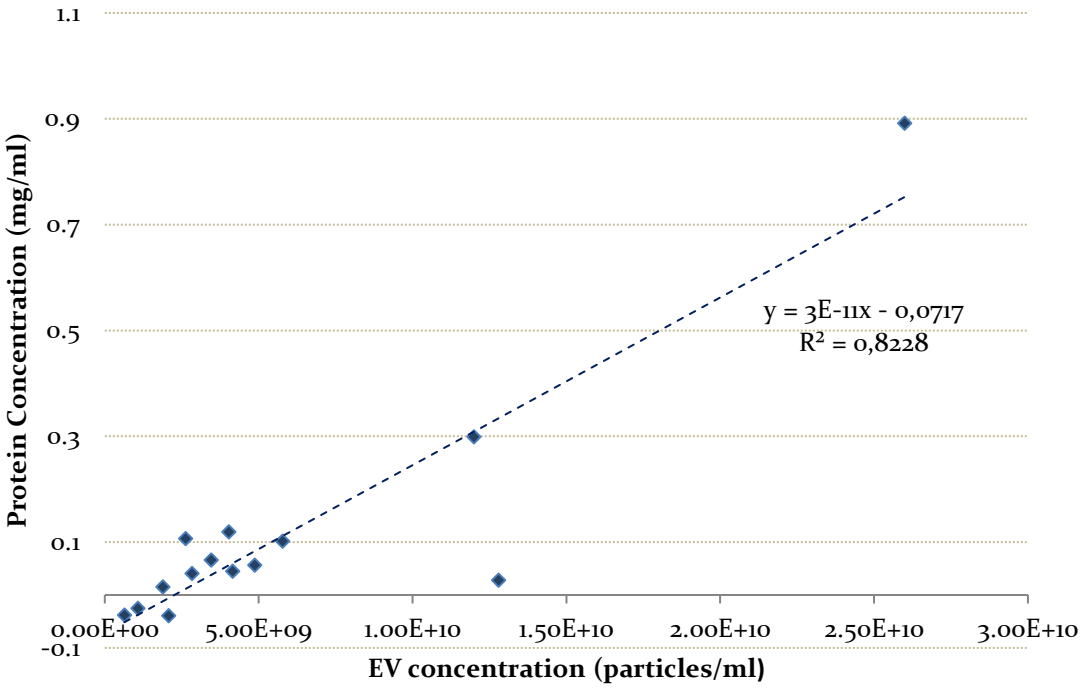

Figure 3.Correlation of soluble protein and EVs concentration in the tumour samples.

The concentration of EVs was detected using the qNano system, whilst the protein concentration was measured by performing Bradford protein assay. The graph shows how protein in-solution and EVs concentration correlate in a proportional way for the same sample. The data was analysed using Pearson's correlation coefficient and the statistical significance was given, **p<0.001, after ANOVA application.

3.1.4 Size Exclusion Chromatography Columns efficiently purify EVs in Glioblastoma

Glioblastoma cells secrete EVs in the tumour microenvironment and in blood circulation (André-Grégoire & Gavard, 2017). The holistic EVs molecular and genomic profile in GBM patients has not been identified. EVs isolation from soluble proteins is important, in order to examine the effect on their target cells separately and build the exact profile of the potential mediating immunosuppressive mechanisms derived by them.

Thus, a novel technique in sample preparation (for mass spectrometry) that includes the separation of EVs from soluble proteins using size-exclusion chromatography was tested here. The SEC-based enrichment of extracellular vesicles was examined in model samples for its efficiency. A model sample of 1 mL serum-free RPMI containing 1 µl/mL CPC200 calibration beads (1E+12 particles/mL), 1 µl/mL CPC100 (1E+13 particles/mL) and 1 µl/mL CPC400 (1E+12 particles/mL) was prepared. The sample was loaded on qEV column and collected in thirty 0.5 mL-fractions. The fractions were tested in EV and soluble protein content by qNano and Bradford protein assay, respectively. These assays determined fractions 1-5 as void volume, fractions 6-12 contain purified EVs, whilst 13-30 are soluble protein-enriched fractions (Figure 4). Alternatively, the EV-enriched fraction can be collected after 2.5 mL void volume and it is in total 3.5 mL. Protein fraction is collected immediately after EVs at a final volume of 9 mL.

Next, qNano was implemented on the seven 0.5 mL EV-enriched fractions (Figure 5). The size profile revealed that most of the EVs had 110-210 nm diameter or 310-410 nm. These two peaks had the same diameter size as the modal beads revealing that qEV does not change EVs characteristics.

A mixture of samples including U251 supernatants, tumour samples and model samples consisting of calibration beads, with different concentrations were tested for EV concentration using qNano before and after qEV size exclusion chromatography (Figure 6). The average EV recovery rate in this procedure was 40%. (***, p = <0.001).

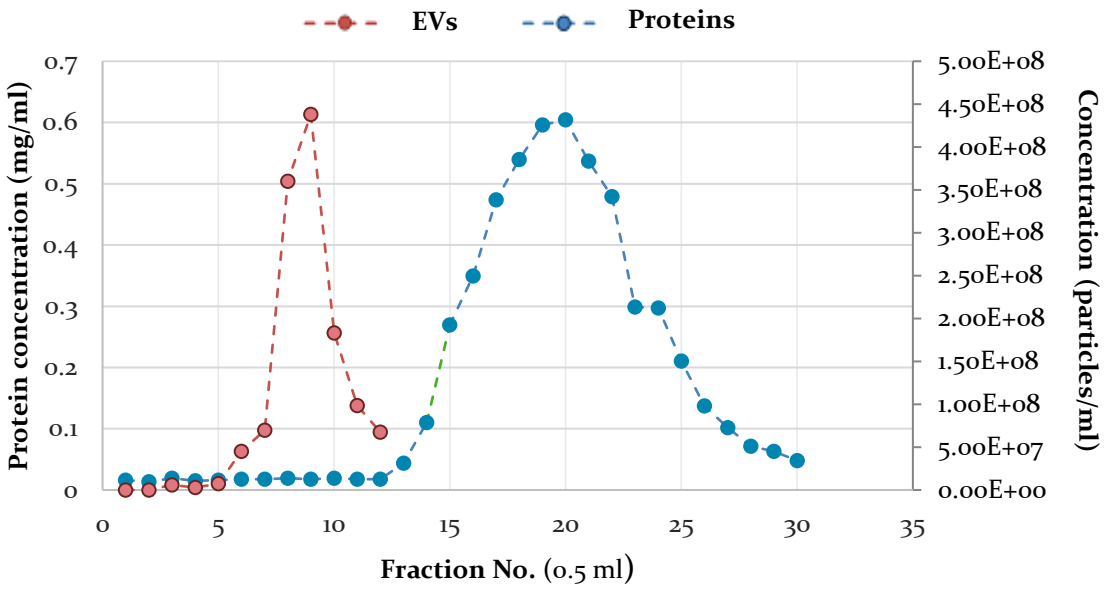

Figure 4.Typical elution profile for EV and Protein Isolation after using qEV SEC columns.

After concentrating the sample into a final volume of 1,5 ml, the sample was added on the top of the qEV column. Up to 30 fractions of 0,5 ml each were collected (15 ml), while the column was continuously being topped up with PBS. In order to verify which fractions contain the vesicles and test the efficiency of the columns, each fractions was tested by the qNano System. Also, the fractions were tested by Bradford protein assay to validate the separation of EVs from soluble proteins.

EVs elute in fractions 6-12 and proteins in fractions 13-30. The samples were calibrated against beads CPC200. Nanopore NP200 was used.

Data analysis performed by Izon Control Suite Software v.3.2. Protein concentration was measured by Bradford Protein Assay. The protein absorbance was measured at 595 nm with the Multiskan™ GO Microplate Spectrophotometer (N=1).

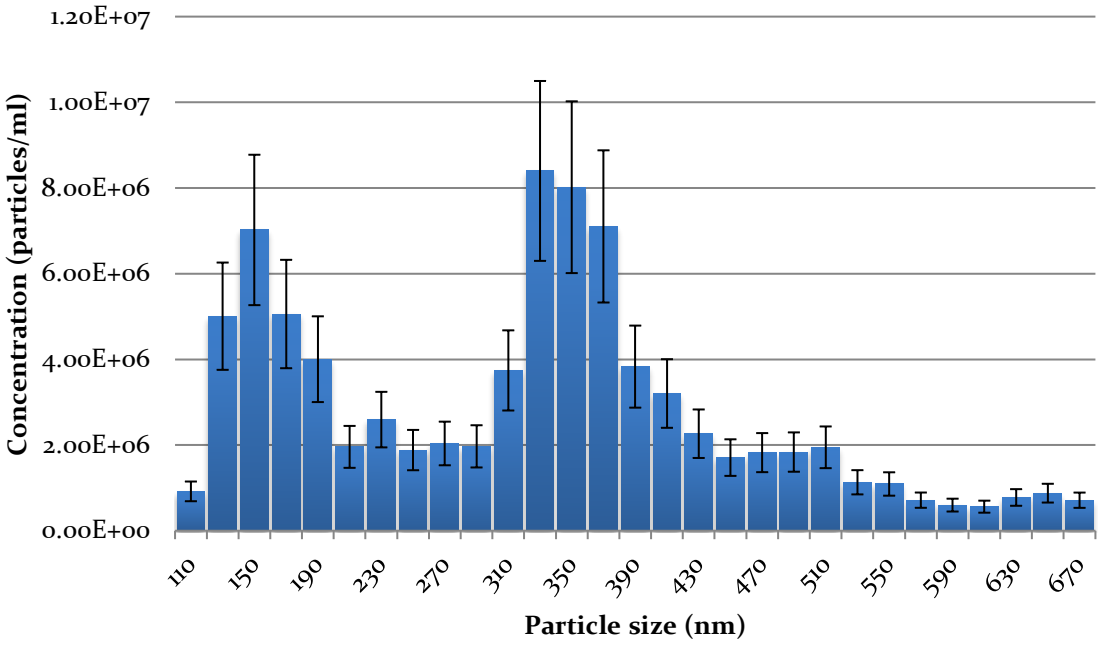

Figure 5. Particle sizing of fractions after qEV SEC.

Polysterene beads of known sizes CPC200 and CPC400 were added to 1,5 ml serum. The sample was added to the top of the qEV column and the EVs fractions were collected, which contained in the 6th-12th fractions following the previous results. These fractions were tested by qNano to detect potential changes in the size (N=1).

The instrument was calibrated using 1 µl/mL CPC200 (1E+12 particles/mL) and 1µl/mL CPC400 (1E+12 particles/mL) modal polysterene beads.

Data is shown as Mean ± SEM. Analysis performed by Izon Control Suite Software v.3.2. Pressure 0.7 kPa, Noise<0.063 RMS, Voltage ~0.40-0.70V.

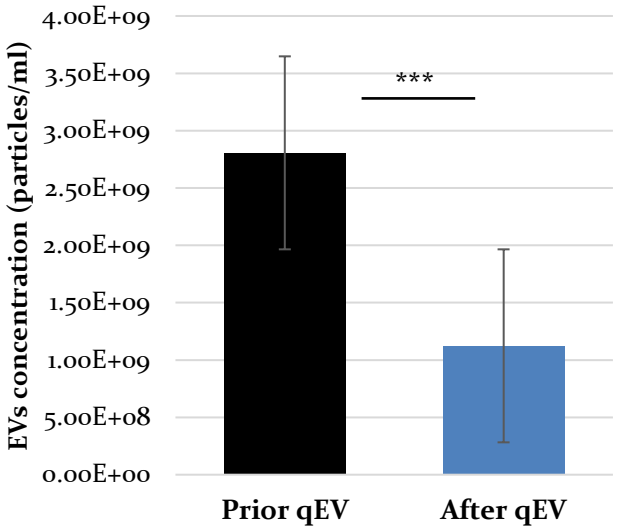

Figure 6. EVs recovery after using qEV columns.

Various samples were tested in their EV content before and after using size exclusion chromatography columns by qNano.

The samples were analysed by Izon Control Suite Software v.3.2. Pressure at 0.7 kPa, Noise<0.063 RMS, Voltage ~0.40-0.70V.

The data is representative of five independent experiments. Bars represent Mean ± SEM, paired t-test, ***, p = <0.001.

3.1.5 Overall Protein Recovery Rate after Sample Preparation.

Centrifugal filters have been introduced to the standard procedure followed for EV purification, in order the right amount of volume to be obtained for further use (Vergauwen et al., 2017). The filters can be used either before qEV SEC, since the maximum loaded volume is 2 mL or after this. The right concentration can be decided based on the steps following.

The efficiency of the whole procedure of sample preparation was studied (Figure 7). The initial protein concentration of tumour samples is tested by NanoDrop and compared with the final concentration (combined EV and protein fraction measurements), as determined by NanoDrop. The overall total protein recovery rate was 55.67%.

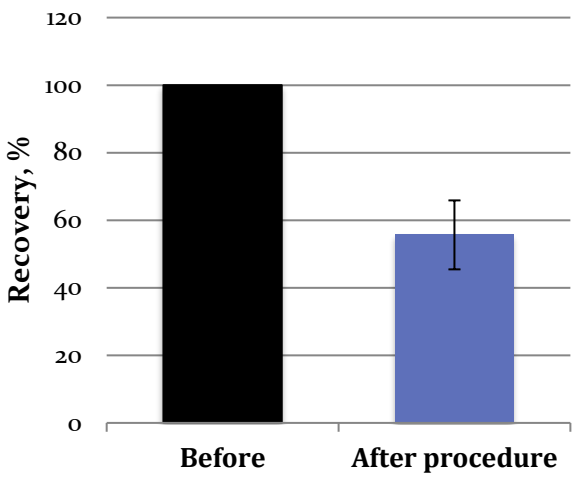

Figure 7. Total protein recovery.

Tumour samples were tested for their protein concentration by NanoDrop prior to sample preparation procedure and after it. Both EV and protein fractions of each sample were tested after qEV and sample concentration MS water was used as blank sample. The protein absorbance was measured at 280 nm. Data is representative of four independent experiments (n=4). Data is shown as Mean ± SEM.

3.1.6 Assessment of sufficient starting concentration

It has been shown that EVs are valid representatives of the tumour state (André-Grégoire & Gavard, 2017). A sufficient EV concentration needs to be established, in order all proteins that form the EV molecular profile to be detected by the mass spectrometer, even when the levels are low. The lowest EV concentration detected in the tumour samples was chosen to be tested, in order to confirm whether the protein amount detected by Mass spec analysis is representative of the actual protein sample profile (Condition 1). EVs concentrations equal to 2x min (Condition 2), 3x min (Concentration 3) were, also, prepared, since ~3 ml of each tumour sample were available and the average EVs concentration (Condition 4) that broadly represents the majority of tumour samples. Samples were prepared from U251 supernatants. Following the procedure described for sample preparation, we isolated vesicles from each sample. Almost the same amount of proteins was identified in all conditions, but most of them, specifically 354 in number, in the Average concentration. Thus, all samples were prepared according to this.

Before adding the samples to the mass spectrometer, the proteins need to be digested into peptides. Digestion in-solution and in-gel digestion were tested and evaluated for their results. U251 supernatants were used as models for the optimisation. More proteins were detected in all cases, when the samples were digested in SDS-PAGE gels. Therefore, this method was chosen and all tumour samples were processed accordingly. Protein concentration of 8 μg,, as detected by Bradford protein assay, in EVs samples and 30 μg of protein in the fraction of soluble factors was aimed for each tumour sample.

Mass spectrometry (MS) refers to conversion of the sample proteins into ions and separates them according to mass-to-charge ratio. MS proteomic analysis using databases (Mascot Daemon and Progenesis QI) defines the identity and quantity of the peptides detected. Proteomic analysis on

EVs fractions identified 354 proteins in total (Table 3). To avoid false positives Mascot sets a threshold for positive IDs of specific proteins within a given sample. Progenesis lowers this threshold for positive identification if a given protein has arisen in other comparator samples. As a result, Progenesis is more likely to positively identify proteins of low abundance than Mascot if a high concentration sample is provided for comparison. The table below displays the actual protein counts in each sample identified with Progenesis. The highest protein amount was identified in the sample containing the average EV concentration. The concentration of EVs in each tumour sample is presented in particles/mL (Figure 8). The threshold of the average EV concentration is, also, spotted and the volume of each sample needed to meet it was estimated.

Table 3. Protein counts of the EVs fractions after Progenesis QI analysis

EVs samples	**Protein number**
Condition 1 - Minimum	332
Condition 2 – Min x2	324
Condition 3 – Min x3	335
Condition 4 - Average	354

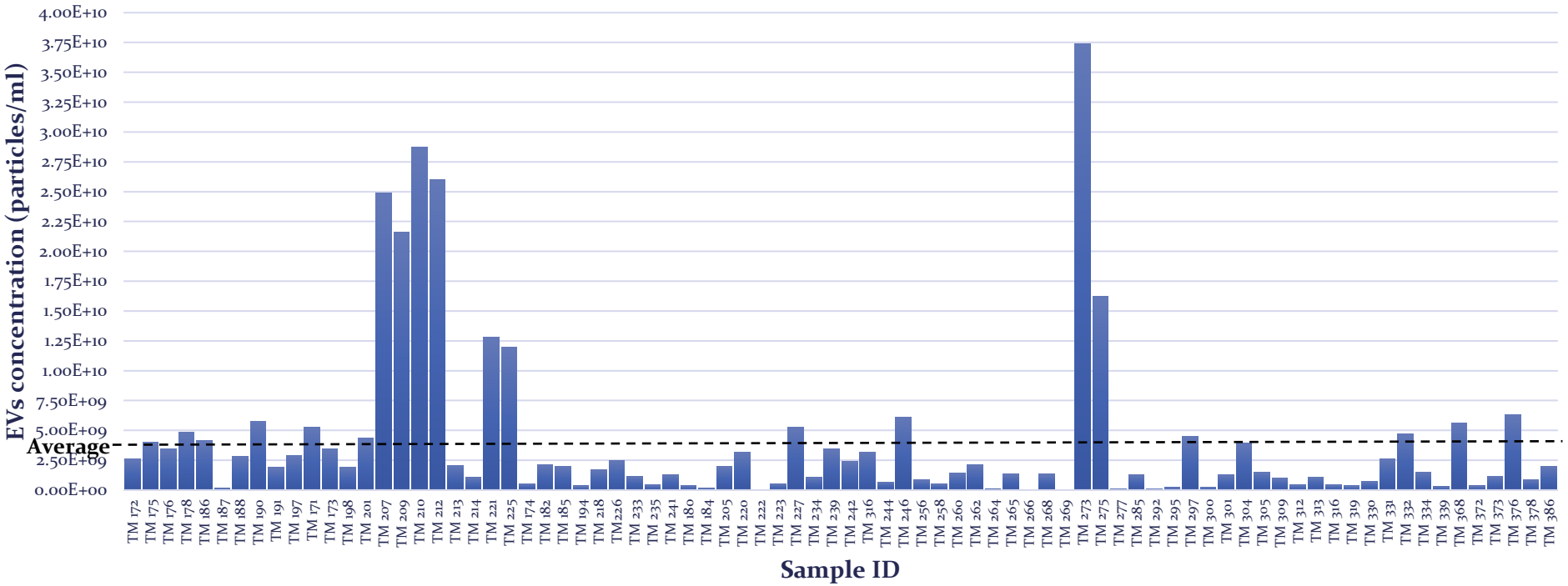

Figure 8. Characterisation of the extracellular vesicles contained in patient-derived tumour samples in terms of their concentration.

The secretome of 79 Glioblastoma tissue biopsy samples was isolated, transferred in transport medium and analysed by the qNano. The EVs secreted in the medium were detected with NP200 nanopore and the concentration is depicted in the graph in particles per millilitre. The dashed line shows the average EVs concentration per mL, which was used as a threshold.

Data was analysed with Izon Control Suite Software v.3.2. Pressure 0.7 kPa, Noise<0.063 RMS, Voltage ~0.40-0.70V.

3.1.7 Established overall workflow for sample preparation

After optimisation, the protocol that was used for tumour sample preparation for proteomic analysis was established. Figure 9 summarises and displays the main steps of this process, which were centrifuging the tumour sample required volume to obtain the average EVs concentration using centrifugal filters, in order to achieve a final volume less than 2 ml. Then, the sample is added on qEV column and vesicles are separated from the proteins into two different fractions. Both the fractions were collected and concentrated using centrifugal filters of 10 kDa for the vesicles and 3 kDa for the proteins in solution to a final volume of 30 µl, in order to be loaded on SDS-PAGE gels. The gels were stained and cut and the proteins were digested into peptides, which were extracted and collected for proteomic analysis with Mass Spectrometry.

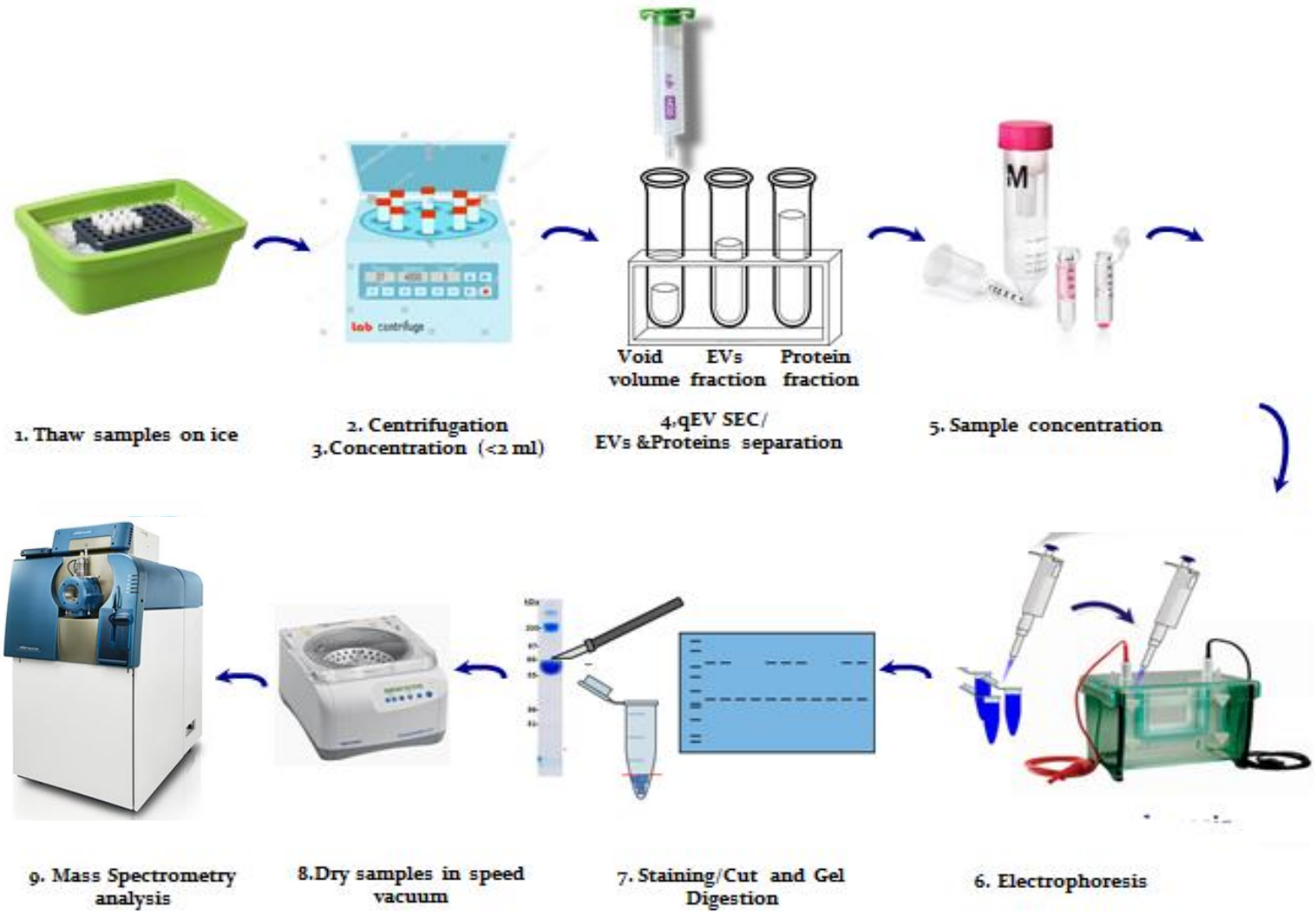

Figure 9. Overall workflow of sample preparation for Proteomic-Mass Spectrometry analysis.
The main steps of the procedure are labelled in the graph.

3.2 BIO-INFORMATIC ANALYSIS AND IDENTIFICATION OF IMMUNOSUPPRESSIVE CANDIDATES

After the samples were prepared for high-throughput liquid chromatography–mass spectrometry (LC-MS/MS) following the above-mentioned established protocol, proteomic analysis was performed, in order to screen and quantify all proteins being present in the tumour microenvironment the moment the tumour was resected from the patients. Previous studies performing proteomic analyses in GBM were most commonly using GBM cell lines or a small number of tumour samples, mostly focusing in identifying genes differentially expressed between healthy and cancer conditions and proposing new biomarkers for GBM diagnosis and prognosis. In contrast, for our study we aimed to analyse the whole secretome of 79 patients, which includes proteins and EVs secreted by both cancer and immune cells of the microenvironment.

3.2.1 Identification of Cell surface proteins in the GBM-derived EV fraction

In the extracellular vesicle fraction, 1397 proteins were identified in total and 1337 in the soluble factor fraction.

The first step to narrow the protein list down was to identify and proceed with the proteins that were expressed in 80% of the tumour samples. The protein analysis was, also, conducted through different databases that are available online. When databases run the gene/protein list against different classification systems, the results given may vary. Thus, use of a number of them would serve the purpose of no information being missed. The databases used are informative regarding the characteristics of the proteins identified, such as the compartment of their expression, their biological functions or the signalling pathways that are implicated.

For the extracellular vesicle fraction, from the 1397 proteins, 1201 were expressed in 80% of the samples. Figure 10-A depicts this network of proteins according to STRING database, which retrieves the functional protein association networks, running the corresponding gene/proteins list against a number of classification systems, such as GO, Pfam and KEGG. The downstream analysis was focused on the proteins expressed on the cell surface (Figure 10-B.i) in an attempt to identify candidates based on the receptor-ligand interactions occurring between the EVs and the recipient cells. Proteins expressed on the external side of the plasma membrane (Figure 10-B.ii) were revealed including cluster differentiation molecules, such as CD276 and CD36, adhesion molecules, like ICAM and NCAM or annexins and transport proteins.

A

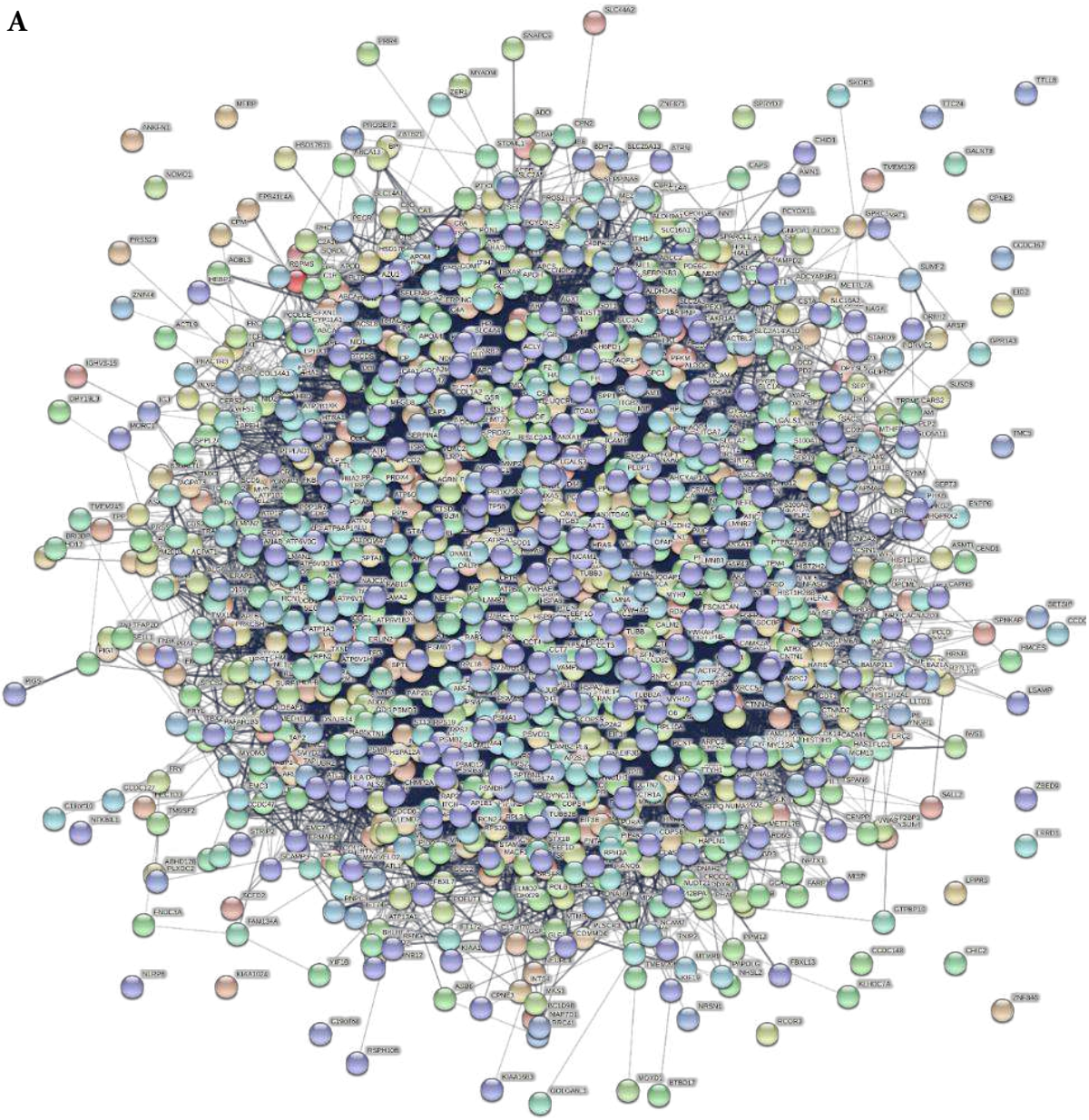

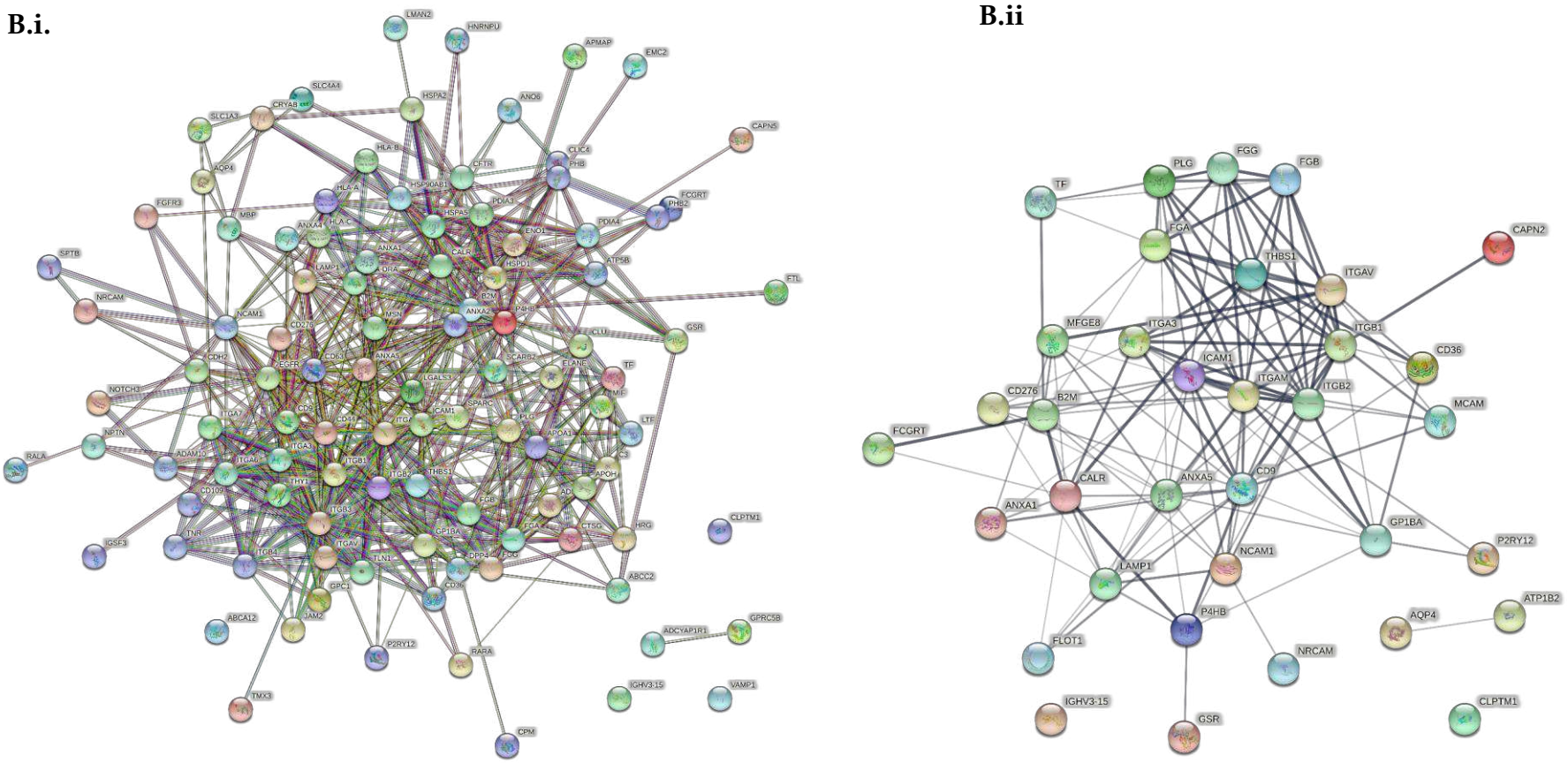

Figure 10. Protein-Protein interaction network in the Extracellular vesicles fraction according to STRING database.

The gene/protein list was added on STRING and labels relevant to ''Cell surface'' were chosen to highlight the proteins expressed on the cell membrane. (A) Network of the proteins that were expressed in 80% of the samples. (B.i.) Representative image of the key proteins detected in the samples to be related to the term "Cell surface". (B.ii.) Network of the proteins expressed in the ''external side of plasma membrane''.

The next step was the proteins of the extracellular vesicle fraction to be sub-grouped according to the cellular component using PANTHER (Protein ANalysis THrough Evolutionary Relationships) Classification System (Figure 11-A) and to focus on those expressed on the plasma membrane, as previously (Figure 11-B). A number of 342 proteins were found to be related to the term ''membrane'', from which 299 were on the plasma membrane. A very small percentage was related to organelle or nuclear membranes and, therefore, were not of our interest. From the downstream analysis, proteins expressed in the cytoplasmic side of the plasma membrane or extrinsic components were excluded, as well (Figure 11-C).

A

Cellular component
Genes 749, Total hits 2512

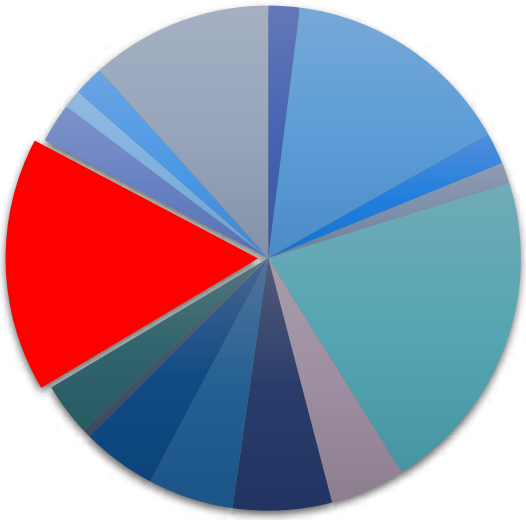

- Cell junction
- Cell periphery
- Cell projection
- Cell surface
- Cytoplasm
- Cytosol
- Endomembrane system
- Extracellular region
- Extracellular space
- Extrinsic component of membrane
- Intrinsic component of membrane
- Membrane
- Membrane-enclosed lumen
- Side of membrane
- Supramolecular complex
- Miscellaneous

B

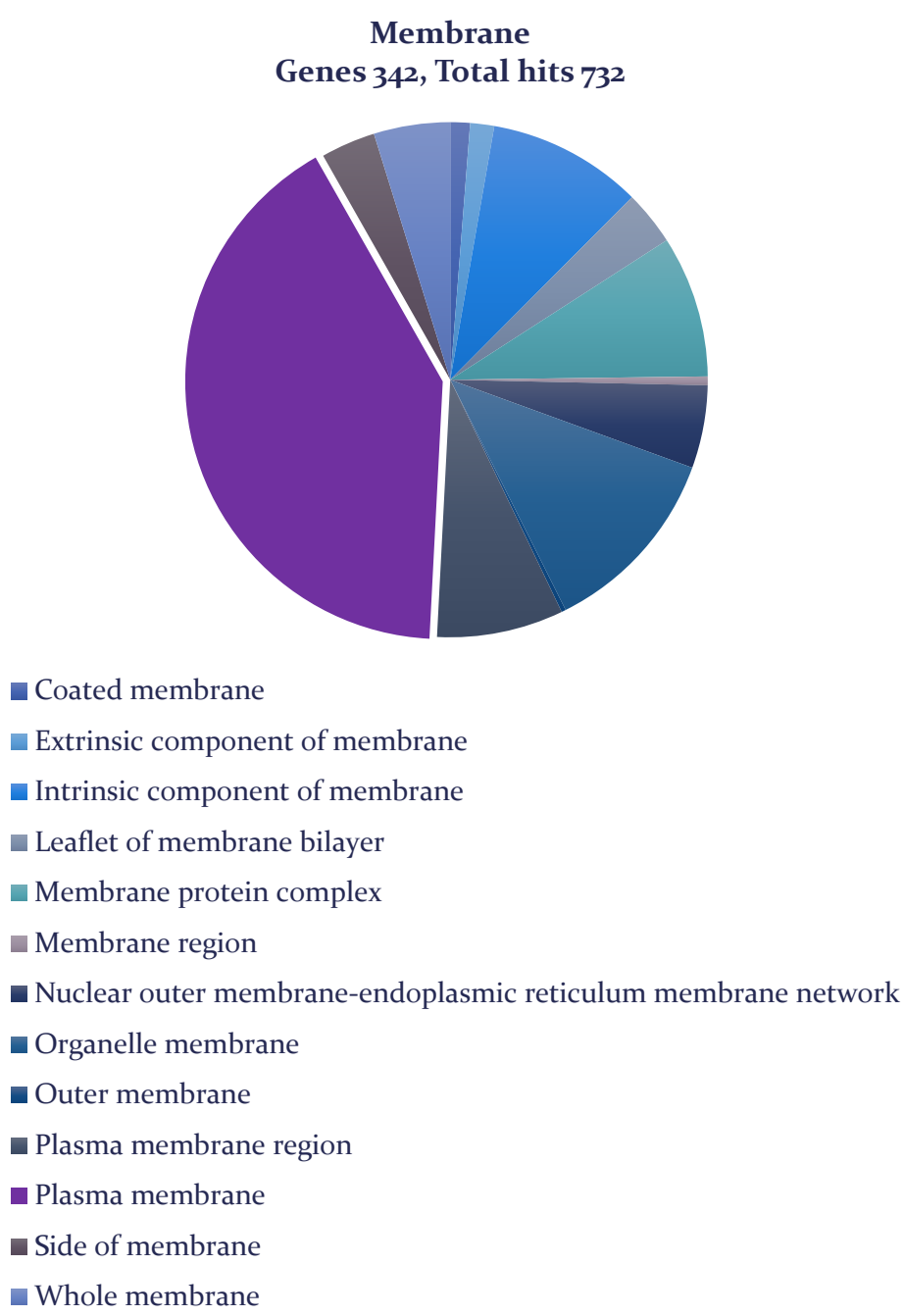
Membrane
Genes 342, Total hits 732
Coated membrane
Extrinsic component of membrane
Intrinsic component of membrane
Leaflet of membrane bilayer
Membrane protein complex
Membrane region
Nuclear outer membrane-endoplasmic reticulum membrane network
Organelle membrane
Outer membrane
Plasma membrane region
Plasma membrane
Side of membrane
Whole membrane

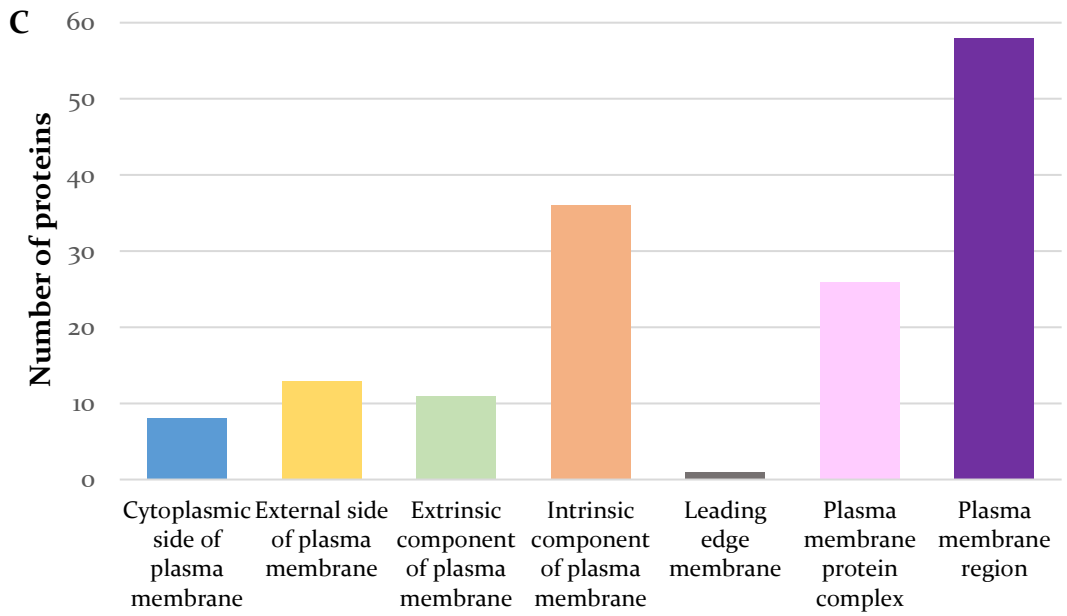

Figure 11. Bioinformatic analysis for the tumour- derived extracellular vesicle fraction according to PANTHER database.

(A). Proteins contained in 80% of the EV fractions categorised based on the cellular component that are expressed. 749 proteins were identified with GO gene ontology, but each one is represented in more than one groups (B). Downstream analysis of figure 10(A). Subcategories for proteins related to the term ''membrane'' are displayed. (C) Proteins sub-groups related to ''plasma membrane''.

The analysis was confirmed and enriched by FunRich software (Functional Enrichment Analysis Tool), which uses FunRich or Uniprot classification. Bioinformatic analysis of the dataset using FunRich confirmed that most of the proteins found in our study in the extracellular vesicle fraction were previously related with the particles or the membrane. Proteins identified under the terms Plasma membrane (80%), Integral to plasma membrane (26,5%), Exosomes (55%) and Cell surface (13%) were relevant to our searching.

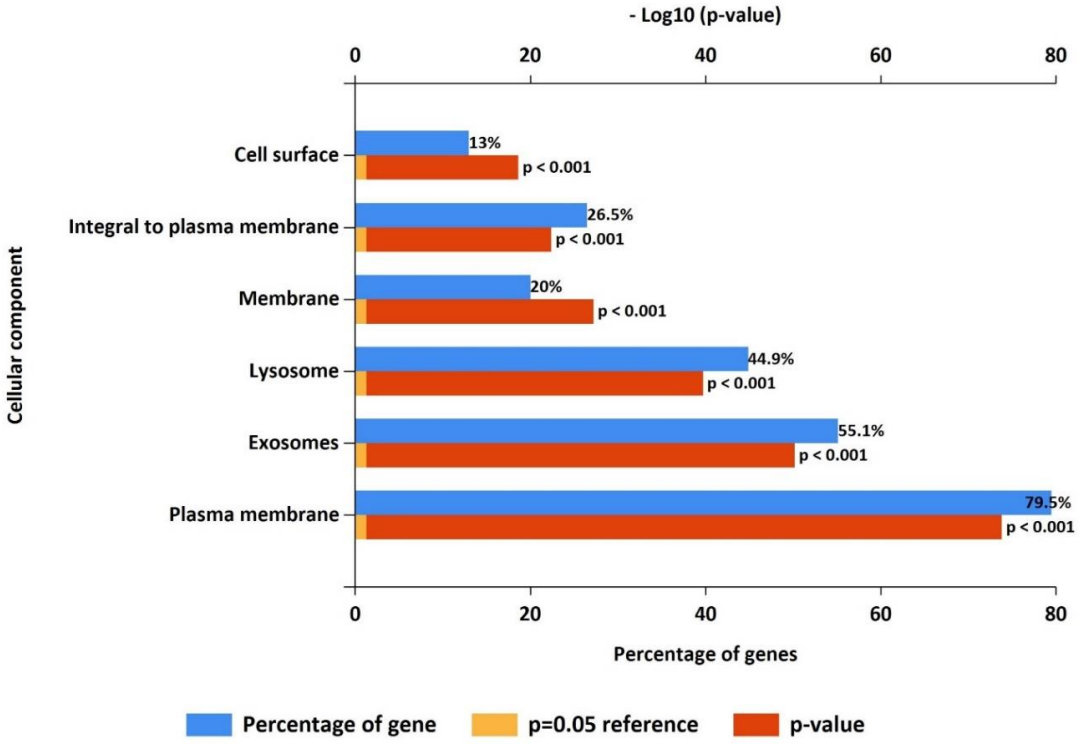

Figure 12. Bioinformatic analysis applied to the proteins detected in Glioblastoma-derived extracellular vesicle fraction.

The gene/protein list found was added to Functional Enrichment Analysis Tool and the proteins identified were categorised based on the cellular component of their expression.

Graph generated by FunRich.

3.2.2 Identification of proteins with immunological function in the tumour EVs fraction

After running the dataset through four different databases (STRING, PANTHER, FunRich and DAVID), the total amount of proteins related to the cell surface was collected. The total number of proteins that were linked to the membrane of either vesicles or cells was 307, from which 145 were found in more than one databases, whilst 165 appeared only in one of them (Figure 13). Due to some vague/broad terms, such as ''membrane'', the list of proteins was examined further. Proteins that were localised on the cytoplasmic side of the membrane or falsely identified as membrane proteins due to interactions with them, were excluded. The proteins that were found to be expressed on the external side of the membrane were 123. Downstream analysis was focused on their function, with the aim to reveal those that potentially are implicated in the immune responses.

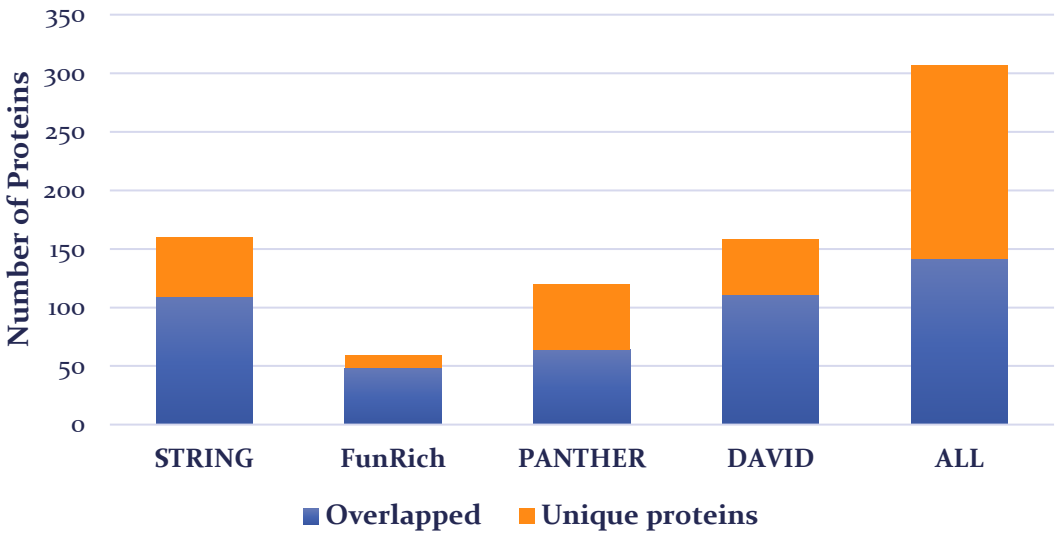

Figure 13. The number of proteins related to the cell surface detected in the EVs fractions using different analysis tools.

The total amount was identified by adding all the proteins found at least one time among the databases. Proteins detected to be expressed on the cell surface by more than one database are labelled as overlapped and they were counted once.

The list of cell surface proteins was re-introduced to the online databases and this time the option to be categorised according to their biological function was chosen. FunRich analysis showed that the majority of them were linked to signal transduction process, transport or cellular communication, which validates our method of sample preparation and vesicle isolation, since the last two are the main EVs functions (Figure 14). 8.6% of cellular proteins was found related to immune responses. Same rationale was followed on STRING, where proteins related to terms, such as 'lymphocyte activation'' and ''immune system process'' were selected for further investigation.

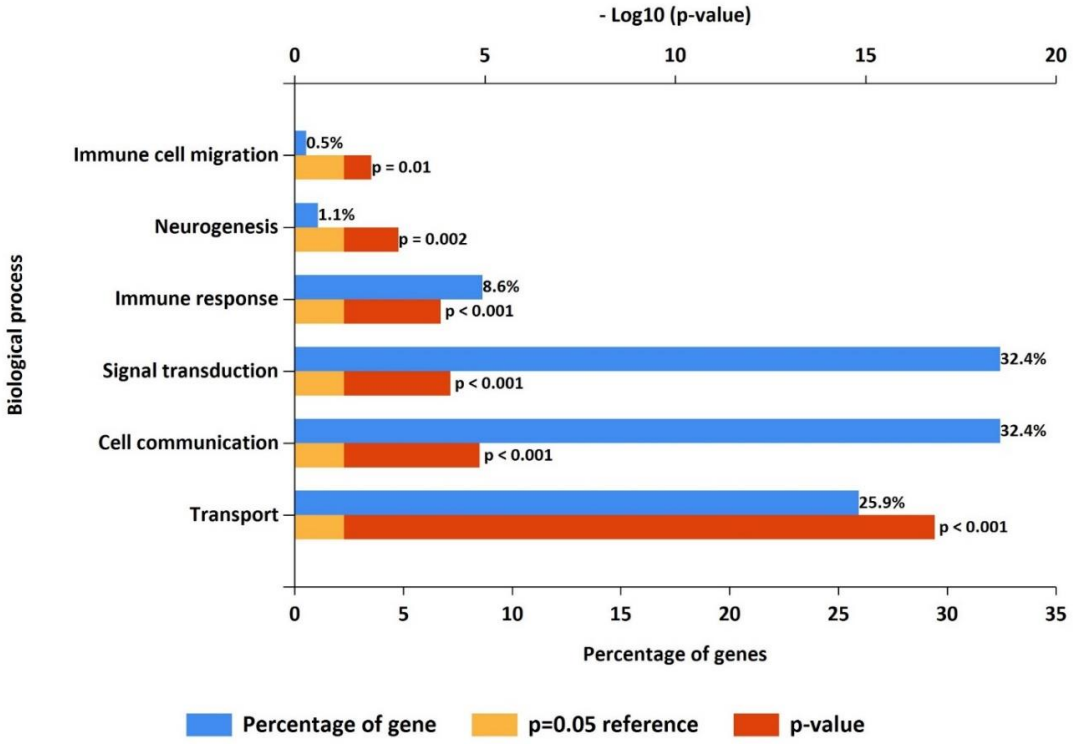

Figure 14. The most representative biological functions of the cell surface proteins contained in the GBM-EVs fraction.

The gene/protein list with the proteins expressed on the cell/vesicle membrane was uploaded on FunRich database and the proteins were subgrouped based on the biological process that are involved. Graph generated by FunRich tool.

In total, 51 proteins were reported to have a potential immunological function. Literature search about their role provided a clearer idea about which ones can serve as immunosuppressive candidates in Glioblastoma multiforme tumours. The flowchart in Figure 15 summarises the main steps of the process followed.

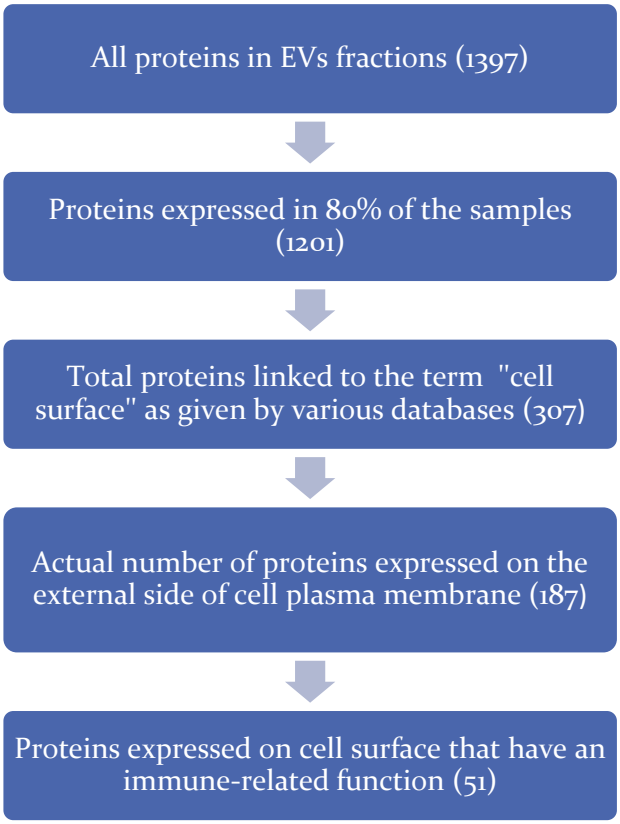

Figure 15. The main steps of the workflow followed to identify the best immunosuppressive candidates in the GBM-derived EVs fraction.

After identifying the proteins expressed on the cell plasma membrane, the dataset was re-analysed, in order proteins with an immune-related function to be determined. The flowchart shows the number of proteins in the narrowing process after each step.

The dataset was analysed with STRING, DAVID, FUNRICH and PANTHER databases.

Three proteins from the extracellular vesicle fraction were chosen to be tested for their effect on T cells responses in further experiments. These were the cluster of differentiation 47 (CD47), the glycoprotein Thrombospondin 1 (THBS1 or TSP-1) and the adhesion molecule ICAM. The main reasons are displayed in Table 4 and more extensively in the next chapter.

Table 4. List of Candidate Immunosuppressive Proteins in the GBM-derived EVs fraction

Thrombospondin (THBS1)	T cell apoptosis, Induction of Tregs
CD47	''don't eat me'' signal that interupts macrophage-mediated phagocytosis
ICAM1	invasion, lymphocyte migration, PD-1-mediated immunosuppression

3.2.3 Bioinformatic analysis for the Soluble proteins in Glioblastoma samples

Similarly working as above for the EVs fraction (Chapter 3.2.2), the protein IDs detected in the soluble protein fraction of the tumour samples, were analysed according to four classification tools. First, the proteins secreted in 80% of the samples were found, which met the number of 1129 proteins. This time, the analysis was directly focused on the factors that may have an immunosuppressive function, since the proteins were in-solution and not attached on the cell membrane.

STRING database revealed the interaction network of the proteins expressed in 80% of the samples (Figure 16-A) and, then, of the proteins with key immunological functions, such as involvement in immune system process (Figure 16-B.i) and lymphocyte activation (Figure 17-B.ii). FunRich revealed that the small percentage of 3,4 of the total proteins was involved in immune response (Figure 17). According to PANTHER database, 36 were the proteins implicated in immune system process, representing 2% of the total number and they were participating in the activation of the immune response, development of the immune system process, leukocyte activation and migration or production of molecular mediator of immune response (Figure 18).

A

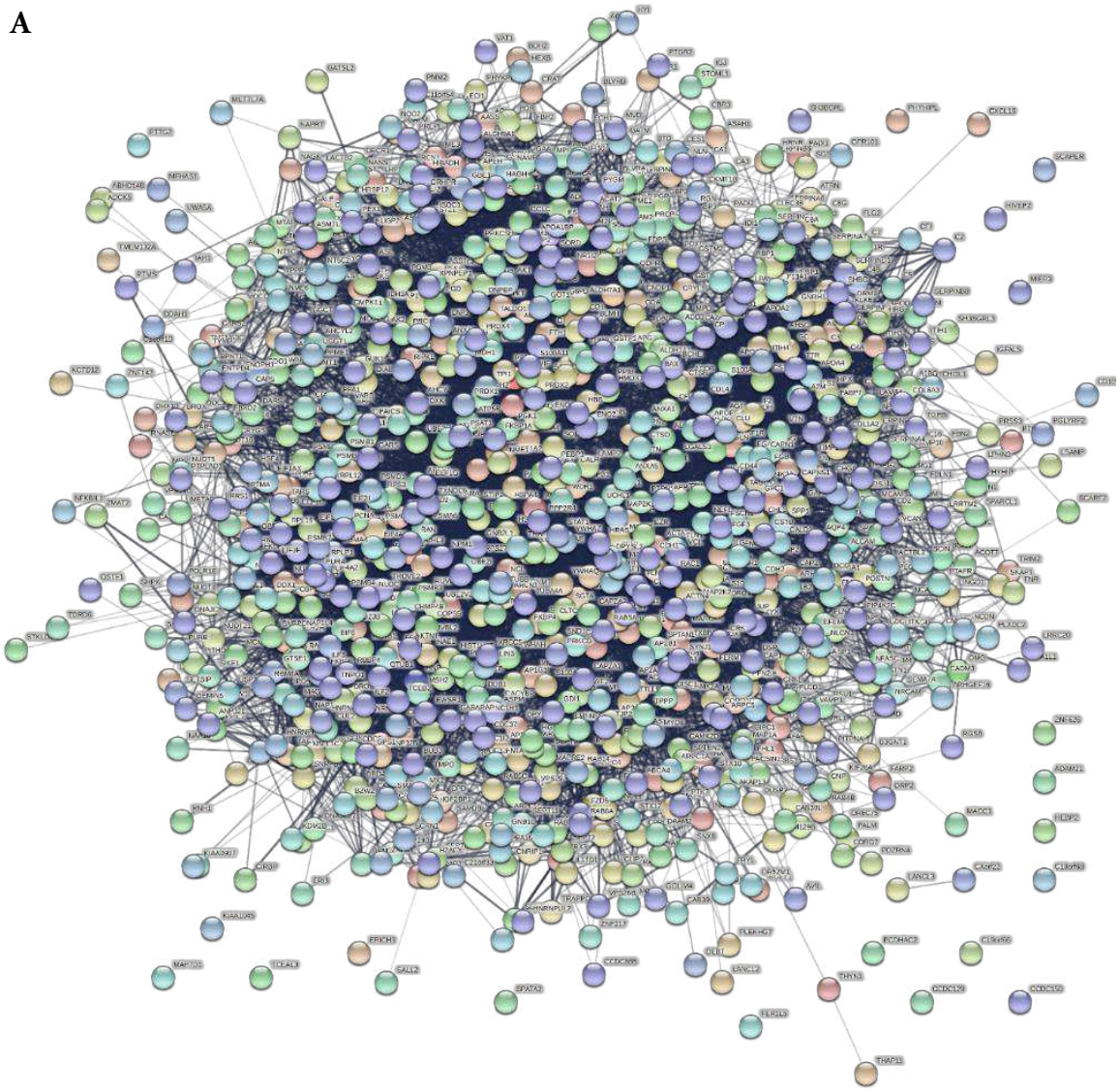

B.i.

B.ii

.

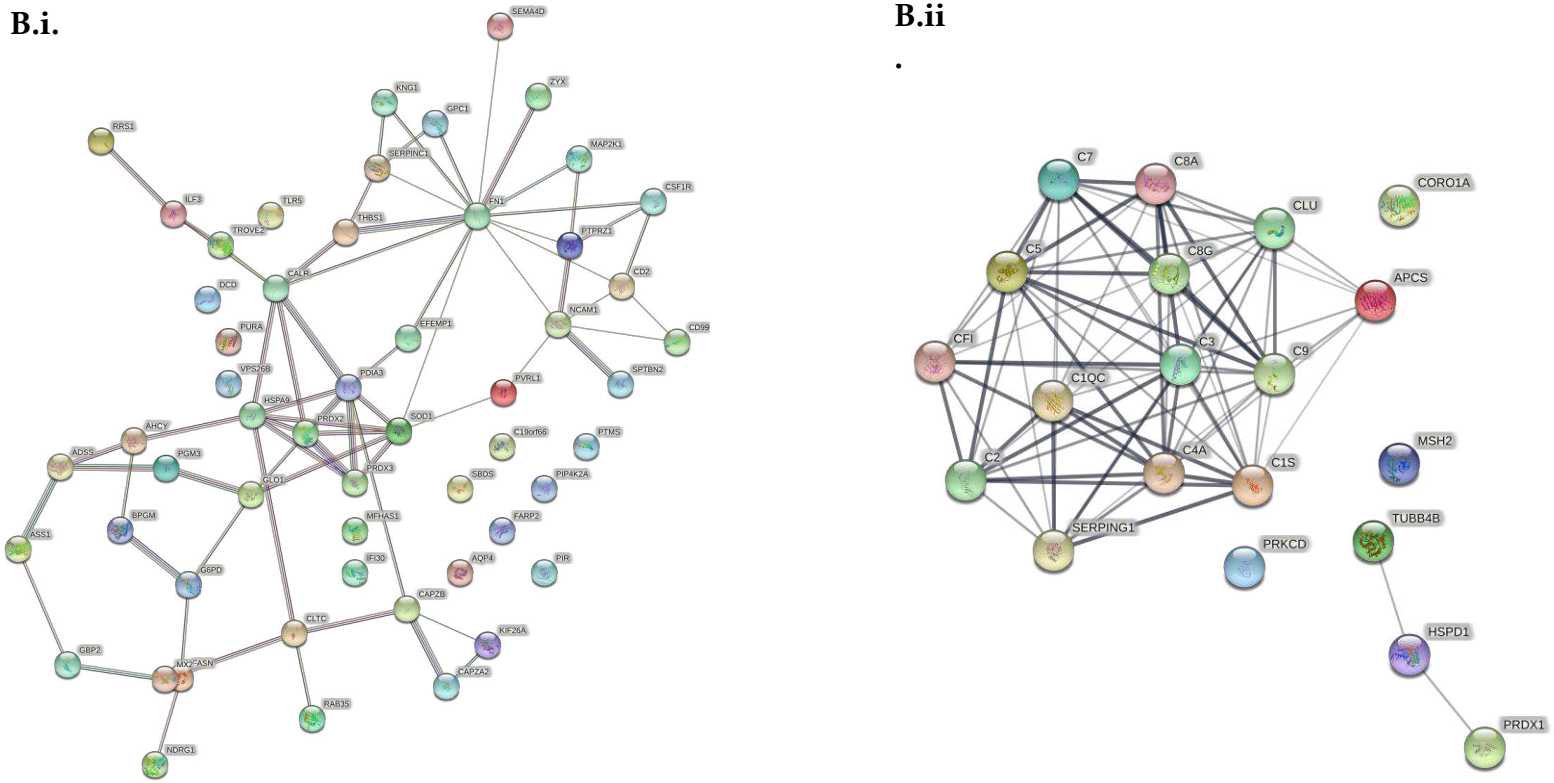

Figure 16. Narrowing down the list of proteins found in the soluble protein fractions of the tumour samples according to STRING database.

of the tumour samples according to STRING database.

The gene/protein list was added on STRING, which runs the dataset against GO, Pham and KEGG classification tools. (A) The network of all proteins expressed in 80% of the soluble protein fractions is displayed. (B.i.) Representative images of the proteins with biological functions related to the label ''immune system process'' and (B.ii) from the network of the proteins implicated in "lymphocyte activation".

A

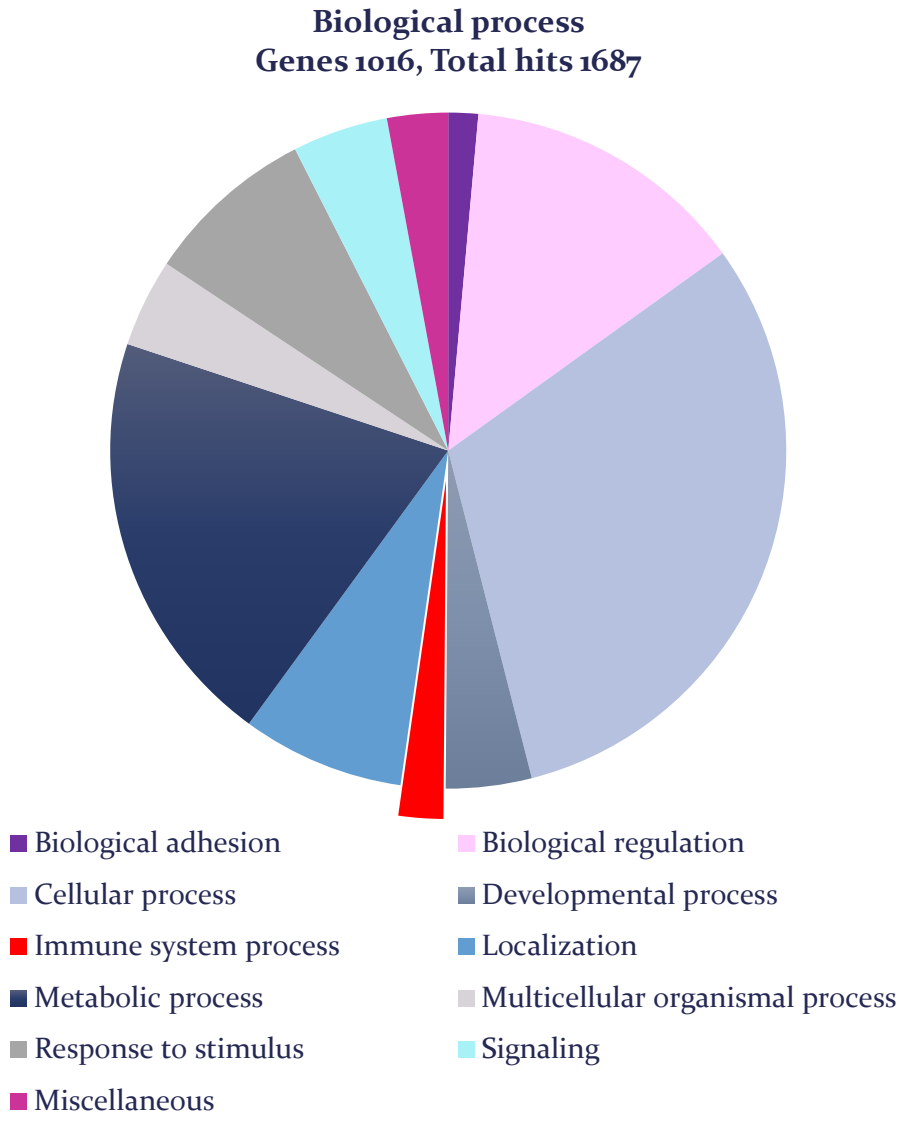
Biological process
Genes 1016, Total hits 1687
Biological adhesion
Biological regulation
Cellular process
Developmental process
Immune system process
Localization
Metabolic process
Multicellular organismal process
Response to stimulus
Signaling
Miscellaneous

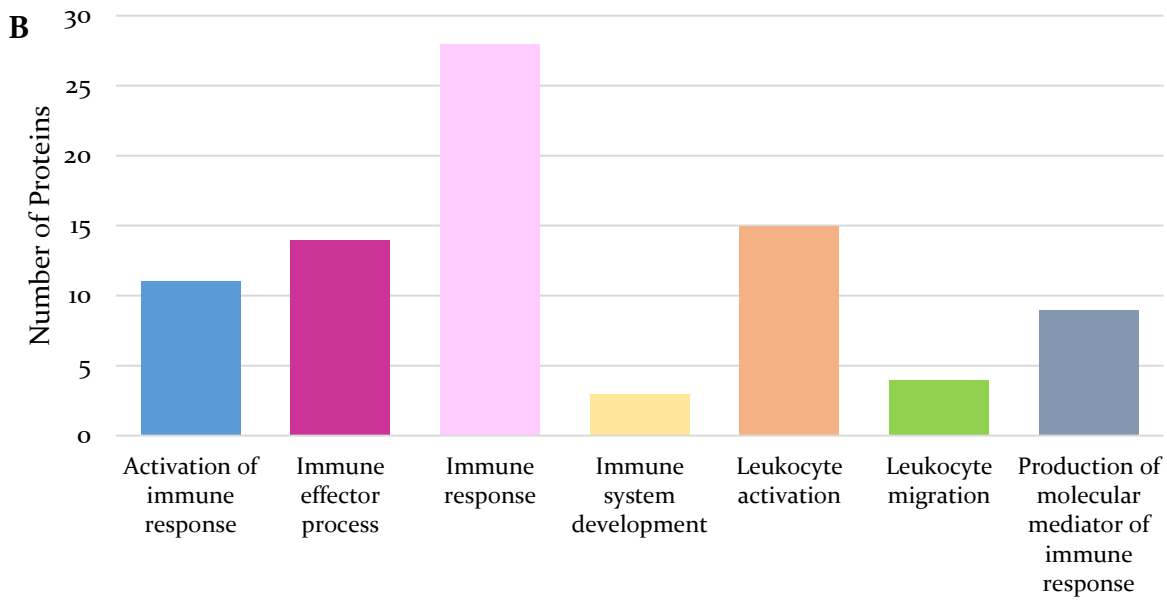

Figure 17. Bioinformatic analysis for the soluble protein fractions according to PANTHER database.

(A) The proteins identified to be contained in 80% of the soluble protein tumour-derived fractions were categorised based on their biological function.1016 proteins were identified according to PANTHER database and are represented by more than one categories. (B) From (16A) downstream analysis. The sub-categories for proteins related to ''immune system process'' are displayed.

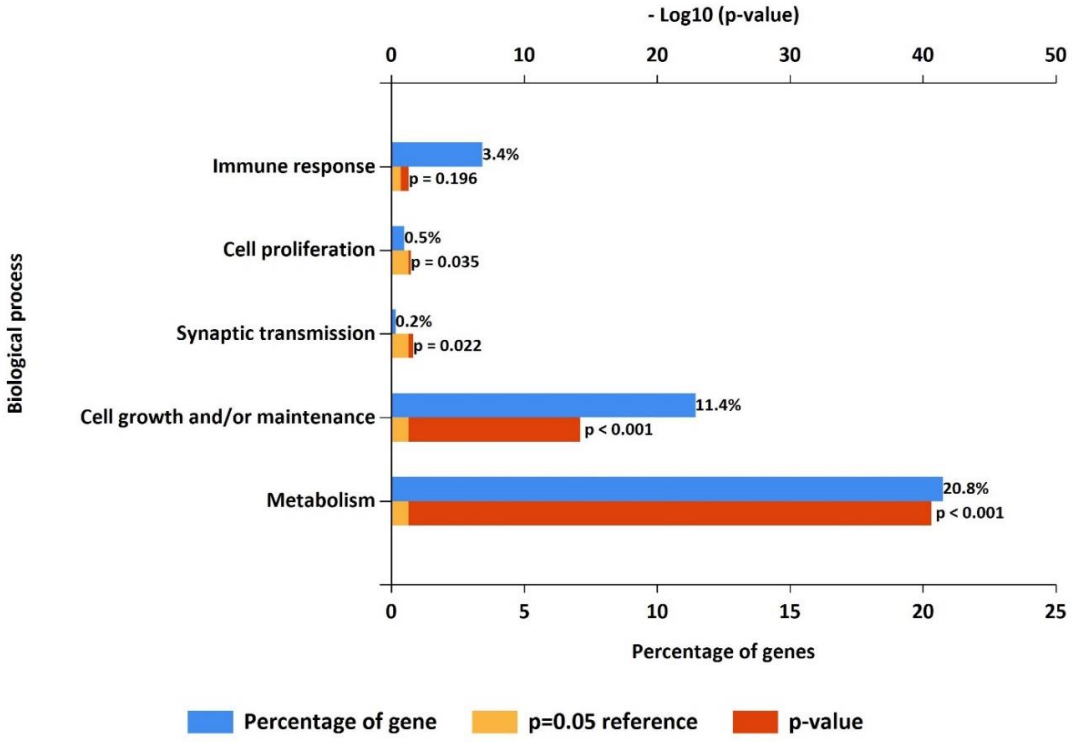

Figure 18. The most representative biological functions of GBM- derived soluble proteins. The gene/protein list with the proteins secreted in the 80% of the patients' soluble factor fractions was uploaded on FunRich database and the proteins were categorised based on their biological processes. Graph generated by FunRich database.

The total amount of proteins having immunological function was added. 219 proteins were uniquely found to be related to immune responses in one of the databases used and 73 overlapped in more than one. After revising the literature, the protein chosen to be examined further for their immunosuppressive impact on T cells in the tumour microenvironment was the macrophage migration inhibitory factor (MIF).

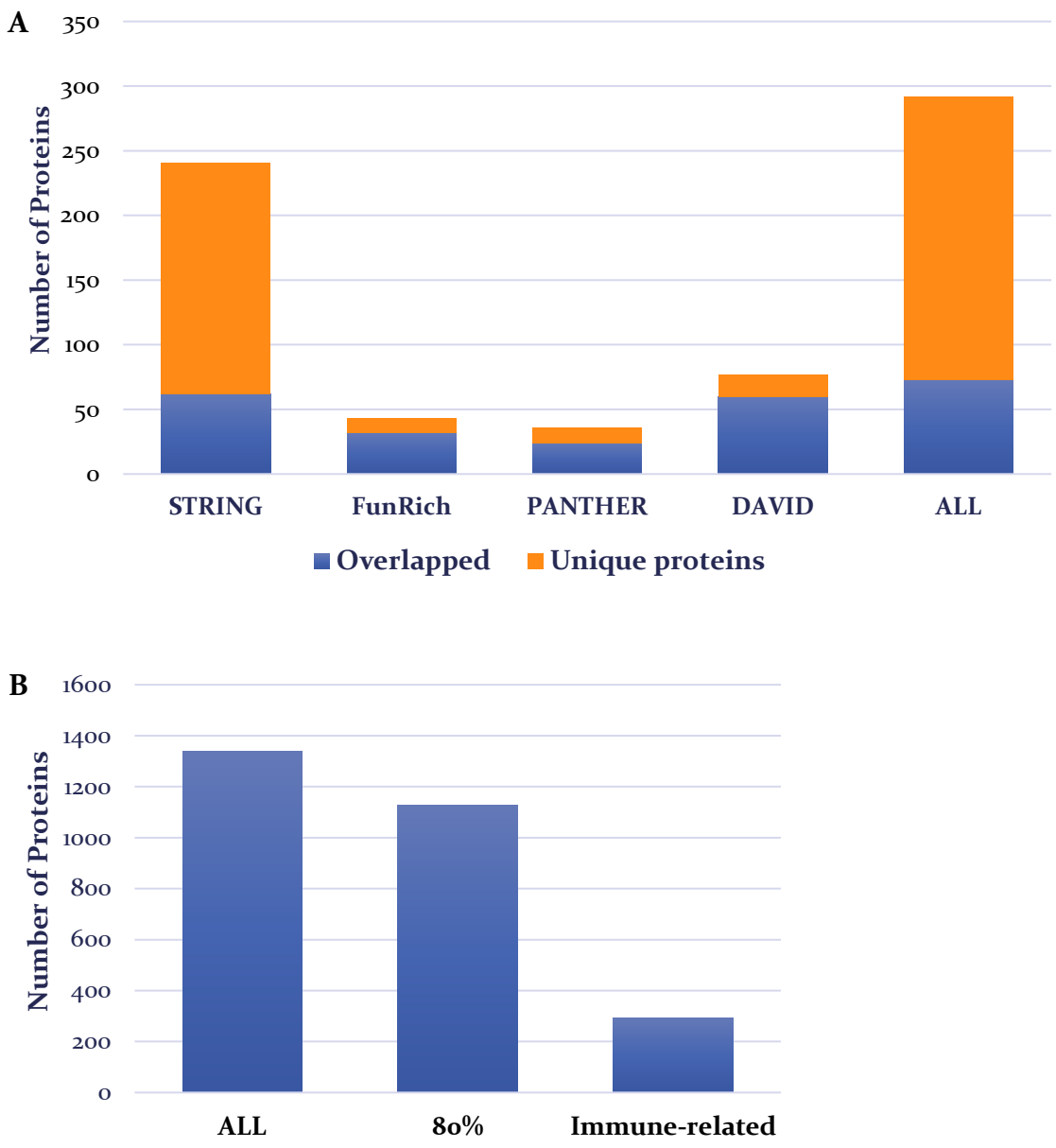

Figure 19. The number of proteins related to the immune system regulation detected in the soluble protein fractions using different analysis tools.

(A) The total amount was identified by adding all the proteins detected at least one time among the databases. Proteins detected by more than one databases are under the term ''overlapped'' and were counted once. (B) Graph shows the number of proteins in the narrowing process after each step.

3.2.4 Comparison between the findings of Glioblastoma-derived EVs and Soluble proteins fraction

From the total amount of proteins detected in each fraction, 395 of them were common in both. From those proteins, the ones expressed in 80% of the tumour samples were identified and analysed further. Approximately the same percentage of proteins, 3,5-4% was involved in immune responses in both fractions. For the soluble proteins, a higher percentage of approximately 21% (***, $p<0.001$) was related to metabolic and energy pathways, compared to 15% (***, $p<0.001$) at the EVs fractions. Additionally, when the proteins were grouped according to their cellular component a higher percentage from the EVs fraction proteins was found to be expressed on plasma membrane, whilst the majority of the soluble factors were related to the cytoplasm. However, the percentage of proteins in solution related to the term ''exosomes'' may indicate that absolute purity between the two fractions was not able to be achieved.

A

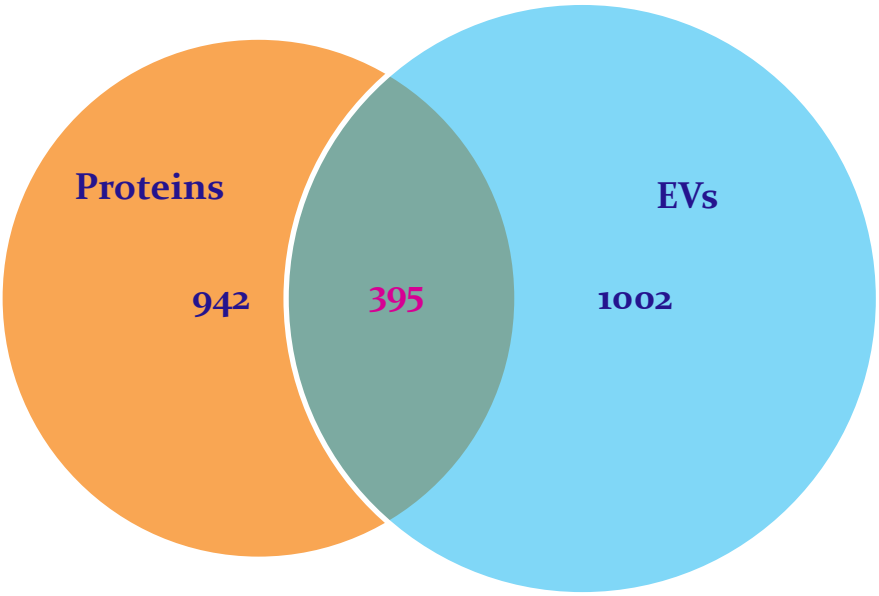
Proteins
942
395
EVs
1002

B

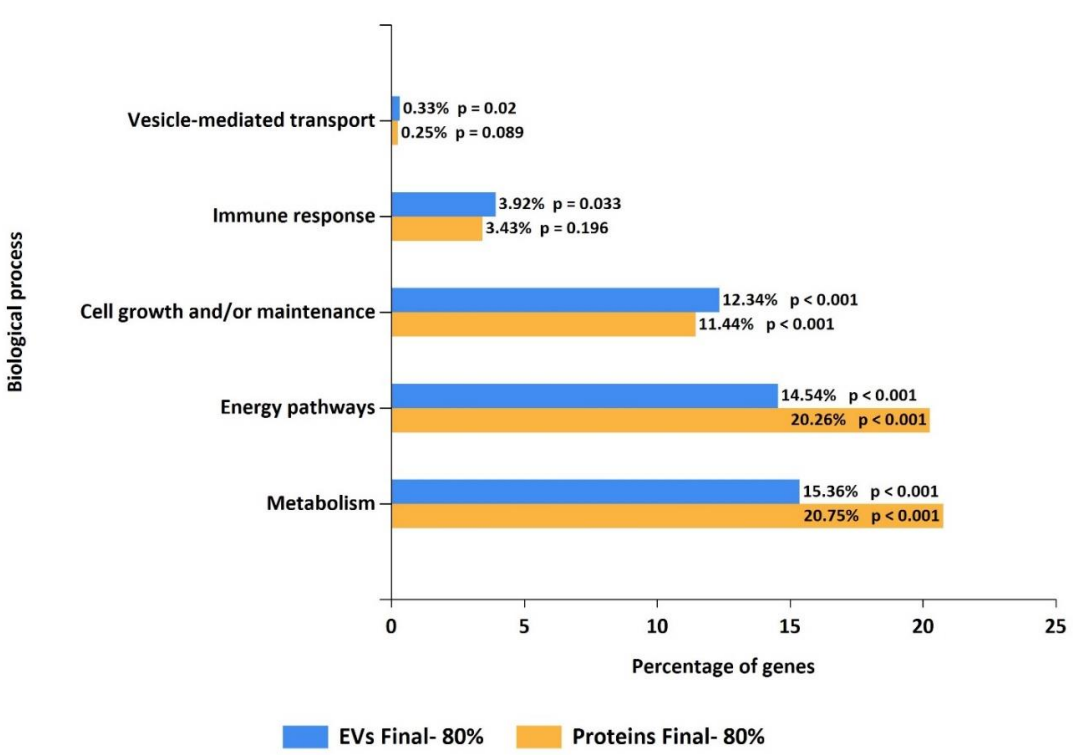
Biological process
Vesicle-mediated transport
0.33% p = 0.02
0.25% p = 0.089
Immune response
3.92% p = 0.033
3.43% p = 0.196
Cell growth and/or maintenance
12.34% p < 0.001
11.44% p < 0.001
Energy pathways
14.54% p < 0.001
20.26% p < 0.001
Metabolism
15.36% p < 0.001
20.75% p < 0.001
0
5
10
15
20
25
Percentage of genes
EVs Final- 80%
Proteins Final- 80%

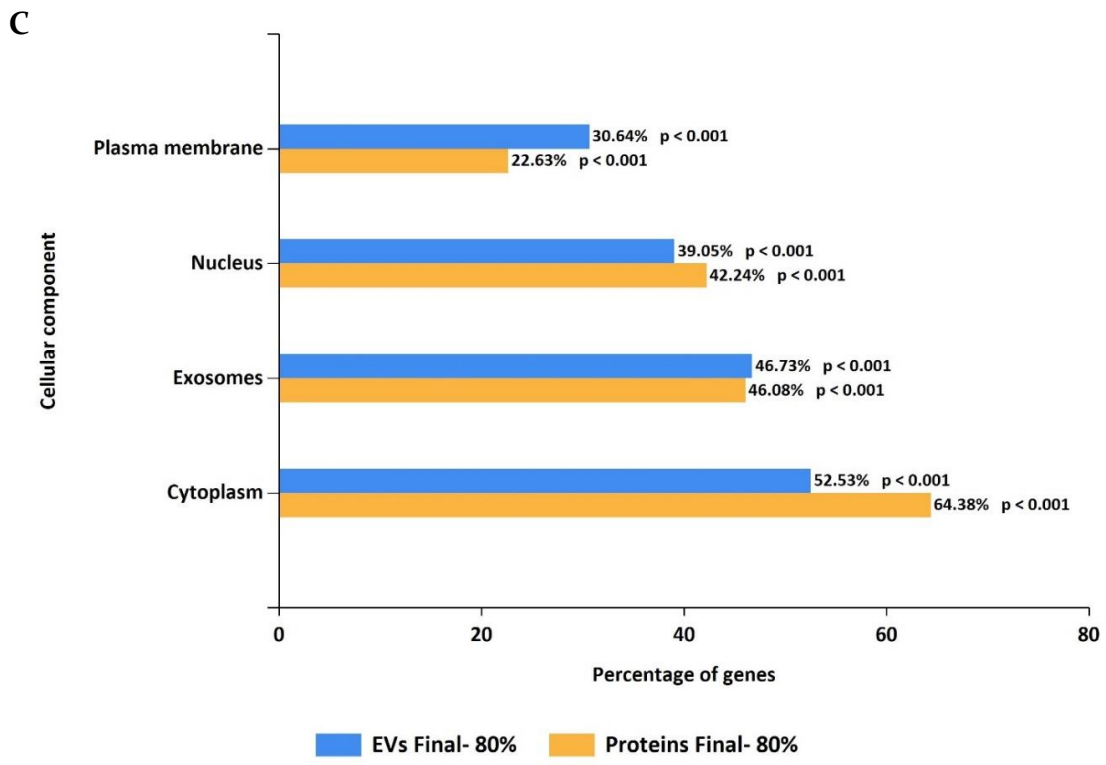

Figure 20. Comparison of EVs and Soluble proteins fractions.

(A) Venn diagram depicts the number of proteins that are unique and common in the two fractions.

(B) Proteins from both fractions compared and categorised according to biological processes.

(C) Subgroups of proteins based on cellular compartment of expression.

The proteins can be represented by more than one categories. The gene/protein lists were added on Functional Enrichment Analysis Tool and the searching was performed by FunRich database.

3.2.5 Molecular subtyping of the tumour samples

In order to test the heterogeneity of the tumour samples, molecular subtyping was performed implementing RQ-PCR. Signature genes for Glioblastoma Multiforme were tested, as they were initially identified by The Cancer Genome Atlas (TCGA) Research Network (2008) and then linked to specific subtypes by Verhaak and his colleagues (Verhaak et al., 2014). The key genes chosen to be investigated regarding their expression levels or any abnormalities are EGFR for total EGFR amplification and EGFRvIII mutants, PDGFRA expression, NF1 and CDKN2A copy number, IDH1 R132H mutation and TP53 gain-of-function (GOF) mutation. The expression levels of these genes and some combinations between them are linked to the four already known glioblastoma subtypes.

The most common genetic abnormality in Classical subtype, appearing in more than 90% of the samples, is within the EGFR gene. EGFR is either enriched or altered with EGFRvIII mutation being present more than half of the times. The vIII variant consists of deletion of exons 2–7 and specifically lack of the amino acids 6–273 (Sugawa et al., 1990) and the mutated amplicons develop as an epigenetic event on the wild type gene (An et al., 2018). Additionally, the classical subclass reportedly was associated with homozygous deletion in CDKN2A gene and higher NF1 expression than the other subtypes (Verhaak et al., 2014).

The mesenchymal subtype is the most aggressive and is characterised by high rate of NF1 mutations, usually deletions, which result in low levels of NF1 transcript. Also, in 32% of the cases a mutation in TP53 gene was observed that offered gain of function advantage to the tumour transforming it into more invasive, migrating and proliferative form capable of escaping apoptosis (Y. Zhang et al., 2018).

The Proneural group was classified based on two main features, the amplifications of the locus at 4q12 chromosome of the PDGFR*A* gene combined with high levels of PDGFRA gene

expression and the high occurrence of mutation in IDH1 gene. Moreover, TP53 GOF was highly linked to the proneural type, in contrast to NF1 expression, which was rather medium or low.

Tumour samples of neural subtype were not identified, since neural markers, such as NEFL, GABRA1, SYT1, SLC12A5 were not included in the screening and because the neural subtype was later identified rather as contaminated tissue.

Interestingly, some of the tumour samples did not follow any of the patterns described above. In our attempt to apply comprehensive and unbiased analysis of the multi-parameter screening dataset, we did not try to fit the profiles observed into the one with the higher number of similarities occurring from the those already known and recognised. Thus, here we present four more glioblastoma subtypes, as they were categorised based on the different combinations of the genes examined (Table 5).

''Classical and Proneural'' subtype is classified based on high the EGFR expression levels, combined with high PDGFRA enrichment, high NF1 expression and either high or low CDKN2A expression.

The ''Classical*'' subtype was classified based on the high NF1 and low CDKN2A expression.

The ''Classical and Proneural *'' subclass was characterised by medium NF1 expression levels and low CDKN2A expression.

The ''Proneural *'' subclass was characterised by medium levels of NF1 expression and high CDKN2A expression.

From the total number of patient samples we obtained, 58 of them were used for genomic profile examination. Most of them and, specifically 17 in number corresponding to 29% of the total, were fit within the Proneural-Verhaak subtype. Thirteen tumour samples (22%) occurred the characteristics of our newly named ''Classical and Proneural *'' type. Eleven of them (19%) follow the well-established Classical subtype features, 8 tumour samples (14%) were categorised as

Classical *, 5 of them were subgrouped as ''Classical and Proneural'' and three samples fit the Mesenchymal molecular subtype (Figure 21). Only one sample was initially identified as Proneural *, but it was decided to be included to the Verhaak-Proneural phenotype instead, in order to be part of the further statistical analysis and not to be considered as an outlier or random result.

Table 5. Molecular subtypes classification system

Classical	Classified based on EGFRVIII expression AND/OR total EGFR expression AND high NF1 expression AND low CDKN2A expression
Proneural	Classified based on IDH1 R132H mutation AND/OR TP53 GOF mutation, high PDGFRA expression with high/med NF1 expression and high/low CDKN2A expression
Mesenchymal	Classified based on low NF1 expression and TP53 GOF mutation
Classical + Proneural	Classified based on high EGFR, high PDGFRA, high NF1 & high/low CDKN2A expression
Classical *	Classified based on the high NF1 expression AND low CDKN2A expression
Proneural *	Classified based on medium NF1 AND high CDKN2A expression
Classical + Proneural *	Classified based on medium NF1 expression AND low CDKN2Aexpression

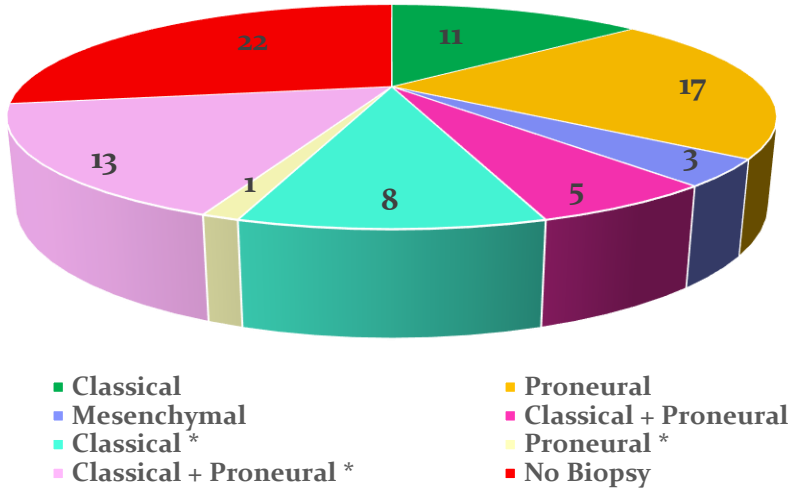

Figure 21. Number of samples represented by each molecular subtype.

RQ-PCR analysis was performed and the Glioblastoma patient samples were tested regarding the expression of specific genes mentioned in Table 5.

The pie chart displays the number of samples following the characteristics of the specific subtype. 22 samples are not included, because no sufficient biopsy volume was available for the analysis.

3.2.6 Comparison among Glioblastoma molecular subtypes based on EVs fraction analysis

The subtypes were tested for similarities or differences amongst their protein content regarding the functions that are implicated. FunRich tool was used and revealed no significant differences in the protein numbers being involved in the most represented functions. 10-15% of the proteins in all subtypes were implicated in signal transduction, around 20% in transport functions, whilst 23-29% in cell growth and maintenance (Figure 22). The Classical* subtype had slighter elevated amounts of transporting proteins(23,23%) and factors participating in cell growth and survival (29,38%) in comparison to the other subtypes.

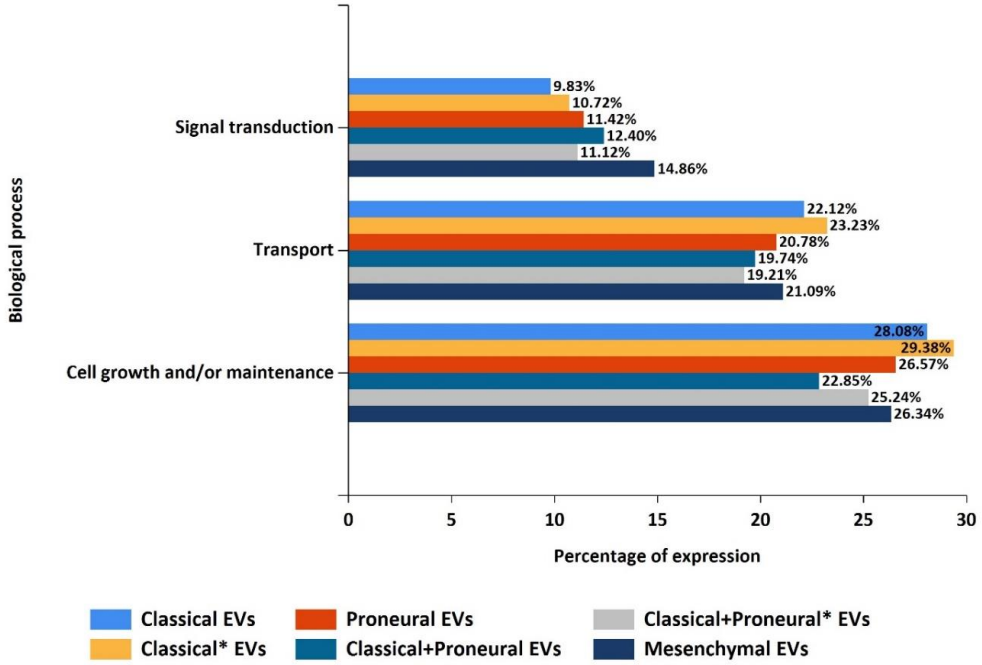

Figure 22. Comparison of the molecular subtypes based on the EVs fractions protein content.

The proteins identified in each molecular subtype were compared and categorised according to the biological processes that are involved. The proteins can be represented by more than one categories. Analysis was performed by Functional Enrichment Analysis Tool, which generated the relative graph.

3.2.7 Molecular subtype- driven potential protein biomarkers in an EV-based analysis

The Principal Component analysis enables us to check for dissociation or correlation of the variables and try to recognise if they follow any trends. In this case, initially the proteins of the EV fraction that following 95% confidence score (ANOVA) were detected, which were 49 in number. The axes F1 and F2 represent the 55,14% of the initial data information. According to Figure 23-A, the subtypes were not quite distinctive one from another. Instead, they presented overlaps regarding their protein expression content. Classical* and Proneural subtypes appeared to be characterized by the same proteins. ''Classical and Proneural'' subtype showed a smaller ellipse with fewer proteins being correlated to it and low to medium expression levels. Classical subtype showed low similarity with the ''Classical and Proneural*'' and the Mesenchymal in terms of protein content, but all three of them were linked with higher expression levels of their key proteins. Mesenchymal and ''Classical and Proneural*'' had a different protein profile with no crosslinks.

In Figure 23-B, the expression of the 49 proteins identified before is shown in a Biplot. The variables investigated were interpreted in terms of angles and PCA dimensions. Narrow angles reflected positively linked variables, in this case proteins that were usually co-expressed, like for example the GDP-mannose 4,6 dehydratase (GMDS gene) with Ras-related protein Rab-11A (RAB11A) or the Complement component C9 (CO9) with the Delta(3,5)-Delta(2,4)-dienoyl-CoA isomerase (ECH1).

Right angles represented variables that are expressed independently and were unrelated with each other, whilst obtuse angles represented negative relationships. In the last case, when one of the variables increased, the other one showed a reduction (one had high values and the other one low), such as Complement component C9 and ATPase plasma membrane Ca2+ transporting 1 (ATP2B1).

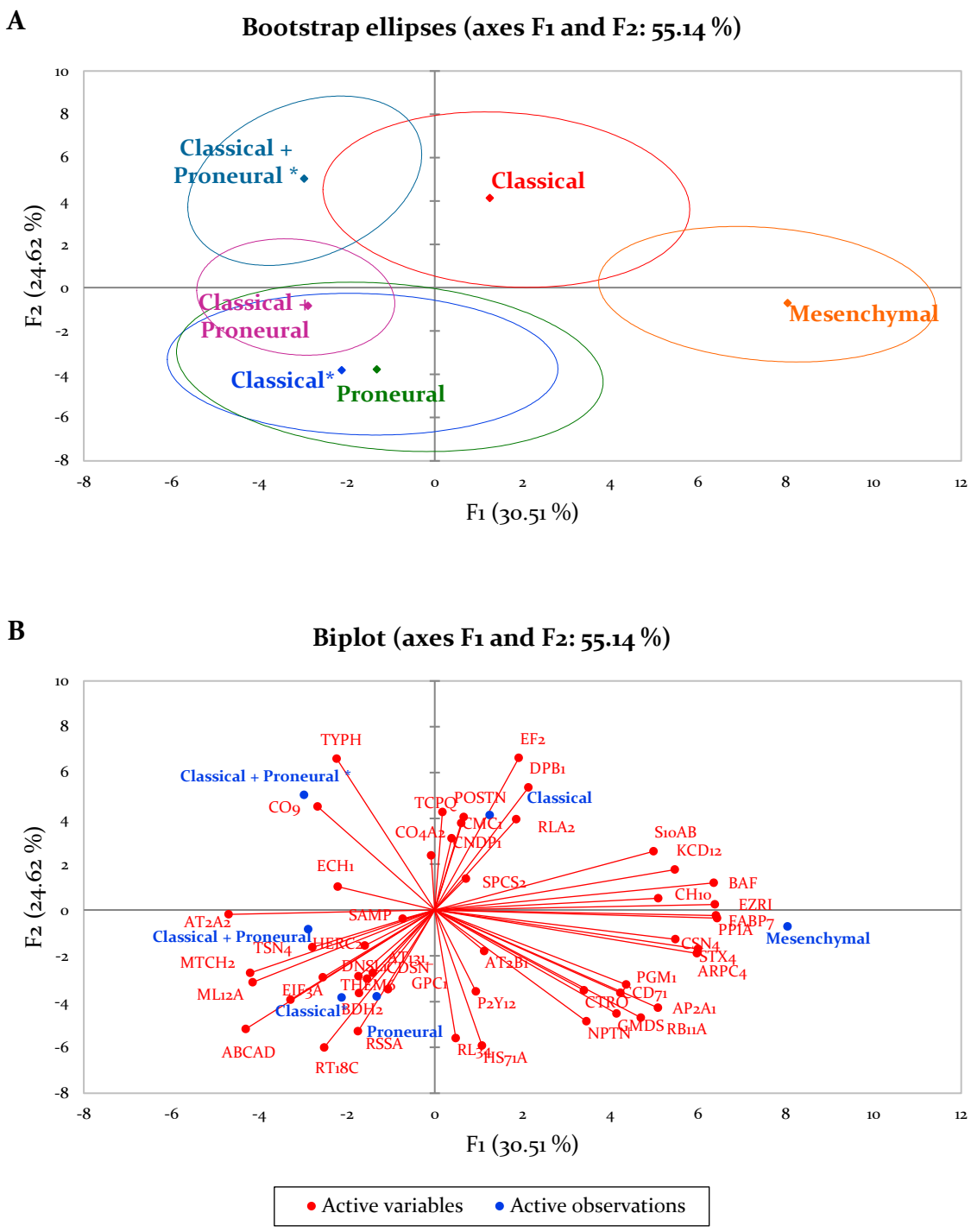

Figure 23. Comparison of the molecular subtypes within the tumour-derived EVs fraction based on the proteins expressed in each one of them.

A) The bootstrap ellipses show how the molecular subtypes overlap with each other, **(B)** the Biplot addresses the proteins that differentiate most amongst them.

The proteins can be represented by more than one categories. Analysis was performed by XLSTAT (ANOVA test, 95% Confidence score).

Trying to reduce the number of variables and identify specific proteins that could serve as new markers of subtype identification, the data was reanalysed using the 99% Confidence score (ANOVA), which was translated to a more limited amount of proteins. In this case, 9 proteins fitted into the confidence interval, as shown in Figure 24. Axes F1 and F2 of the bootstrap ellipses represented almost 65% of the initial data, which was higher than before. However, with fewer parameters taken into account, the subtype phenotype seemed more overlapped than before. The ''Classical and Proneural*'' subclass was more distinct in this case, characterized mainly by the high expression of the Complement component C9 and a lower co-expression of ECH1. Moreover, Classical and Classical* followed different patterns with the first one being the one correlated with 60S acidic ribosomal protein P2 (RPLP2) high expression and the latter one with low expression of ATP-binding cassette sub-family A member 13 (ABCA13), Mitochondrial carrier homolog 2 (MTCH2) and GDP-mannose 4,6 dehydratase (GMDS). The Mesenchymal, Proneural and ''Classical and Proneural'' subtypes had small differences in the co-expression profiles of ATP2B1, RAB11A, GMDS and Glypican-1 (GPC1).

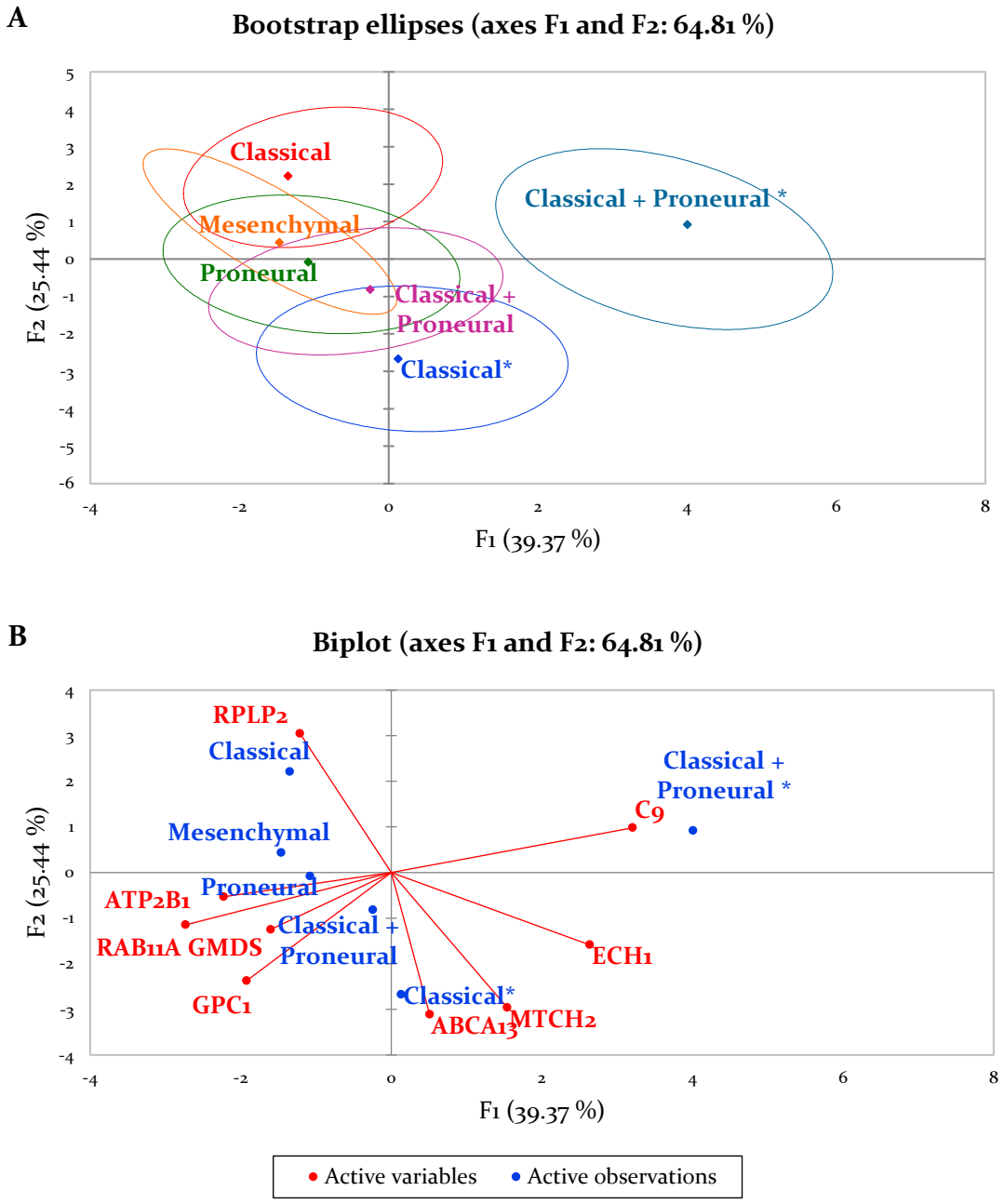

Figure 24. Comparison of the molecular subtypes within the extracellular vesicle fractions based on the proteins expressed in each one of them.

(A) The bootstrap ellipses show how the molecular subtypes overlap with each other, **(B)** the Biplot addresses the proteins that differentiate most amongst them.

The proteins can be represented by more than one categories. Analysis was performed by XLSTAT (ANOVA test, 99% Confidence score).

3.2.8 Comparison among Glioblastoma molecular subtypes based on Soluble protein fraction analysis

In the soluble protein fraction, molecular subtyping revealed no differences regarding the biological functions that are involved (Figure 25). From the proteins that were identified, the highest percentage had a biological function related to transportation with the mesenchymal subtype having a 32.64% of the proteins linked to that function. Fewer proteins had an implication in the signal transduction pathways and cellular growth and maintenance, especially when compared with the percentages given in the EVs fraction. Among the subclasses the ''Classical and Proneural*'' had the high percentages of 13.71% of the protein IDs related to processes transmitting extracellular signals to the cells and 11% participated in processes of cell growth. For the same biological function, the ''Classical and Proneural'' subtype had the lowest percentage of representative proteins with 12.5% being implicated in signal transduction and 9% in cell maintenance. Nevertheless, the differences were insignificant among the subtypes, since it was observed that almost the same amount of proteins was involved in the above-mentioned most representative biological functions.

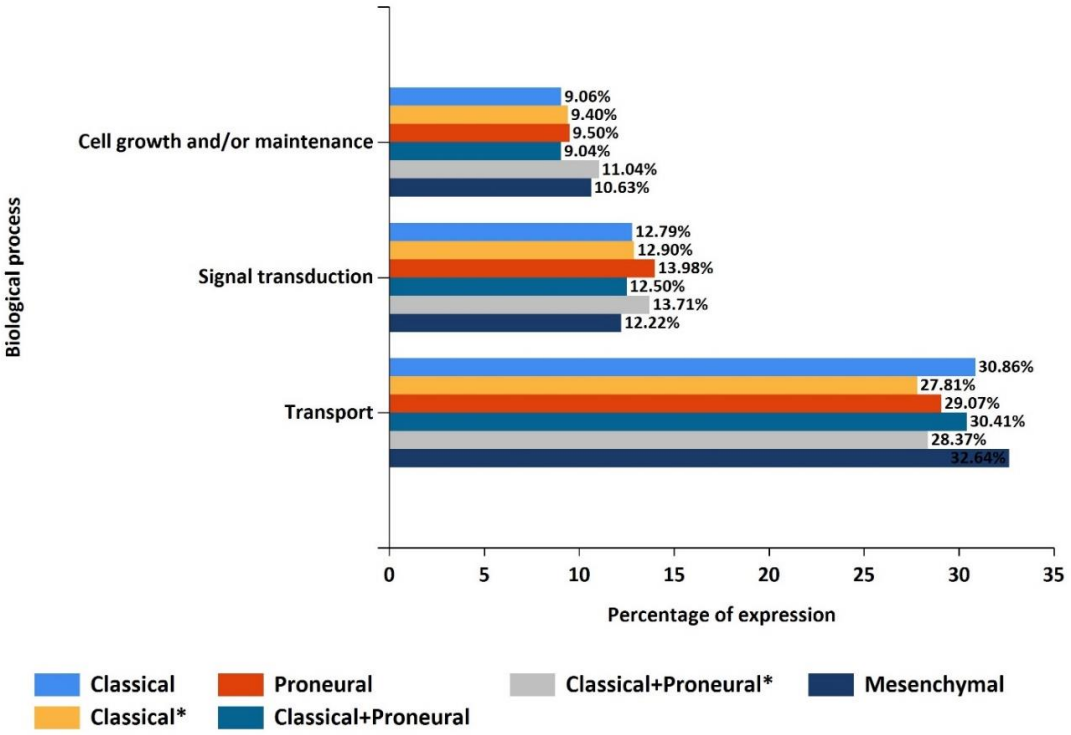

Figure 25. Comparison of the molecular subtypes based on biological functions of the soluble proteins detected.

The most representative biological processed that the proteins found in each molecular type are shown in the graph.

The analysis was performed by FunRich database. The graph was obtained by the same tool

3.2.9 Potential protein biomarker for molecular subtype identification in GBM based on secretome-derived soluble proteins analysis

The proteins identified in the soluble protein fraction of each tumour sample were categorised according to their molecular subtype and were normalised regarding their abundance. The average normalized abundancy of each protein in the each molecular subtype was calculated and analysed with the XLSTAT Software, in order to be assessed for trends/patterns that could serve for subtyping identification.

First, the proteins following the 99% Confidence score according to ANOVA were identified, which were 30 in total (Fig. 26A). These proteins were used for further analysis. Axes F1 and F2 represented the 84,14% of the initial information. Most of the subtypes showed overlaps, especially with the Proneural subclass, which had the broader ellipsis. The Mesenchymal subtype was distinct than the Classical* and the ''Classical and Proneural''. Furthermore, the ''Classical and Proneural*'' was characterised by different protein pattern than the Classical*.

The angles that the variables were interpreted were important and can be explained the same way as mentioned in Figure 25. As it is depicted in Figure 26B, the mesenchymal type was linked to low co-expression of 60S acidic ribosomal protein P2 (PLP2), Insulin-Like Growth Factor Binding Protein 2 (IBP2), Osteopontin (OSTP) and Y-box-binding proteins 1 and 2 (YBOX). The obtuse angles revealed that expression of the above proteins was negatively correlated with expression of Leucine aminopeptidase 2 (LAP2A), Lysosomal alpha-glucosidase (LYAG), 14-3-3 protein gamma (1433G), Prostaglandin-H2 D-isomerase (PTGDS), Transgelin (TAGL3), Creatine kinase (KCRU), Pyridoxal phosphate phosphatase (PPLP), Calcium/calmodulin-dependent protein kinase (KCC2A), Malate dehydrogenase (MDHC), 2-phospho-D-glycerate hydro-lyase (ENOG), Cathepsin D (CATD), Dihydropyridine receptor (DHPR), Neuronal growth regulator 1 (NEGR1), which were correlated with the Classical* subtype. ''Classical and Proneural'' subclass was linked to the signature proteins Bcl-2-associated X protein (BAX), Eukaryotic translation

initiation factor 3 subunit F (EIF3F) and Ras-related C3 botulinum toxin substrate 1 (RAC1). The Classical and the Proneural subtypes did not show any specific phenotype for protein-based subtype classification.

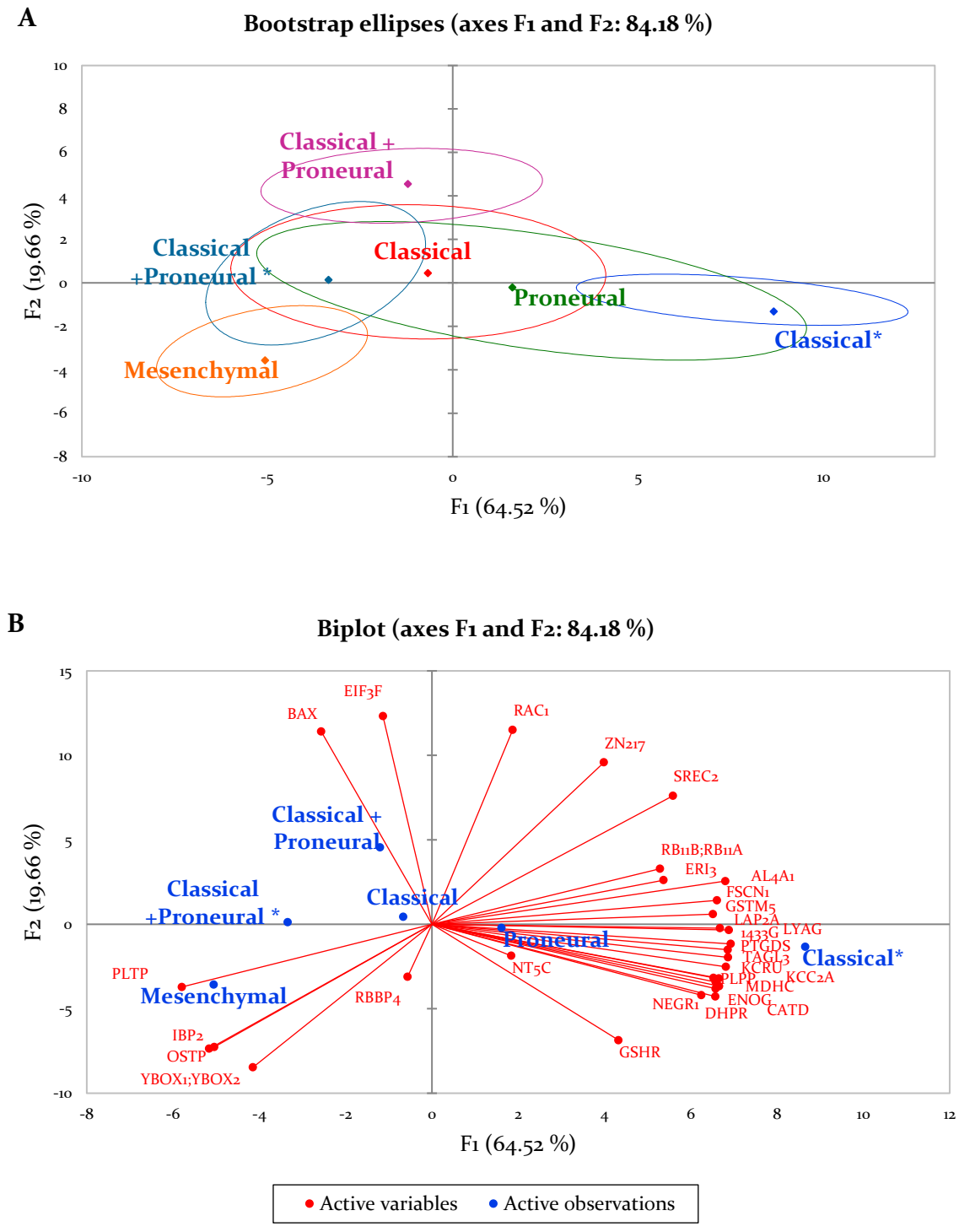

Figure 26. Comparison of the molecular subtypes within the soluble protein fractions based on the proteins expressed in each one of them.

(A) The bootstrap ellipses show how the molecular subtypes overlap with each other, **(B)** the Biplot addresses the proteins that differentiate most amongst them.

The proteins can be represented by more than one categories. Analysis was performed by XLSTAT (ANOVA test, 99% Confidence score).

The nine subtype-signature proteins in the GBM extracellular vesicle fractions were added on Functional Enrichment Analysis Tool and analysed based on the biological functions that were implicated. Some of the proteins were involved in more than one biological functions. A percentage of 33,3 was involved in cellular communication or signal transduction (Figure 27). These proteins were GPC1, RAB11A and MTCH2. The Complement component C9 was the only protein implicated in immune responses. RPLP2 was part of the protein metabolic pathways, GMDS and ECH1 were involved in energy pathways, whilst ABCA13 and ATP2B1 participated in transport process.

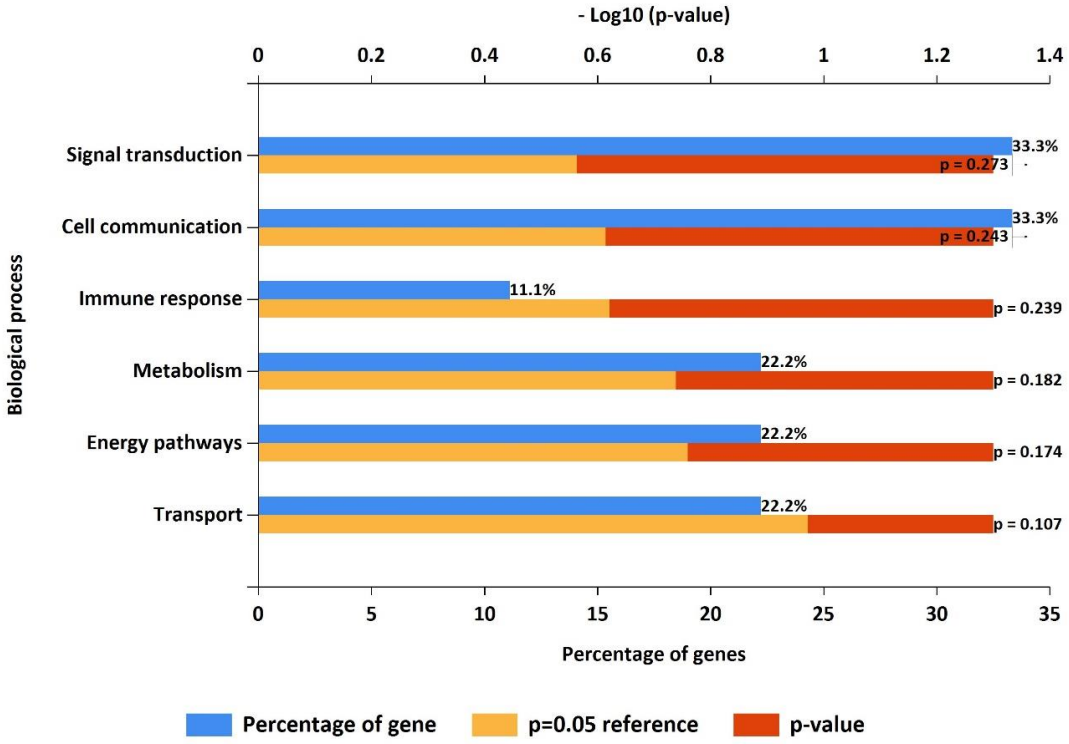

Figure 27. Most represented biological processes, in which the key proteins of the different molecular subtypes are implicated in tumour-derived EVs fraction.

The gene/protein list of potential subtype-biomarker was added on FunRich database and the proteins were categorised based on their functions. Proteins can be represented by more than one categories.

From the 30 soluble proteins named in this project as potential subtype-markers, the main biological processes that were part of were presented. Figure 28 shows that the majority of the proteins were involved in the energy pathways (38.7%, **, $p<0.001$) and metabolism (35.5%, **, $p<0.001$). Processes, such as nuclear organisation an biogenesis, regulation of the cell cycle and cell adhesion are represented by a much lower percentage of 3.2% of the total proteins in each case.

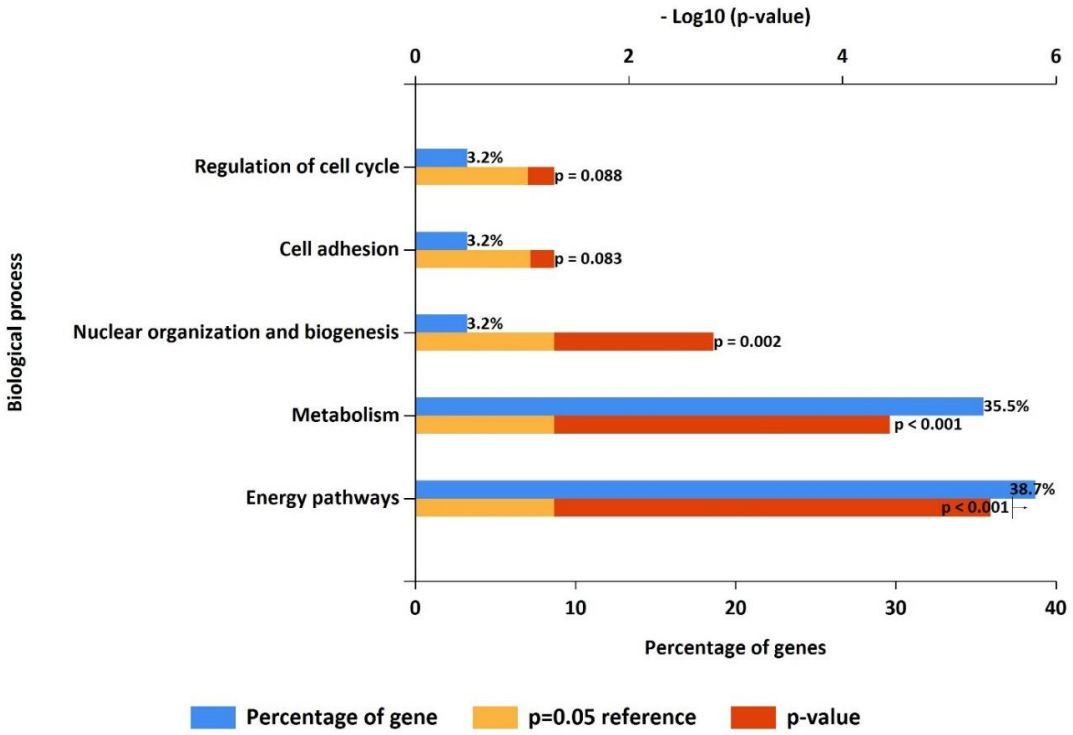

Figure 28. Most represented biological processes, in which the key proteins of the different molecular subtypes are implicated in GBM patients' soluble protein fraction.
The soluble proteins found to be linked with the GBM the molecular subtyping were analysed with FunRich for the biological functions that are implicated. Each protein can be represented by more than one categories.

3.3 Effect of Glioblastoma-derived Extracellular Vesicles and Soluble Proteins on T cells

Extracellular vesicles from Glioblastoma cell lines have been reported to suppress T cell anti-tumour responses through various mechanisms, some of the suggested are through expressing PD-L1 on their surface, or according to a more recent study through CD73 expression, which inhibits T cell expansion clones (Ricklefs et al., 2018; M. Wang et al., 2021). PD-L1 blockade has reversed T cell suppression to some extend and only in subtypes containing exosomes with high PD-L1 expression, such as the mesenchymal. In contrast, eliminating CD73-positive TDEVs showed to inhibit glioblastoma cell proliferation, but no T cell activity restoration was reported.

Several soluble proteins secreted in the GBM tumour microenvironment have, also, been suggested to favour cancer progression and immunosuppression via inhibiting T cell responses or preferentially promoting Treg expansion. Angiogenic VEGF is the most well-studied factor (Bourhis et al., 2021). Despite anti-VEGF therapy having been approved by FDA, the patients survival rate has not been improved (Yu & Quail, 2021). Moreover, cytokines, such as the immunosuppressive TGFβ have been extensively studied in GBM TME. However, TGFβ pathway targeting has not been clinically successful, due to failure to completely eliminate TGFβ production or high dose toxicity (Papachristodoulou et al., 2019).

Thus, there is an urgent need of other potential immunosuppressive mechanisms that EVs or soluble proteins utilise to suppress CD4+ T cells to be identified and attempted to be targeted alone or combined for therapeutic reasons.

The exact impact of the GBM tumours on T cell phenotype and secretion profile remains unclear. Thus, we generated a multi-parameter flow cytometry assay to assess the effects of EVs and proteins released in the secretome of GBM patients on T cell survival and several T cell markers utilising CD4+ T cell populations, which are the most suppressed cells in GBM, from

healthy donors and co-culturing them with tumour-derived EVs. Furthermore, our chosen immunosuppressive candidate were stratified to be tested for their effects on T cells accordingly.

3.3.1 Effect of EVs from GBM patients on T cell counts

GBM tumour microenvironment is highly immunosuppressive. Glioblastoma cells use a variety of mechanisms to evade the immune response. Extracellular vesicles in the TME can suppress the host anti-tumour immunity and promote a shift to pro-tumoural cell phenotypes (Maia et al., 2018).

In the current subchapter, the ability of tumour-derived extracellular vesicles to suppress human CD4+ T cells was tested. CD4+ T cells were isolated from whole blood of healthy donors, cultured at a density of 2.5 x 10^4 cells per well and stimulated with anti-CD3/CD28 coated beads at a ratio 1:2. Concentrated EVs from GBM patients were titrated over the T cells for 5 days. CD4+ T cells, were, also, seeded alone as a control sample. After harvesting the total cell amount, CD4+ cells were stained with anti-human CD4 antibody and analysis was implemented via flow cytometry. The cell counts are expressed as a percentage of the maximum response, which is observed, where T cells are cultured with stimulation beads alone.

Figure 29 showed suppression on CD4+ T cell response in a dose-dependent manner with the maximal inhibition shown after exposure to the Full dose of EVs. This can be either a result of T cell apoptosis or lack of proliferation. The cell counts are expressed as a percentage of the maximum response, which is observed, where T cells are cultured with stimulation beads alone. Figure 29C shows how the lymphocyte gate changes along the EVs addition with 76.4% of the initial cells being gated as lymphocytes to gradually shifting to 65.7%.

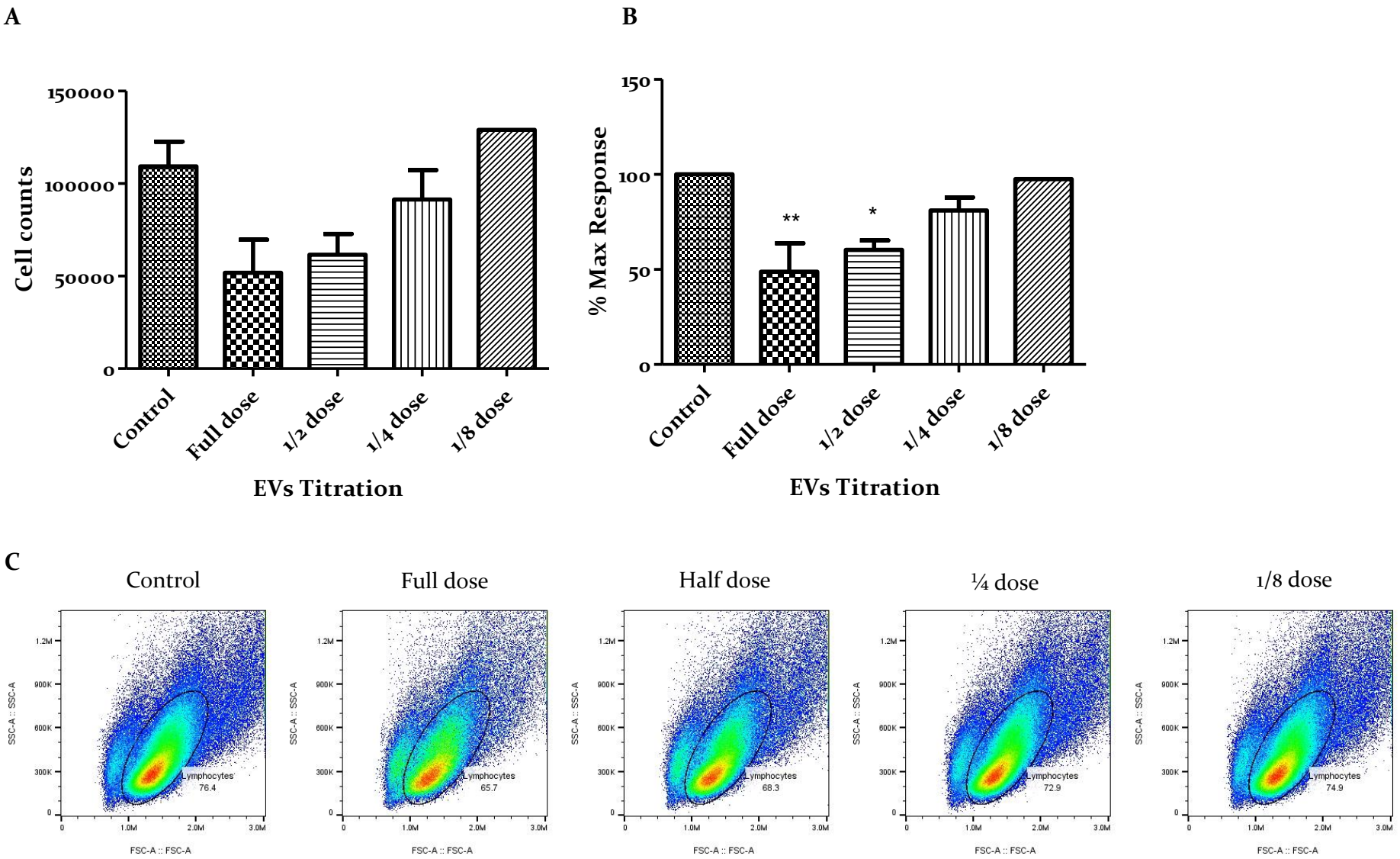
A
150000
100000
50000
0
Cell counts
Control
Full dose
1/2 dose
1/4 dose
1/8 dose
EVs Titration
B
150
100
50
0
% Max Response
**
*
Control
Full dose
1/2 dose
1/4 dose
1/8 dose
EVs Titration
C
Control
Full dose
Half dose
¼ dose
1/8 dose
SSC-A :: SSC-A
FSC-A :: FSC-A
Lymphocytes
76.4
65.7
68.3
72.9
74.9

D

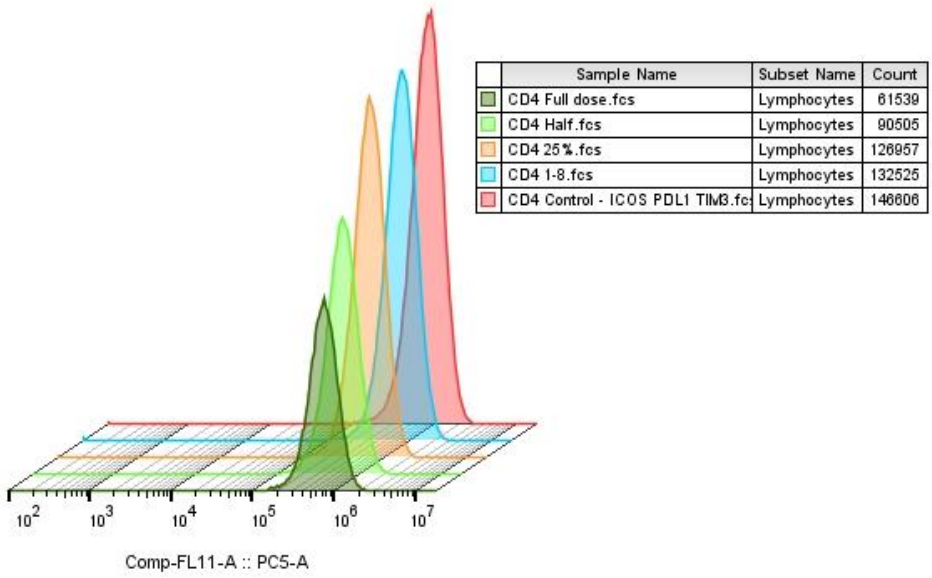

Figure 29. Concentrated tumour extracellular vesicles affect CD4+ T cell viability in high concentrations.

2.5 x 10^4 CD4+ T cells were cultured with 5x10^4 CD3/CD28 Human T-activator Dynabeads alone or in the presence of indicated tumour EVs ratios. After 5 days cells were harvested and stained for surface CD4 antibody. **(A)** Cell viability is shown using the total number of cells **(B)** Cell viability is presented as a percentage of the control in response to different concentrations after treatment with concentrated GBM patients' EVs. **(C)** Representative dot plots and **(D)** stagger plot show the cells detected by the flow cytometer and the lymphocyte gate, when cultured alone (first panel), or in the presence of decreasing concentrations of tumour EVs. The results are representative of 5 experiments (N=5). Bars represent means and SEM is shown .*, p = <0.05, **, p = <0.01.

3.3.2 Effect of GBM EVs on T cell surface markers

Extracellular vesicles suppress T cell proliferation, as observed in before (3.3.1). In order to understand the way EVs regulate the T cell responses, a deeper insight into T cell exhaustion and activation status and cytokine secretion profile was aimed. GBM cells have been reported to increase the expression of immune checkpoint inhibitors, such as PD-1 and TIM-3, on the surface of infiltrating T cells, but it is unclear if this effect was caused by EV release. In the current chapter, the CD4+ T cells were characterised for the expression of inhibitory and stimulatory immune checkpoints, such as the cell surface markers of exhaustion TIM-3 and PD-1 and the ICOS marker of activation, upon treatment with GBM patient- derived extracellular vesicles.

In optimising a multi-parameter panel for flow cytometry, first we confirmed efficient cell staining with individual surface markers. Therefore, CD4+ T cells, sorted from peripheral blood of healthy human donors, were cultured with CD3/CD28 Dynabeads for 5 days. Then, the total cell volume was harvested, stained for CD4 and compared with samples stained for CD4 combined with any of the PD-1, TIM-3 or ICOS each time. As displayed in Figure 30, when TIM-3 was added, 28% of the CD4+ population shifted to CD4+TIM3+ profile. Accordingly, almost half of the isolated CD4+ T cells expressed PD-1, whilst 31% of them expressed ICOS.

To test the effect of EVs on the expression of specific cell surface markers, CD4+ T cells were sorted and cultured alone with CD3/CD28 activation Dynabeads or treated with ascending doses of isolated extracellular vesicles for 5 days. After harvesting, the cells were stained with CD4, TIM-3, PD-1 and ICOS antibodies and analysed with flow cytometry.

Exposure of isolated CD4+ T cells to higher doses of tumour-derived extracellular vesicles resulted in a smaller amount of cells expressing the exhaustion marker TIM-3.

Accordingly, PD-1 expression was analysed on CD4+ T cells and it was found that fewer cells express the exhaustion marker after treatment with high doses of EVs. Interestingly, though, when examining the mean fluorescence intensity, it was revealed that although the cells were fewer, MFI levels of PD-1 were higher.

Treatment with glioblastoma EVs resulted in a decrease in the number of T cells expressing ICOS, but exposure to high doses of EVs showed that the percentage of ICOS+ve cells was increased, when compared to the total amount of cells present in each condition. Approximately 31% of the CD4+ T cells in the control group express ICOS, after treatment with the Full dose of EVs (Figure 31-C.i.), whilst the percentage of the MFI reported was elevated by almost 50%. This could indicate that ICOS had higher expression on a per cell basis after EV treatment (Figure 31- C.ii).

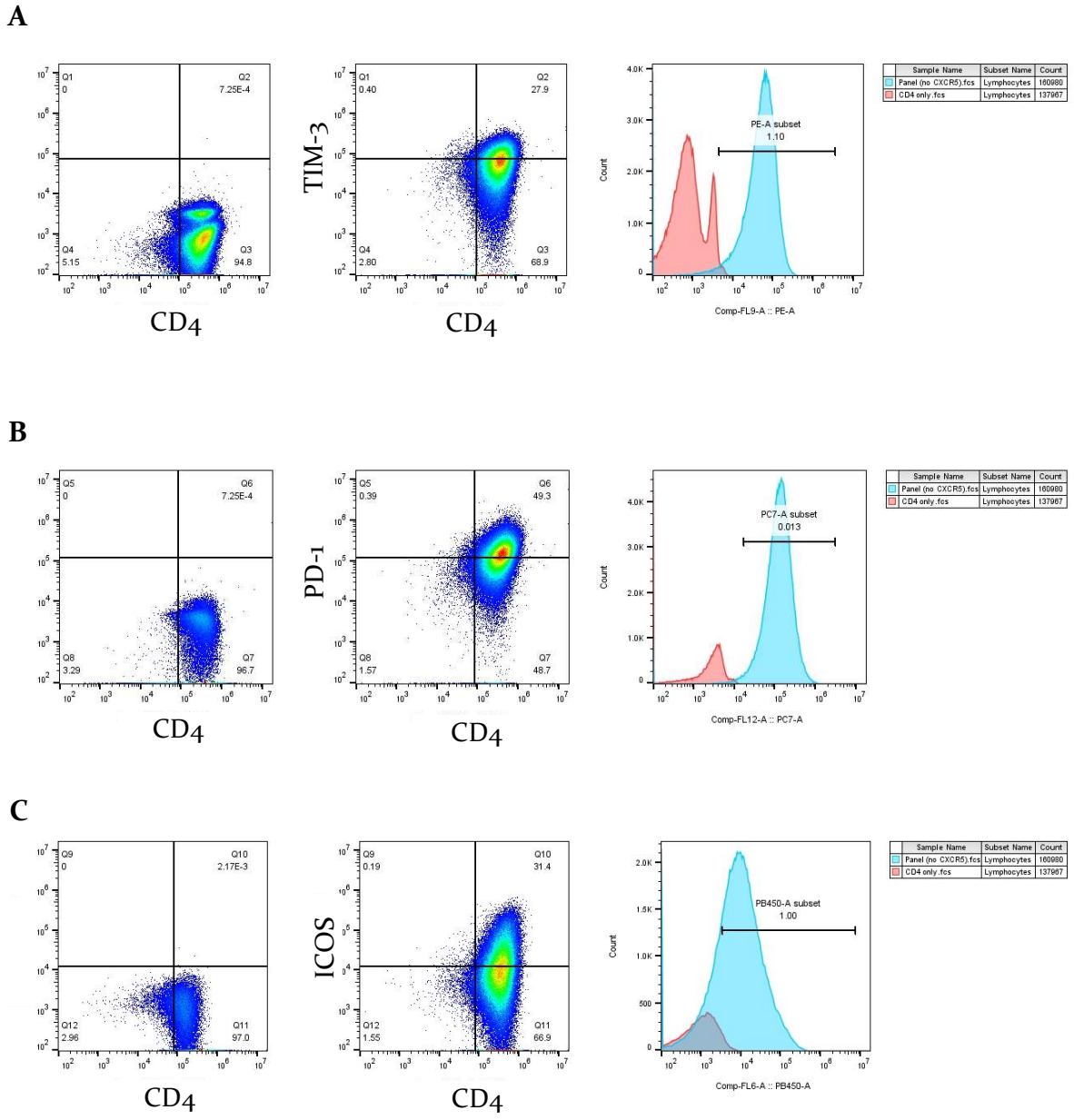

Figure 30. T cell staining for cell surface markers.

Isolated T cells were cultured for 5 days and then stained with anti-human CD4 alone (left panels) or in the presence of surface markers (A) TIM-3, (B) PD-1, (C) ICOS (middle panels). Representative histograms show the shift towards positive populations in all cases right panels). Cells were isolated from peripheral blood of a human healthy donor and analysed by flow cytometry.

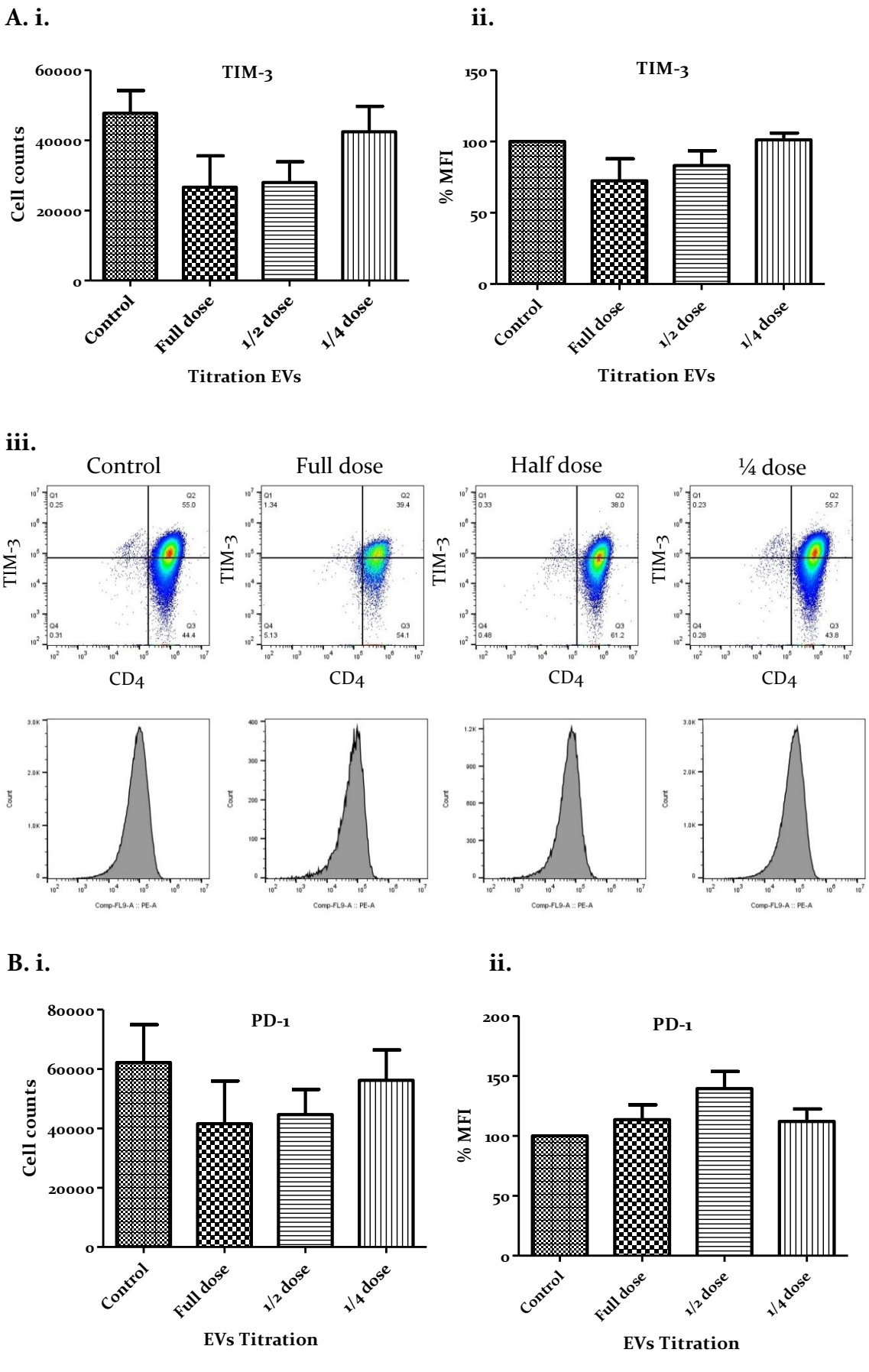
A. i.
TIM-3
Cell counts
60000
40000
20000
0
Control
Full dose
1/2 dose
1/4 dose
Titration EVs
ii.
TIM-3
% MFI
150
100
50
0
Control
Full dose
1/2 dose
1/4 dose
Titration EVs
iii.
Control
Full dose
Half dose
¼ dose
TIM-3
CD4
Q1 0.25
Q2 55.0
Q4 0.31
Q3 44.4
Q1 1.34
Q2 39.4
Q4 5.13
Q3 54.1
Q1 0.33
Q2 38.0
Q4 0.48
Q3 61.2
Q1 0.23
Q2 55.7
Q4 0.28
Q3 43.8
Count
Comp-FL9-A :: PE-A
B. i.
PD-1
Cell counts
80000
60000
40000
20000
0
Control
Full dose
1/2 dose
1/4 dose
EVs Titration
ii.
PD-1
% MFI
200
150
100
50
0
Control
Full dose
1/2 dose
1/4 dose
EVs Titration

iii.

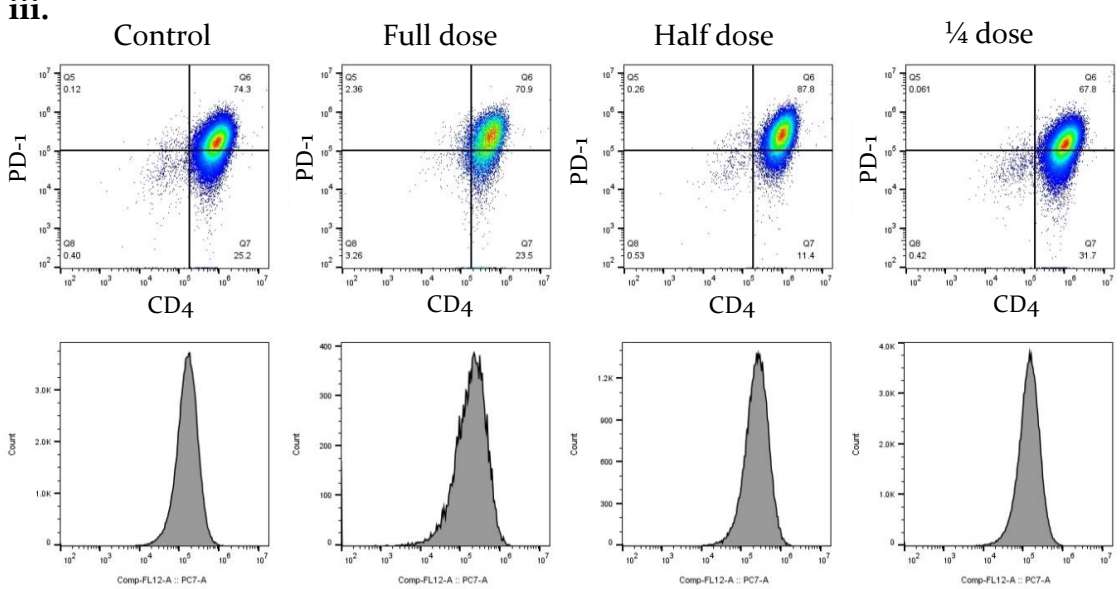
Control
Full dose
Half dose
¼ dose
PD-1
CD4
Q5 0.12
Q6 74.3
Q8 0.40
Q7 25.2
Q5 2.36
Q6 70.9
Q8 3.26
Q7 23.5
Q5 0.26
Q6 87.8
Q8 0.53
Q7 11.4
Q5 0.061
Q6 67.8
Q8 0.42
Q7 31.7
Count
Comp-FL12-A :: PC7-A

C. i.

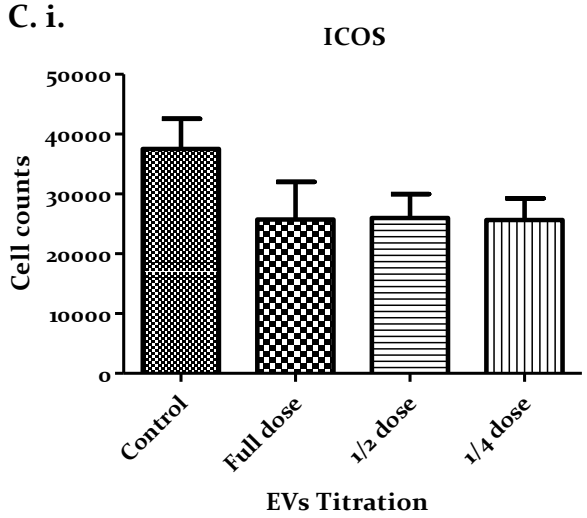
ICOS
Cell counts
50000
40000
30000
20000
10000
0
Control
Full dose
1/2 dose
1/4 dose
EVs Titration

ii.

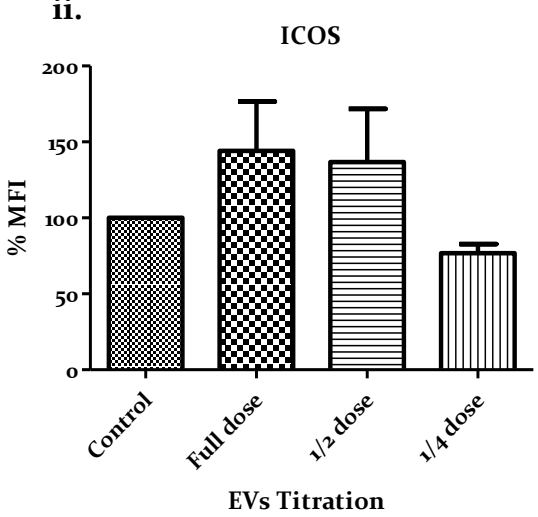
ICOS
% MFI
200
150
100
50
0
Control
Full dose
1/2 dose
1/4 dose
EVs Titration

iii.

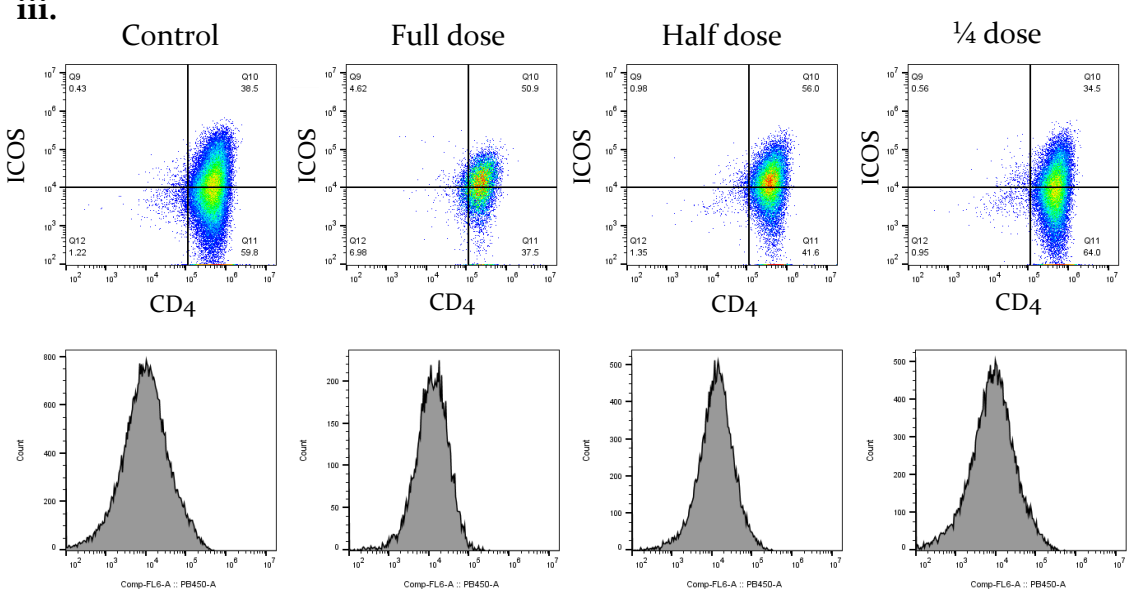

Figure 31. Cell surface markers expression in response to decreasing concentrations of tumour EVs.

CD4+ isolated T cells from peripheral blood of healthy human donor were cultured with 5 x 10^4 CD3/CD28 Human T-activator Dynabeads alone or in the presence of EVs in indicated ratios. After 5 days cells were stained for surface CD4 and (A) TIM-3, (B) PD-1, or (C) ICOS antibodies. A.i.-C.i. Graphs show the number of cells expressing the markers in each condition, while A.ii-C.ii graphs show the Maximum Fluorescence Intensity of each marker as a percentage relative to the control, where no concentrated EVs were added on the cells.

A.iii.-C.iii Representative dot plots show the expression of each cell surface marker by CD4+ T cells, when cultured alone (first panel), or in the presence of the tumour EVs.

Data is representative of 5 experiments (n=5). Bars represent means and SEM is shown. *, p = <0.05, **, p = <0.01.

3.3.3 Effect of the Glioblastoma –derived EVs on the cytokine output of T cells

The cytokine secretion profile of immune cells can be dramatically altered resulting into a more favourable microenvironment for the tumour progression. Here, the expression of signature cytokines for different CD4+ T cell subsets was studied, in order to assess whether extracellular vesicles derived from patient samples are able of skewing the cytokine milieu towards immunosuppression.

Intracellular cytokine staining was validated by using CD4+ unstained cells as a control opposed to single-cytokine CD4+ cells. Following cell stimulation, a percentage of 46% CD4+ T cells was shown to be TGFβ+ve (Fig. 32-A). CD4+ isolated cells were also producing the pro-inflammatory cytokines TNFα (53.6%) and IFNγ (31.1%) (Fig. 33B-C), whilst low levels of IL-21, IL-13 and IL-17 were, also, efficiently detected (Fig. 32D-F).

A

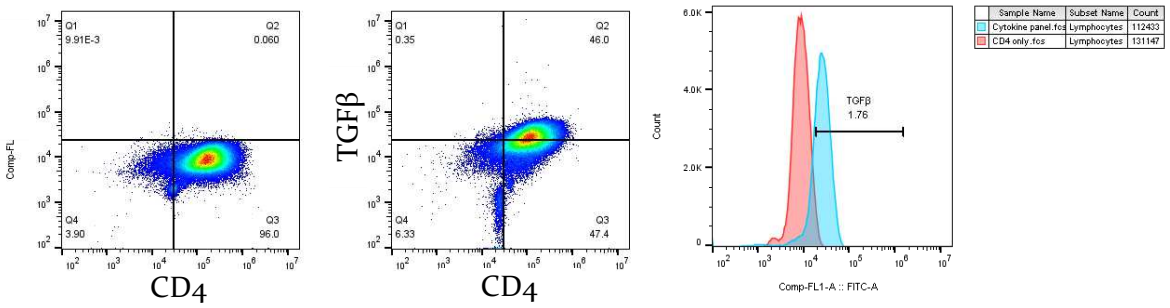
Q1
9.91E-3
Q2
0.060
Q4
3.90
Q3
96.0
Comp-FL
CD4
Q1
0.35
Q2
46.0
Q4
6.33
Q3
47.4
TGFβ
CD4
TGFβ
1.76
Count
Comp-FL1-A :: FITC-A
Sample Name
Subset Name
Count
Cytokine panel.fcs
Lymphocytes
112433
CD4 only.fcs
Lymphocytes
131147

B

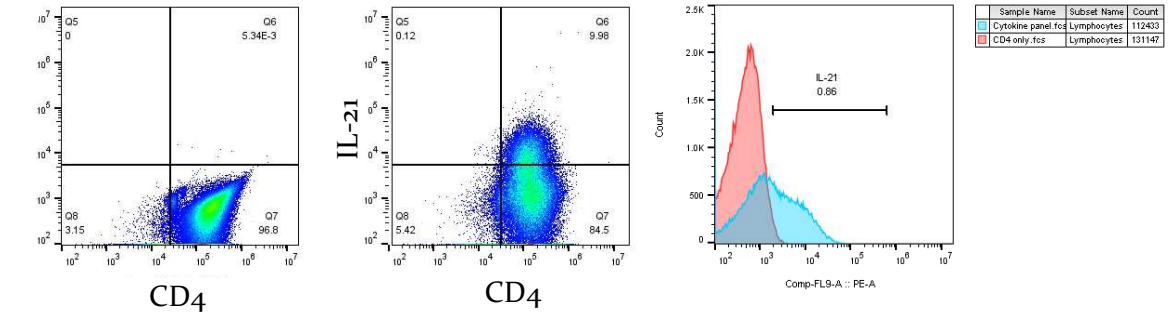
Q5
0
Q6
5.34E-3
Q8
3.15
Q7
96.8
CD4
Q5
0.12
Q6
9.98
Q8
5.42
Q7
84.5
IL-21
CD4
IL-21
0.86
Count
Comp-FL9-A :: PE-A
Sample Name
Subset Name
Count
Cytokine panel.fcs
Lymphocytes
112433
CD4 only.fcs
Lymphocytes
131147

C

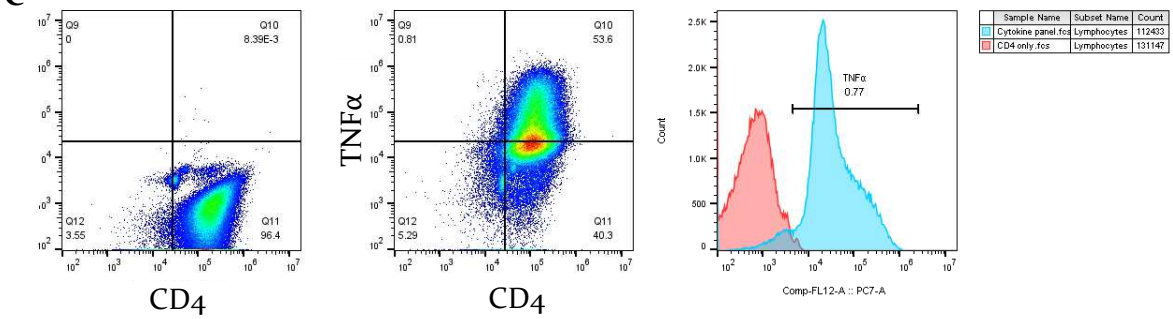
Q9
0
Q10
8.39E-3
Q12
3.55
Q11
96.4
CD4
Q9
0.81
Q10
53.6
Q12
5.29
Q11
40.3
TNFα
CD4
TNFα
0.77
Count
Comp-FL12-A :: PC7-A
Sample Name
Subset Name
Count
Cytokine panel.fcs
Lymphocytes
112433
CD4 only.fcs
Lymphocytes
131147

D

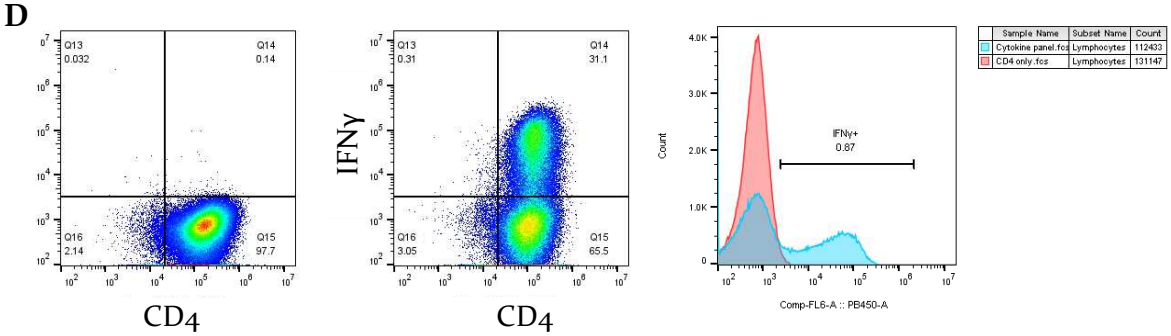
Q13
0.032
Q14
0.14
Q16
2.14
Q15
97.7
CD4
Q13
0.31
Q14
31.1
Q16
3.05
Q15
65.5
IFNγ
CD4
IFNγ+
0.87
Count
Comp-FL6-A :: PB450-A
Sample Name
Subset Name
Count
Cytokine panel.fcs
Lymphocytes
112433
CD4 only.fcs
Lymphocytes
131147

E

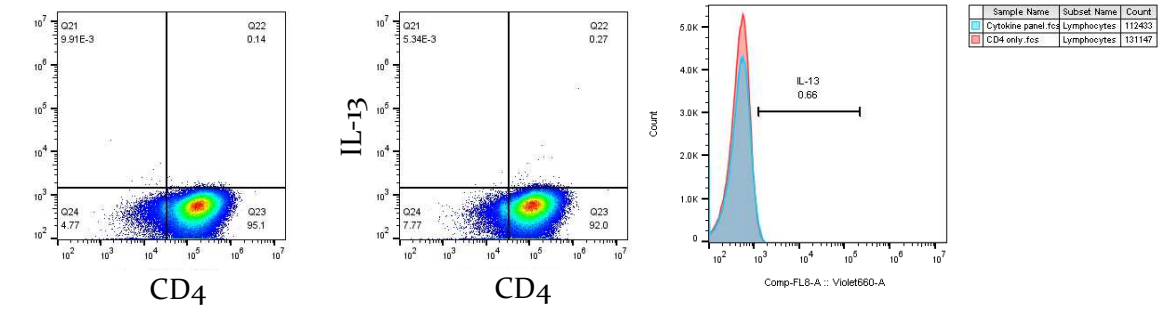

F

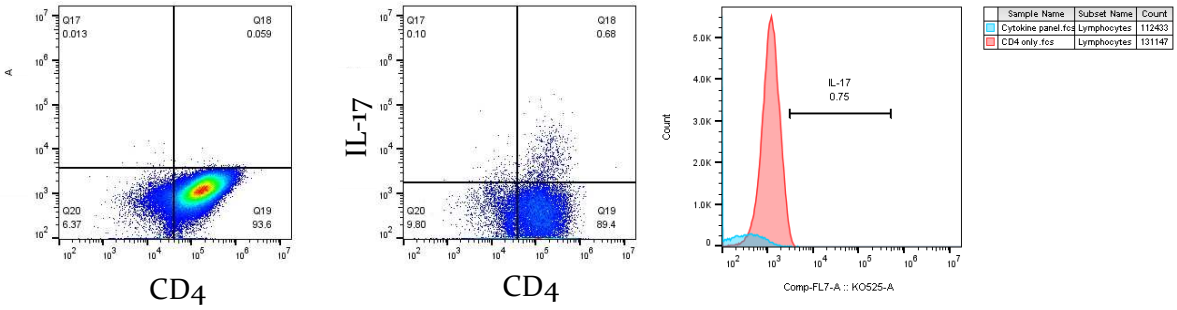

Figure 32. T cell staining for intracellular cytokines.

Isolated T cells seeded for 5 days and following re-stimulation, they were stained with anti-human CD4 antibody alone (left panels) or in the presence of (A) TGFβ, (B) IL-21, (C) TNFα, (D) IFNγ, (E) IL-13 or (F) IL-17 (middle panels). Representative histograms show the shift towards positive populations in all cases right panels).

Cells were isolated from peripheral blood of a human healthy donor and analysed by flow cytometry.

Isolated by gradient centrifugation from peripheral human blood, CD4+ cells were cultured with CD3/CD28 Dynabeads alone or over different EVs concentration for 4 days. Then, the cells were re-stimulated using a PMA-Ionomycin based cocktail to produce cytokines. After 2 hours, Brefeldin A was used, before overnight incubation. The next day, the total amount of cells was harvested and after fixing and permeabilising them, the cells were stained for CD4 and the main intracellular cytokines of different immune cells, TGFβ, TNFα, IFNγ, IL-21, IL-13, IL-17 and analysed with flow cytometry.

Induced expression of TGFβ in CD4+ conventional cells transforms them into regulatory T cell phenotype with immunosuppressive capacity. CD4+ T cells counts expressing TGFβ were almost 50% fewer in the Full EV dose in comparison to the control CD4+ T cells that received no treatment. However, from the MFI graph we see that the total amount of TGFβ secreted remained almost the same as the control group among treatment with different EV doses (Figure 33-A.ii).

The same pattern was followed in the expression levels of IL-21 and TNFα with fewer cells secreting the cytokines as a result to ascending concentrations of GBM EVs addition to the culture, but with the T cells producing almost the same percentage of cytokines as the control group, where no EVs were added (Fig. 33B-C). IFNγ, IL-17 and IL-13 secretion was impaired upon exposure to high doses of extracellular vesicles (Fig. 33D-F). An interesting observation was that when 25% of the EV Full dose was added on CD4+ T cells, the amount of secreted cytokines was slightly boosted.

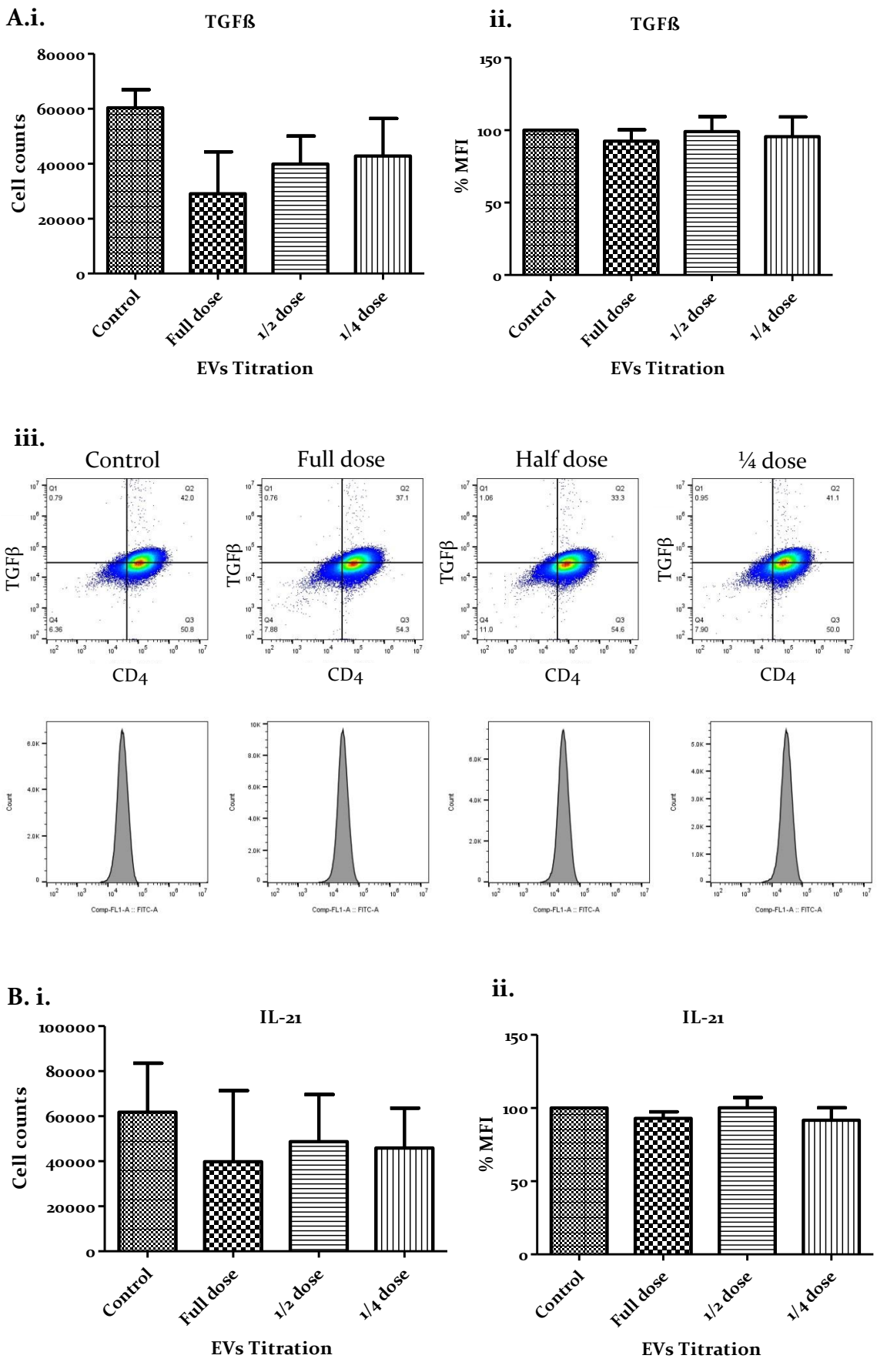
A.i.
TGFß
Cell counts
80000
60000
40000
20000
0
Control
Full dose
1/2 dose
1/4 dose
EVs Titration
ii.
TGFß
% MFI
150
100
50
0
Control
Full dose
1/2 dose
1/4 dose
EVs Titration
iii.
Control
Full dose
Half dose
¼ dose
TGFβ
CD4
Q1 0.79
Q2 42.0
Q4 6.36
Q3 50.8
Q1 0.76
Q2 37.1
Q4 7.88
Q3 54.3
Q1 1.06
Q2 33.3
Q4 11.0
Q3 54.6
Q1 0.95
Q2 41.1
Q4 7.90
Q3 50.0
Count
Comp-FL1-A :: FITC-A
B. i.
IL-21
Cell counts
100000
80000
60000
40000
20000
0
Control
Full dose
1/2 dose
1/4 dose
EVs Titration
ii.
IL-21
% MFI
150
100
50
0
Control
Full dose
1/2 dose
1/4 dose
EVs Titration

iii.

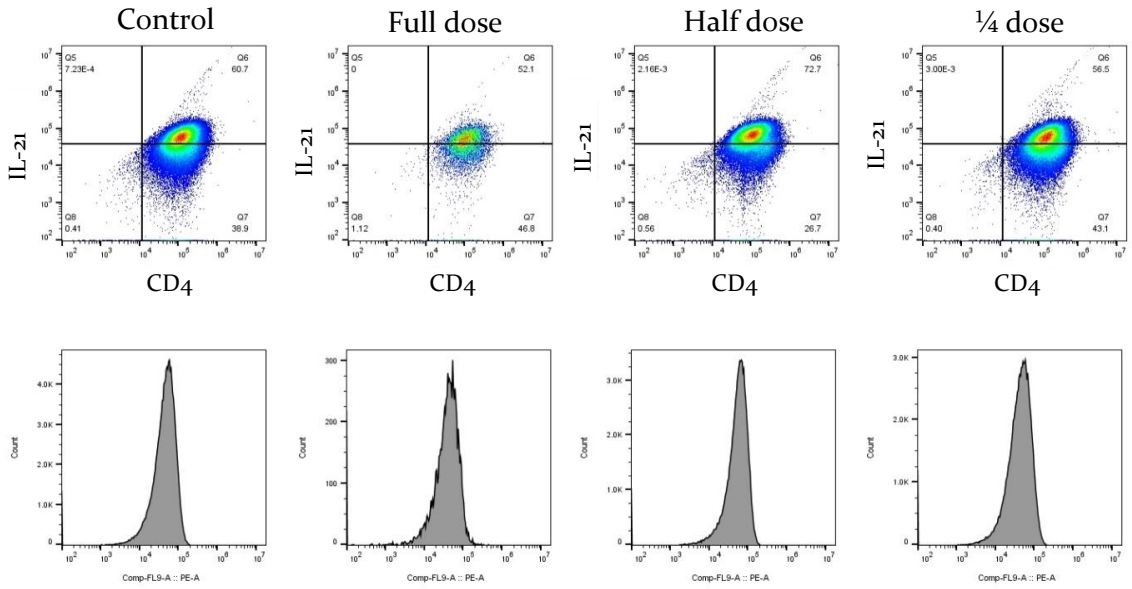
Control
Full dose
Half dose
¼ dose
IL-21
CD4
Count
Comp-FL9-A :: PE-A

C. i.

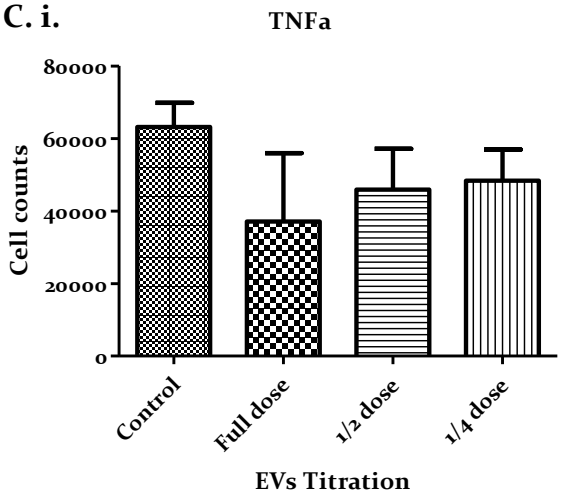
TNFa
Cell counts
80000
60000
40000
20000
0
Control
Full dose
1/2 dose
1/4 dose
EVs Titration

ii.

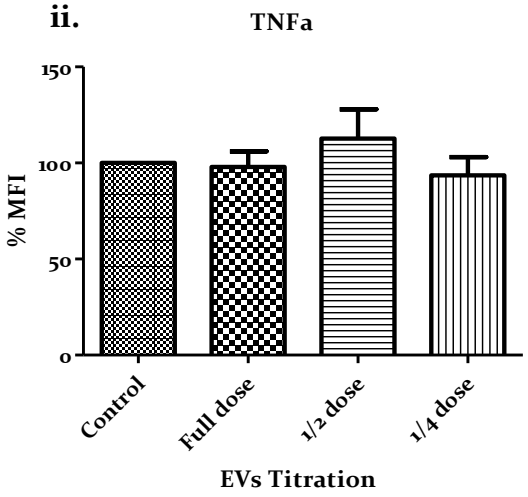
TNFa
% MFI
150
100
50
0
Control
Full dose
1/2 dose
1/4 dose
EVs Titration

iii.

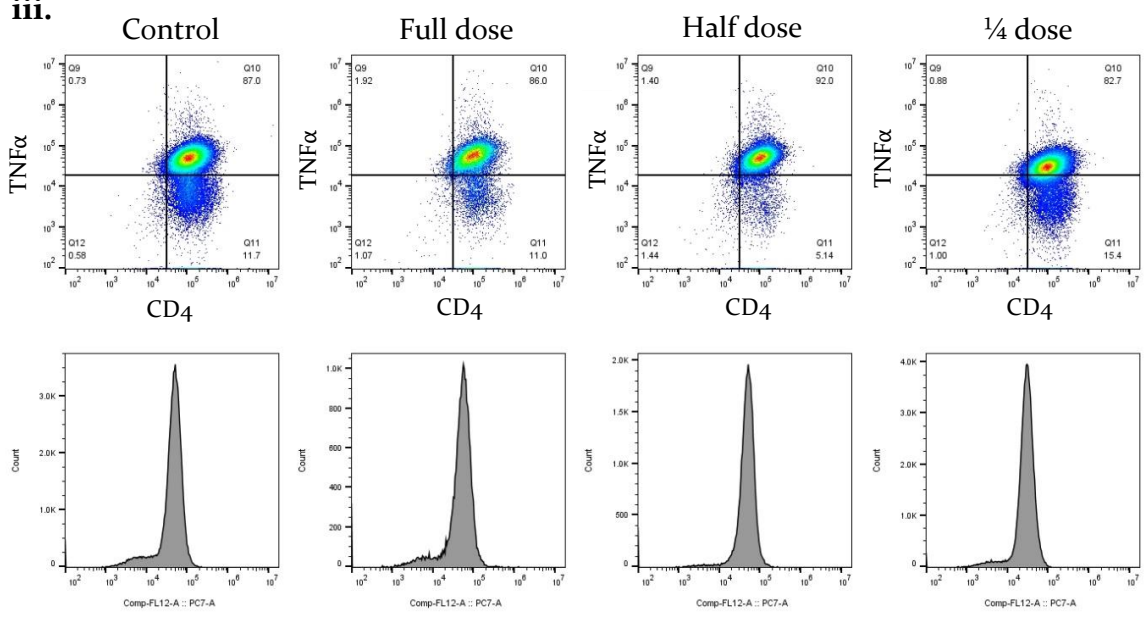
Control
Full dose
Half dose
¼ dose
TNFα
CD4
Count
Comp-FL12-A :: PC7-A

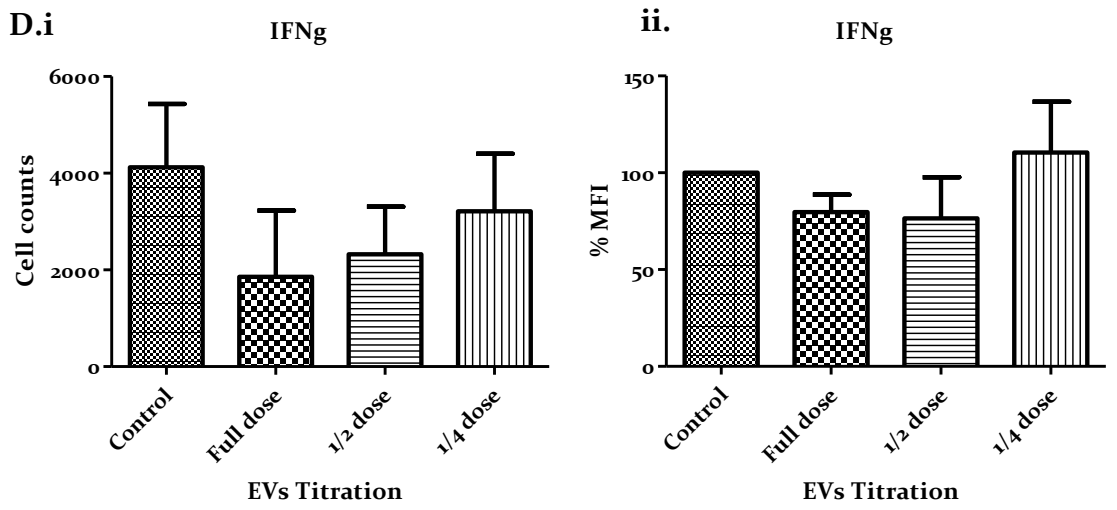
D.i
IFNg
Cell counts
6000
4000
2000
0
Control
Full dose
1/2 dose
1/4 dose
EVs Titration
ii.
IFNg
% MFI
150
100
50
0
Control
Full dose
1/2 dose
1/4 dose
EVs Titration

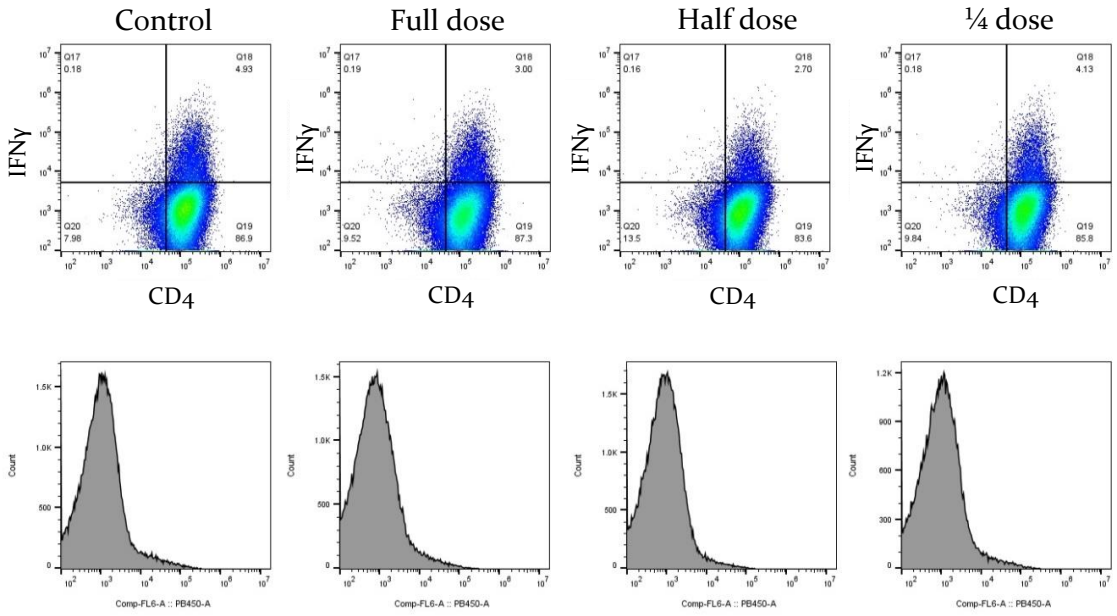
iii.
Control
Full dose
Half dose
¼ dose
IFNγ
CD4
Q17 0.18
Q18 4.93
Q20 7.98
Q19 86.9
Q17 0.19
Q18 3.00
Q20 9.52
Q19 87.3
Q17 0.16
Q18 2.70
Q20 13.5
Q19 83.6
Q17 0.18
Q18 4.13
Q20 9.84
Q19 85.8
Count
Comp-FL6-A :: PB450-A

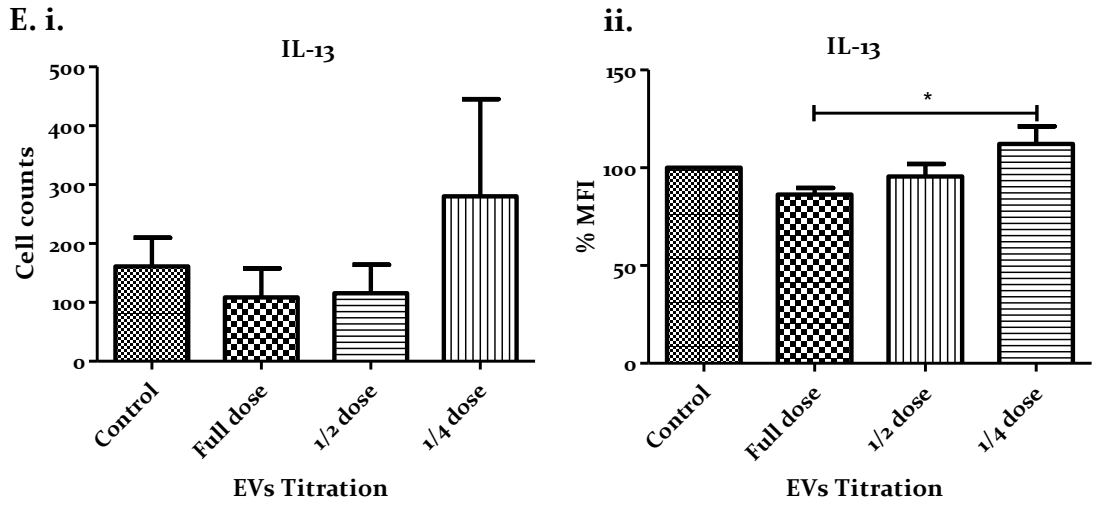
E. i.
IL-13
Cell counts
500
400
300
200
100
0
Control
Full dose
1/2 dose
1/4 dose
EVs Titration
ii.
IL-13
% MFI
150
100
50
0
*
Control
Full dose
1/2 dose
1/4 dose
EVs Titration

iii.

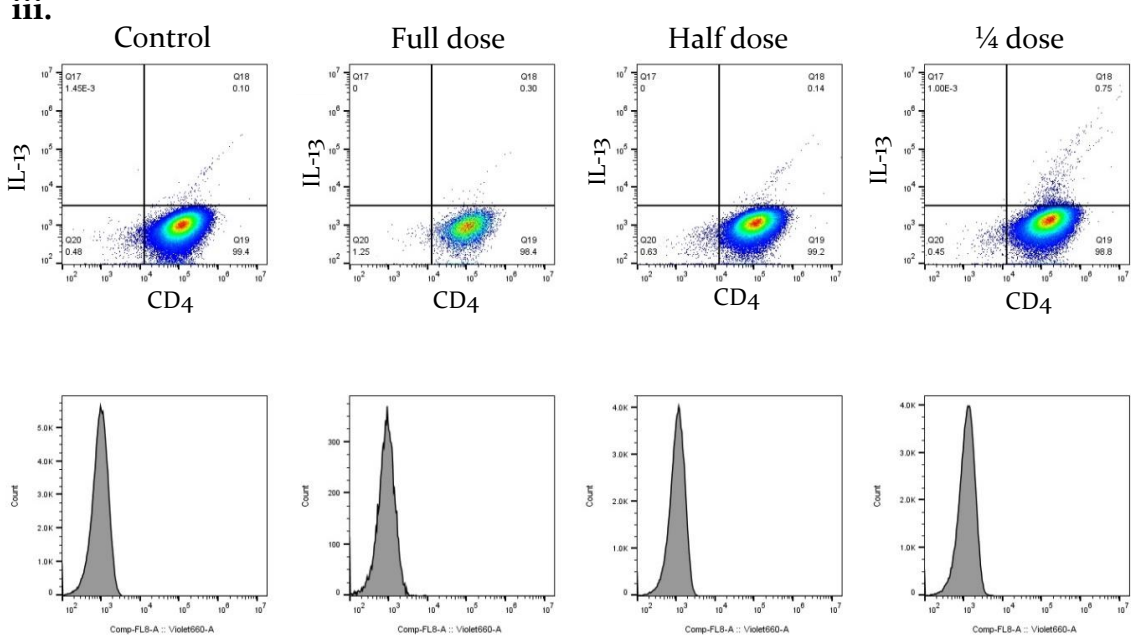
Control
Full dose
Half dose
¼ dose
IL-13
CD4
Q17
1.45E-3
Q18
0.10
Q20
0.48
Q19
99.4
Q17
0
Q18
0.30
Q20
1.25
Q19
98.4
Q17
0
Q18
0.14
Q20
0.63
Q19
99.2
Q17
1.00E-3
Q18
0.75
Q20
0.45
Q19
98.8
Count
Comp-FL8-A :: Violet660-A

F. i.

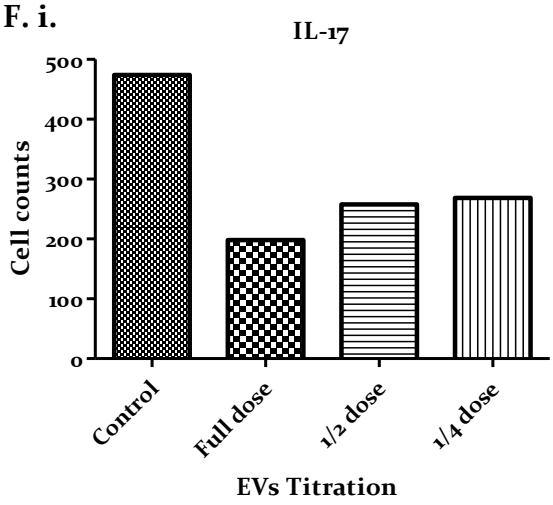
IL-17
Cell counts
500
400
300
200
100
0
Control
Full dose
1/2 dose
1/4 dose
EVs Titration

ii.

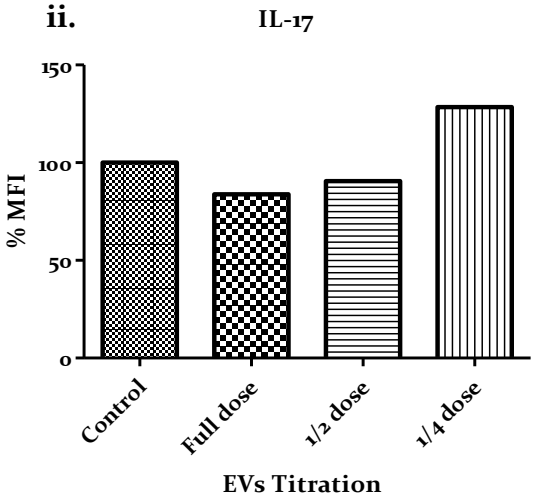
IL-17
% MFI
150
100
50
0
Control
Full dose
1/2 dose
1/4 dose
EVs Titration

iii.

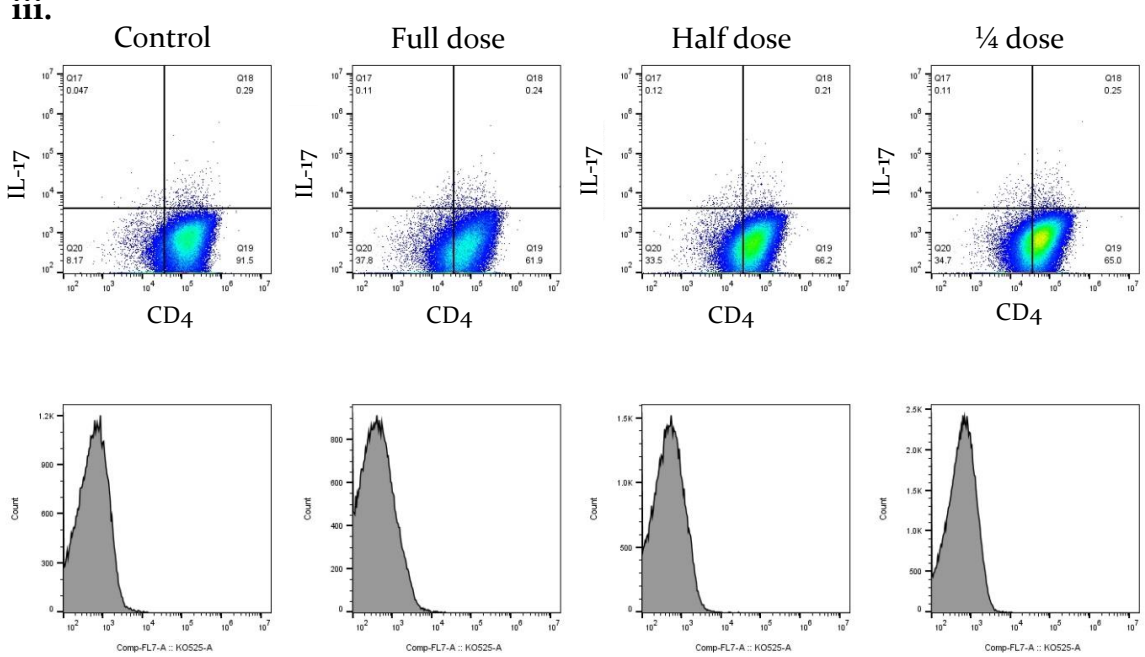

Figure 33. Production of cytokines in response to indicated concentrations of tumour EVs.

2.5x10⁴ CD4+ T cells were seeded with 5x10⁴ CD3/CD28 Human T-activator Dynabeads alone or in the presence of EVs titration. After 5 days cells were restimulated and stained for intracellular (A) TGFβ, (B) IL-21, (C) TNFα, (D) IFNγ, (E) IL-17 or (F) IL-13 with the surface CD4 antibody.

A.i.-F.i Graphs show the change in the number of cells expressing each marker in each condition.

A.ii-F.ii graphs show the MFI as a percentage relative to the control condition with no EVs from the tumour.

A.iii.-F.iii Representative dot plots show the expression of each cytokine by CD4+ T cells in different GBM EVs concentrations.

Data, and SEM is shown for 5 experiments. *, p = <0.05, **, p = <0.01.

3.3.4 Effect of the tumour-derived EVs on T cell transcription factors expression

The CD4+ T cells were, also, tested for transcription factors, because these master regulators can be major indicators of the T cell phenotype and identity (Vahedi et al., 2013). CD4+ T cells were cultured alone or treated with Full dose, Half dose and ¼ dose of EVs and incubated for 5 days. Then, the total amount of cells was harvested, fixed and permeabilised. Next, the cells were stained for CD4 and GATA-3, RoRγT, Bcl-6, T-bet and FoxP3 antibodies and were analysed by flow cytometric assay.

GATA-3 is the master regulator of the anti-inflammatory Th2 cells and did not show any significant difference in the expression levels after exposure to high doses of EVs (Fig. 34-A). RoRγT transcription factor characterizes the Th17 cell subset that is involved in inflammation and autoimmune responses (Luckheeram et al., 2012). RoRγT showed an increase in expression levels, when glioblastoma extracellular vesicles were added in Half or Full dose, but the cell counts of the RoRγT+ve cells appear to be lower (Fig. 34-B). Bcl-6 expression indicates the presence of T follicular helper cells (Tfh) cells, which are implicated in the germinal centres' and high affinity antibody formation ((Luckheeram et al., 2012). Treatment with EVs resulted in impairment of Bcl-6 expression on CD4+ T cells in a dose-dependent manner (Fig. 34-C). Furthermore, the pro-inflammatory Th1 cells are related to the expression of the transcription factor T-bet. T-bet was expressed in almost the same percentage of cells when Full dose of EVs was added, but it should be considered that the total cell counts were approximately at 80% of the control. In Half and in ¼ EV dose treatment, instead, the counts CD4+ cells expressing T-bet were much higher by 16% and 21%, respectively (Fig. 34-D). Finally, the Treg specific master transcription factor, FoxP3, was elevated in levels of expression when the cells were treated with tumour EVs showing the peak of expression up to almost 126% in Half dose addition (Fig 34-E).

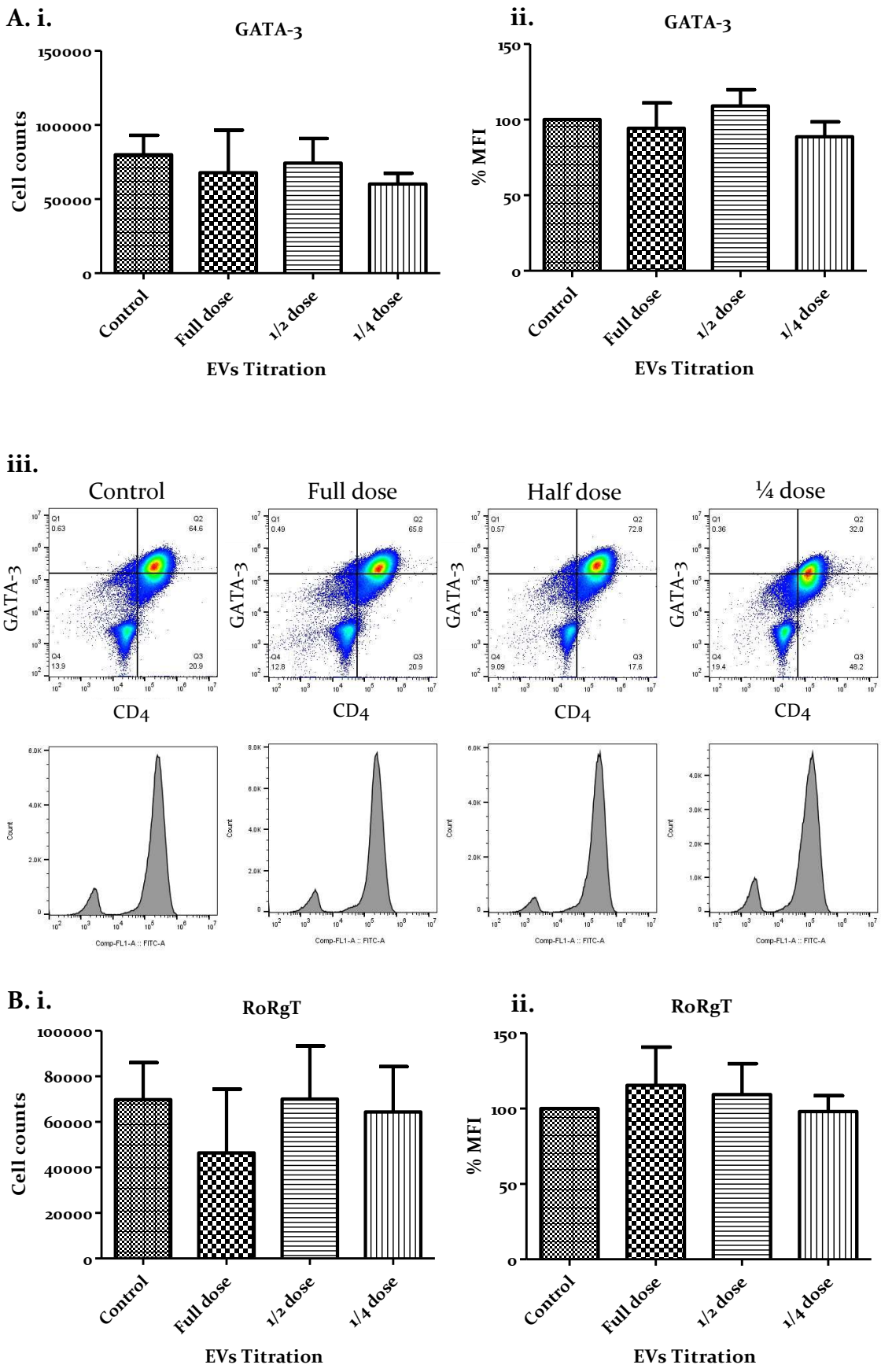
A. i.
GATA-3
Cell counts
150000
100000
50000
0
Control
Full dose
1/2 dose
1/4 dose
EVs Titration
ii.
GATA-3
% MFI
150
100
50
0
Control
Full dose
1/2 dose
1/4 dose
EVs Titration
iii.
Control
Full dose
Half dose
¼ dose
GATA-3
CD4
Q1 0.63
Q2 64.6
Q4 13.9
Q3 20.9
Q1 0.49
Q2 65.8
Q4 12.8
Q3 20.9
Q1 0.57
Q2 72.8
Q4 9.09
Q3 17.6
Q1 0.36
Q2 32.0
Q4 19.4
Q3 48.2
Count
Comp-FL1-A :: FITC-A
B. i.
RoRgT
Cell counts
100000
80000
60000
40000
20000
0
Control
Full dose
1/2 dose
1/4 dose
EVs Titration
ii.
RoRgT
% MFI
150
100
50
0
Control
Full dose
1/2 dose
1/4 dose
EVs Titration

iii.

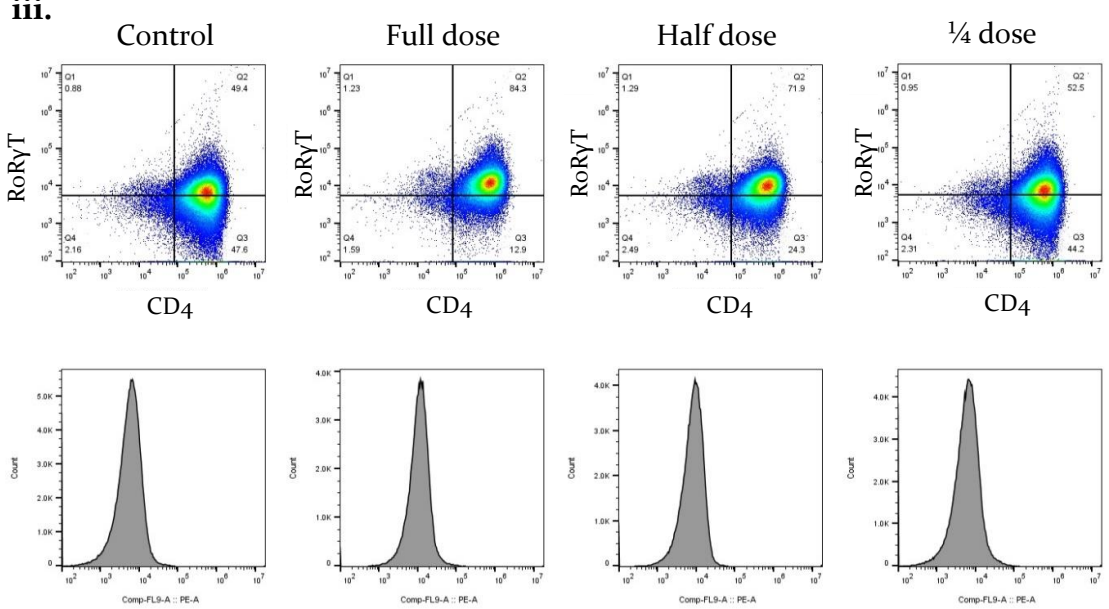
Control
Full dose
Half dose
¼ dose
RoRyT
CD4
Count
Comp-FL9-A :: PE-A

C. i.

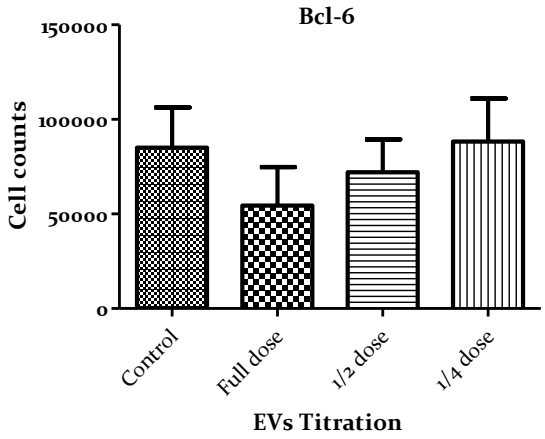
Bcl-6
Cell counts
150000
100000
50000
0
Control
Full dose
1/2 dose
1/4 dose
EVs Titration

ii.

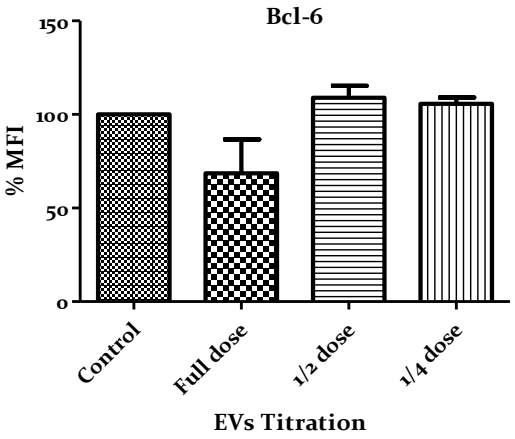
Bcl-6
% MFI
150
100
50
0
Control
Full dose
1/2 dose
1/4 dose
EVs Titration

iii.

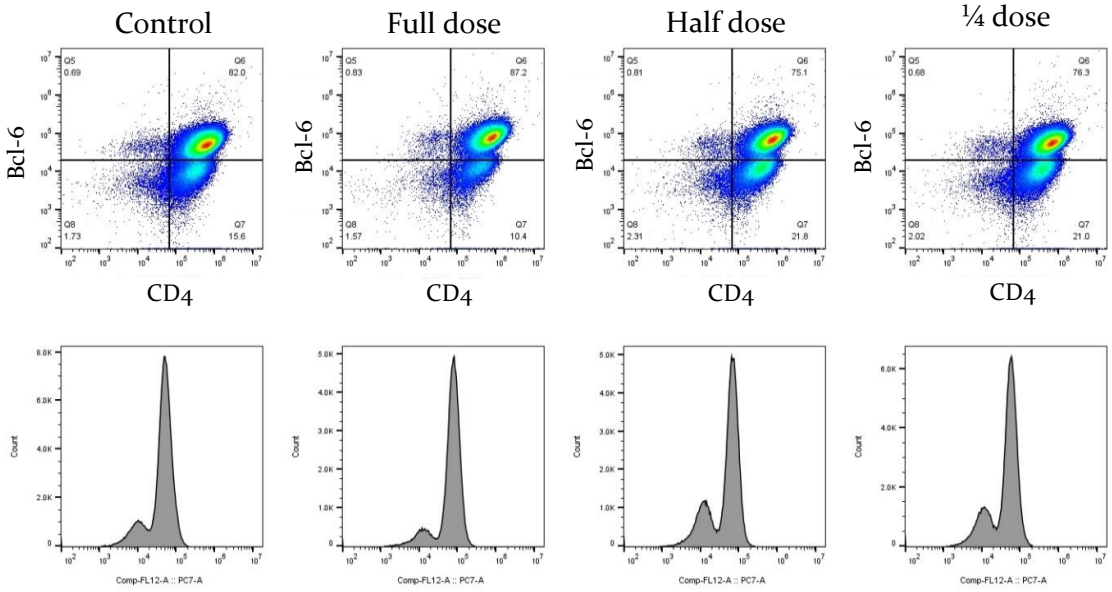
Control
Full dose
Half dose
¼ dose
Bcl-6
CD4
Count
Comp-FL12-A :: PC7-A

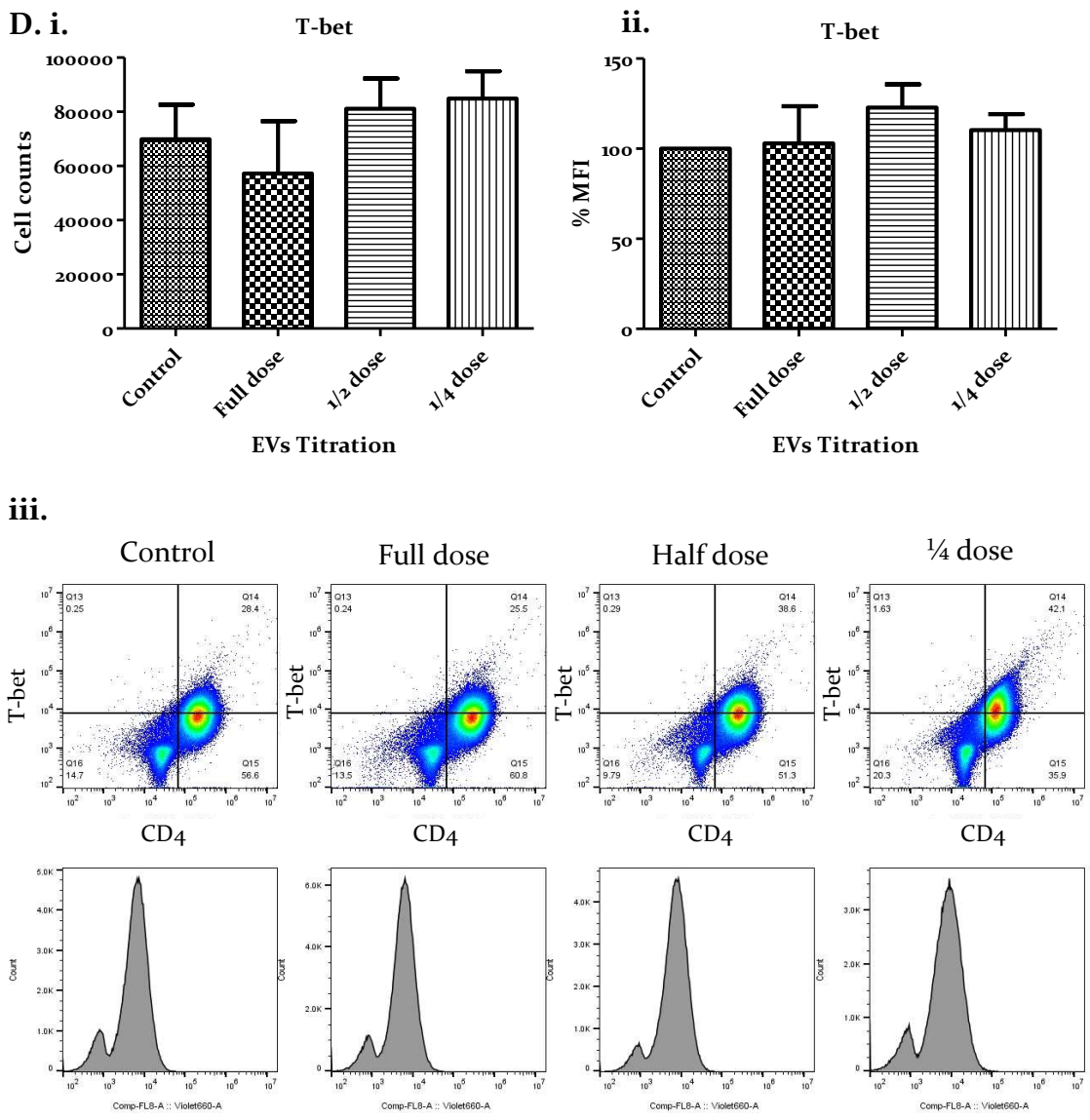
D. i.
T-bet
Cell counts
100000
80000
60000
40000
20000
0
Control
Full dose
1/2 dose
1/4 dose
EVs Titration
ii.
T-bet
% MFI
150
100
50
0
Control
Full dose
1/2 dose
1/4 dose
EVs Titration
iii.
Control
Full dose
Half dose
¼ dose
T-bet
CD4
Q13 0.25
Q14 28.4
Q16 14.7
Q15 56.6
Q13 0.24
Q14 25.5
Q16 13.5
Q15 60.8
Q13 0.29
Q14 38.6
Q16 9.79
Q15 51.3
Q13 1.63
Q14 42.1
Q16 20.3
Q15 35.9
Count
Comp-FL8-A :: Violet660-A

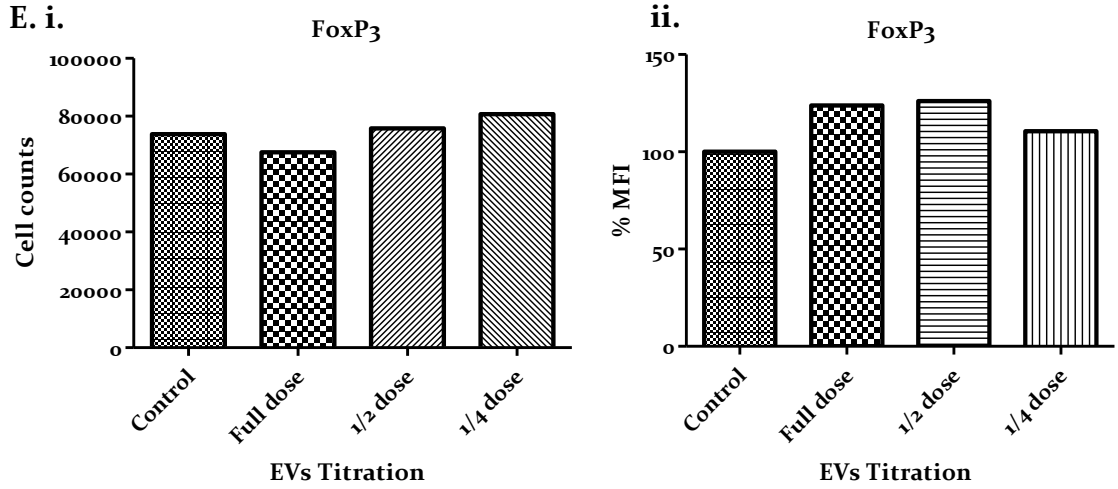
E. i.
FoxP3
Cell counts
100000
80000
60000
40000
20000
0
Control
Full dose
1/2 dose
1/4 dose
EVs Titration
ii.
FoxP3
% MFI
150
100
50
0
Control
Full dose
1/2 dose
1/4 dose
EVs Titration

iii.

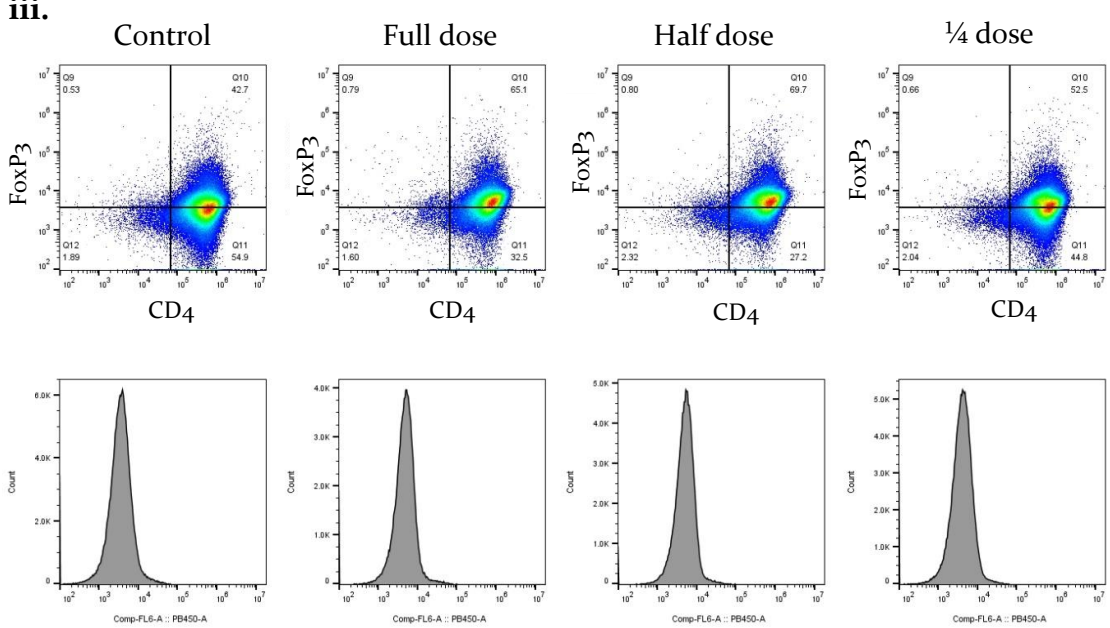

Figure 34. The transcription factors expression levels upon indicated concentrations of Glioblastoma-derived vesicles.

2.5 x 10^4 CD4+ T cells were seeded with 5 x 10^4 CD3/CD28 Human T-activator Dynabeads alone or in the presence of increasing tumour EVs ratios. After 5 days, the cells were stained for intracellular (A) GATA-3, (B) RoRγT, (C) Bcl-6, (D) T-bet, (E) FoxP3 antibodies and surface CD4. A.i.-E.i. Graphs show how the counts of cells expressing each factor change in response to different concentrations of tumour EVs.

A.ii-E.ii. Graphs represent the MFI in percentages related to the control condition where no EVs from the tumour tissue were added on the cultures.

A.iii-E.iii Dot plots representative for the above descriptions are presented for each condition and transcription factor. The experiment performed for n=5.

3.3.5 Effect of Glioblastoma tumour- derived proteins in solution on T cell counts

Soluble proteins derived from glioblastoma patients samples were added on isolated from human peripheral blood CD4+ T cells in descending doses. As it is presented in the Figure 35, the proteins contained in the secretome have an immunosuppressive effect on the T cell subset, with addition of high doses resulting in a decrease on the cell counts. Figure 35C shows the shift on the lymphocyte gate. The initial percentage of the lymphocytes detected was reduced, whilst the dead cell population increased. The same result is obvious from the stagger plot (Fig. 35D), where the accuracy of the gates is visually more obvious and the differences of the populations in the experimental set in comparison to the control group can be detected due to the different peaks at the overlays.

A

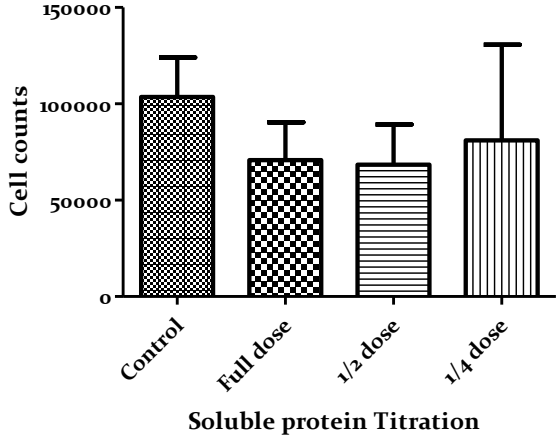
150000
100000
50000
0
Cell counts
Control
Full dose
1/2 dose
1/4 dose
Soluble protein Titration

B

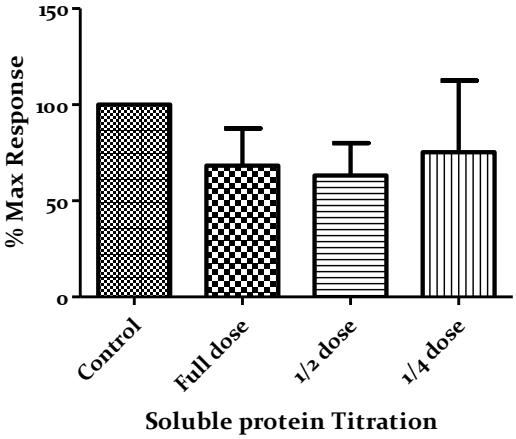
150
100
50
0
% Max Response
Control
Full dose
1/2 dose
1/4 dose
Soluble protein Titration

C

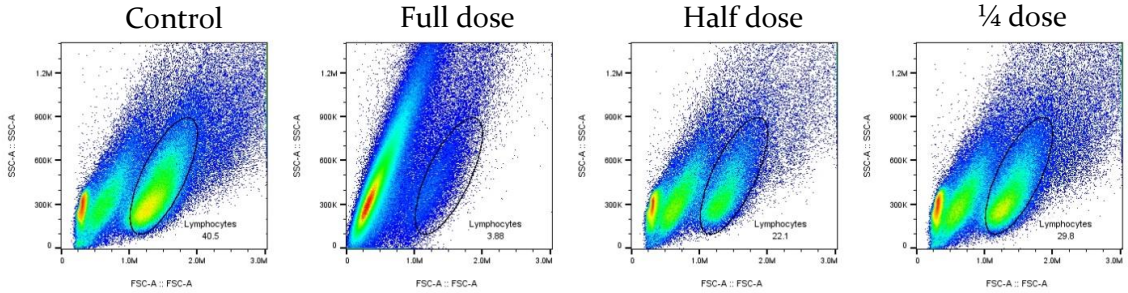
Control
Full dose
Half dose
¼ dose
Lymphocytes
40.5
Lymphocytes
3.88
Lymphocytes
22.1
Lymphocytes
29.8
SSC-A :: SSC-A
FSC-A :: FSC-A

D

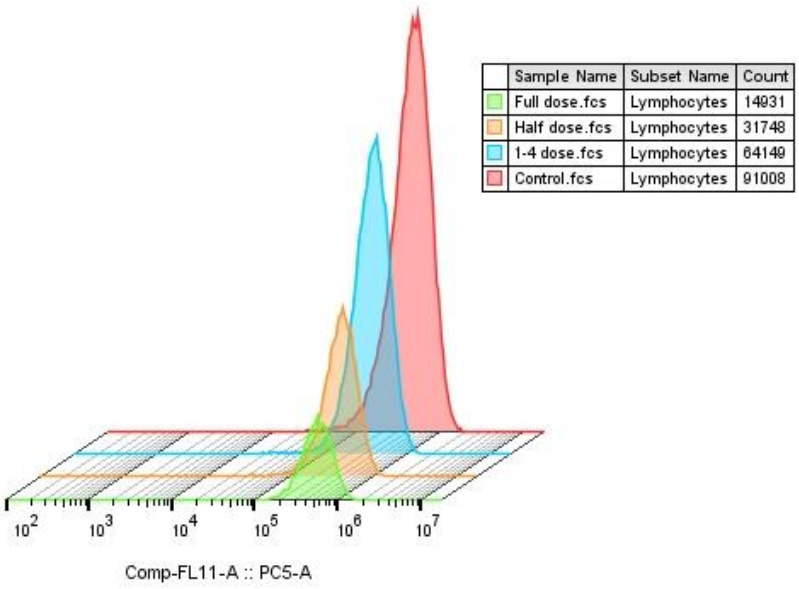

Figure 35. Concentrated tumour soluble proteins reduce CD4+ T cell viability in high concentrations.

Isolated CD4+ cells were seeded with CD3/CD28 T-activator Dynabeads in 2:1 ratio alone or in the presence of GBM-derived Soluble proteins. After 5 days, cells were harvested and stained for surface ani-human CD4.

(A) Cell viability is shown using the total number of cells **(B)** Cell viability is presented as a percentage of the control in response to different concentrations after treatment with concentrated tumour proteins. **(C)** Representative dot plots and (D) stagger plot show the cells detected by the flow cytometer, when cultured alone (first panel), or in the presence of decreasing concentrations of tumour proteins and the lymphocyte gate.

The results are representative of 4 experiments (N=4). Error bars that represent SEM are shown *, p = <0.05, **, p = <0.01.

3.3.6 Effect of GBM Soluble factors on T cell surface markers expression

Similarly working as with the EVs, in order to test on the expression levels of cell surface markers, we isolated CD4+ T cells and plated them alone with CD3/CD28 activation Dynabeads or treated them with doses of soluble proteins for 5 days. Next, we harvested the whole cell volume, stained them with CD4, TIM-3, PD-1 and ICOS antibodies and analysed with flow cytometry.

Cells counts expressing the exhaustion marker TIM-3 show a decrease after being treated with Full, Half or ¼ doses of soluble proteins. However, the mean fluorescence intensity was higher over ascending doses of treatment to the culture. As showed in Figure 36-A, the TIM-3-positive CD4+ population increased by 25% after exposure to Full dose of tumour soluble proteins in comparison to the control group (Fig. 36-B). The immune checkpoint inhibitor and marker of exhaustion, PD-1, is expressed by fewer cells in absolute number over soluble protein serial dilution. PD-1 MFI was significantly higher in Full dose of treatment up to 131% (**, p=0.0042) in comparison to ¼ dose and the control group, where no soluble proteins were added to the cells. ICOS surface expression on T cells was impaired after addition of tumour proteins in the culture. The expression of the activation marker was lowered in a dose-dependent manner (Fig. 36-C).

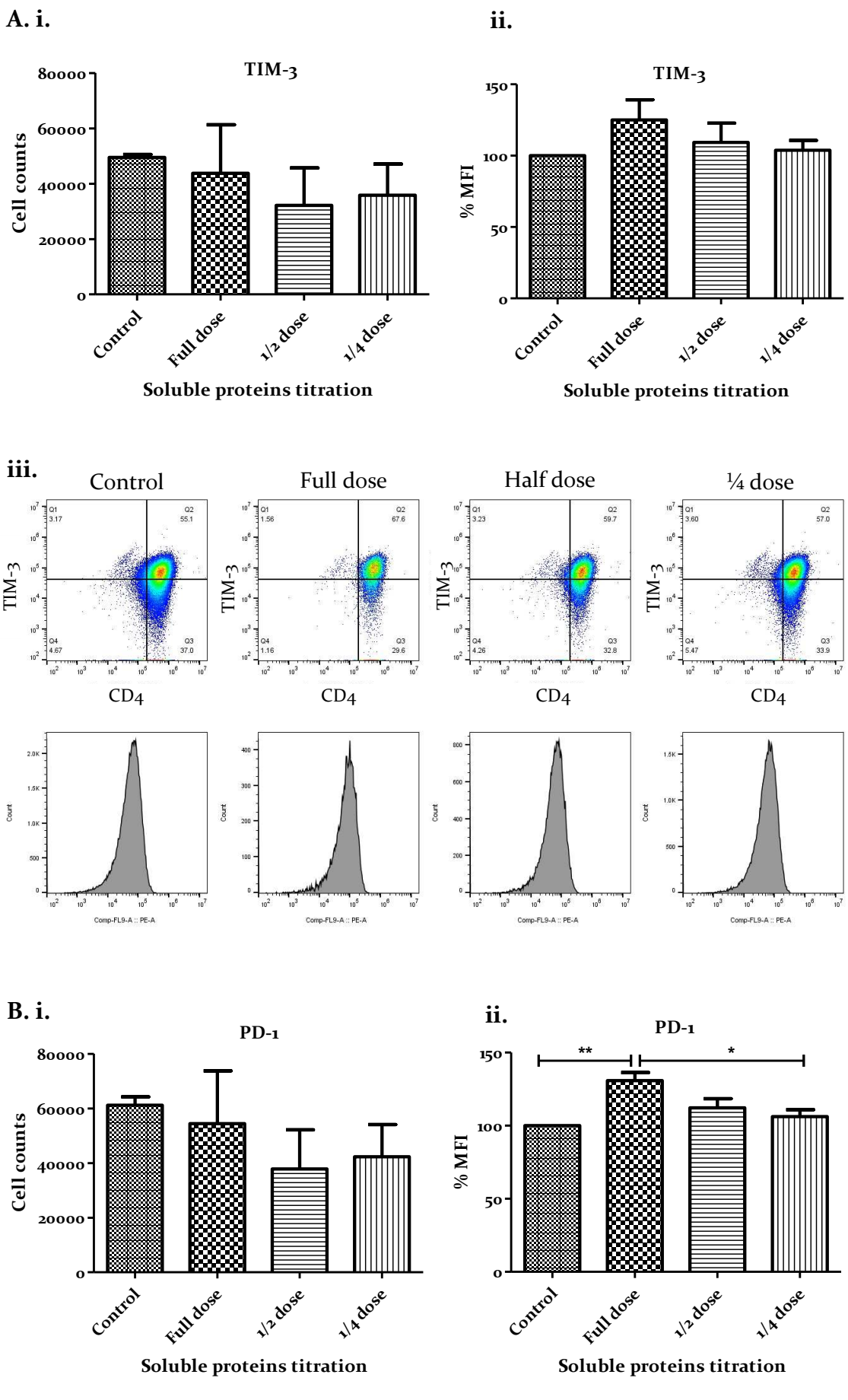
A. i.
TIM-3
Cell counts
80000
60000
40000
20000
0
Control
Full dose
1/2 dose
1/4 dose
Soluble proteins titration
ii.
TIM-3
% MFI
150
100
50
0
Control
Full dose
1/2 dose
1/4 dose
Soluble proteins titration
iii.
Control
Full dose
Half dose
¼ dose
TIM-3
CD4
Q1 3.17
Q2 55.1
Q4 4.67
Q3 37.0
Q1 1.56
Q2 67.6
Q4 1.16
Q3 29.6
Q1 3.23
Q2 59.7
Q4 4.26
Q3 32.8
Q1 3.60
Q2 57.0
Q4 5.47
Q3 33.9
Count
Comp-FL9-A :: PE-A
B. i.
PD-1
Cell counts
80000
60000
40000
20000
0
Control
Full dose
1/2 dose
1/4 dose
Soluble proteins titration
ii.
PD-1
**
*
% MFI
150
100
50
0
Control
Full dose
1/2 dose
1/4 dose
Soluble proteins titration

iii.

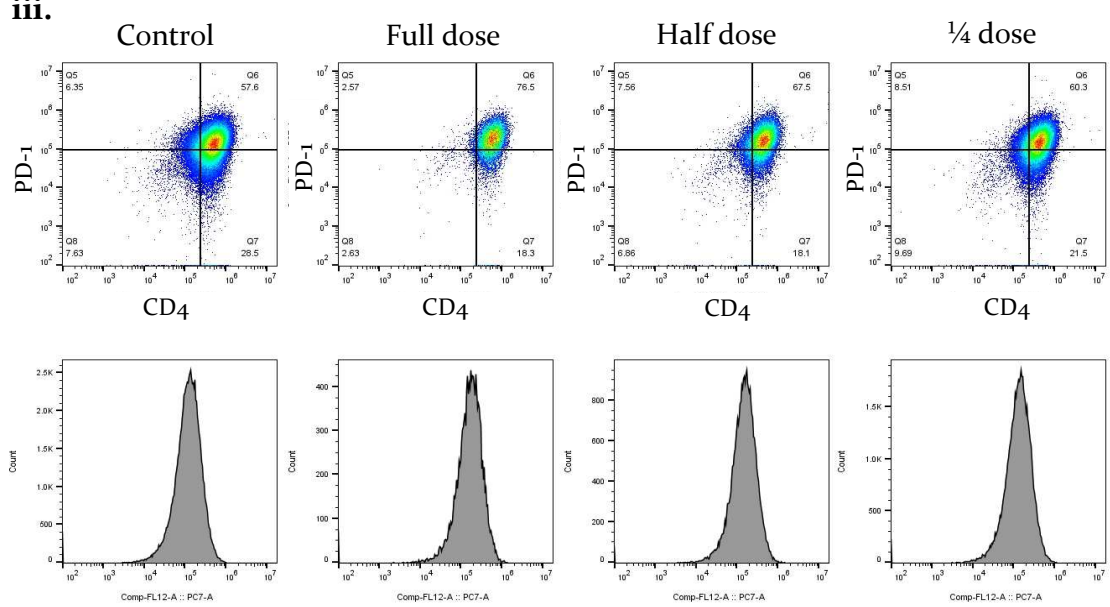
Control
Full dose
Half dose
¼ dose
PD-1
CD4
Q5 6.35
Q6 57.6
Q8 7.63
Q7 28.5
Q5 2.57
Q6 76.5
Q8 2.63
Q7 18.3
Q5 7.56
Q6 67.5
Q8 6.86
Q7 18.1
Q5 8.51
Q6 60.3
Q8 9.69
Q7 21.5
Count
Comp-FL12-A :: PC7-A

C. i.

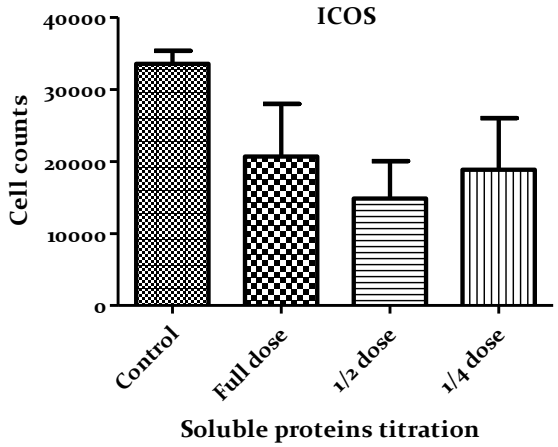
ICOS
Cell counts
40000
30000
20000
10000
0
Control
Full dose
1/2 dose
1/4 dose
Soluble proteins titration

ii.

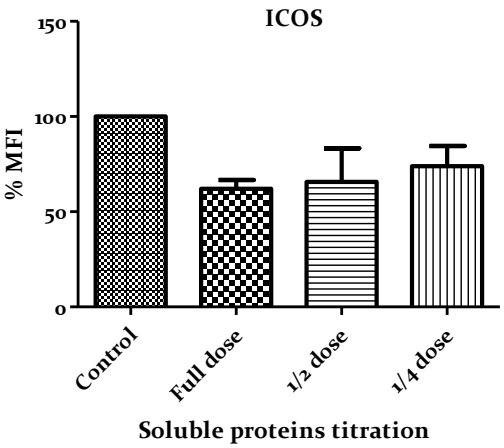
ICOS
% MFI
150
100
50
0
Control
Full dose
1/2 dose
1/4 dose
Soluble proteins titration

iii.

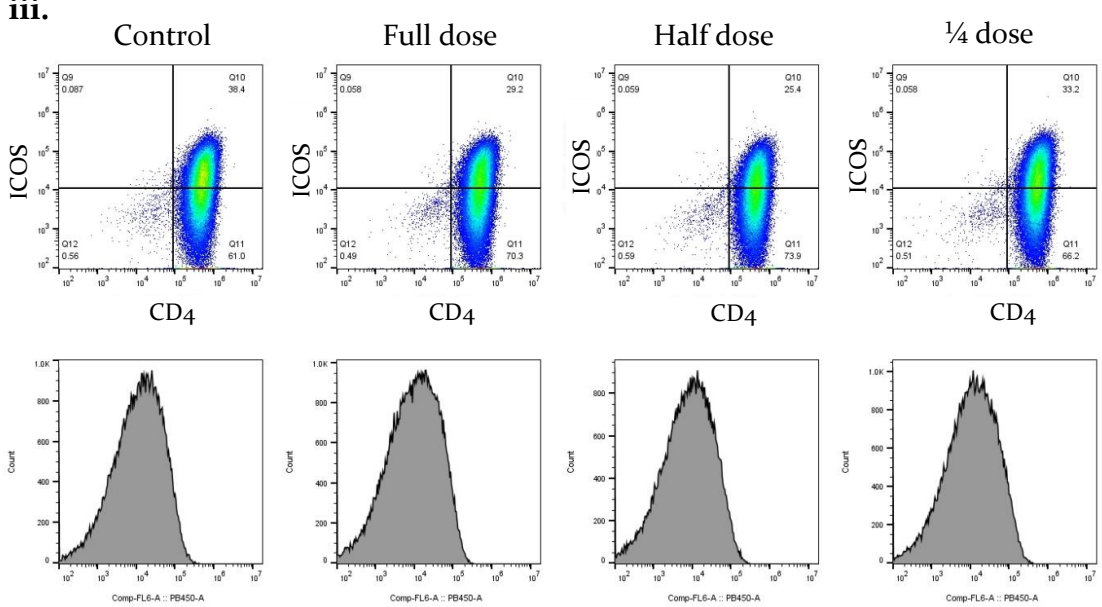

Figure 36. Expression levels of cell surface markers upon the descending concentration of tumour Soluble proteins.

Seeded CD4+ T cells (2.5x10⁴ cells/well) alone or with indicated tumour Soluble protein ratios were incubated for 5 days. Then, the cells were harvested and stained for surface (A) TIM-3, (B) PD-1, (C) ICOS and CD4 antibodies.

A.i.-C.i. Graphs show the change in cells numbers expressing the specific markers under the different conditions. A.ii-C.ii Graphs show the MFI of the markers in a percentage format relative to the control, where no GBM-derived proteins were added to the cells.

A.iii.-C.iii Representative dot plots show the levels of the surface markers on CD4+ T cells, when cultured alone (left panel), or in the presence of the tumour proteins.

Data is representative of 4 experiments (n=4). *, p = <0.05, **, p = <0.01.

3.3.7 Effect of soluble factors from GBM patients on T cell cytokine production

The expression profile and potential altering of certain cytokines-drivers of specific immune cell subsets was examined over GBM soluble protein serial dilution following the same procedure as previously with the EVs (details in Chapter 3.3.3).

T cell-mediated TGFβ secretion was decreased after the soluble protein addition in the culture. The amount of cells found to release TGFβ and the expression of the particular stained marker was imoicantly lower in the CD4+ cells receiving the Full dose soluble proteins (Fig. 37-A).. IL-21 was secreted by fewer cells and MFI was lower after treatment with soluble proteins from glioblastoma patients (Fig. 37-B). TNFα secretion were significantly impaired, when CD4+ T cells were exposed to Full dose of GBM proteins in solution (Fig. 37C). Moreover, IL-13 did not show any notable difference regarding release from T cells upon exposure to tumour proteins (Fig. 37-E). IL-17 was expressed by more cells, as ¼ of the Full dose of soluble proteins was added to the culture. Furthermore, expression of IL-17 was constantly higher than the control group in all conditions, while elevated production was observed in response to Half and Full dose soluble proteins (Fig. 37-F).

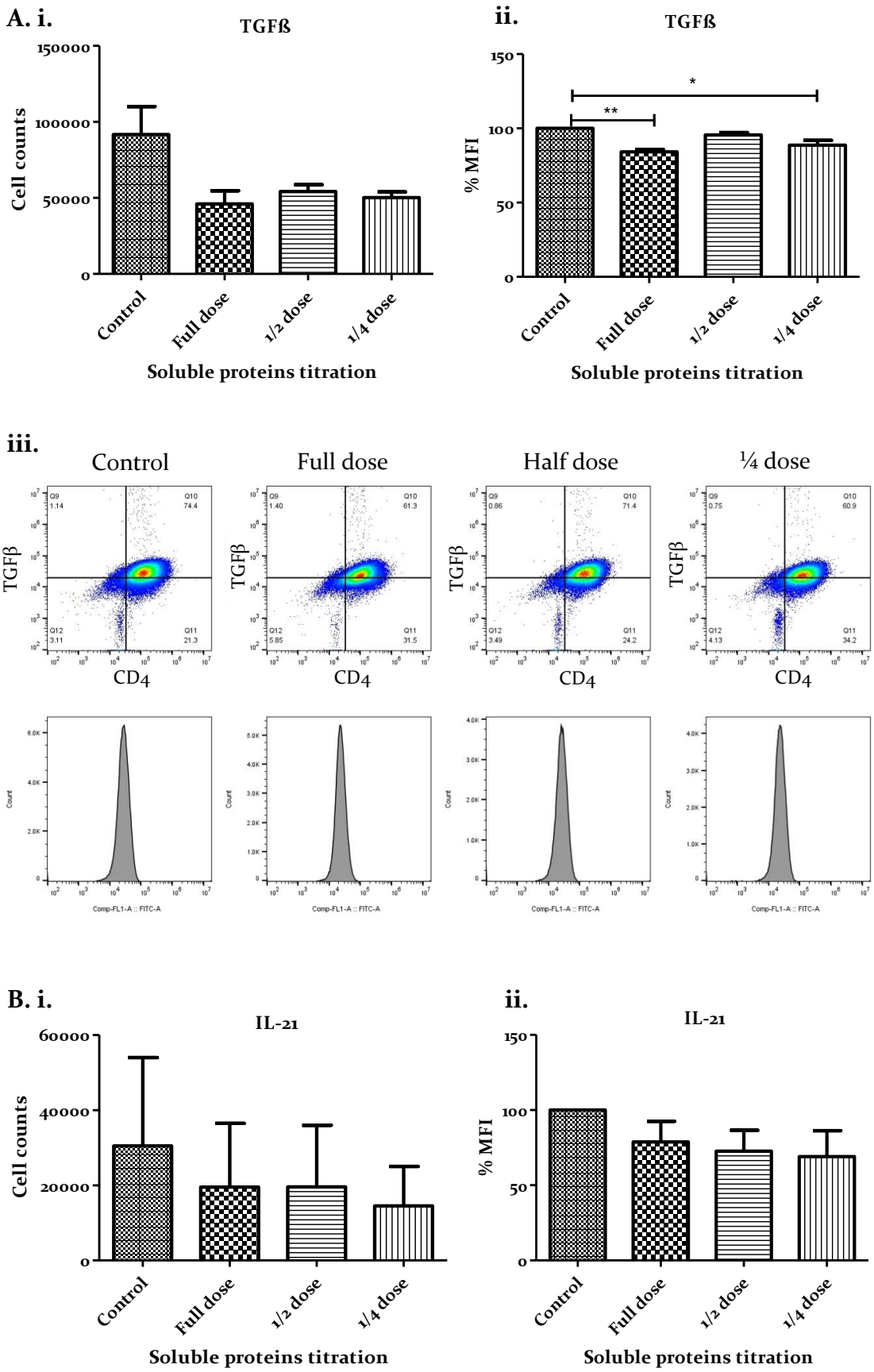
A. i.
TGFß
Cell counts
150000
100000
50000
0
Control
Full dose
1/2 dose
1/4 dose
Soluble proteins titration
ii.
TGFß
% MFI
150
100
50
0
*
**
Control
Full dose
1/2 dose
1/4 dose
Soluble proteins titration
iii.
Control
Full dose
Half dose
¼ dose
TGFβ
CD4
Q9 1.14
Q10 74.4
Q12 3.11
Q11 21.3
Q9 1.40
Q10 61.3
Q12 5.85
Q11 31.5
Q9 0.86
Q10 71.4
Q12 3.49
Q11 24.2
Q9 0.75
Q10 60.9
Q12 4.13
Q11 34.2
Count
Comp-FL1-A :: FITC-A
B. i.
IL-21
Cell counts
60000
40000
20000
0
Control
Full dose
1/2 dose
1/4 dose
Soluble proteins titration
ii.
IL-21
% MFI
150
100
50
0
Control
Full dose
1/2 dose
1/4 dose
Soluble proteins titration

iii.

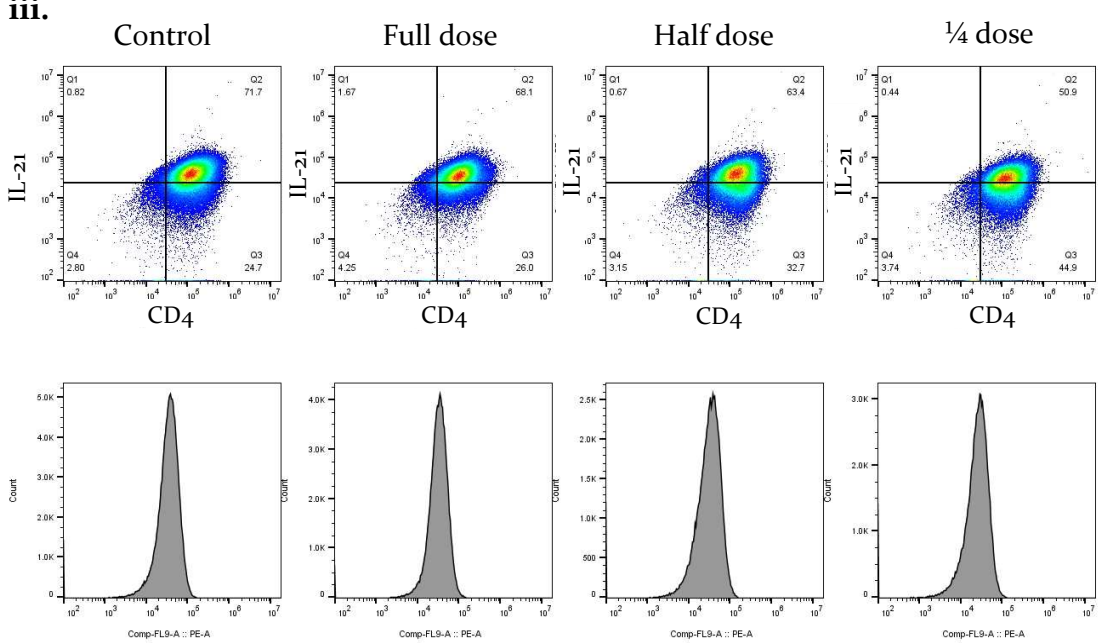
Control
Full dose
Half dose
¼ dose
IL-21
CD4
Q1 0.82
Q2 71.7
Q4 2.80
Q3 24.7
Q1 1.67
Q2 68.1
Q4 4.25
Q3 26.0
Q1 0.67
Q2 63.4
Q4 3.15
Q3 32.7
Q1 0.44
Q2 50.9
Q4 3.74
Q3 44.9
Count
Comp-FL9-A :: PE-A

C. i.

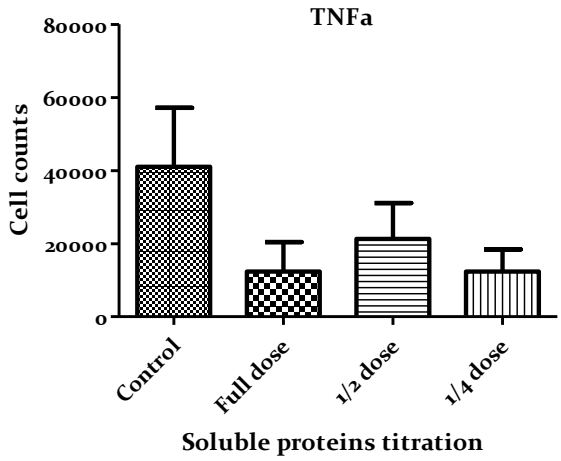
TNFa
Cell counts
80000
60000
40000
20000
0
Control
Full dose
1/2 dose
1/4 dose
Soluble proteins titration

ii.

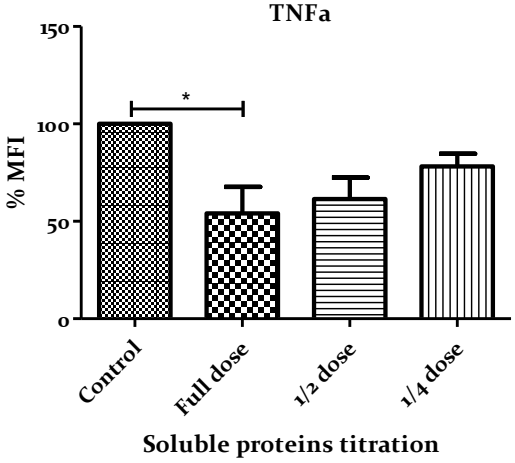
TNFa
% MFI
150
100
50
0
*
Control
Full dose
1/2 dose
1/4 dose
Soluble proteins titration

iii.

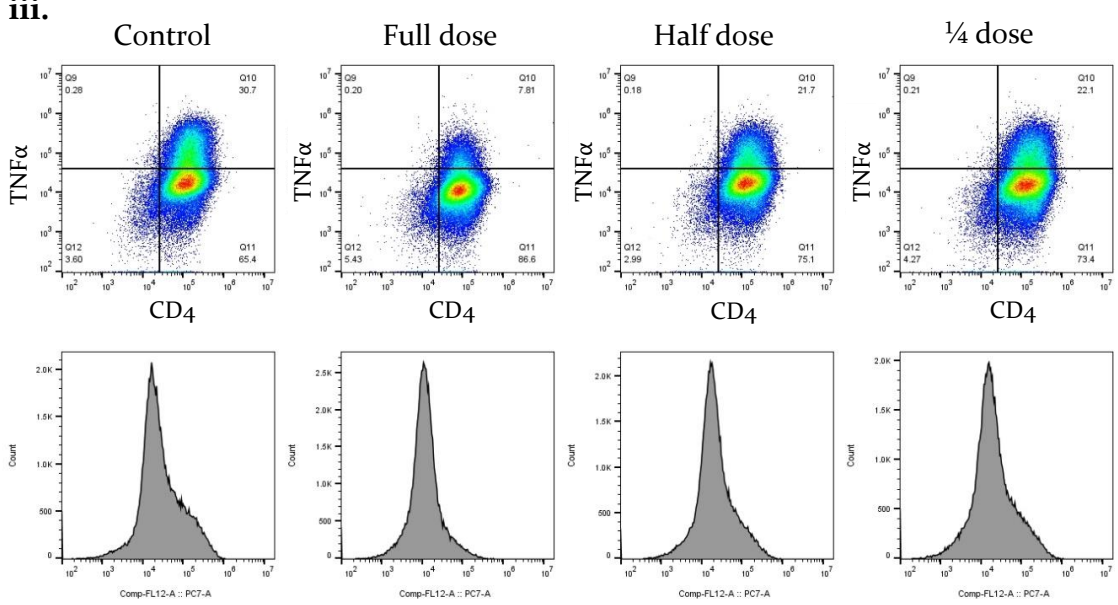
Control
Full dose
Half dose
¼ dose
TNFα
CD4
Q9 0.28
Q10 30.7
Q12 3.60
Q11 65.4
Q9 0.20
Q10 7.81
Q12 5.43
Q11 86.6
Q9 0.18
Q10 21.7
Q12 2.99
Q11 75.1
Q9 0.21
Q10 22.1
Q12 4.27
Q11 73.4
Count
Comp-FL12-A :: PC7-A

D. i.

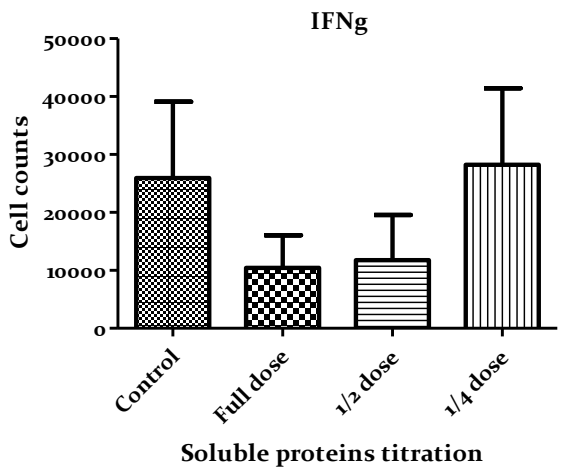
IFNg
Cell counts
50000
40000
30000
20000
10000
0
Control
Full dose
1/2 dose
1/4 dose
Soluble proteins titration

ii.

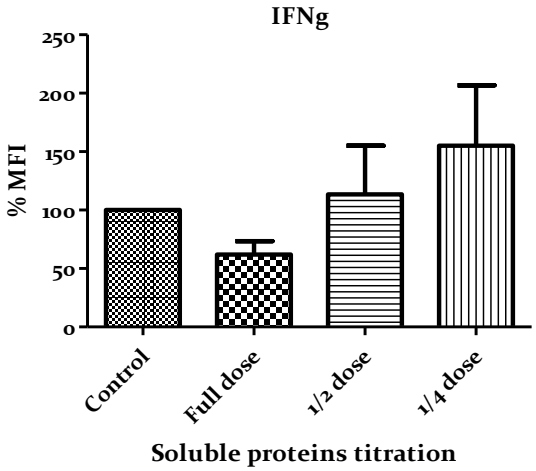
IFNg
% MFI
250
200
150
100
50
0
Control
Full dose
1/2 dose
1/4 dose
Soluble proteins titration

iii.

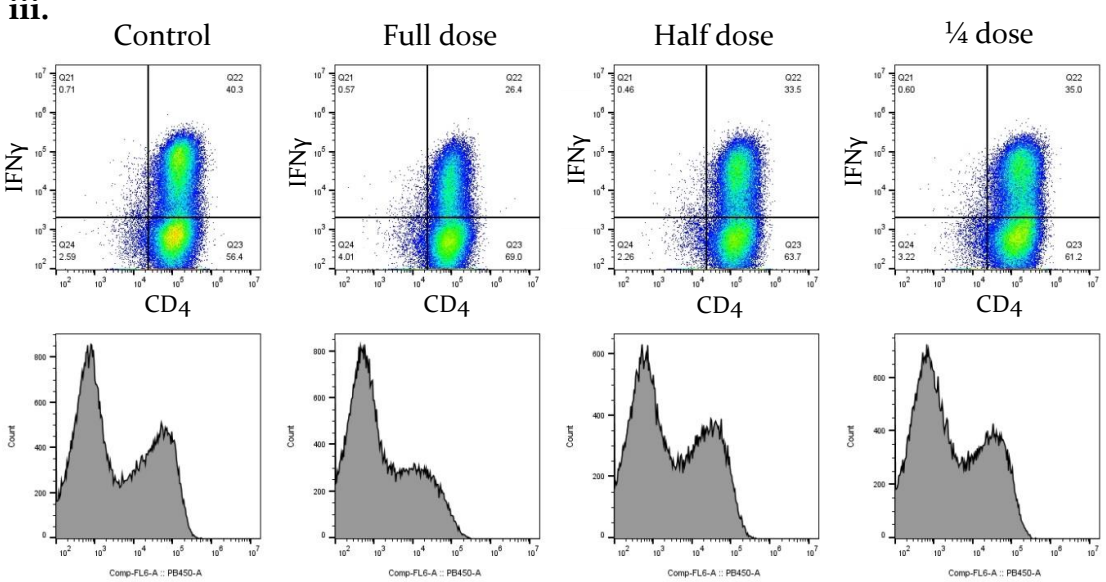
Control
Full dose
Half dose
¼ dose
IFNγ
CD4
Q21 0.71
Q22 40.3
Q24 2.59
Q23 56.4
Q21 0.57
Q22 26.4
Q24 4.01
Q23 69.0
Q21 0.46
Q22 33.5
Q24 2.26
Q23 63.7
Q21 0.60
Q22 35.0
Q24 3.22
Q23 61.2
Count
Comp-FL6-A :: PB450-A

E. i.

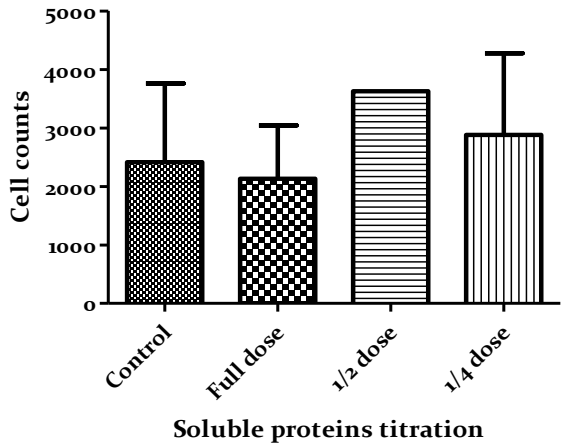
IL-13
Cell counts
5000
4000
3000
2000
1000
0
Control
Full dose
1/2 dose
1/4 dose
Soluble proteins titration

ii.

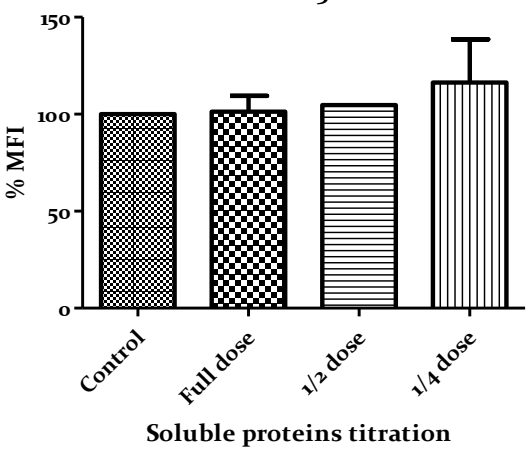
IL-13
% MFI
150
100
50
0
Control
Full dose
1/2 dose
1/4 dose
Soluble proteins titration

iii.

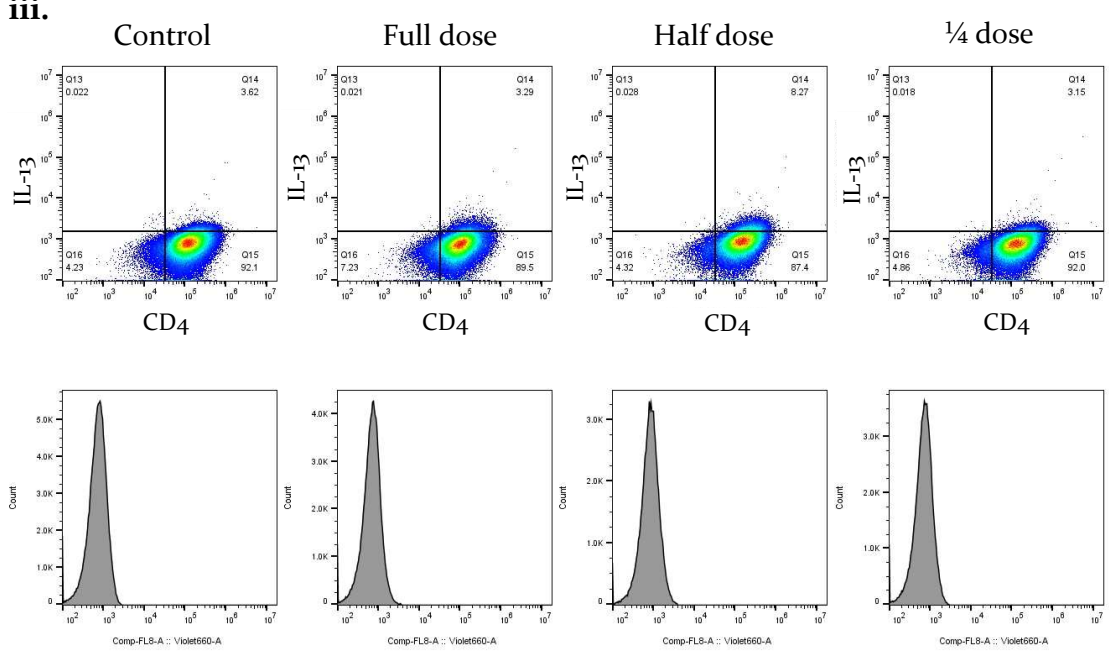
Control
Full dose
Half dose
¼ dose
IL-13
CD4
Q13 0.022
Q14 3.62
Q16 4.23
Q15 92.1
Q13 0.021
Q14 3.29
Q16 7.23
Q15 89.5
Q13 0.028
Q14 8.27
Q16 4.32
Q15 87.4
Q13 0.018
Q14 3.15
Q16 4.86
Q15 92.0
Count
Comp-FL8-A :: Violet660-A

F. i.

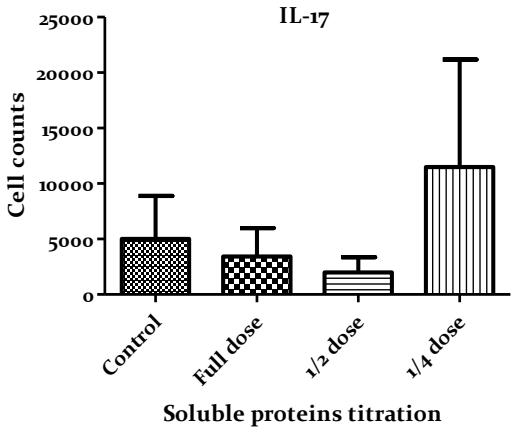
IL-17
Cell counts
25000
20000
15000
10000
5000
0
Control
Full dose
1/2 dose
1/4 dose
Soluble proteins titration

ii.

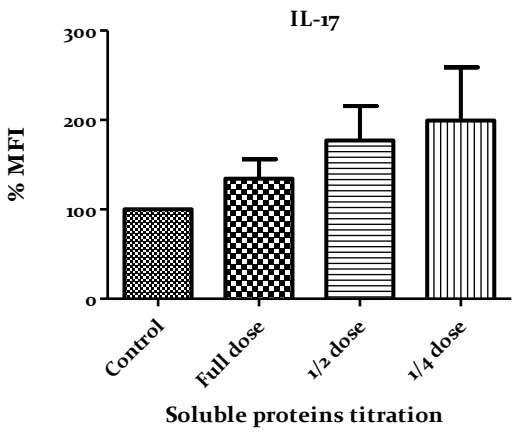
IL-17
% MFI
300
200
100
0
Control
Full dose
1/2 dose
1/4 dose
Soluble proteins titration

iii.

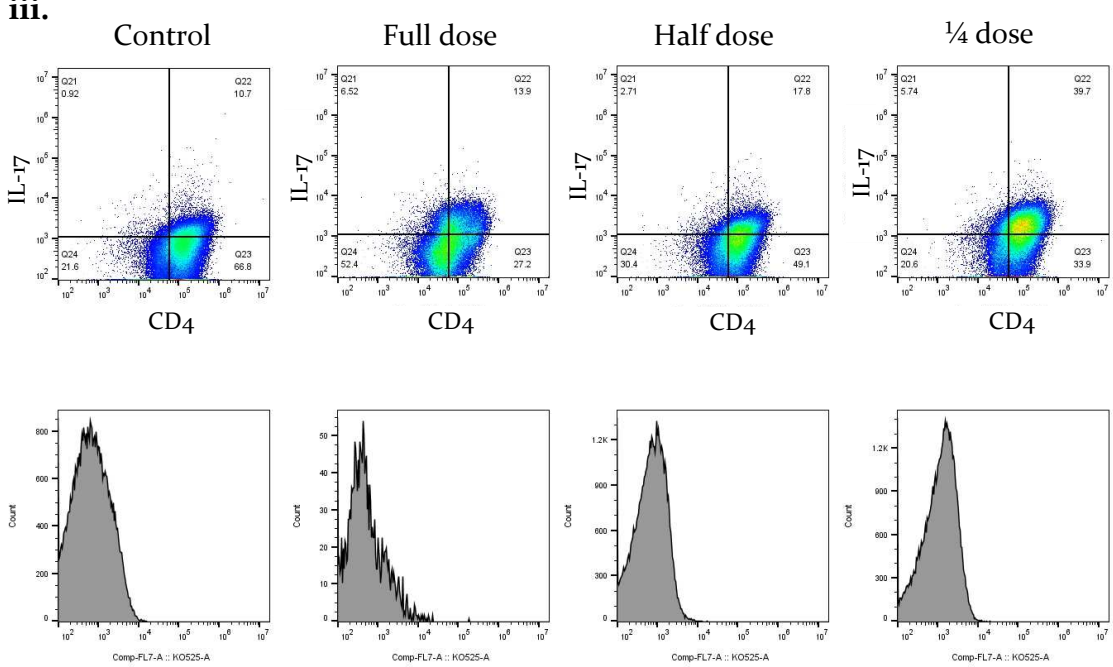

Figure 37. Production of cytokines upon the titration of the purified tumour Soluble proteins.

CD4+ T cells were cultured at 2.5 x 10^4 cells/well density with CD3/CD28 Human T-activator Dynabeads in 1:2 ratio, alone or with indicated tumour soluble protein concentrations for 5 days. Then, the cells were restimulated and stained for intracellular (A) TGFβ, (B) IL-21, (C) TNFα, (D) IFNγ, (E) IL-17, (F) IL-13 antibodies and anti-human CD4.

A.i.-F.i Graphs show the change in counts expressing the selected cytokines in response to decreasing ratios of GBM-derived soluble proteins. in a percentage format. A.ii-F.ii Graphs show the MFI of the markers in a percentage format relative to the control, where no GBM-derived proteins were added to the cells. A.iii.-F.iii Dot plots are representative of the effect described on T cells.

Data is representative of 4 experiments (n=4). SEM is shown. *, p = <0.05, **, p = <0.01.

3.3.8 Effect of tumour soluble proteins on T cell transcription factors expression

The master transcription regulators were, also, examined for their altering expression upon tumour soluble proteins titration.

GATA-3 and RoRγT were produced by a slightly smaller count of cells as the concentration of soluble proteins increased, but the expression levels of the cytokines (MFI) remained stable in all conditions (Fig. 38A-B). Bcl-6 expression is reduced as the concentration of proteins in solution increased, showing a significant decrease of 30% when the Full dose was added (*, p=0.0263). FoxP3 transcription factor was expressed by fewer CD4+ T cells upon the titrated soluble proteins exposure, but the mean fluorescence intensity followed the opposite pattern. After co-culture of the isolated T cells with Full dose soluble factors, the expression level of FoxP3 was similar to the control group, where no tumour proteins were introduced to the cells. Finally, T-bet was expressed by a smaller number of cells, when the tumour was added to the culture, but T-bet+ve CD4+ T cells demonstrated high expression, equal to the control condition.

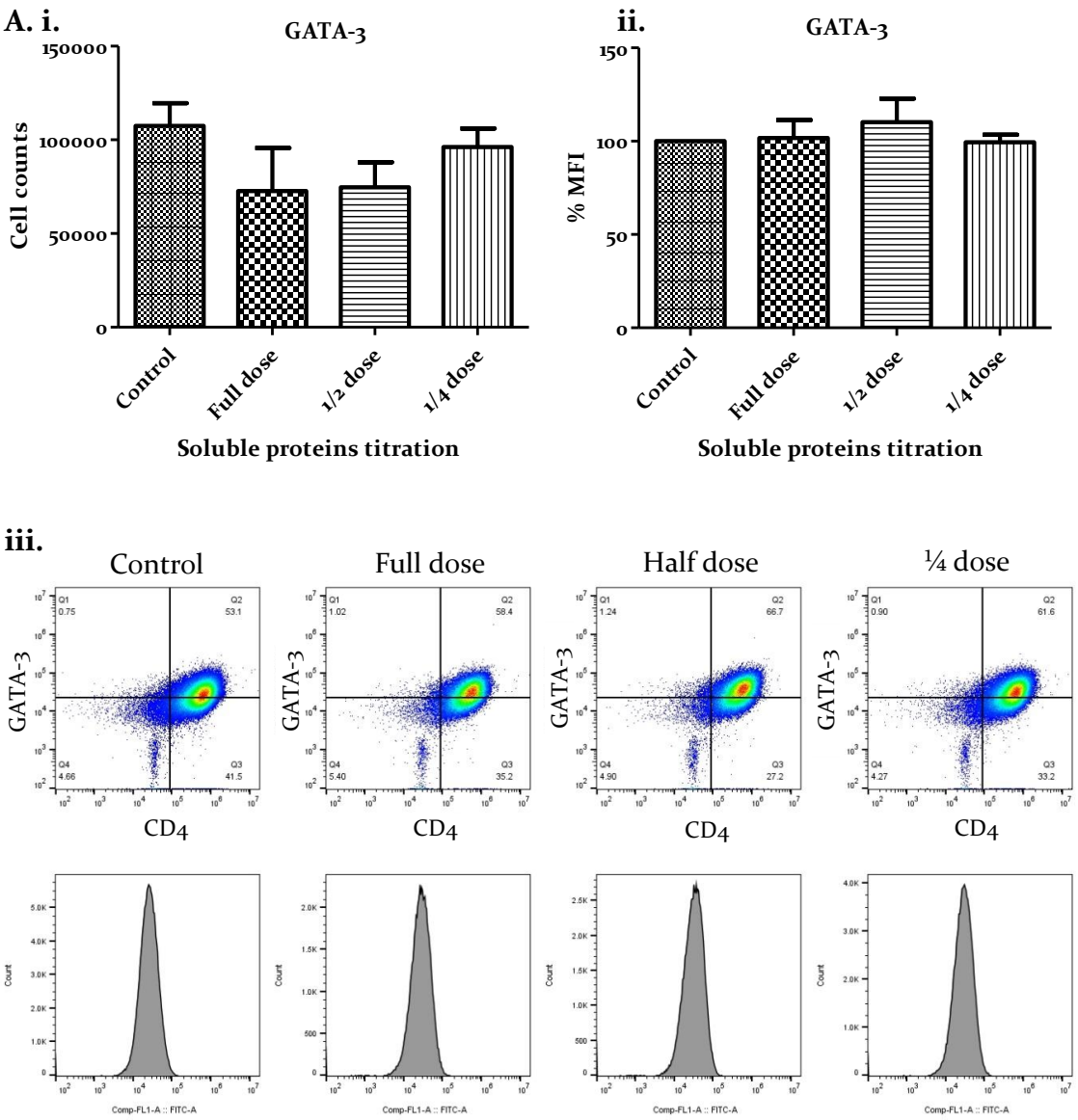
A. i.
GATA-3
150000
100000
50000
0
Cell counts
Control
Full dose
1/2 dose
1/4 dose
Soluble proteins titration
ii.
GATA-3
150
100
50
0
% MFI
Control
Full dose
1/2 dose
1/4 dose
Soluble proteins titration
iii.
Control
Full dose
Half dose
¼ dose
GATA-3
CD4
Q1 0.75
Q2 53.1
Q4 4.66
Q3 41.5
Q1 1.02
Q2 58.4
Q4 5.40
Q3 35.2
Q1 1.24
Q2 66.7
Q4 4.90
Q3 27.2
Q1 0.90
Q2 61.6
Q4 4.27
Q3 33.2
Count
Comp-FL1-A :: FITC-A

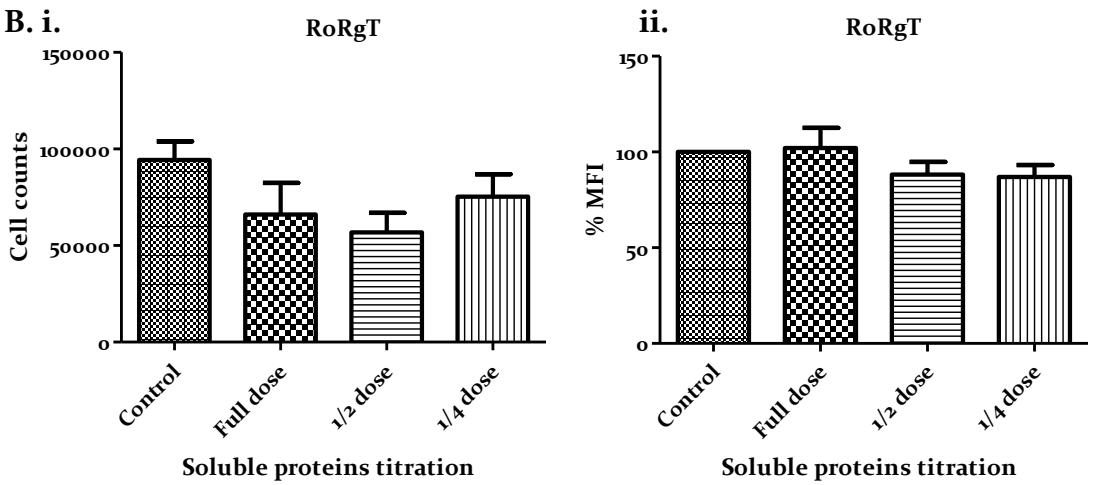
B. i.
RoRgT
150000
100000
50000
0
Cell counts
Control
Full dose
1/2 dose
1/4 dose
Soluble proteins titration
ii.
RoRgT
150
100
50
0
% MFI
Control
Full dose
1/2 dose
1/4 dose
Soluble proteins titration

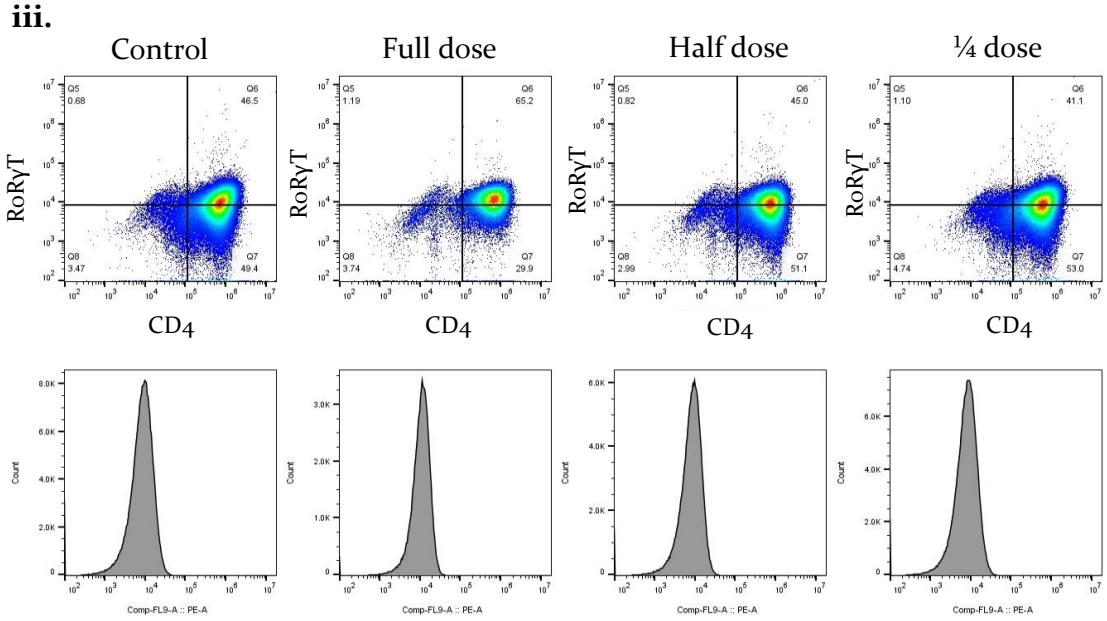
iii.
Control
Full dose
Half dose
¼ dose
RoRyT
CD4
Q5 0.68
Q6 46.5
Q8 3.47
Q7 49.4
Q5 1.19
Q6 65.2
Q8 3.74
Q7 29.9
Q5 0.82
Q6 45.0
Q8 2.99
Q7 51.1
Q5 1.10
Q6 41.1
Q8 4.74
Q7 53.0
Count
Comp-FL9-A :: PE-A

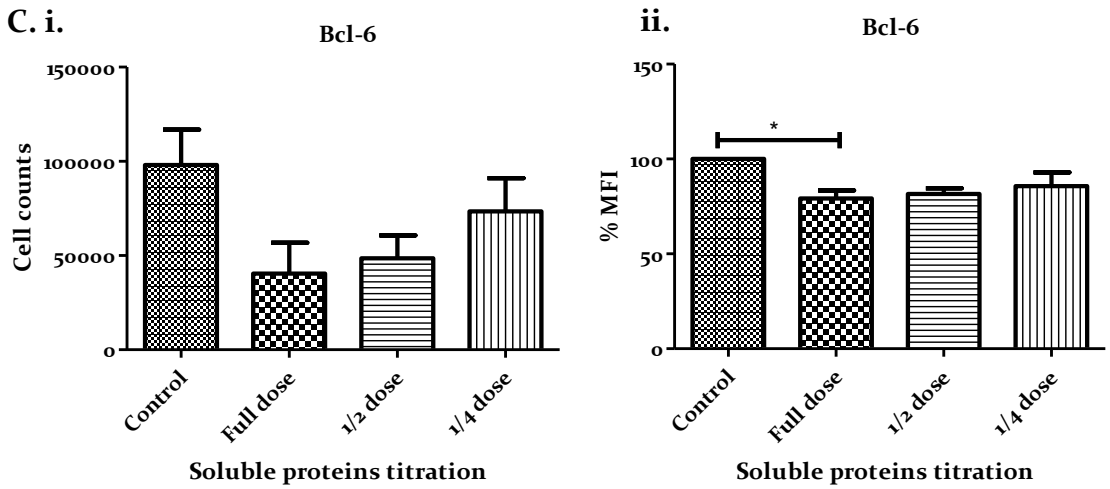
C. i.
Bcl-6
Cell counts
150000
100000
50000
0
Control
Full dose
1/2 dose
1/4 dose
Soluble proteins titration
ii.
Bcl-6
% MFI
150
100
50
0
*
Control
Full dose
1/2 dose
1/4 dose
Soluble proteins titration

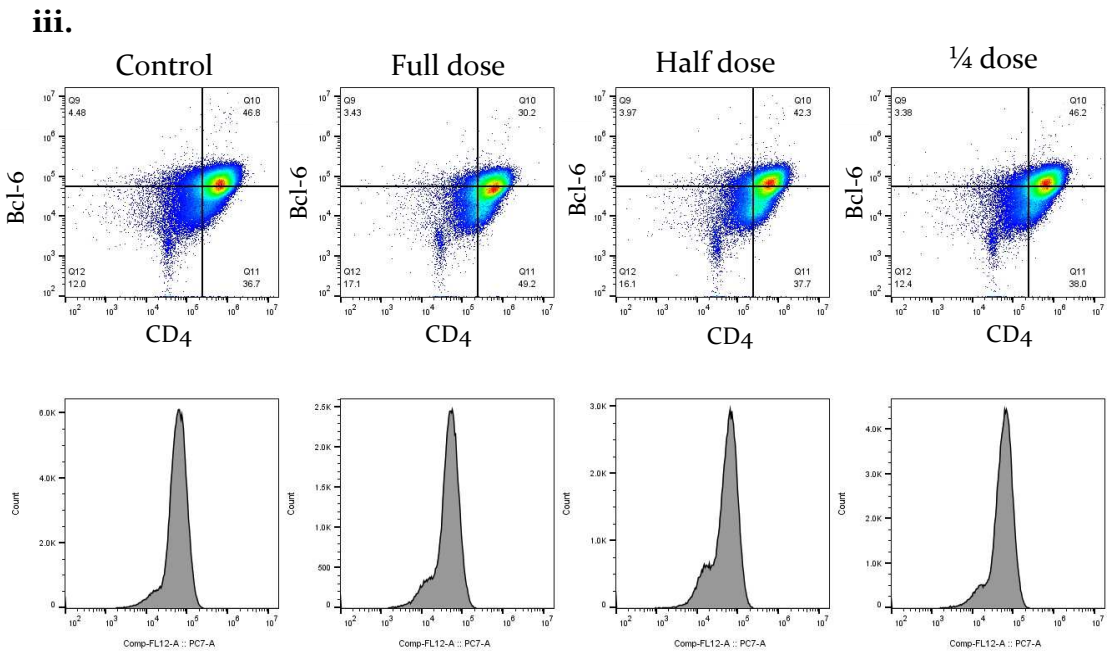
iii.
Control
Full dose
Half dose
¼ dose
Bcl-6
CD4
Q9 4.48
Q10 46.8
Q12 12.0
Q11 36.7
Q9 3.43
Q10 30.2
Q12 17.1
Q11 49.2
Q9 3.97
Q10 42.3
Q12 16.1
Q11 37.7
Q9 3.38
Q10 46.2
Q12 12.4
Q11 38.0
Count
Comp-FL12-A :: PC7-A

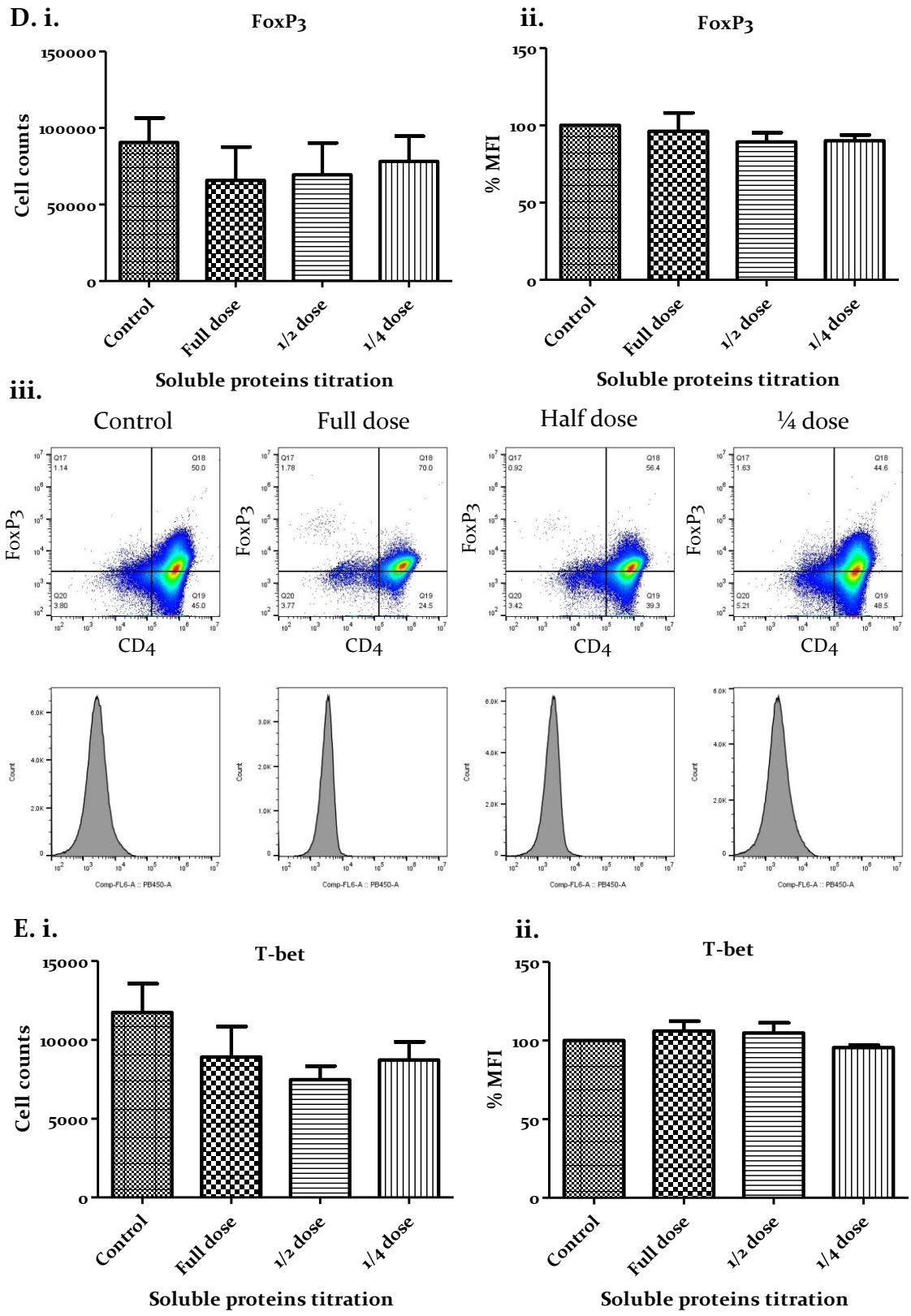
D. i.
FoxP3
Cell counts
150000
100000
50000
0
Control
Full dose
1/2 dose
1/4 dose
Soluble proteins titration
ii.
FoxP3
% MFI
150
100
50
0
Control
Full dose
1/2 dose
1/4 dose
Soluble proteins titration
iii.
Control
Full dose
Half dose
¼ dose
FoxP3
CD4
Q17 1.14
Q18 50.0
Q20 3.80
Q19 45.0
Q17 1.78
Q18 70.0
Q20 3.77
Q19 24.5
Q17 0.92
Q18 56.4
Q20 3.42
Q19 39.3
Q17 1.63
Q18 44.6
Q20 5.21
Q19 48.5
Count
Comp-FL6-A :: PB450-A
E. i.
T-bet
Cell counts
15000
10000
5000
0
Control
Full dose
1/2 dose
1/4 dose
Soluble proteins titration
ii.
T-bet
% MFI
150
100
50
0
Control
Full dose
1/2 dose
1/4 dose
Soluble proteins titration

iii.

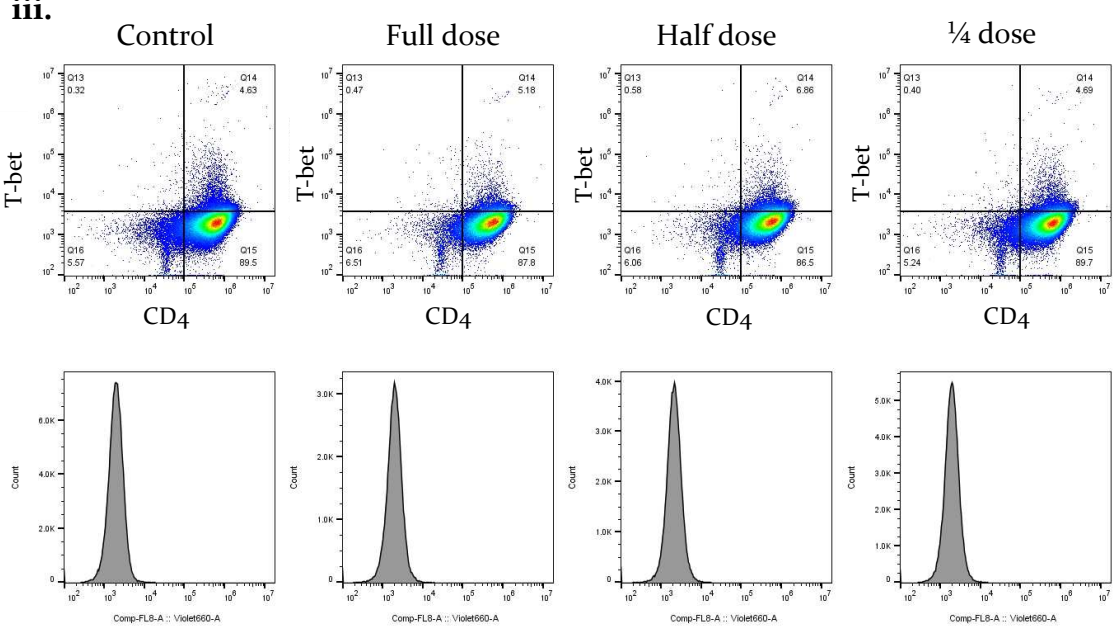

Figure 38. The transcription factors expression levels upon the titrated tumour Soluble proteins.

CD4+ T cells were seeded with CD3/CD28 Human T-activator Dynabeads (ratio 1:2) alone or in the presence of indicated tumour Soluble protein ratios. 5 days later, cells were stained for intracellular (A) GATA-3, (B) RoRγT, (C) Bcl-6, (D) FoxP3, (E) T-bet antibodies and anti-human CD4.

A.i.-E.i Graphs show the effect in cell counts expression of each factor in response to different concentrations of GBM-derived soluble proteins. A.ii-E.ii Graphs represent the MFI related to the control condition where no soluble proteins were added on the cultures in a percentage format. A.iii-E.iii Dot plots representative for the above descriptions are presented for each condition and transcription factor

Data is representative of 4 experiments (n=4). Bars represent means and SEM is shown for 4 experiments. *, p = <0.05.

3.3.9 Assessment of Immunosuppressive effect of candidate proteins on T cells

The protein profile of EVs and soluble factors in the secretome of 79 GBM patients was revealed following high throughput MS and analysed for identification of proteins that mediate the receptor-ligand immunosuppression in the TME, as described in previous chapters. Here, in order to assess the ability of chosen proteins to suppress T cell responses, ICAM-1, CD47, THBS1 and MIF were added to isolated CD4+ T cells in indicated concentrations suggested in the literature.

CD4+ T cells sorted from peripheral blood of healthy human donors and cultured, with CD3/CD28 Dynabeads in descending concentrations of ICAM-1, CD47, THBS1 or MIF for 5 days. Then, the total cell volume was harvested and stained for CD4 and the T cell responses were assessed by implementing flow cytometry.

No significant effect was reported in the CD4+ T cell counts after treatment with the immunosuppressive protein candidates (Fig. 39). The numbers of cells were slightly elevated as a response to the ¼ dose treatment of each protein. However, cell counts in Half and Full dose were equal or borderline lower than the control CD4+ cells that received no protein treatment.

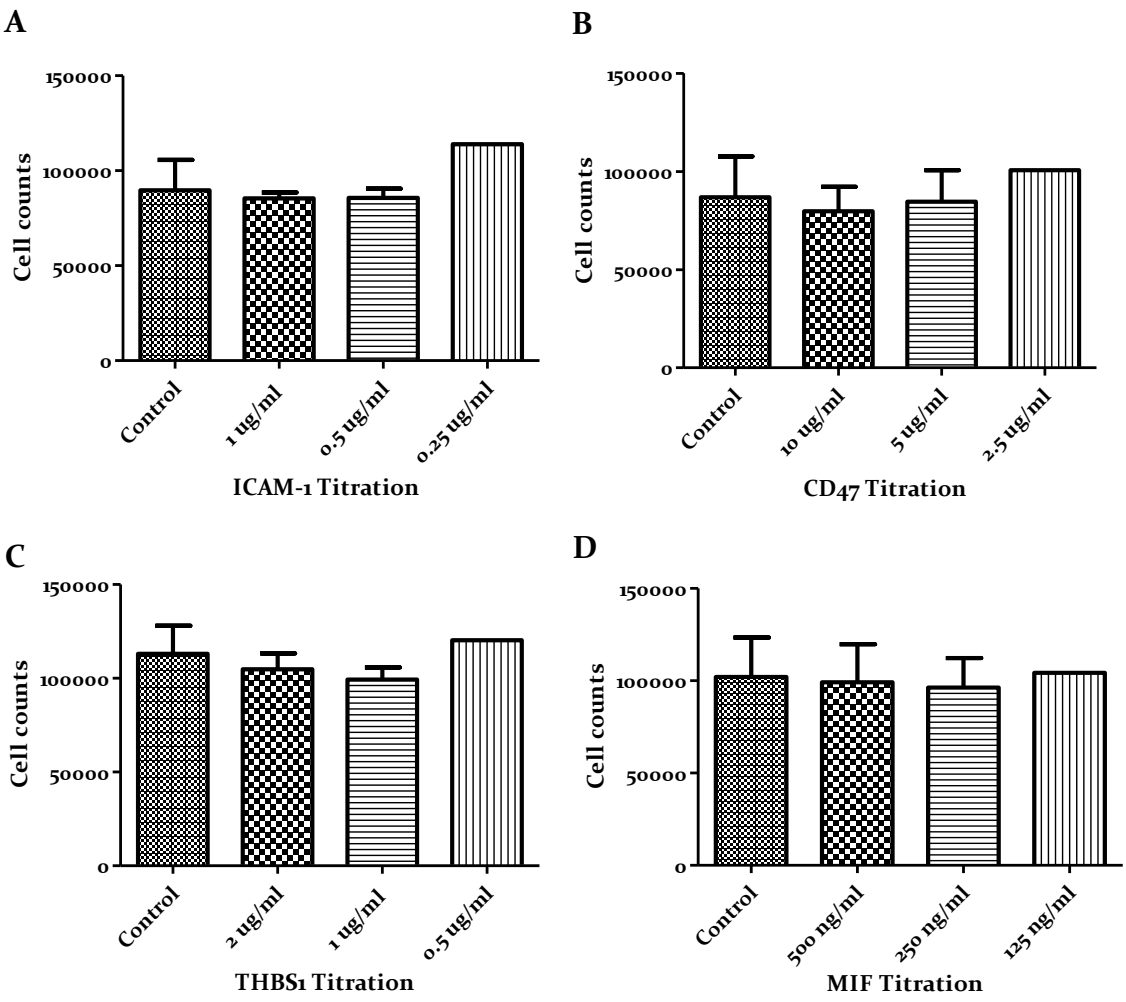
A
150000
100000
50000
0
Cell counts
Control
1 ug/ml
0.5 ug/ml
0.25 ug/ml
ICAM-1 Titration
B
150000
100000
50000
0
Cell counts
Control
10 ug/ml
5 ug/ml
2.5 ug/ml
CD47 Titration
C
150000
100000
50000
0
Cell counts
Control
2 ug/ml
1 ug/ml
0.5 ug/ml
THBS1 Titration
D
150000
100000
50000
0
Cell counts
Control
500 ng/ml
250 ng/ml
125 ng/ml
MIF Titration

E. i.

ICAM-1

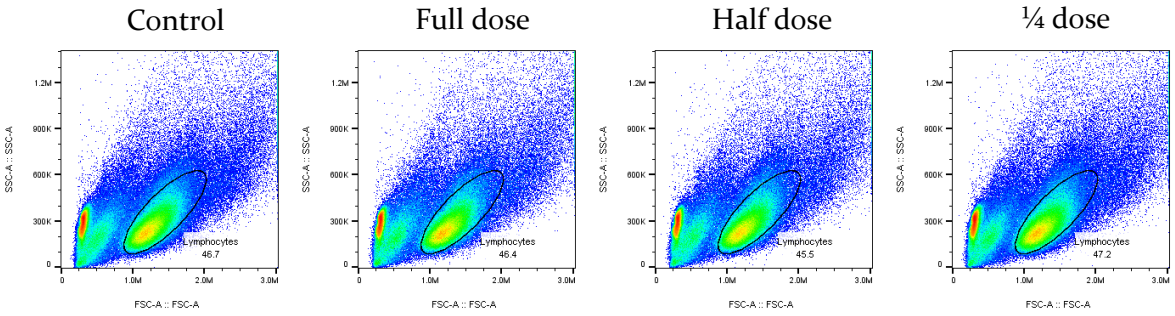
Control
Full dose
Half dose
¼ dose
SSC-A :: SSC-A
FSC-A :: FSC-A
Lymphocytes
46.7
46.4
45.5
47.2

E. ii.

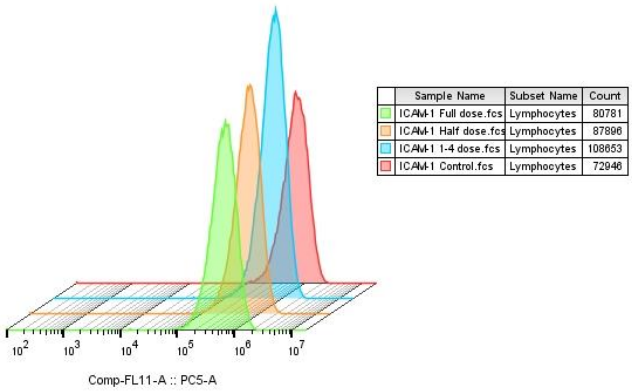

F. i. **CD47**

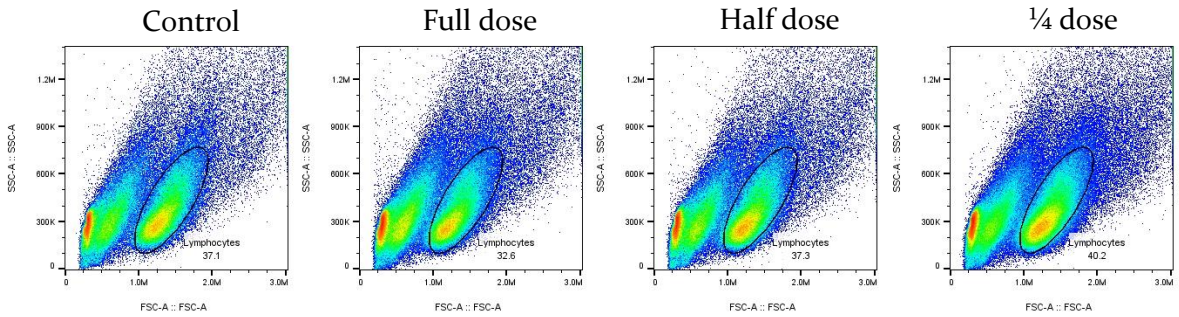

F. ii.

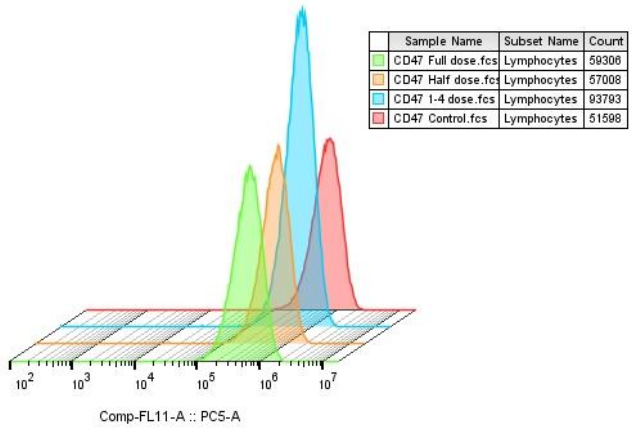

G. i. **THBS1**

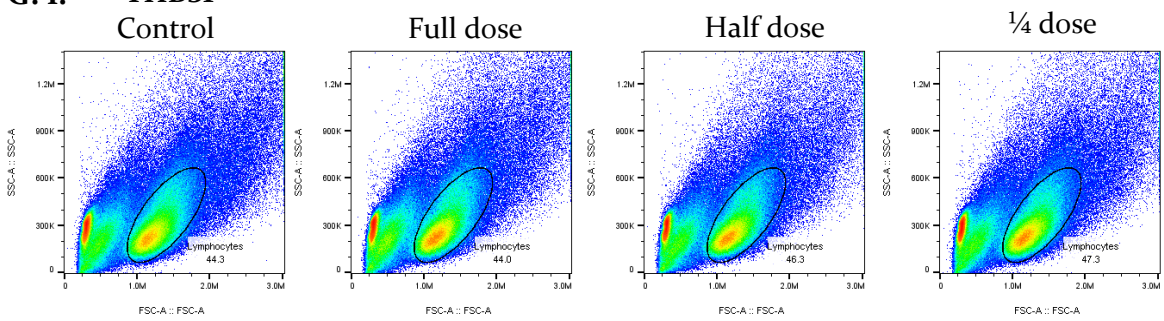

G. ii.

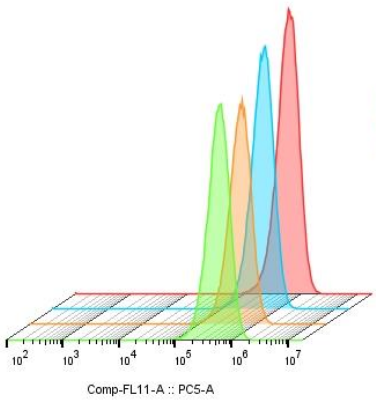

	Sample Name	Subset Name	Count
	THBS1 Full dose.fcs	Lymphocytes	118487
	THBS1 Half dose.fcs	Lymphocytes	111223
	THBS1 1-4 dose (only CD4).fcs	Lymphocytes	133626
	THBS1 Control.fcs	Lymphocytes	141821

H. i. **MIF**

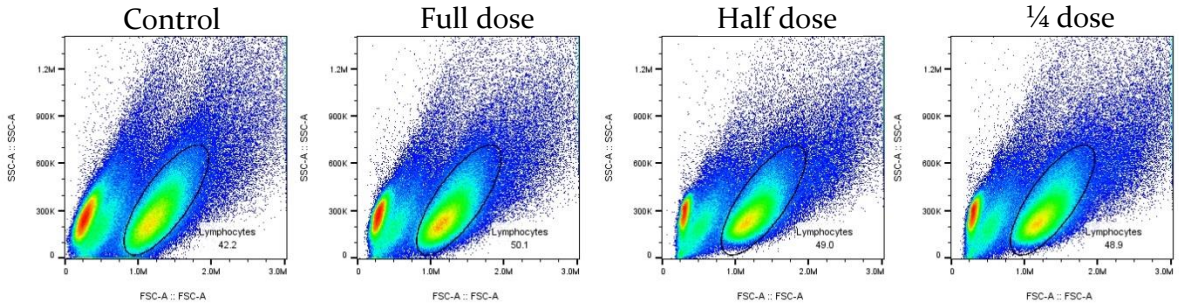

H. ii.

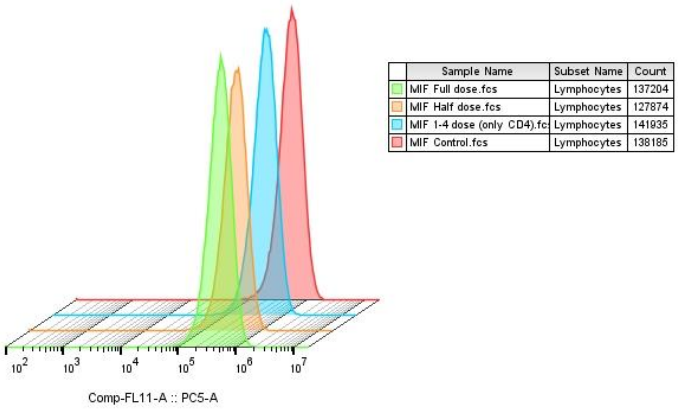

Figure 39. The effect of protein candidates on CD4+ cell counts.

Isolated CD4+ T cells were cultured with CD3/CD28 Human T-activator Dynabeads alone or in the presence of indicated protein candidate concentrations. After 5 days, cells were stained for surface CD4 mAb.

(A-D) Graphs show the change in cell numbers upon titration of (A) ICAM-1, (B) CD47, (C) THBS1, (D) MIF.

(E.i.-H-i) Representative dot plots and (Eii-H.ii) Stagger histograms show the lymphocytes, when cultured alone (left panel), or in the presence of the proteins.

Data is representative of 3 experiments (n=3).

CHAPTER 4 – DISCUSSION

4.1 OPTIMISATION PROTOCOL

Glioblastoma Multiforme tumours use multiple mechanisms to eradicate immune responses. GBM extracellular vesicles play a pivotal role in cell-to-cell communication and are known to promote tumour progression (Maia et al., 2018), but little is known about the mechanisms and the receptor-ligand interactions they ustilise to modulate the immune system towards immunosuppression. The overall aim of this project is therefore to identify EV-driven immunosuppressive mechanisms that can be targeted therapeutically to promote anti-GBM immune responses in patients. In order to identify EV-bound immunosuppressive candidates, work within this report has focused on devising and optimising an EV isolation strategy suitable for downstream mass spectrometric analyses.

In the present study, glioblastoma fresh biopsies from the patients were transferred into transport medium. Using transport medium, the release of the EVs from the tumour was confirmed. This finding suggests that transport medium could serve as a liquid biopsy for diagnostic reasons in the future and provides insight for the development of new therapeutic methods. We first studied the size and concentration of the extracellular vesicles derived from glioblastoma fresh biopsies in the tumour samples using Tunable Resistive Pulse Sensing (TRPS) technology provided by the qNano system. Numerous of extracellular vesicles were found to be released in the tumour secretome, as expected, since the number of EVs is strongly correlated with the aggressiveness of the disease (Hellwinkel et al., 2016). TRPS was chosen because it is accurate, reproducible, is high-throughput and, critically when dealing with patient samples of limited availability, it requires only a small sample volume. We found that most EVs were 70-300 nm and had an average diameter of 147 nm, and a mode diameter of 103 nm. TRPS was also used to determine the profile of the EVs- contained in U251 supernatants for optimisation reasons. For these samples, the average EV size was 180 nm, whilst the mode was 110 nm. The two test samples had approximately the same size. Thus, EVs from

U251 supernatants have similar size characteristics with those derived from newly resected tumours, and were chosen as a model system for GBM EVs for further experimental optimisation. Their small size reveals that the majority are exosomes, which is consistent with the study conducted by Ricklefs and colleagues (2018), who showed that the average EV diameter of Glioblastoma stem cells (GSCs) EVs is 120-130 nm. In another study, Hallal et al. (2019), confirmed a distribution of EVs size between 30–150 nm, when derived from GBM stem-like cell line, whilst a slightly smaller mode size was reported for the EVs from a variety of GBM cell lines, such as 86.6 nm for LN18, 86.3 nm for U87, 94.6 nm for U118, 80.48 nm for G166 and 81.5 nm for GS090 (Lane et al., 2019).

To examine the whole secretome, we also aimed to undertake mass spectrometric analyses of the non-EV-bound soluble protein fraction isolated from our GBM tumour samples. This is because soluble proteins are critical effectors of immune responses and are known to modulate immune cell activity. We therefore, as a first step, determined the soluble protein concentration in our biopsy supernatant samples using the Bradford assay. The colorimetric Bradford protein assay detects the shift in absorbance, when the dye Coomassie Brilliant Blue G-250 binds to proteins in solution that have been denatured. We noted a significant correlation between EV and soluble protein concentration, which means that the samples with the highest concentrations of EVs, as have been determined in the previous step, also demonstrated the highest in-solution protein content.

In order to investigate the protein profile of the extracellular vesicles in Glioblastoma and the potential ligand-receptor interactions that lead to suppression of anti-tumour immunity, an effective method for EV isolation and separation from soluble proteins needed to be established. The most widespread method for EV isolation for years has been ultracentrifugation, which applies a centrifugal force to separate biological materials based on their density. However,

ultracentrifugation has a number of significant limitations including a lack of EV purity and EV aggregation and fusion, altering their morphologic integrity (Stranska et al., 2018), which in the case of our study that investigates the effect of EVs and proteins in solution separately was a major drawback. As an alternative approach, we tested a recently developed technique for EV isolation based on Size Exclusion Chromatography (SEC). These qEV columns utilise a gel with pores of 70 nm in diameter that function as a filter (Ohlendieck & Harding, 2018). Proteins enter the filter pores whilst extracellular vesicles, which are larger than 70nm, are excluded from the pores and are rapidly eluted. This method efficiently resulted in an EV-enriched fraction of 3.5 mL and a soluble protein fraction of 9 mL. To validate this method, we examined the two fractions for the presence of EVs and confirmed that the vast majority were indeed in the extracellular vesicle fraction, with negligible contamination in the soluble protein fraction. After qEV isolation, the average recovery rate was approximately 40% for a variety of samples. However, critically, the average EV diameter was 145 nm. Thus, although the qEV SEC columns afford fairly poor recovery, they do not alter EV morphological characteristics or produce aggregates.

Due to the fact that some of the samples have initial volumes higher than the qEV column maximum loading volume (which is up to 2 mL), it was necessary to utilise an effective method of sample concentration prior to EV isolation. After qEV the two fractions need to be concentrated, in order to be loaded on the gel. The efficiency of the method after several steps (qEV SEC, sample concentration before and after qEV) was tested based on the total protein concentration, as it was determined by NanoDrop. In order to ensure a good recovery, centrifugal filters of 10 kDa was decided to be used for the EV fraction based on their size and 3kDa maximum pore size for the soluble protein fraction concentration.

After establishing a workflow for EV isolation, we used U251 supernatant-derived samples at a range of concentrations to establish the concentration required for mass spectrometry. Four EV samples were constructed from the U251 supernatants containing: the minimum concentration of EVs that was detected in the tumour samples, twice the minimum, three times the minimum and one sample representing the average concentration. In-gel digestion was performed for the four EV fractions. As expected, Mascot Daemon analysis recognised many more proteins in the sample representing the average EV concentration than in those representing the minimum, 2x or 3x. However, analysis with Progenesis QI software revealed almost the same number of proteins across all fractions. These differences are due to the way each piece of software processes the data. Mascot analyses each sample in isolation and applies a threshold below which very low abundance proteins are not positively identified. Progenesis further analyses these low abundance proteins to determine whether they are present in comparison samples, and if so, they are reported as positively identified, thereby increasing the total number of proteins reported. In total 354 unique proteins were identified across the EV fractions, with EV protein markers among them, such as CD81 and proteins of the 14-3-3 pathway (Yáñez-Mó et al., 2015). Based on these results, we decided to prepare the tumour samples at an initial EV concentration representing the average, as this resulted in the greatest number of positively identified proteins.

Different methods for protein digestion were tried using U251 supernatants, in order to evaluate the most appropriate one for cleaner samples, good result quality and high peptide detection levels. In-gel digestion was considered for the proteins, whilst for the EV fractions also in-solution digestion using trypsin or SMART Digest™ Trypsin Kit with Magnetic Bulk Resin option with SOLAμ/collection plate (ThermoFisher Scientific, UK) were under investigation. The pilot samples were analysed by Mass spectrometry. The results revealed that in-gel digestion was for both the most effective one, since more proteins were identified using the pilot U251-supernatant derived

sample and, therefore, all tumour samples were prepared according to be proceeded to the mass spectrometer.

4.2 ANALYSIS OF THE DATA COLLECTED FROM MASS SPECTROMETRY - PROTEOMICS

GBM tumour-derived samples from 79 patients that had surgical resection were prepared for Mass spectrometric analysis, after extracellular vesicles and soluble protein fractions had been separated. The results were collected and analysed by Mascot Daemon Software. Proteomic analysis revealed a detailed and holistic protein profile of GBM EVs and soluble proteins. For the protein fraction, 1337 proteins were positively identified, whilst more almost 1397 proteins were detected in the EVs fraction. 395 of the proteins identified were common in both fractions and the rest are unique. Additionally, EV surface markers, such as CD81, CD63 and CD9 and 14-3-3 proteins (Fernandes et al., 2017) were detected again and only into the extracellular vesicle fraction. The above results show that the qEV columns can successfully separate the secretome into two fractions not fully overlapped. According to Vesiclepedia, the maximum protein ID number associated with Glioblastoma that has been detected in previous studies is 309 and the corresponding for soluble proteins is 601 (Heroux et al., 2014). That proves that the approach used here is more reliable and sensitive, since it even identifies proteins with low expression levels. In addition, proteins that have never been linked to Glioblastoma have also been detected. Using samples that derive directly from the actual tumour offers the advantage of detecting proteins that are present in the tumour microenvironment, but are not exclusively secreted by the cancer cells. Immune cells such as antigen presenting cells lke dendritic cells or macrophages constitute approximately 50% of the cells in the TME and definitely participate in the configuration of the protein milieu (Hambardzumyan et al., 2016). In previous studies, the experiments were performed on

Glioblastoma cell lines or primary cell cultures. However, these do not completely represent the diverse cells in the tumour microenvironment, but they are focused instead on the actual cancer cells. Since almost half of the tumour, though, consists of immune cells, these should not be excluded from the research. Another published study used homogenised GBM tissue biopsy (Vesiclepedia). This can include all cells in the TME, nonetheless the purity of the samples is lower, since more intracellular components may be included in the analysis due to the honogenisation.

The dataset was analysed using a number of online available tools. Each of them runs the input sequences against specific databases, which result in outputs that may vary. Database resources provide information about biological functions of the proteins, intracellular signalling pathways, the compartment of the cell that are expressed, protein-protein interaction network, gene ontologies and superfamilies, protein structures and more. Here, we show how the two gene datasets were analysed in a different way. For the extracellular vesicle fraction, the analysis was focused in initially identifying all those proteins that are expressed on the membrane of cells or EVs, in order to detect potential receptor-ligand interactions that can easily be targeted therapeutically by using antibodies that bind on the cell surface. However, different softwares screen the dataset against different databases, so the results may vary. For this reason, more than one tools were stratified for the analysis.

The first step in the process of downsizing the list of proteins was to identify those that are expressed in at least 80% of the samples. The rationale for this is because we are aiming in a widely applicable treatment that can be effective in a lot of patients. However, most of the proteins were expressed in 80% of the samples or more, with 1201 proteins fitting this criteria. Using PANTHER database to group the genes according to their cellular compartment, the list of genes/proteins expressed on the plasma membrane was narrowed down to 120. According to FunRich classification

against FunRich database, the amount of gene IDs was 59, according to DAVID, which runs the dataset against Uniprot database, the number of proteins related to the membrane was 158, whilst STRING identified 160 proteins. Considerable redundancy is observed in the output though, since each one of the proteins can be associated with more than one functions or subcellular components, but also because different terms can be used to ultimately describe the same thing (Hutchins, 2014). From the total proteins, some of them were overlapped and given as a positive result from more than one databases. Therefore, the total number of proteins that were expressed on the surface, after considering and excluding the overlaps was 307. Meta-analysis on those and search through the literature for structural details and localisation, some of the proteins were excluded, since they were actually expressed on the cytoplasmic side of the plasma membrane or just interacting with membrane proteins. After that clearance step, the protein IDs with a true positive correlation with the extracellular side of the plasma/vesicle membrane were 187. The corresponding gene IDs were added again on the databases and this time categorised based on their biological function. Among the 187 membrane proteins, 51 were the ones that may play an immunosuppressive role through ligand-receptor interactions. Three of the proteins were chosen as the best candidates, after extensive search in the literature about the way they participate in immune responses regarding the signalling pathways, the interactions with other proteins and most importantly any known implications in cancer and the effect on T cells. A list of potential culprits for GBM pathogenesis was constructed and more details are given below.

The gene list identified in the fraction with the proteins in solution was analysed based on the biological processes that the corresponding proteins are implicated, without a prior need to detect which proteins are expressed on the cell membrane. First, 1229 proteins were found to be expressed

in 80% of the samples. Then, these proteins were grouped with PANTHER classification system selecting the group of interest, which in this case was under the label the ''immune system process''. The subcategories are revealed with the number and the ID of the genes related to each. Similarly working, the soluble proteins with potential suppressive immunological function were identified using FunRich, DAVID and STRING. The total number of proteins that was linked to immune responses, after removing the ones given as a positive result from more than one databases was 292. From this step and downstream, reviewing proteins through literature was the only indicator of which ones can be targeted therapeutically in an attempt to restore immunosuppression of T cells in the tumour microenvironment.

The one protein selected in the current project to be assessed regarding its effect on CD4+ T cell responses and phenotype was MIF.

FunRich outnumbered PANTHER in subcategories used in each case, offering more detailed information for the function of the protein or where it can be found. Also, analysis with FunRich showed that the proteins in both EV and soluble protein fractions were distributed into categories following almost the same pattern with each other. The percentages of proteins representing each category appeared to be similarly high or low in the two fractions. However, more proteins from the soluble protein fraction had a metabolic-related activity and participating in energy pathways. EV protein content was more related to immune responses and cell growth and maintenance. This comes in agreement with another study conducted by Setti and his colleagues (2015), who have shown that EVs in GBM induce cell growth and proliferation in *in vitro* and *in vivo* models in a pathway dependent on CLIC-1 expression (Setti et al., 2015). Furthermore, EVs are part of the maintenance of glioma stem cells properties, they contribute to tumour growth and proliferation through anti-angiogenic and growth factors they contain (Graner, 2019; Yekula et al., 2019).

Considerable redundancy is observed in the output though, since each one of the proteins can be associated with more than one functions or subcellular components, but also because different annotation is given to describe actually the same term (Hutchins, 2014).

4.3 MOLECULAR PROFILING OF THE TUMOUR SAMPLES

The molecular subtyping of the samples was performed by our collaborators at Wolverhampton University (UK) by Dr Farjana Rowther, who implemented RQ-PCR analysis on them based signature gene alterations, as described by Verhaak and his colleagues in 2010. The genes under investigation were EGFR, PDGFR, CDKN2A, NF1, TP53 and IDH1, which are growth factors, tumour suppression genes implicating in cell cycle and DNA damage/repair mechanisms. The original classification by Verhaak divides Glioblastoma Multiforme tumours into 4 molecular subtypes, Classical, Proneural, Mesenchymal and Neural based on combinations of high or low expression of the above mentioned genes or mutations on them. Neural subtype, however, was identified as contaminated tissue. In our study, categorising the samples available was not clear, since some of the genes expression was not particularly high or low, but median and, also, different combinations were reported. However, something like this should not be surprising, since heterogeneity is one of the hallmarks in Glioblastoma, with tumours consisting of heterogeneous cells between different focuses or even within the same focus. Therefore, in an attempt to do meta-analysis on what it was initially observed, the samples were given the names of group with the corresponding signatures reported. Nonetheless, in order to keep our study unbiased and not force the samples to fit in groups established more than a decade ago, we decided to keep them distinct. Thus, 7 subtypes were identified, three of which were the Classical, Proneural and Mesenchymal, as has been

described before. The Neural subtype did not constitute one of the options, since no neural markers were including in the experiment performance.

So, the Classical subtype was classified based on EGFRVIII expression and/or total EGFR expression, combined with high NF1 expression and low CDKN2A. The Proneural identification was based on detection of the IDH1 R132H mutation, and/or TP53 GOF mutation, high PDGFRA expression with high or median NF1 expression and high/low CDKN2A expression. The Mesenchymal type was classified based on low NF1 expression and the mutation in TP53 gene.

The new classification emerged as a need due to missing information. Classical* subtype was identified based on high NF1 expression and low CDKN2A. As it is obvious, the same pattern is followed in the Classical subtype, but in the case of the first one no amplification was observed in the EGFR gene, which is the major characteristic of the Classical type. Accordingly, the rest of the new subtypes were distinguished from the already known ones. The Proneural* was lacking the amplified expression of PDGFR gene, but since ultimately it was only one sample falling into this category, it was grouped as the original Proneural. The ''Classical and Proneural'' subclass had characteristics from both namely mentioned groups, showing high EGFR and PDGFR expression levels, high NF1 and either high or low CDKN2A. The ''Classical and Proneural *''is recognised due to absence of EGFR and PDGFR amplification, medium NF1 had low CDKN2A expression.

A number of samples were not available for RQ-PCR. However, some of these samples were included in the Mass Spectrometric analysis for their proteomic content. From the rest, the majority (17) were identified as the original Proneural subtype, the new ''Classical and Proneural *'' (13) and the original Verhaak-Classical (11). That comes into agreement with the literature, as most of the tumours were Proneural (Phillips et al., 2006; Verhaak et al., 2010). However, Proneural was the most common subtype among the secondary GBM lesions, but we cannot confirm or reject this,

since no further information or background data regarding the patient donors were accessible. EGFR is one of the most mutated genes in GBM, so it was expected a lot of cases to be classified as the Classical subtype. Mesenchymal was reported in the literature as the most frequent primary GBM tumour arising de novo, but in our study, three were the samples identified as mesenchymal.

The protein IDs as identified in each molecular subtype were added on the Functional Enrichment Tool with the average normalised abundancy that was reported per subtype, in order to be categorised according to the cellular compartment of expression or their biological functions and be tested for similarities or deviations amongst the subclasses. No significant differences were observed the amount of proteins representing each category. Proteins in the EVs fractions were implicating, as expected, in transport and besides that, in cell growth and maintenance, as mentioned in previous chapter and signal transduction.

A more solid analysis was undertaken using XLSTAT to detect if the proteins of the different subtypes follow any particular trends and expression patterns and how they overlap (in a 95% confidence score). Most of the subtypes, original and new, were overlapped, confirming that the profiles are not quite distinct one from another. Moreover, our new labelled subtype ''Classical and Proneural*'' showed a diverse profile from subtypes, such as Mesenchymal, Classical* and Proneural. That was even more obvious, when the analysis was focused on the protein IDs that were in the 99% Confidence interval according to ANOVA, where there was no overlap with the other subtypes and the identification of the particular subclass was based on the C9 and ECH1 co-expression. Since this protein was strongly correlated with the ''Classical and Proneural*'' profile, it can serve as a new biomarker in the subtype recognition and classification. Nine were the proteins, which following various combinations, could be indicating the presence of specific GBM subtypes. The disadvantage of analysing the dataset from 95% to 99% confidence score is that from 49

proteins that we had in the first case, we ended up with 9 in the latter one. Since a lot of the ''pointing'' subtype markers were excluded in the second case, the different subclasses showed a bigger overlap. However, with nine proteins we are narrowing down the screening dataset to the most necessary and valuable proteins. Although several studies have identified protein biomarkers of Glioblastoma (Heroux et al., 2014; Elstner et al., 2011; Ghantasala et al., 2020; Popescu et al., 2014), this is the first study identified protein biomarkers specific for each molecular subtype.

Similarly working for the soluble proteins fraction, after adding the dataset on FunRich with the proteins expressed divided according to their molecular profile and abundance, the component of expression and the biological processes they are part of revealed. No differences were observed again among the subtypes regarding the portion of the total amount being represented by each subcategory. The same amount of proteins and most importantly in most cases the same proteins were present in all subtypes. A higher percentage than the EVs was implicated in signal transduction process, something that comes into agreement with our previous observations.

XLSTAT analysis in the 99% confidence interval, which gave as a positive result 30 protein IDs, revealed a big overlap among the subtypes. The Mesenchymal subtype again seemed to be distinct from the Classical* and the ''Classical and Proneural'' one. The Mesenchymal subtype was classified based on the expression of RKP2, IBP2, OSTP and YBOX. The ''Classical and Proneural'' is characterised by the presence of BAX and EIF3F, whilst for the Classical* detection several proteins are participating, such as CATD, TAGL3, 14-3-3G, PTGDS, ENOG, etc. The Proneural type had a very broad profile with proteins form almost all the other subtypes being present here.

The key proteins were added back on the FunRich Tool to get more information about the pathways they are implicated. In the case of EVs fraction, proteins were mostly participating in cell

communication and signal transduction, whilst for the proteins in solution the pathways that were upregulated were the energy and metabolism.

The datasets received from the Mass Spectrometric analysis and the molecular subtyping, if studied extensively, can extrapolate valuable information for the disease diagnosis and treatment improvement. Here, we have reported new potential protein biomarkers for each of our GBM subtype, which if we take into consideration the capacity of extracellular vesicles to serve as a liquid biopsy, could offer a time-effective, alternative diagnostic tool. The list of protein IDs was extensive and the limited time for the current project could not be sufficient to study each of the hundreds of proteins that were detected for its immunosuppressive properties. Four of them were chosen though to be investigated in further experimental set-ups, in order to evaluate their ability in inhibiting CD_4+ T cell responses and altering their marker and cytokine secretion profile. Although we chose some of them, the full list of proteins is available for further study in the Appendix 3.

4.4 GBM EVs AND SOLUBLE PROTEIN – MEDIATED SUPPRESSION

Initially, we tested the ability of soluble proteins and EVs to affect T cell suppression. Proteins and extracellular vesicles derived from U251 concentrated supernatant. The results, were assayed once, since being the model sample and revealed that both fractions have immunosuppressive capacity on conventional T cells at high doses.

Following this, the isolated extracellular vesicles from the patients were added in descending concentrations to the culture with the stimulated CD4+ T cells. The Full and Half dose EVs had resulted in a significant reduction in T cell number to 48,8% and 60% (p=0.0028, **) of the maximum response observed in the control group, where no EVs were present. This comes in agreement with a number of other studies, where CD73+ GBM cell-derived EVs could be uptaken up by T-lymphocytes and inhibit the clonal proliferation (Wang et al., 2021). Hellwinkel el al. (2016) and Domenis et al. (2017) reported that exposure of CD4+ T cells, when within PBMCs, to GSCs-derived exosomes from GBM patients resulted in notably impaired T cell proliferation. Interestingly, in the latter study, when isolated CD4+ T cells were exposed to the exosomes, they were activated more even in the absence of CD3/CD28 stimulation and they were inducing the expression of CD25 marker on CD4+ T cells, suggesting that maybe EVs are providing the cells with some co-stimulatory molecules, such as CD80/86 or ICOS. (Domenis et al., 2017). Moreover, RIcklefs reported the inhibition of CD4+ and CD8+ cells by GSCs GBM EVs (Ricklefs et al., 2018), which contradicts the Domenis' group study, who mentioned no inhibition in the CD8+ population. Ricklefs and colleagues showed that the T cell suppression is mediated by PD-L1 is expressed on a number of stem cells and by both PD-L1high and PD-L1low EVs by directly suppressing TCR-stimulated T cells. However, PD-L1 blockade can only partially restore T cell activity and only after exposure to PD-L1 high EVs. Thus, there are clearly other important ligands implicated that have

not yet been identified (Ricklefs et al., 2018). In contrast to our work, the majority of the studies did not use EVs isolated directly from the tumour, but from GBM cells that have been cultured in stem cell enrichment conditions, except Domenis' group, who isolated EVs from patients' plasma. It is not clear what effect culture conditions have on protein expression in these cells, so it remains unclear whether their study accurately represents the GBM secretome. Moreover, Ricklefs and colleagues isolated EVs by ultracentrifugation and not qEV SEC columns, so it is unclear whether the *in vitro* activity of these EVs has been altered by morphological changes. Ricklefs et al., did not provide co-stimulation in their T cell assays, which suggests that the responses would be limited to memory T cells. Of major significance, this study noted that PD-L1 was only found on EVs from a subset of patients, most commonly of the mesenchymal type. Our proteomic analyses on U251 supernatant and on GBM tumour biopsies did not identify PD-L1 on EVs, which is interesting, because it indicates that other mediators of suppression must be at play.

Exposure of monocytes to Glioblastoma EVs can alter their expression profile in terms of cell surface markers and secretion of cytokines (Vrij et al., 2015). Oushy et al. (2018) showed that astrocytes elevated their cytokine production and acquired a more pro-tumoural profile after treatment with glioma EVs (Oushy et al., 2018). It has been an interest by other groups to investigate the effect of GBM EVs on monocytes, their turning into TAMs and how this is reflected on the phenotype (Vrij et al., 2015; Broekman et al., 2018). Glioblastoma EVs have been linked to inducing Th2 responses and production, M2 macrophage polarization and pushing NK cells towards type II NK with protumourigenic potency (Broekman et al., 2018). However, here we are going to report the changes on specific markers of CD4+ T cell subset.

TIM-3 molecule is a marker of T cell exhaustion and acts as an immune checkpoint inhibitory signal selectively expressed on the surface of IFNγ-producing CD4+ Th1 and CD8+ T cells, FoxP3+ Treg

cells, macrophages and DCs, which upon binding to its ligands can induce suppression (Das et al., 2017). TIM-3 expression was found to be upregulated in glioma patients in glioma cells, GSCs and Tregs (Li et al., 2017), in monocytes and TAMS in other cancer types, such as gastric cancer (Q. Wang et al., 2017) and was linked with enhanced dysfunction of CD4+ T cells. EVs derived from GBM patients' CSF contained one of TIM-3 ligands, galectin-9, which after binding to TIM-3 downregulated DC-mediated antigen presentation and CD8+ T cell responses. However, different roles have been reported for TIM-3 in different immune cell populations. It has been suggested that TIM-3-LGALS9 interaction results in Th cell apoptosis, and CD8+ exhaustion, but can stimulate CD4+ and NK T cells (M. Wang et al., 2020). Here, we observed that the amount of CD4+ T cells expressing the marker was decreased in ascending EVs concentration. However, the fluorescence intensity of the marker was almost the same as the control group, where no EVs were added on the CD4+ T cells, whilst a very small increase was shown in when cells were treated with ¼ of the EV concentration. The fact that fewer cells express the exhaustion marker when the tumour EVs are added can be explained by the fact that the survival rate of the CD4+ T cells in response to Glioblastoma was lowered and the cells were lacking the ability to proliferate. Nonetheless, the marker was expressed in increased amounts per cell, whilst in low concentration of EVs, where the CD4+ cells have high survival rate, the MFI was even more upregulated than the control (Figure 32A). High expression of TIM-3 would imply suppressed T cell functions and promotion of tumour escape and, in patients, it was linked with poor prognosis (G. Li et al., 2017).

PD-L1 is a well-known and studied exhaustion marker and immune checkpoint inhibitor, which when binding to its receptor PD-1, expressed on T cells, induces apoptosis. PD-1/PD-L1 pathway is upregulated in a several types of cancer and its presence is correlated with poor survival, such as in

melanoma, lung, gastric cancer and glioma (Dart et al., 2021; Saito et al., 2019; Scheffel et al., 2021). Treatment of CD4+ T cells with extracellular vesicles from the tumour samples showed to decrease the cell counts expressing the specific marker in high doses of EVs. However, the MFI showed higher levels of expression per cell by almost 15% in the Full dose and 28% in the Half dose. This result did not come as a surprise, since we already have mentioned the PD-L1 elevated expression levels on GBM cells and EVs by Ricklefs et al. and their immunosuppressive effect on T cells (Ricklefs et al., 2018). PD-1 has the same response as TIM-3 in glioma suppressing activation signalling in macrophages and T cells and when co-expressed, the cells had a more exhausted phenotype (Li et al., 2017). In another study, it was showed that PD-1+TIM3+ CD4 T effector cells were enriched in tumour, a profile that matches the one we identified, were dysfunctional in terms of proliferation, and co-blockade of PD-1 and TIM-3 could be more beneficial than anti-PD-1 monotherapy (Goods et al., 2017).

ICOS acts a costimulatory molecule for the activated T cells (CD4+, CD8) and promotes their proliferation, expansion and differentiation into Tfh cells. Co-stimulation through ICOS elevates secretion of IL-21, TNFα and IFNγ and CXCR5 cell surface expression (Amatore et al., 2020; Sainson et al., 2020). ICOS is also expressed on regulatory T cells and activation signal via this promotes effective CD4+ T cell inhibition and production of anti-inflammatory cytokines, such as IL-10, IL-4, IL-6 (Sainson et al., 2020). Here we noticed that the ICOS-expressing CD4+ T cell counts were lower, when the tumour EVs were introduced into the culture. However, those cells were expressing high amounts of this specific marker in Full dose (14% more than the control) and in Half dose EVs (8% more). This result may indicate an inducible level of ICOS by the CD4+ T cells over the basal as the tumour signals are enhanced, in an attempt to offer alternative signalling pathways to the cells and resist suppression. ICOS expression in Th can be stimulated by interaction of the T cell receptor with the peptides presented by DCs on MHC class II molecules (Bellinghausen et al., 2004).

Binding of ICOS with ICOSL, which is also expressed by glioma cells can increase CD4+ICOS+ and CD8+ cells, the ratio of T effector cells (Teff)/Tregs, enhance the IFNγ and TNFa production with enhanced efficacy when combined with anti-CTLA-4 treatment (Schreiner et al., 2003; Fan et al., 2014). Therefore, another explanation could be that the secretome contains factors that can induce ICOS expression augmenting the antitumour immune responses. However, engagement of ICOS-ICOSL, also, induces secretion of IL-4, IL-10 and promotes Treg-mediated immunosuppression (Schreiner et al., 2003), thus, ICOS role in cancer is dual and in some studies targeting of this pathway is utilised in immunotherapy.

Our results come in agreement with a recently published paper by Davidson et al (2020), where TILs isolated by patient tumours had elevated expression levels of both exhaustion and activation markers, such as PD-1, TIM-3 and ICOS.

The cytokines TGFβ, IL-21 and TNFα seemed to follow a similar pattern regarding their amounts of production by the CD4+ T cells. In all cases, the frequency of the positive cells secreting each one of those cytokines was lower, when high doses of Glioblastoma patients-derived EVs were added in the culture, but the levels of secretion according to Fluorescence excited by them was almost counterbalancing the control group. IFNγ secretion was impaired by 21%, after treatment with the Full EVs dose. TGFβ induction in CD4+ T cells has been reported by Donkor et al. (2012) to promote cancer development in mice prostate models, whilst blocking of TGFβ enhanced the CTL-mediated immune responses. That suggests that CD4+ T cells turn into a more immunosuppressive phenotype after exposure to EVs (Donkor et al., 2012). Nonetheless, TGFβ production in CD4+ cells, despite not being necessary, is capable for the induction of differentiation into Th17 cells (Ghoreschi et al., 2010), which implication in cancer has been controversial. Treatment with high doses of GBM patient EVs, as expected, lowered the frequency of the anti-tumoural IL-21, TNFα and IFNγ -

producing CD4+ T cells in the microenvironment. This comes into agreement with the literature, where significant reduction in the total amount of TNFα and IFNγ secretion was showed, as a response to GBM EV treatment (Domenis et al., 2017). In that study, Domenis and her group tested the effect of EVs on PBMCs utilising GSCs supernatant. However, further analysis to our results revealed that the although the proliferative CD4+ T cells producing these cytokines were fewer and the total cytokine production less than the control, we noticed that even after high doses of EVs treatment, the secretion level per cell was almost equally high as the control. Similar results, with the TNFα secretion from pericytes increasing after 72h of co-culture with Glioblastoma cell-derived supernatant was reported by Valdor et al. (2017), but without focusing on the specific effect of the EVs on them (Valdor et al., 2017). Additionally, Goods et al. (2017) found that CD4 effector cells from GBM patients proliferation was disrupted, but the cells were still capable of secreting pro-inflammatory cytokines, such as IFNγ. Altering in the endogenous production levels of IL-21 by CD4+ T cells, upon treatment with cancer cell lines or EVs has not been investigated in detail before though, in order to compare how the cytokine output was affected in other studies.

The frequency of the IL-13+ CD4+ T cells and its secretion levels were found to be significantly higher than the control and the Full dose groups, when ¼ EV dose was added in the culture. The survival rate of T effector cells in Full and Half dose of EVs was quite low, so the most possible explanation of the result would be that EVs stimulate the production of IL-13 in CD4+ T cells in low doses and tend to turn them into the anti-inflammatory Th2 phenotype, but in very high concentrations they are rather lethal for the cells. An increasing number of IL-13-producing peripheral blood CD4+ T cells was, also, reported in patients with T cell cutaneous lymphoma and leukaemia and it was linked with progression of the disease (Geskin et al., 2015). IL-13 production in CD4+ cells and NKT cells in breast cancer *in vitro* and *in vivo* models has been shown to drive tumour development by enhancing Th2 polarisation of DCs and suppression of CD8+ T cells. In

some cells, IL-13 production was also combined with IFNγ, showing plasticity in switching between Th1 and Th2 cell phenotype (Aspord et al., 2007). The same disruption on the immune surveillance was observed colon carcinoma lung metastasis and fibrosarcoma (Terabe et al., 2004), but no data are available about induction of IL-13 in CD4+ T cells by EVs in GBM.

IL-17 was expressed by fewer CD4+ T cells in all EVs conditions, but the levels of expression were higher than the control in the ¼ dose and almost equal to it in the higher doses. In a previous publication, where it was reported that the CD4+ IL-17A+ cell frequency is 17% in GBM. The levels of IL-17A expression, as measured by mRNA levels, were higher in astrocytoma and even more in oligodendroglioma and glioblastoma. However, IL-17A expression was similar to the T cell counts, after normalising it to the expression levels of CD3ε in mice models (Wainwright et al., 2010). Nonetheless, we should take into consideration the co-expression of other cytokines and transcription factors, since the CD4+IL-17+IFN-γ+ and CD4+IL-17+FoxP3+ populations were found increase by 10.5% and 22%, respectively, in glioma (Wainwright et al., 2010). The role of IL-17 in cancer has been contradictory. When co-expressed with IFNγ can shift the cells towards Th1 responses, but in several cases IL-17 has been promoting tumour growth and turn Th17 cells into a more Treg-related phenotype, when co-expressed with TGFβ, IL-6, IL-23 (Bettelli et al., 2006). Data for the direct effect of the GBM EVs though on IL-17 expression were not available for comparison.

The CD4+ T cell signature was tested upon exposure to different GBM-derived EV concentrations, also, in terms of the expression levels of the master regulators of transcription. GATA-3 drives Th cells towards Th2 responses, RORγt to a Th17 phenotype, Bcl6 transforms CD4+ cells to Tfh, T-bet to Th1 and FoxP3 to regulatory T cells. The expression of these transcription factors is usually mutually exclusive, but it has been reported that they can also be co-expressed offering an extent of plasticity to the cells (Fang & Zhu, 2017). As it was expected, the anti-inflammatory GATA-3 and

RORγt levels were high as the tumour was introduced to the CD4+ T cells, with RORγt being expressed 15% more than the control group at the Full dose, despite the RORγt+CD4+ cells at this condition being fewer by approximately 34%. Accordingly, FoxP3 expression was increased, whilst Bcl6 expression was impaired at the Full EV dose, but upregulated at lower doses. Interestingly, T-bet levels were upregulated in all conditions. After treatment with GBM neoantigen, CD4 Th cells showed an elevated expression of GATA-3, RORγt, and FoxP3, as we mentioned. However, the levels of T-bet were found to be downregulated (Johanns et al., 2019) unlike the results of our study. The intratumoural Th17 cells expressing IL-17 and IFNγ, as mentioned before, express not only RORγt, but also the Th1 master regulator, T-bet (Dobrzanski, 2013). At a recently published paper, Bcl6 expression levels has been shown to be significantly increased in peripheral T cells, after vaccination of melanoma patients (Czerwinska et al., 2020). This data is consistent with our observations, since in controlled low doses of the cancer antigen induction, Bcl6 expression seems to increase. Bcl6 enhanced expression, after patients' immunisation, and a concurrent upregulation of the TGFβ levels turned the naïve CD4+ T cells into Tfh cells, whilst increased TNFα turned them into Th effector or memory CD4+ cells (Czerwinska et al., 2020). In gastric and ovarian cancer patients, an increased density of infiltrated T-bet+ lymphocytes was reported in the tumour microenvironment, which was an indicator of better survival (Xu et al., 2017; Hennequin et al., 2016). In colorectal cancer, T cells in the tumour microenvironment that are positive for ICOS expression, produced increased levels of T-bet and IFNγ (DiToro & Basu, 2021; Y. Zhang et al., 2016), whilst ICOS-based CAR Tc cells induced both T-bet and RORγt expression in the Teff cells (Guedan et al., 2014). The number of CD4+CD25+FoxP3+ cells were found to be elevated in glioblastoma multiforme tumours in comparison to the control normal brain tissue (El Andaloussi & Lesniak, 2006). In addition, CD4 expression was decreased and FoxP3 was elevated, when T cells cultured with GBM cells or with MSC-EVs expressing mir-503 (Wang et al., 2021). These findings support our data. However, Scholl

et al. (2020) showed that glioma-derived EVs reduced tumour growth, CD4+ populations, including suppressive cells and FoxP3 expression (Scholl et al., 2020).

Experiments were performed to evaluate the effect of the glioblastoma-derived proteins in solution on the CD4+ T cells. We reported that the proteins contained in GBM secretome were suppressive for the T cell counts in high doses. Crane et al. (2012) have shown that soluble factors from GBM cells can suppress T cell proliferation and preferentially expand Treg clones. However, in that study condition medium from GBM cell lines was utilised for the experiments and not isolated soluble proteins, which can mean that the effect reported can also be a result of the EVs secreted in the TCM. In glioma-bearing mice a reduction in the frequency of both CD4+ and CD8+ counts was shown and subsequent decrease in those immune cell numbers in the peripheral blood (Ayasoufi et al., 2020).

Soluble proteins secreted in glioblastoma tumour microenvironment can alter expression of the cell surface markers of monocytes and affect the cytokine output (Zou et al., 1999). Altered profiles of monocytes have, also been reported in Glioblastoma and are linked with the systemic immunosuppression these tumours cause (Gustafson et al., 2010). Here, we focused on the soluble-protein-mediating effect on CD4+ T cells phenotype and their potential to become immunosuppressive and favour tumour progression.

Exhaustion markers TIM-3 and PD-1 expression followed similar trend, as in the EVs treatment with the frequency of CD4+ T cells carrying on their cell surface the specific markers being lower than the control group, where no soluble proteins were added in the culture, but with a high MFI level. CD4+ T cells have faced a level of death, when the tumour proteins were introduced to them and the numbers are fewer and the cells remaining show a more exhausted profile in a dose-dependent manner, since the expression levels were significantly higher in the Full dose. Approximately 25%

more TIM-3 was identified by cell counts decreased by 11,6% in comparison to the control. Also, PD-1 expression was 30% more than the control and 24% higher than the ¼ dose of soluble proteins.

In contrast to what we observed, when we treated the cells with GBM-derived EVs, activation marker ICOS expression was downregulated as the concentrations of soluble proteins increased. In this case, it is difficult to predict what the total amount of ICOS expression by the CD4+ T cells was, since the secretome in the tumour microenvironment consists of both EVs and factors in solution that had different effect on the marker, but the protein fraction may contain factors causing a more suppressive reaction.

Soluble proteins secreted in the microenvironment of glioblastoma altered the secretion profile of cytokines by CD4+ T cells. TGFβ and IL-21, as observed in treated cells with EVs were produced by fewer CD4+ numbers. Interestingly, it was shown that TGFβ secretion was significantly reduced, when cells were treated with Full dose soluble proteins, but, when considering the reduction in the cell counts, the expression of the marker is not lower, but almost equal as he control instead. Donkor and his group (2012) have suggested, though, that TGFβ from activated CD4+ T cells promotes tumour evasion. TNFα secretion showed a greater reduction, when the soluble proteins added on the T cells, especially in the Full dose, where the cytokine production was lower by 45%. IFNγ was produced by a smaller amount of cells in all conditions, but the expression level in Half and ¼ dose was higher than the untreated cells and impaired in the Full dose. According to Zou et al. (1999), the secretion of TNFα and IFNγ was decreased in PBMCs, when treated with GSCs, whilst anti-inflammatory cytokine production was increased. PD-1+CD4+ cells produce high levels of IFNγ, which in turn has been reported to increase the PD-L1 expression on glioma and melanoma cells promoting immunosuppression (Goods et al., 2017; Thiem et al., 2019). IL-13 production levels seem not to be affected by the tumour soluble protein treatment, while IL-17 production was higher

in all conditions than the control, after incubation of the CD4+ T cells with the soluble factors and especially when lower doses were added, as described in the EV treatment.

The expression of the transcription factors, as a result to the incubation of CD4+ T cells with the glioblastoma tumour-derived soluble factors follow the exact same trends as in the treatment with the extracellular vesicles described above.

4.5 THE EFFECT OF THE PROTEINS OF INTEREST ON T CELLS

The bioinformatic analysis helped in narrowing down the proteins. A list of the potential culprits for Glioblastoma pathogenesis was constructed and the best candidates were targeted for therapeutic purposes. Our chosen proteins of interest were studied further for their capacity to inhibit CD4+ T cell response or alter their fate, activating mechanisms of inflammation or immunosuppression.

ICAM-1 is an adhesion molecule with contradictory effects on tumour lymphocytes according to different studies. It has been reported that expression of ICAM-1 molecule on GBM cells promotes tumour invasion and lymphocyte migration (Kuppner et al., 1990). Also, in glioblastoma mouse model with resistance to anti-angiogenic agent bevacizumab, ICAM-1 knock down was linked with better prognosis and lower levels of tumour infiltrating macrophages (Piao et al., 2017). However, overexpression of ICAM-1 on cells of renal cancer promotes CTL function over the PGE2-promoted immunosuppression of CD8+ responses (Morgan, 2018). Upon binding to LFA-1, ICAM-1 can provide costimulatory signal to NK cells and induce cytotoxicity (Chong et al., 1994). Nonetheless, co-expression of ICAM-1 is crucial in antigen presentation through HLA-DR for induction of activation in T cells (Altmann et al., 1989). Moreover, a very recently published study has shown

that ICAM-1 interaction with LFA-1 on CD8+ T cells is necessary for EVs PD-L1-mediated immunosuppression and disruption of this pathway can enhance CD8+ activation (W. Zhang et al., 2022). The findings about ICAM-1 and its role in promoting or inhibiting the immune-mediated responses made it an interesting candidate for further investigation, since previous studies have investigated its implication in GBM, in EVs and on immune cell populations separately, but not combined.

CD47 is an antiphagocytic molecule overexpressed on macrophages and several cancers, including glioblastoma cells. Moreover higher levels of CD47 have been detected in higher grade gliomas than lower and are linked to poorer prognosis (J. Yang et al., 2021). It provides cancer cells with a ''don't eat me signal'' against macrophages, since upon binding to the innate myeloid immune checkpoint signal regulatory protein-α (SIRPα), which is expressed on myeloid cell surface, inhibits phagocytosis and allows immune evasion (Gauttier et al., 2020). However, blockade of CD47-SIRPα interaction, induces CD8+ T cells responses, but the opposite has been reported regarding the effects on CD4+ T cell activation. Additionally, the anti-CD47 treatment, restored phagocytosis and, therefore, improved antigen presentation processes (Tseng et al., 2013). A later study, though supports that targeting should be focused on the SIRPα blockade, since they have showed that CD47 antibodies impaired T cell activation and proliferation in mice models bearing tumours (Gauttier et al., 2020). Primary results of targeting CD47 alone or in combined therapy in Glioblastoma cells and xenografts seem promising (Zhang et al., 2016; Y. Zhang et al., 2018; Ma et al., 2015). CD47 role in GBM EVs or soluble protein- mediated T cell suppression has not been investigated yet.

THBS1 is another interaction molecule for CD47, which is expressed on T cells. Upon binding to CD47, it induces regulatory T cell response (Grimbert et al., 2006). It has, also, been reported that when THBS1 is expressed in high level can induce apoptosis in T cells (Lamy et al., 2007). In glioma,

THBS1 expression results in cancer cell migration and indirectly in inhibition of the CD8+ T cell responses (Ma et al., 2015). In addition, THBS1-expressing CD35+ B cells have a downregulated expression of the CD80/86 costimulatory molecules in dendritic cells and an elevated conversion level of naïve CD4+ cells to Tregs (H.-P. Zhang et al., 2013).

These three proteins contained in the EV GBM fraction were chosen for further experiments, in order to evaluate their potential immunosuppressive effects on CD4+ T cells. MIF protein was selected from the proteins in solution to be examined further.

Macrophage migration inhibitory factor (MIF) has been described as a pro-inflammatory cytokine binding to CD74 receptor to regulate innate immune response (Calandra & Roger, 2003). In cancers including Glioblastoma, MIF is implicated in enhanced tumourigenicity by initiating signalling pathways that inhibit apoptosis, impeding NK-mediated cancer cell lysis, induction of MDSCs (Simpson et al., 2012), inhibition of T lymphocyte activation (Yan et al., 2006; Mangano et al., 2018) and sustained tumour-associated macrophage/microglia M2 polarization (Ghoochani et al., 2016). Attempts of targeting MIF in GBM *in vitro* and *in vivo* have beneficial results (Mangano et al., 2018).

In terms of cell counts, CD4+ T cells did not show any significant reduction, even after exposure to high protein concentrations. This result was not different from what expected, since addition from only one protein from the tumour in each case, is not apparently sufficient to cause an effect of T cell suppression, equal to what we observed, when we added the whole fractions of EVs or soluble proteins expressed in the TME. Multiple factors are contained in the whole secretome that can interact with the cells or each other and cause a greater co-inhibitory effect on T cells. That can, also, be concluded from the fact that monotherapy has not been proved to be adequately efficient for the treatment of Glioblastoma patients over the years.

The effect that ICAM-1, THBS1, CD47 and MIF have on the CD4+ T cell phenotype has not been studied before. Incubation the T cells with these proteins in indicated concentrations may affect their cell surface expression profile and the cytokine secretion output and (Appendix 1). Amongst the proteins, THBS1 showed to slightly elevate the exhaustion markerks PD-1 and TIM-3 and downregulate the ICOS costimulatory molecule. CD47 was showed to have an immunosuppressive effect on T cells cytokine profile by impairing IL-21, TNFα and IFNγ production and slightly increasing IL-13, proposing that it could be a good target for immunotherapeutic purposes. Our findings come into agreement with previous studies, where CD47 expression was found to modulate the immune responses in monocytes and DCs by being a negative regulator of the Th1 phenotype, promoting skewing towards Th2 cell development through inhibiting IL-12, TNFα and IFNγ cytokines (Avice et al., 2000; Bouguermouh et al., 2008). Most likely, reversing the anti-inflammatory CD4+ phenotype would be more effective, if combined with other suppressive factors for the cells.

However, the experiments need to be repeated, since they were performed only once and are lacking the statistical analysis.

In order to have a more robust understanding of the overall interactions in the tumour microenvironment, the Treg-mediated suppression needs, also, to be added in the equation. FoxP3+ regulatory T cells are overrepresented in the TME, accounting for almost 38.5% of the infiltrating immune cells (Heimberger et al., 2008; Crane et al., 2012). A low CD8+ T cell to FoxP3+Treg ratio has been correlated with poorer prognosis and recurrence (Sayour et al., 2015), and depletion of Tregs reversed T cell inhibition in mice with malignant brain tumours (El Andaloussi & Lesniak., 2006). In this report, an *in vitro* human primary Treg-mediated suppression assay started to be established. Conventional T cells and regulatory T cells were magnetically isolated from PBMCs of

a healthy blood donor. Tregs suppressed the T concv cells in a dose-dependent manner, after activation of Tconv with CD3/CD28 Dynabeads (1:5 Dynabeads:Tconv). However, the experiment was performed once and needs to be repeated, in order to confirm the data. Addition of tumour-derived EVs and soluble proteins in the culture would address the overall potential immunosuppressive effect on T cells directly or through Treg-mediated suppression.

In general, this project showed that as the disease progresses and the tumourigenic factors, such as extracellular vesicles and soluble proteins released in the microenvironment, multiply, they have anti-proliferative or rather fatal for the T cells, as indicated by their low numbers. However, an interesting finding was that the CD4+ T cell ''survivors'', despite demonstrating a more exhausted phenotype, they were still able of producing cytokines and transcription factors. The total expression levels of the markers tested maybe were lower, as it was shown by the mean fluorescence intensity parameter, but in many cases was comparable with the control group. That suggested that the expression amount produced per cell was becoming higher. T cells in TME may try to replenish the suppressed store by potentiating their inflammatory signals seeking for support from other immune subsets, such as CD8+ T cells, NKs or monocytes. Nonetheless, anti-inflammatory factors were, also, produced in highs, inevitably promoting the shift of a number of CD4+ T cells to a more Th2-immunosuppressive phenotype. Previous studies have shown that exhausted CD4+ cells can secrete high amounts of IFNγ to enhance migration of other T helper cells to TME, but sometimes they are dysfunctional (Goods, et al., 2017). Additional single-cell studies may be useful in unravelling the functionality of tumour CD4+ cells and how co-expression of different markers drives their response. Identifying and overcoming the ligand-receptor interactions that are responsible for GBM immunosuppression would be highly important in the design of a novel immunotherapy for the treatment of Glioblastoma brain tumours.

4.6 LIMITATIONS

Due to the nature of the samples, one of the limitations in the current study was the size of the biopsy tissue resected from the GBM patients that was available for research purposes. The small sample size restricted the number of experiments that could be conducted on them and set up the maximum protein concentrations used for Mass spectrometric analysis. Additionally, based on the timeline of the respective grant, the repeats of the experiments investigating the role of the protein candidates on T cell immunosuppression were not performed. Experiments addressing the role of EVs and soluble proteins on T cell proliferation and apoptosis and attempts to block the candidate ligands should be the performed as the next step and they are discussed further in the next section.

4.7 FUTURE WORK

Future studies can include the repeat and confirmation of the preliminary results taken from the candidate protein-mediated T cell inhibition assays and the Treg suppression assays. In addition, the actual effect of extracellular vesicles and soluble factors on T cell proliferation and apoptosis can be assessed by flow cytometry by monitoring the Carboxyfluorescein succinimidyl ester (CFSE) and modified annexin V/propidium iodide respectively. Also, the effect of the GBM proteins and extracellular vesicles on Treg behaviour can be examined, whilst co-cultures of Tregs and Tconv cells with the protein and EV fractions would be useful to be tested to have a more representative idea of the tumour microenvironment, how these cells interact and what effect they have on T cell markers.

Targeting of immunosuppressive candidates identified by mass spectrometry can be attempted by utilising specific antibodies or siRNAs in T cell co-cultures *in vitro,* and analysed by flow cytometry. Combined therapy approaches using existing promising targets, such as PD-L1 or STAT3 can, also, be undertaken. Identifying and overcoming the ligand-receptor interactions that are responsible for GBM immunosuppression would be highly important in the design of a novel immunotherapy for the treatment of Glioblastoma brain tumours.

4.8 Concluding Remarks

The limited efficacy of standard treatment leads to high mortality rates in Glioblastoma Multiforme patients. The GBM tumour microenvironment is highly immunosuppressive. GBM-derived extracellular vesicles mediate intercellular communication and cancer spreading. Optimisation of the sample preparation protocol for mass spectrometry has examined the EVs size profiling by qNano, the efficiency of EVs and soluble proteins separation by qEV SEC columns and sample digestion. Mass spectrometry analysis on patient tumour samples was, then, undertaken to screen and identify all the proteins that are present in the TME and focus the ligand-receptor interactions that may cause GBM immunosuppression. The proteins detected were analysed for discovering similarities and differences across the molecular subtypes and potential new markers for subtype identification. This study explored the capacity of GBM-derived EVs/soluble proteins to reduce T cell growth and alter the fate of CD4+ T cells by changing the expression profile of the cell surface markers, master regulator transcription factors and cytokine secretion. Subtype-non-specific pathogenic candidates were attempted to be listed, evaluated and the best of them to examined further for their potential to inhibit CD4+ T cells. Further work will reveal if the candidates chosen are ideal to be targeted. If successful, this PhD project will address an important clinical need, as

resistance to Temozolomide and inadequate T cell restoration is a challenging clinical problem in Glioblastoma.

REFERENCES

Abels, E. R., Maas, S. L. N., Nieland, L., Wei, Z., Cheah, P. S., Tai, E., Kolsteeg, C.-J., Dusoswa, S. A., Ting, D. T., Hickman, S., El Khoury, J., Krichevsky, A. M., Broekman, M. L. D., & Breakefield, X. O. (2019). Glioblastoma-Associated Microglia Reprogramming Is Mediated by Functional Transfer of Extracellular miR-21. *Cell Reports*, *28*(12), 3105-3119.e7. https://doi.org/10.1016/j.celrep.2019.08.036

Adeegbe, D. O., & Nishikawa, H. (2013). Natural and induced T regulatory cells in cancer. *Frontiers in Immunology*, *4*, 190. https://doi.org/10.3389/fimmu.2013.00190

Al-Nedawi, K., Meehan, B., Kerbel, R. S., Allison, A. C., & Rak, J. (2009). Endothelial expression of autocrine VEGF upon the uptake of tumor-derived microvesicles containing oncogenic EGFR. *Proceedings of the National Academy of Sciences of the United States of America*, *106*(10), 3794–3799. https://doi.org/10.1073/pnas.0804543106

Altmann, D. M., Hogg, N., Trowsdale, J., & Wilkinson, D. (1989). Cotransfection of ICAM-1 and HLA-DR reconstitutes human antigen-presenting cell function in mouse L cells. *Nature*, *338*, 512–514. https://doi.org/10.1038/338512a0

Amatore, F., Ortonne, N., Lopez, M., Orlanducci, F., Castellano, R., Ingen-Housz-Oro, S., De Croos, A., Salvado, C., Gorvel, L., Goubard, A., Collette, Y., Bouabdallah, R., Schiano, J.-M., Bonnet, N., Grob, J.-J., Gaulard, P., Bagot, M., Bensussan, A., Berbis, P., & Olive, D. (2020). ICOS is widely expressed in cutaneous T-cell lymphoma, and its targeting promotes potent killing of malignant cells. *Blood Advances*, *4*(20), 5203–5214. https://doi.org/10.1182/bloodadvances.2020002395

An, Z., Aksoy, O., Zheng, T., Fan, Q.-W., & Weiss, W. A. (2018). Epidermal growth factor receptor and EGFRvIII in glioblastoma: Signaling pathways and targeted therapies. *Oncogene*, *37*(12), Article 12. https://doi.org/10.1038/s41388-017-0045-7

André-Grégoire, G., & Gavard, J. (2017). Spitting out the demons: Extracellular vesicles in glioblastoma. *Cell Adhesion & Migration*, *11*(2), 164–172. https://doi.org/10.1080/19336918.2016.1247145

Andreu, Z., & Yáñez-Mó, M. (2014). Tetraspanins in extracellular vesicle formation and function. *Frontiers in Immunology*, *5*, 442. https://doi.org/10.3389/fimmu.2014.00442

Aspord, C., Pedroza-Gonzalez, A., Gallegos, M., Tindle, S., Burton, E. C., Su, D., Marches, F., Banchereau, J., & Palucka, A. K. (2007). Breast cancer instructs dendritic cells to prime interleukin 13–secreting CD4+ T cells that facilitate tumor development. *Journal of Experimental Medicine*, *204*(5), 1037–1047. https://doi.org/10.1084/jem.20061120

Avice, M. N., Rubio, M., Sergerie, M., Delespesse, G., & Sarfati, M. (2000). CD47 ligation selectively inhibits the development of human naive T cells into Th1 effectors. *Journal of Immunology (Baltimore, Md.: 1950)*, *165*(8), 4624–4631. https://doi.org/10.4049/jimmunol.165.8.4624

Ayasoufi, K., Pfaller, C. K., Evgin, L., Khadka, R. H., Tritz, Z. P., Goddery, E. N., Fain, C. E., Yokanovich, L. T., Himes, B. T., Jin, F., Zheng, J., Schuelke, M. R., Hansen, M. J., Tung, W., Parney, I. F., Pease, L. R., Vile, R. G., & Johnson, A. J. (2020). Brain cancer induces systemic immunosuppression through release of non-steroid soluble mediators. *Brain: A Journal of Neurology*, *143*(12), 3629–3652. https://doi.org/10.1093/brain/awaa343

Bai, R.-Y., Staedtke, V., & Riggins, G. J. (2011). Molecular targeting of glioblastoma: Drug discovery and therapies. *Trends in Molecular Medicine*, *17*(6), 301–312. https://doi.org/10.1016/j.molmed.2011.01.011

Barrow, A. D., & Colonna, M. (2019). Innate lymphoid cell sensing of tissue vitality. *Current Opinion in Immunology*, *56*, 82–93. https://doi.org/10.1016/j.coi.2018.11.004

Bellinghausen, I., Klostermann, B., Böttcher, I., Knop, J., & Saloga, J. (2004). Importance of the inducible costimulator molecule for the induction of allergic immune responses and its decreased expression on T helper cells after venom immunotherapy. *Immunology*, *112*(1), 80–86. https://doi.org/10.1111/j.1365-2567.2004.01845.x

Berghoff, A. S., Kiesel, B., Widhalm, G., Rajky, O., Ricken, G., Wöhrer, A., Dieckmann, K., Filipits, M., Brandstetter, A., Weller, M., Kurscheid, S., Hegi, M. E., Zielinski, C. C., Marosi, C., Hainfellner, J. A., Preusser, M., & Wick, W. (2015). Programmed death ligand 1 expression and tumor-infiltrating lymphocytes in glioblastoma. *Neuro-Oncology*, *17*(8), 1064–1075. https://doi.org/10.1093/neuonc/nou307

Bergmann, N., Delbridge, C., Gempt, J., Feuchtinger, A., Walch, A., Schirmer, L., Bunk, W., Aschenbrenner, T., Liesche-Starnecker, F., & Schlegel, J. (2020). The Intratumoral Heterogeneity Reflects the Intertumoral Subtypes of Glioblastoma Multiforme: A Regional Immunohistochemistry Analysis. *Frontiers in Oncology*, *10*. https://www.frontiersin.org/article/10.3389/fonc.2020.00494

Bettelli, E., Carrier, Y., Gao, W., Korn, T., Strom, T. B., Oukka, M., Weiner, H. L., & Kuchroo, V. K. (2006). Reciprocal developmental pathways for the generation of pathogenic effector TH17 and regulatory T cells. *Nature*, *441*(7090), 235–238. https://doi.org/10.1038/nature04753

Black, K. L., Chen, K., Becker, D. P., & Merrill, J. E. (1992). Inflammatory leukocytes associated with increased immunosuppression by glioblastoma. *Journal of Neurosurgery*, *77*(1), 120–126. https://doi.org/10.3171/jns.1992.77.1.0120

Bloch, O., Crane, C. A., Kaur, R., Safaee, M., Rutkowski, M. J., & Parsa, A. T. (2013). GLIOMAS PROMOTE IMMUNOSUPPRESSION THROUGH INDUCTION OF B7-H1 EXPRESSION

IN TUMOR-ASSOCIATED MACROPHAGES. *Clinical Cancer Research : An Official Journal of the American Association for Cancer Research*, *19*(12), 3165–3175. https://doi.org/10.1158/1078-0432.CCR-12-3314

Bouguermouh, S., Van, V. Q., Martel, J., Gautier, P., Rubio, M., & Sarfati, M. (2008). CD47 Expression on T Cell Is a Self-Control Negative Regulator of Type 1 Immune Response. *The Journal of Immunology*, *180*(12), 8073–8082. https://doi.org/10.4049/jimmunol.180.12.8073

Bourhis, M., Palle, J., Galy-Fauroux, I., & Terme, M. (2021). Direct and Indirect Modulation of T Cells by VEGF-A Counteracted by Anti-Angiogenic Treatment. *Frontiers in Immunology*, *12*. https://www.frontiersin.org/article/10.3389/fimmu.2021.616837

Broekman, M. L., Maas, S. L. N., Abels, E. R., Mempel, T. R., Krichevsky, A. M., & Breakefield, X. O. (2018). Multidimensional communication in the microenvirons of glioblastoma. *Nature Reviews. Neurology*, *14*(8), 482–495. https://doi.org/10.1038/s41582-018-0025-8

Brown, N. F., Carter, T. J., Ottaviani, D., & Mulholland, P. (2018). Harnessing the immune system in glioblastoma. *British Journal of Cancer*, *119*(10), Article 10. https://doi.org/10.1038/s41416-018-0258-8

Buonfiglioli, A., & Hambardzumyan, D. (2021). Macrophages and microglia: The cerberus of glioblastoma. *Acta Neuropathologica Communications*, *9*(1), 54. https://doi.org/10.1186/s40478-021-01156-z

Calandra, T., & Roger, T. (2003). Macrophage migration inhibitory factor: A regulator of innate immunity. *Nature Reviews. Immunology*, *3*(10), 791–800. https://doi.org/10.1038/nri1200

Cancer Genome Atlas Research Network. (2008). Comprehensive genomic characterization defines human glioblastoma genes and core pathways. *Nature*, *455*(7216), 1061–1068. https://doi.org/10.1038/nature07385

Carlsson, S. K., Brothers, S. P., & Wahlestedt, C. (2014). Emerging treatment strategies for glioblastoma multiforme. *EMBO Molecular Medicine*, *6*(11), 1359–1370. https://doi.org/10.15252/emmm.201302627

Carson, M. J., Doose, J. M., Melchior, B., Schmid, C. D., & Ploix, C. C. (2006). CNS immune privilege: Hiding in plain sight. *Immunological Reviews*, *213*, 48–65. https://doi.org/10.1111/j.1600-065X.2006.00441.x

Cervantes-Barragan, L., Lewis, K. L., Firner, S., Thiel, V., Hugues, S., Reith, W., Ludewig, B., & Reizis, B. (2012). Plasmacytoid dendritic cells control T-cell response to chronic viral infection. *Proceedings of the National Academy of Sciences of the United States of America*, *109*(8), 3012–3017. https://doi.org/10.1073/pnas.1117359109

Chaplin, D. D. (2010). Overview of the Immune Response. *The Journal of Allergy and Clinical Immunology*, *125*(2 Suppl 2), S3-23. https://doi.org/10.1016/j.jaci.2009.12.980

Chong, A. S.-F., Boussy, I. A., Jiang, X. L., Lamas, M., & Graf, L. H. (1994). CD54/ICAM-1 Is a Costimulator of NK Cell-Mediated Cytotoxicity. *Cellular Immunology*, *157*(1), 92–105. https://doi.org/10.1006/cimm.1994.1208

Clarke, J., Butowski, N., & Chang, S. (2010). Recent advances in therapy for glioblastoma. *Archives of Neurology*, *67*(3), 279–283. https://doi.org/10.1001/archneurol.2010.5

Crane, C. A., Ahn, B. J., Han, S. J., & Parsa, A. T. (2012). Soluble factors secreted by glioblastoma cell lines facilitate recruitment, survival, and expansion of regulatory T cells: Implications for immunotherapy. *Neuro-Oncology*, *14*(5), 584–595. https://doi.org/10.1093/neuonc/nos014

Curtin, J. F., King, G. D., Candolfi, M., Greeno, R. B., Kroeger, K. M., Lowenstein, P. R., & Castro, M. G. (2005). Combining cytotoxic and immune-mediated gene therapy to treat brain

tumors. *Current Topics in Medicinal Chemistry*, *5*(12), 1151–1170. https://doi.org/10.2174/156802605774370856

Czerwinska, P., Rucinski, M., Wlodarczyk, N., Jaworska, A., Grzadzielewska, I., Gryska, K., Galus, L., Mackiewicz, J., & Mackiewicz, A. (2020). Therapeutic melanoma vaccine with cancer stem cell phenotype represses exhaustion and maintains antigen-specific T cell stemness by up-regulating BCL6. *OncoImmunology*, *9*(1), 1710063. https://doi.org/10.1080/2162402X.2019.1710063

Dart, S. J., Cook, A. M., Millward, M. J., McDonnell, A. M., Chin, W. L., Hakeem, M. U., Meniawy, T. M., & Bowyer, S. E. (2021). Changes in expression of PD-L1 on peripheral T cells in patients with melanoma and lung cancer treated with PD-1 inhibitors. *Scientific Reports*, *11*(1), Article 1. https://doi.org/10.1038/s41598-021-93479-z

Das, S., & Marsden, P. A. (2013). Angiogenesis in glioblastoma. *The New England Journal of Medicine*, *369*(16), 1561–1563. https://doi.org/10.1056/NEJMcibr1309402

De Vleeschouwer, S., & Bergers, G. (2017). Glioblastoma: To Target the Tumor Cell or the Microenvironment? In S. De Vleeschouwer (Ed.), *Glioblastoma*. Codon Publications. http://www.ncbi.nlm.nih.gov/books/NBK469984/

de Vrij, J., Maas, S. L. N., Kwappenberg, K. M. C., Schnoor, R., Kleijn, A., Dekker, L., Luider, T. M., de Witte, L. D., Litjens, M., van Strien, M. E., Hol, E. M., Kroonen, J., Robe, P. A., Lamfers, M. L., Schilham, M. W., & Broekman, M. L. D. (2015). Glioblastoma-derived extracellular vesicles modify the phenotype of monocytic cells. *International Journal of Cancer*, *137*(7), 1630–1642. https://doi.org/10.1002/ijc.29521

Desjardins, P., Hansen, J. B., & Allen, M. (2009). Microvolume protein concentration determination using the NanoDrop 2000c spectrophotometer. *Journal of Visualized Experiments: JoVE*, *33*, 1610. https://doi.org/10.3791/1610

DiToro, D., & Basu, R. (2021). Emerging Complexity in CD4+T Lineage Programming and Its Implications in Colorectal Cancer. *Frontiers in Immunology*, *12*. https://www.frontiersin.org/article/10.3389/fimmu.2021.694833

Dobrzanski, M. J. (2013). Expanding Roles for CD4 T Cells and Their Subpopulations in Tumor Immunity and Therapy. *Frontiers in Oncology*, *3*, 63. https://doi.org/10.3389/fonc.2013.00063

Domenis, R., Cesselli, D., Toffoletto, B., Bourkoula, E., Caponnetto, F., Manini, I., Beltrami, A. P., Ius, T., Skrap, M., Di Loreto, C., & Gri, G. (2017). Systemic T Cells Immunosuppression of Glioma Stem Cell-Derived Exosomes Is Mediated by Monocytic Myeloid-Derived Suppressor Cells. *PLoS ONE*, *12*(1), e0169932. https://doi.org/10.1371/journal.pone.0169932

Donkor, M. K., Sarkar, A., & Li, M. O. (2012). Tgf-β1 produced by activated CD4+ T Cells Antagonizes T Cell Surveillance of Tumor Development. *Oncoimmunology*, *1*(2), 162–171. https://doi.org/10.4161/onci.1.2.18481

Dörsam, B., Reiners, K. S., & von Strandmann, E. P. (2018). Cancer-derived extracellular vesicles: Friend and foe of tumour immunosurveillance. *Philosophical Transactions of the Royal Society of London. Series B, Biological Sciences*, *373*(1737), 20160481. https://doi.org/10.1098/rstb.2016.0481

Dunn, G. P., Old, L. J., & Schreiber, R. D. (2004). The Three Es of Cancer Immunoediting. *Annual Review of Immunology*, *22*(1), 329–360. https://doi.org/10.1146/annurev.immunol.22.012703.104803

El Andaloussi, A., & Lesniak, M. S. (2006). An increase in CD4+CD25+FOXP3+ regulatory T cells in tumor-infiltrating lymphocytes of human glioblastoma multiforme. *Neuro-Oncology*, *8*(3), 234–243. https://doi.org/10.1215/15228517-2006-006

Ellor, S. V., Pagano-Young, T. A., & Avgeropoulos, N. G. (2014). Glioblastoma: Background, standard treatment paradigms, and supportive care considerations. *The Journal of Law, Medicine & Ethics: A Journal of the American Society of Law, Medicine & Ethics*, *42*(2), 171–182. https://doi.org/10.1111/jlme.12133

Elstner, A., Stockhammer, F., Nguyen-Dobinsky, T.-N., Nguyen, Q. L., Pilgermann, I., Gill, A., Guhr, A., Zhang, T., von Eckardstein, K., Picht, T., Veelken, J., Martuza, R. L., von Deimling, A., & Kurtz, A. (2011). Identification of diagnostic serum protein profiles of glioblastoma patients. *Journal of Neuro-Oncology*, *102*(1), 71–80. https://doi.org/10.1007/s11060-010-0284-8

Esteller, M., & Herman, J. G. (2004). Generating mutations but providing chemosensitivity: The role of O6-methylguanine DNA methyltransferase in human cancer. *Oncogene*, *23*(1), 1–8. https://doi.org/10.1038/sj.onc.1207316

Fang, D., & Zhu, J. (2017). Dynamic balance between master transcription factors determines the fates and functions of CD4 T cell and innate lymphoid cell subsets. *Journal of Experimental Medicine*, *214*(7), 1861–1876. https://doi.org/10.1084/jem.20170494

Fecci, P. E., Mitchell, D. A., Whitesides, J. F., Xie, W., Friedman, A. H., Archer, G. E., Herndon, J. E., Bigner, D. D., Dranoff, G., & Sampson, J. H. (2006). Increased regulatory T-cell fraction amidst a diminished CD4 compartment explains cellular immune defects in patients with malignant glioma. *Cancer Research*, *66*(6), 3294–3302. https://doi.org/10.1158/0008-5472.CAN-05-3773

Fernandes, C., Costa, A., Osório, L., Lago, R. C., Linhares, P., Carvalho, B., & Caeiro, C. (2017). Current Standards of Care in Glioblastoma Therapy. In S. De Vleeschouwer (Ed.), *Glioblastoma*. Codon Publications. http://www.ncbi.nlm.nih.gov/books/NBK469987/

Fontenot, J. D., Rasmussen, J. P., Williams, L. M., Dooley, J. L., Farr, A. G., & Rudensky, A. Y. (2005). Regulatory T cell lineage specification by the forkhead transcription factor foxp3. *Immunity*, *22*(3), 329–341. https://doi.org/10.1016/j.immuni.2005.01.016

Fourcade, J., Sun, Z., Pagliano, O., Guillaume, P., Luescher, I. F., Sander, C., Kirkwood, J. M., Olive, D., Kuchroo, V., & Zarour, H. M. (2012). CD8(+) T cells specific for tumor antigens can be rendered dysfunctional by the tumor microenvironment through upregulation of the inhibitory receptors BTLA and PD-1. *Cancer Research*, *72*(4), 887–896. https://doi.org/10.1158/0008-5472.CAN-11-2637

Gabrusiewicz, K., Li, X., Wei, J., Hashimoto, Y., Marisetty, A. L., Ott, M., Wang, F., Hawke, D., Yu, J., Healy, L. M., Hossain, A., Akers, J. C., Maiti, S. N., Yamashita, S., Shimizu, Y., Dunner, K., Zal, M. A., Burks, J. K., Gumin, J., … Heimberger, A. B. (2018). Glioblastoma stem cell-derived exosomes induce M2 macrophages and PD-L1 expression on human monocytes. *Oncoimmunology*, *7*(4), e1412909. https://doi.org/10.1080/2162402X.2017.1412909

Gasser, S., Orsulic, S., Brown, E. J., & Raulet, D. H. (2005). The DNA damage pathway regulates innate immune system ligands of the NKG2D receptor. *Nature*, *436*(7054), 1186–1190. https://doi.org/10.1038/nature03884

Gauttier, V., Pengam, S., Durand, J., Biteau, K., Mary, C., Morello, A., Néel, M., Porto, G., Teppaz, G., Thepenier, V., Danger, R., Vince, N., Wilhelm, E., Girault, I., Abes, R., Ruiz, C., Trilleaud, C., Ralph, K., Trombetta, E. S., … Poirier, N. (2020). Selective SIRPα blockade reverses tumor T cell exclusion and overcomes cancer immunotherapy resistance. *The Journal of Clinical Investigation*, *130*(11), 6109–6123. https://doi.org/10.1172/JCI135528

Geskin, L. J., Viragova, S., Stolz, D. B., & Fuschiotti, P. (2015). Interleukin-13 is overexpressed in cutaneous T-cell lymphoma cells and regulates their proliferation. *Blood*, *125*(18), 2798–2805. https://doi.org/10.1182/blood-2014-07-590398

Ghantasala, S., Gollapalli, K., Epari, S., Moiyadi, A., & Srivastava, S. (2020). Glioma tumor proteomics: Clinically useful protein biomarkers and future perspectives. *Expert Review of Proteomics*, *17*(3), 221–232. https://doi.org/10.1080/14789450.2020.1731310

Ghiringhelli, F., Puig, P. E., Roux, S., Parcellier, A., Schmitt, E., Solary, E., Kroemer, G., Martin, F., Chauffert, B., & Zitvogel, L. (2005). Tumor cells convert immature myeloid dendritic cells into TGF-beta-secreting cells inducing CD4+CD25+ regulatory T cell proliferation. *The Journal of Experimental Medicine*, *202*(7), 919–929. https://doi.org/10.1084/jem.20050463

Ghoochani, A., Schwarz, M. A., Yakubov, E., Engelhorn, T., Doerfler, A., Buchfelder, M., Bucala, R., Savaskan, N. E., & Eyüpoglu, I. Y. (2016). MIF-CD74 signaling impedes microglial M1 polarization and facilitates brain tumorigenesis. *Oncogene*, *35*(48), 6246–6261. https://doi.org/10.1038/onc.2016.160

Ghoreschi, K., Laurence, A., Yang, X.-P., Tato, C. M., McGeachy, M. J., Konkel, J. E., Ramos, H. L., Wei, L., Davidson, T. S., Bouladoux, N., Grainger, J. R., Chen, Q., Kanno, Y., Watford, W. T., Sun, H.-W., Eberl, G., Shevach, E. M., Belkaid, Y., Cua, D. J., … O'Shea, J. J. (2010). Generation of pathogenic T(H)17 cells in the absence of TGF-β signalling. *Nature*, *467*(7318), 967–971. https://doi.org/10.1038/nature09447

Ghouzlani, A., Kandoussi, S., Tall, M., Reddy, K. P., Rafii, S., & Badou, A. (2021). Immune Checkpoint Inhibitors in Human Glioma Microenvironment. *Frontiers in Immunology*, *12*. https://www.frontiersin.org/article/10.3389/fimmu.2021.679425

Gonda, D. D., Akers, J. C., Kim, R., Kalkanis, S. N., Hochberg, F. H., Chen, C. C., & Carter, B. S. (2013). Neuro-oncologic applications of exosomes, microvesicles, and other nano-sized extracellular particles. *Neurosurgery*, *72*(4), 501–510. https://doi.org/10.1227/NEU.0b013e3182846e63

Gonzalez, H., Hagerling, C., & Werb, Z. (2018). Roles of the immune system in cancer: From tumor initiation to metastatic progression. *Genes & Development*, *32*(19–20), 1267–1284. https://doi.org/10.1101/gad.314617.118

Goods, B. A., Hernandez, A. L., Lowther, D. E., Lucca, L. E., Lerner, B. A., Gunel, M., Raddassi, K., Coric, V., Hafler, D. A., & Love, J. C. (2017). Functional differences between PD-1+ and PD-1- CD4+ effector T cells in healthy donors and patients with glioblastoma multiforme. *PLOS ONE*, *12*(9), e0181538. https://doi.org/10.1371/journal.pone.0181538

Graner, M. W. (2019). Roles of Extracellular Vesicles in High-Grade Gliomas: Tiny Particles with Outsized Influence. *Annual Review of Genomics and Human Genetics*, *20*, 331–357. https://doi.org/10.1146/annurev-genom-083118-015324

Grimaldi, A., Serpe, C., Chece, G., Nigro, V., Sarra, A., Ruzicka, B., Relucenti, M., Familiari, G., Ruocco, G., Pascucci, G. R., Guerrieri, F., Limatola, C., & Catalano, M. (2019). Microglia-Derived Microvesicles Affect Microglia Phenotype in Glioma. *Frontiers in Cellular Neuroscience*, *13*, 41. https://doi.org/10.3389/fncel.2019.00041

Grimbert, P., Bouguermouh, S., Baba, N., Nakajima, T., Allakhverdi, Z., Braun, D., Saito, H., Rubio, M., Delespesse, G., & Sarfati, M. (2006). Thrombospondin/CD47 interaction: A pathway to generate regulatory T cells from human CD4+ CD25- T cells in response to inflammation. *Journal of Immunology (Baltimore, Md.: 1950)*, *177*(6), 3534–3541. https://doi.org/10.4049/jimmunol.177.6.3534

Groh, V., Wu, J., Yee, C., & Spies, T. (2002). Tumour-derived soluble MIC ligands impair expression of NKG2D and T-cell activation. *Nature*, *419*(6908), 734–738. https://doi.org/10.1038/nature01112

Guedan, S., Chen, X., Madar, A., Carpenito, C., McGettigan, S. E., Frigault, M. J., Lee, J., Posey, A. D., Scholler, J., Scholler, N., Bonneau, R., & June, C. H. (2014). ICOS-based chimeric

antigen receptors program bipolar TH17/TH1 cells. *Blood*, *124*(7), 1070–1080. https://doi.org/10.1182/blood-2013-10-535245

Gustafson, M. P., Lin, Y., New, K. C., Bulur, P. A., O'Neill, B. P., Gastineau, D. A., & Dietz, A. B. (2010). Systemic immune suppression in glioblastoma: The interplay between CD14+HLA-DRlo/neg monocytes, tumor factors, and dexamethasone. *Neuro-Oncology*, *12*(7), 631–644. https://doi.org/10.1093/neuonc/noq001

Hambardzumyan, D., Gutmann, D. H., & Kettenmann, H. (2016). The role of microglia and macrophages in glioma maintenance and progression. *Nature Neuroscience*, *19*(1), Article 1. https://doi.org/10.1038/nn.4185

Han, J., Alvarez-Breckenridge, C. A., Wang, Q.-E., & Yu, J. (2015). TGF-β signaling and its targeting for glioma treatment. *American Journal of Cancer Research*, *5*(3), 945–955.

Hanif, F., Muzaffar, K., Perveen, K., Malhi, S. M., & Simjee, S. U. (2017). Glioblastoma Multiforme: A Review of its Epidemiology and Pathogenesis through Clinical Presentation and Treatment. *Asian Pacific Journal of Cancer Prevention : APJCP*, *18*(1), 3–9. https://doi.org/10.22034/APJCP.2017.18.1.3

Hao, C., Parney, I. F., Roa, W. H., Turner, J., Petruk, K. C., & Ramsay, D. A. (2002). Cytokine and cytokine receptor mRNA expression in human glioblastomas: Evidence of Th1, Th2 and Th3 cytokine dysregulation. *Acta Neuropathologica*, *103*(2), 171–178. https://doi.org/10.1007/s00401010100448

Hardee, M. E., & Zagzag, D. (2012). Mechanisms of glioma-associated neovascularization. *The American Journal of Pathology*, *181*(4), 1126–1141. https://doi.org/10.1016/j.ajpath.2012.06.030

Harshyne, L. A., Nasca, B. J., Kenyon, L. C., Andrews, D. W., & Hooper, D. C. (2016). Serum exosomes and cytokines promote a T-helper cell type 2 environment in the peripheral

blood of glioblastoma patients. *Neuro-Oncology*, *18*(2), 206–215. https://doi.org/10.1093/neuonc/nov107

Hatanpaa, K. J., Burma, S., Zhao, D., & Habib, A. A. (2010). Epidermal growth factor receptor in glioma: Signal transduction, neuropathology, imaging, and radioresistance. *Neoplasia (New York, N.Y.)*, *12*(9), 675–684. https://doi.org/10.1593/neo.10688

He, Y., Rivard, C. J., Rozeboom, L., Yu, H., Ellison, K., Kowalewski, A., Zhou, C., & Hirsch, F. R. (2016). Lymphocyte-activation gene-3, an important immune checkpoint in cancer. *Cancer Science*, *107*(9), 1193–1197. https://doi.org/10.1111/cas.12986

Heimberger, A. B., Abou-Ghazal, M., Reina-Ortiz, C., Yang, D. S., Sun, W., Qiao, W., Hiraoka, N., & Fuller, G. N. (2008). Incidence and prognostic impact of FoxP3+ regulatory T cells in human gliomas. *Clinical Cancer Research: An Official Journal of the American Association for Cancer Research*, *14*(16), 5166–5172. https://doi.org/10.1158/1078-0432.CCR-08-0320

Hennequin, A., Derangère, V., Boidot, R., Apetoh, L., Vincent, J., Orry, D., Fraisse, J., Causeret, S., Martin, F., Arnould, L., Beltjens, F., Ghiringhelli, F., & Ladoire, S. (2016). Tumor infiltration by Tbet+ effector T cells and CD20+ B cells is associated with survival in gastric cancer patients. *Oncoimmunology*, *5*(2), e1054598. https://doi.org/10.1080/2162402X.2015.1054598

Heroux, M. S., Chesnik, M. A., Halligan, B. D., Al-Gizawiy, M., Connelly, J. M., Mueller, W. M., Rand, S. D., Cochran, E. J., LaViolette, P. S., Malkin, M. G., Schmainda, K. M., & Mirza, S. P. (2014). Comprehensive characterization of glioblastoma tumor tissues for biomarker identification using mass spectrometry-based label-free quantitative proteomics. *Physiological Genomics*, *46*(13), 467–481. https://doi.org/10.1152/physiolgenomics.00034.2014

Hopkin, K. (2016). Core Concept: Extracellular vesicles garner interest from academia and biotech. *Proceedings of the National Academy of Sciences of the United States of America*, *113*(33), 9126–9128. https://doi.org/10.1073/pnas.1611700113

Hosseinkhani, N., Derakhshani, A., Kooshkaki, O., Abdoli Shadbad, M., Hajiasgharzadeh, K., Baghbanzadeh, A., Safarpour, H., Mokhtarzadeh, A., Brunetti, O., Yue, S. C., Silvestris, N., & Baradaran, B. (2020). Immune Checkpoints and CAR-T Cells: The Pioneers in Future Cancer Therapies? *International Journal of Molecular Sciences*, *21*(21), E8305. https://doi.org/10.3390/ijms21218305

Humphries, W., Wei, J., Sampson, J. H., & Heimberger, A. B. (2010). The Role of Tregs in Glioma-Mediated Immunosuppression: Potential Target for Intervention. *Neurosurgery Clinics of North America*, *21*(1), 125–137. https://doi.org/10.1016/j.nec.2009.08.012

Hutchins, J. (2014). What's that gene (or protein)? Online resources for exploring functions of genes, transcripts, and proteins. *Molecular Biology of the Cell*, *25*, 1187–1201. https://doi.org/10.1091/mbc.E13-10-0602

Johanns, T. M., Miller, C. A., Liu, C. J., Perrin, R. J., Bender, D., Kobayashi, D. K., Campian, J. L., Chicoine, M. R., Dacey, R. G., Huang, J., Fritsch, E. F., Gillanders, W. E., Artyomov, M. N., Mardis, E. R., Schreiber, R. D., & Dunn, G. P. (2019). Detection of neoantigen-specific T cells following a personalized vaccine in a patient with glioblastoma. *Oncoimmunology*, *8*(4), e1561106. https://doi.org/10.1080/2162402X.2018.1561106

Kalra, H., Drummen, G. P. C., & Mathivanan, S. (2016). Focus on Extracellular Vesicles: Introducing the Next Small Big Thing. *International Journal of Molecular Sciences*, *17*(2), 170. https://doi.org/10.3390/ijms17020170

Kamath, A. A., Friedman, D. D., Akbari, S. H. A., Kim, A. H., Tao, Y., Luo, J., & Leuthardt, E. C. (2019). Glioblastoma Treated With Magnetic Resonance Imaging-Guided Laser Interstitial

Thermal Therapy: Safety, Efficacy, and Outcomes. *Neurosurgery*, *84*(4), 836–843. https://doi.org/10.1093/neuros/nyy375

Kane, A., & Yang, I. (2010). Interferon-gamma in brain tumor immunotherapy. *Neurosurgery Clinics of North America*, *21*(1), 77–86. https://doi.org/10.1016/j.nec.2009.08.011

Kannappan, V., Butcher, K., Trela, M., Nicholl, I., Wang, W., & Attridge, K. (2017). Interleukin 21 inhibits cancer-mediated FOXP3 induction in naïve human CD4 T cells. *Cancer Immunology, Immunotherapy: CII*, *66*(5), 637–645. https://doi.org/10.1007/s00262-017-1970-6

Kennedy, M. A. (2010). A Brief Review of the Basics of Immunology: The Innate and Adaptive Response. *Veterinary Clinics: Small Animal Practice*, *40*(3), 369–379. https://doi.org/10.1016/j.cvsm.2010.01.003

Khatami, M. (2012). *Inflammation, Chronic Diseases and Cancer—Cell and Molecular Biology, Immunology and Clinical Bases*. https://doi.org/10.5772/1219

Kim, J. E., & Lim, M. (2015). The role of checkpoints in the treatment of GBM. *Journal of Neuro-Oncology*, *123*(3), 413–423. https://doi.org/10.1007/s11060-015-1747-8

Kim, R., Emi, M., & Tanabe, K. (2007). Cancer immunoediting from immune surveillance to immune escape. *Immunology*, *121*(1), 1–14. https://doi.org/10.1111/j.1365-2567.2007.02587.x

Komori, T. (2015). Pathology and genetics of diffuse gliomas in adults. *Neurologia Medico-Chirurgica*, *55*(1), 28–37. https://doi.org/10.2176/nmc.ra.2014-0229

Kozlowska, A. K., Tseng, H.-C., Kaur, K., Topchyan, P., Inagaki, A., Bui, V. T., Kasahara, N., Cacalano, N., & Jewett, A. (2016). Resistance to cytotoxicity and sustained release of interleukin-6 and interleukin-8 in the presence of decreased interferon-γ after differentiation of glioblastoma by human natural killer cells. *Cancer Immunology, Immunotherapy: CII*, *65*(9), 1085–1097. https://doi.org/10.1007/s00262-016-1866-x

Kumar, R., de Mooij, T., Peterson, T. E., Kaptzan, T., Johnson, A. J., Daniels, D. J., & Parney, I. F. (2017). Modulating glioma-mediated myeloid-derived suppressor cell development with sulforaphane. *PloS One*, *12*(6), e0179012. https://doi.org/10.1371/journal.pone.0179012

Kuppner, M. C., van Meir, E., Hamou, M. F., & de Tribolet, N. (1990). Cytokine regulation of intercellular adhesion molecule-1 (ICAM-1) expression on human glioblastoma cells. *Clinical and Experimental Immunology*, *81*(1), 142–148. https://doi.org/10.1111/j.1365-2249.1990.tb05305.x

Lamy, L., Foussat, A., Brown, E. J., Bornstein, P., Ticchioni, M., & Bernard, A. (2007). Interactions between CD47 and thrombospondin reduce inflammation. *Journal of Immunology (Baltimore, Md.: 1950)*, *178*(9), 5930–5939. https://doi.org/10.4049/jimmunol.178.9.5930

Lane, R., Simon, T., Vintu, M., Solkin, B., Koch, B., Stewart, N., Benstead-Hume, G., Pearl, F. M. G., Critchley, G., Stebbing, J., & Giamas, G. (2019). Cell-derived extracellular vesicles can be used as a biomarker reservoir for glioblastoma tumor subtyping. *Communications Biology*, *2*(1), Article 1. https://doi.org/10.1038/s42003-019-0560-x

Li, C. C., Eaton, S. A., Young, P. E., Lee, M., Shuttleworth, R., Humphreys, D. T., Grau, G. E., Combes, V., Bebawy, M., Gong, J., Brammah, S., Buckland, M. E., & Suter, C. M. (2013). Glioma microvesicles carry selectively packaged coding and non-coding RNAs which alter gene expression in recipient cells. *RNA Biology*, *10*(8), 1333–1344. https://doi.org/10.4161/rna.25281

Li, C. C. Y., Eaton, S. A., Young, P. E., Lee, M., Shuttleworth, R., Humphreys, D. T., Grau, G. E., Combes, V., Bebawy, M., Gong, J., Brammah, S., Buckland, M. E., & Suter, C. M. (2013). Glioma microvesicles carry selectively packaged coding and non-coding RNAs which alter gene expression in recipient cells. *RNA Biology*, *10*(8), 1333–1344. https://doi.org/10.4161/rna.25281

Li, G., Wang, Z., Zhang, C., Liu, X., Cai, J., Wang, Z., Hu, H., Wu, F., Bao, Z., Liu, Y., Zhao, L., Liang, T., Yang, F., Huang, R., Zhang, W., & Jiang, T. (2017). Molecular and clinical characterization of TIM-3 in glioma through 1,024 samples. *Oncoimmunology*, *6*(8), e1328339. https://doi.org/10.1080/2162402X.2017.1328339

Linsley, P. S., Greene, J. L., Brady, W., Bajorath, J., Ledbetter, J. A., & Peach, R. (1994). Human B7-1 (CD80) and B7-2 (CD86) bind with similar avidities but distinct kinetics to CD28 and CTLA-4 receptors. *Immunity*, *1*(9), 793–801. https://doi.org/10.1016/s1074-7613(94)80021-9

Liu, Z., Han, H., He, X., Li, S., Wu, C., Yu, C., & Wang, S. (2016). Expression of the galectin-9-Tim-3 pathway in glioma tissues is associated with the clinical manifestations of glioma. *Oncology Letters*, *11*(3), 1829–1834. https://doi.org/10.3892/ol.2016.4142

Louis, D. N., Holland, E. C., & Cairncross, J. G. (2001). Glioma classification: A molecular reappraisal. *The American Journal of Pathology*, *159*(3), 779–786. https://doi.org/10.1016/S0002-9440(10)61750-6

Louveau, A., Harris, T. H., & Kipnis, J. (2015). Revisiting the concept of CNS immune privilege. *Trends in Immunology*, *36*(10), 569–577. https://doi.org/10.1016/j.it.2015.08.006

Lowin, B., Hahne, M., Mattmann, C., & Tschopp, J. (1994). Cytolytic T-cell cytotoxicity is mediated through perforin and Fas lytic pathways. *Nature*, *370*(6491), 650–652. https://doi.org/10.1038/370650a0

Lu, J., Li, H., Chen, Z., Fan, L., Feng, S., Cai, X., & Wang, H. (2019). Identification of 3 subpopulations of tumor-infiltrating immune cells for malignant transformation of low-grade glioma. *Cancer Cell International*, *19*, 265. https://doi.org/10.1186/s12935-019-0972-1

Luckheeram, R. V., Zhou, R., Verma, A. D., & Xia, B. (2012). CD4+T Cells: Differentiation and Functions. *Clinical and Developmental Immunology*, *2012*, 925135. https://doi.org/10.1155/2012/925135

Ma, Y., Qu, B., Xia, X., Yang, L., Kuang, Y., Yang, T., Cheng, J., Sun, H., Fan, K., & Gu, J. (2015). Glioma-derived thrombospondin-1 modulates cd14+ cell tolerogenic properties. *Cancer Investigation*, *33*(4), 152–157. https://doi.org/10.3109/07357907.2015.1010089

Maia, J., Caja, S., Strano Moraes, M. C., Couto, N., & Costa-Silva, B. (2018). Exosome-Based Cell-Cell Communication in the Tumor Microenvironment. *Frontiers in Cell and Developmental Biology*, *6*, 18. https://doi.org/10.3389/fcell.2018.00018

Mair, M. J., Kiesel, B., Feldmann, K., Widhalm, G., Dieckmann, K., Wöhrer, A., Müllauer, L., Preusser, M., & Berghoff, A. S. (2021). LAG-3 expression in the inflammatory microenvironment of glioma. *Journal of Neuro-Oncology*, *152*(3), 533–539. https://doi.org/10.1007/s11060-021-03721-x

Mak, T. W., Saunders, M. E., & Jett, B. D. (2014). *Primer to The Immune Response: Second Edition*. 1–674.

Mangano, K., Mazzon, E., Basile, M. S., Di Marco, R., Bramanti, P., Mammana, S., Petralia, M. C., Fagone, P., & Nicoletti, F. (2018). Pathogenic role for macrophage migration inhibitory factor in glioblastoma and its targeting with specific inhibitors as novel tailored therapeutic approach. *Oncotarget*, *9*(25), 17951–17970. https://doi.org/10.18632/oncotarget.24885

Marcus, A., Gowen, B. G., Thompson, T. W., Iannello, A., Ardolino, M., Deng, W., Wang, L., Shifrin, N., & Raulet, D. H. (2014). Recognition of tumors by the innate immune system and natural killer cells. *Advances in Immunology*, *122*, 91–128. https://doi.org/10.1016/B978-0-12-800267-4.00003-1

McBride, M. A., Patil, T. K., Bohannon, J. K., Hernandez, A., Sherwood, E. R., & Patil, N. K. (2021). Immune Checkpoints: Novel Therapeutic Targets to Attenuate Sepsis-Induced

Immunosuppression. *Frontiers in Immunology*, *11*. https://www.frontiersin.org/article/10.3389/fimmu.2020.624272

Medawar, P. B. (1948). Immunity to Homologous Grafted Skin. III. The Fate of Skin Homographs Transplanted to the Brain, to Subcutaneous Tissue, and to the Anterior Chamber of the Eye. *British Journal of Experimental Pathology*, *29*(1), 58–69.

Mittal, D., Gubin, M. M., Schreiber, R. D., & Smyth, M. J. (2014). New insights into cancer immunoediting and its three component phases—Elimination, equilibrium and escape. *Current Opinion in Immunology*, *27*, 16–25. https://doi.org/10.1016/j.coi.2014.01.004

Mittelbronn, M., Platten, M., Zeiner, P., Dombrowski, Y., Frank, B., Zachskorn, C., Harter, P. N., Weller, M., & Wischhusen, J. (2011). Macrophage migration inhibitory factor (MIF) expression in human malignant gliomas contributes to immune escape and tumour progression. *Acta Neuropathologica*, *122*(3), 353–365. https://doi.org/10.1007/s00401-011-0858-3

Mondal, A., Kumari Singh, D., Panda, S., & Shiras, A. (2017). Extracellular Vesicles As Modulators of Tumor Microenvironment and Disease Progression in Glioma. *Frontiers in Oncology*, *7*, 144. https://doi.org/10.3389/fonc.2017.00144

Morgan, F. S. B. and D. J. (2018). ICAM-1 overexpression counteracts immune-suppression by tumour cell-derived PGE2 to restore CTL function. *Journal of Immunological Sciences*, *2*(1). https://www.immunologyresearchjournal.com/articles/icam1-overexpression-counteracts-immunesuppression-by-tumour-cellderived-pgesub2sub-to-restore-ctl-function.html

Mori, S., Jewett, A., Murakami-Mori, K., Cavalcanti, M., & Bonavida, B. (1997). The participation of the Fas-mediated cytotoxic pathway by natural killer cells is tumor-cell-dependent. *Cancer Immunology, Immunotherapy: CII*, *44*(5), 282–290. https://doi.org/10.1007/s002620050384

Motz, G. T., & Coukos, G. (2013). Deciphering and reversing tumor immune suppression. *Immunity*, *39*(1), 61–73. https://doi.org/10.1016/j.immuni.2013.07.005

Mulcahy, L. A., Pink, R. C., & Carter, D. R. F. (2014). Routes and mechanisms of extracellular vesicle uptake. *Journal of Extracellular Vesicles*, *3*. https://doi.org/10.3402/jev.v3.24641

Müller-Hermelink, N., Braumüller, H., Pichler, B., Wieder, T., Mailhammer, R., Schaak, K., Ghoreschi, K., Yazdi, A., Haubner, R., Sander, C. A., Mocikat, R., Schwaiger, M., Förster, I., Huss, R., Weber, W. A., Kneilling, M., & Röcken, M. (2008). TNFR1 signaling and IFN-gamma signaling determine whether T cells induce tumor dormancy or promote multistage carcinogenesis. *Cancer Cell*, *13*(6), 507–518. https://doi.org/10.1016/j.ccr.2008.04.001

Nduom, E. K., Weller, M., & Heimberger, A. B. (2015). Immunosuppressive mechanisms in glioblastoma. *Neuro-Oncology*, *17 Suppl 7*, vii9–vii14. https://doi.org/10.1093/neuonc/nov151

Negi, N., & Das, B. K. (2018a). CNS: Not an immunoprivilaged site anymore but a virtual secondary lymphoid organ. *International Reviews of Immunology*, *37*(1), 57–68. https://doi.org/10.1080/08830185.2017.1357719

Negi, N., & Das, B. K. (2018b). CNS: Not an immunoprivilaged site anymore but a virtual secondary lymphoid organ. *International Reviews of Immunology*, *37*(1), 57–68. https://doi.org/10.1080/08830185.2017.1357719

Noerholm, M., Balaj, L., Limperg, T., Salehi, A., Zhu, L. D., Hochberg, F. H., Breakefield, X. O., Carter, B. S., & Skog, J. (2012). RNA expression patterns in serum microvesicles from patients with glioblastoma multiforme and controls. *BMC Cancer*, *12*(1), 22. https://doi.org/10.1186/1471-2407-12-22

Noman, M. Z., Hasmim, M., Messai, Y., Terry, S., Kieda, C., Janji, B., & Chouaib, S. (2015). Hypoxia: A key player in antitumor immune response. A Review in the Theme: Cellular Responses to Hypoxia. *American Journal of Physiology - Cell Physiology*, *309*(9), C569–C579. https://doi.org/10.1152/ajpcell.00207.2015

Nurieva, R. I., Liu, X., & Dong, C. (2009). Yin-Yang of costimulation: Crucial controls of immune tolerance and function. *Immunological Reviews*, *229*(1), 88–100. https://doi.org/10.1111/j.1600-065X.2009.00769.x

Ohgaki, H., & Kleihues, P. (2013). The definition of primary and secondary glioblastoma. *Clinical Cancer Research: An Official Journal of the American Association for Cancer Research*, *19*(4), 764–772. https://doi.org/10.1158/1078-0432.CCR-12-3002

Ohlendieck, K., & Harding, S. E. (2018). Centrifugation and Ultracentrifugation. In A. Hofmann & S. Clokie (Eds.), *Wilson and Walker's Principles and Techniques of Biochemistry and Molecular Biology* (8th ed., pp. 424–453). Cambridge University Press. https://doi.org/10.1017/9781316677056.014

Okada, H., Kohanbash, G., Zhu, X., Kastenhuber, E. R., Hoji, A., Ueda, R., & Fujita, M. (2009). Immunotherapeutic Approaches for Glioma. *Critical Reviews in Immunology*, *29*(1), 1–42.

Ooi, Y. C., Tran, P., Ung, N., Thill, K., Trang, A., Fong, B. M., Nagasawa, D. T., Lim, M., & Yang, I. (2014). The role of regulatory T-cells in glioma immunology. *Clinical Neurology and Neurosurgery*, *119*, 125–132. https://doi.org/10.1016/j.clineuro.2013.12.004

Ostrom, Q. T., Gittleman, H., Liao, P., Rouse, C., Chen, Y., Dowling, J., Wolinsky, Y., Kruchko, C., & Barnholtz-Sloan, J. (2014). CBTRUS Statistical Report: Primary Brain and Central Nervous System Tumors Diagnosed in the United States in 2007–2011. *Neuro-Oncology*, *16*(Suppl 4), iv1–iv63. https://doi.org/10.1093/neuonc/nou223

Oushy, S., Hellwinkel, J. E., Wang, M., Nguyen, G. J., Gunaydin, D., Harland, T. A., Anchordoquy, T. J., & Graner, M. W. (2018). Glioblastoma multiforme-derived extracellular vesicles drive normal astrocytes towards a tumour-enhancing phenotype. *Philosophical Transactions of the Royal Society of London. Series B, Biological Sciences*, *373*(1737), 20160477. https://doi.org/10.1098/rstb.2016.0477

Papachristodoulou, A., Silginer, M., Weller, M., Schneider, H., Hasenbach, K., Janicot, M., & Roth, P. (2019). Therapeutic Targeting of TGFβ Ligands in Glioblastoma Using Novel Antisense Oligonucleotides Reduces the Growth of Experimental Gliomas. *Clinical Cancer Research: An Official Journal of the American Association for Cancer Research*, *25*(23), 7189–7201. https://doi.org/10.1158/1078-0432.CCR-17-3024

Pardoll, D. M. (2012). The blockade of immune checkpoints in cancer immunotherapy. *Nature Reviews Cancer*, *12*(4), Article 4. https://doi.org/10.1038/nrc3239

Park, J. H., Kim, H.-J., Kim, C. W., Kim, H. C., Jung, Y., Lee, H.-S., Lee, Y., Ju, Y. S., Oh, J. E., Park, S.-H., Lee, J. H., Lee, S. K., & Lee, H. K. (2021). Tumor hypoxia represses γδ T cell-mediated antitumor immunity against brain tumors. *Nature Immunology*, *22*(3), 336–346. https://doi.org/10.1038/s41590-020-00860-7

Perng, P., & Lim, M. (2015). Immunosuppressive Mechanisms of Malignant Gliomas: Parallels at Non-CNS Sites. *Frontiers in Oncology*, *5*, 153. https://doi.org/10.3389/fonc.2015.00153

Phillips, H. S., Kharbanda, S., Chen, R., Forrest, W. F., Soriano, R. H., Wu, T. D., Misra, A., Nigro, J. M., Colman, H., Soroceanu, L., Williams, P. M., Modrusan, Z., Feuerstein, B. G., & Aldape, K. (2006). Molecular subclasses of high-grade glioma predict prognosis, delineate a pattern of disease progression, and resemble stages in neurogenesis. *Cancer Cell*, *9*(3), 157–173. https://doi.org/10.1016/j.ccr.2006.02.019

Piao, Y., Henry, V., Tiao, N., Park, S. Y., Martinez-Ledesma, J., Dong, J. W., Balasubramaniyan, V., & de Groot, J. F. (2017). Targeting intercellular adhesion molecule-1 prolongs survival in mice bearing bevacizumab-resistant glioblastoma. *Oncotarget*, *8*(57), 96970–96983. https://doi.org/10.18632/oncotarget.18859

Pirro, V., Alfaro, C. M., Jarmusch, A. K., Hattab, E. M., Cohen-Gadol, A. A., & Cooks, R. G. (2017). Intraoperative assessment of tumor margins during glioma resection by desorption electrospray ionization-mass spectrometry. *Proceedings of the National Academy of Sciences of the United States of America*, *114*(26), 6700–6705. https://doi.org/10.1073/pnas.1706459114

Popescu, I. D., Codrici, E., Albulescu, L., Mihai, S., Enciu, A.-M., Albulescu, R., & Tanase, C. P. (2014). Potential serum biomarkers for glioblastoma diagnostic assessed by proteomic approaches. *Proteome Science*, *12*(1), 47. https://doi.org/10.1186/s12953-014-0047-0

Ratajczak, J., Wysoczynski, M., Hayek, F., Janowska-Wieczorek, A., & Ratajczak, M. Z. (2006). Membrane-derived microvesicles: Important and underappreciated mediators of cell-to-cell communication. *Leukemia*, *20*(9), Article 9. https://doi.org/10.1038/sj.leu.2404296

Redzic, J. S., Balaj, L., van der Vos, K. E., & Breakefield, X. O. (2014). Extracellular RNA mediates and marks cancer progression. *Seminars in Cancer Biology*, *28*, 14–23. https://doi.org/10.1016/j.semcancer.2014.04.010

Ribatti, D. (2016). The concept of immune surveillance against tumors: The first theories. *Oncotarget*, *8*(4), 7175–7180. https://doi.org/10.18632/oncotarget.12739

Rich, R. R., Fleisher, T. A., Shearer, W. T., Schroeder, H. W., Frew, A. J., & Weyand, C. (2012). *Clinical immunology: Principles and practice: Fourth edition* (p. 1295).

Ricklefs, F. L., Alayo, Q., Krenzlin, H., Mahmoud, A. B., Speranza, M. C., Nakashima, H., Hayes, J. L., Lee, K., Balaj, L., Passaro, C., Rooj, A. K., Krasemann, S., Carter, B. S., Chen, C. C.,

Steed, T., Treiber, J., Rodig, S., Yang, K., Nakano, I., … Chiocca, E. A. (2018). Immune evasion mediated by PD-L1 on glioblastoma-derived extracellular vesicles. *Science Advances*, *4*(3), eaar2766. https://doi.org/10.1126/sciadv.aar2766

Ricklefs, F., Mineo, M., Rooj, A. K., Nakano, I., Charest, A., Weissleder, R., Breakefield, X. O., Chiocca, E. A., Godlewski, J., & Bronisz, A. (2016). Extracellular Vesicles from High-Grade Glioma Exchange Diverse Pro-oncogenic Signals That Maintain Intratumoral Heterogeneity. *Cancer Research*, *76*(10), 2876–2881. https://doi.org/10.1158/0008-5472.CAN-15-3432

Rodrigues, J. C., Gonzalez, G. C., Zhang, L., Ibrahim, G., Kelly, J. J., Gustafson, M. P., Lin, Y., Dietz, A. B., Forsyth, P. A., Yong, V. W., & Parney, I. F. (2010). Normal human monocytes exposed to glioma cells acquire myeloid-derived suppressor cell-like properties. *Neuro-Oncology*, *12*(4), 351–365. https://doi.org/10.1093/neuonc/nop023

Roessler, K., Suchanek, G., Breitschopf, H., Kitz, K., Matula, C., Lassmann, H., & Koos, W. T. (1995). Detection of tumor necrosis factor-α protein and messenger RNA in human glial brain tumors: Comparison of immunohistochemistry with in situ hybridization using molecular probes. *Journal of Neurosurgery*, *83*(2), 291–297. https://doi.org/10.3171/jns.1995.83.2.0291

Ronquist, K. G., Sanchez, C., Dubois, L., Chioureas, D., Fonseca, P., Larsson, A., Ullén, A., Yachnin, J., Ronquist, G., & Panaretakis, T. (2016). Energy-requiring uptake of prostasomes and PC3 cell-derived exosomes into non-malignant and malignant cells. *Journal of Extracellular Vesicles*, *5*, 29877. https://doi.org/10.3402/jev.v5.29877

Rosa-Fernandes, L., Rocha, V. B., Carregari, V. C., Urbani, A., & Palmisano, G. (2017). A Perspective on Extracellular Vesicles Proteomics. *Frontiers in Chemistry*, *5*, 102. https://doi.org/10.3389/fchem.2017.00102

Roth, P., Mittelbronn, M., Wick, W., Meyermann, R., Tatagiba, M., & Weller, M. (2007). Malignant glioma cells counteract antitumor immune responses through expression of lectin-like transcript-1. *Cancer Research*, *67*(8), 3540–3544. https://doi.org/10.1158/0008-5472.CAN-06-4783

Sagini, K., Costanzi, E., Emiliani, C., Buratta, S., & Urbanelli, L. (2018). Extracellular Vesicles as Conveyors of Membrane-Derived Bioactive Lipids in Immune System. *International Journal of Molecular Sciences*, *19*(4), E1227. https://doi.org/10.3390/ijms19041227

Saito, H., Shimizu, S., Kono, Y., Murakami, Y., Shishido, Y., Miyatani, K., Matsunaga, T., Fukumoto, Y., Ashida, K., & Fujiwara, Y. (2019). PD-1 Expression on Circulating CD8+ T-Cells as a Prognostic Marker for Patients With Gastric Cancer. *Anticancer Research*, *39*(1), 443–448. https://doi.org/10.21873/anticanres.13132

Sakaguchi, S., Wing, K., Onishi, Y., Prieto-Martin, P., & Yamaguchi, T. (2009). Regulatory T cells: How do they suppress immune responses? *International Immunology*, *21*(10), 1105–1111. https://doi.org/10.1093/intimm/dxp095

Santiago-Dieppa, D. R., Steinberg, J., Gonda, D., Cheung, V. J., Carter, B. S., & Chen, C. C. (2014). Extracellular vesicles as a platform for 'liquid biopsy' in glioblastoma patients. *Expert Review of Molecular Diagnostics*, *14*(7), 819–825. https://doi.org/10.1586/14737159.2014.943193

Sayour, E. J., McLendon, P., McLendon, R., De Leon, G., Reynolds, R., Kresak, J., Sampson, J. H., & Mitchell, D. A. (2015). Increased proportion of FoxP3+ regulatory T cells in tumor infiltrating lymphocytes is associated with tumor recurrence and reduced survival in patients with glioblastoma. *Cancer Immunology, Immunotherapy: CII*, *64*(4), 419–427. https://doi.org/10.1007/s00262-014-1651-7

Scheffel, T. B., Grave, N., Vargas, P., Diz, F. M., Rockenbach, L., & Morrone, F. B. (2021). Immunosuppression in Gliomas via PD-1/PD-L1 Axis and Adenosine Pathway. *Frontiers in Oncology*, *10*. https://www.frontiersin.org/article/10.3389/fonc.2020.617385

Scholl, J. N., Dias, A. de F., Pizzato, P. R., Lopes, D. V., Moritz, C. E. J., Jandrey, E. H. F., Souto, G. D., Colombo, M., Rohden, F., Sévigny, J., Pohlmann, A. R., Guterres, S. S., Battastini, A. M. O., & Figueiró, F. (2020). Characterization and antiproliferative activity of glioma-derived extracellular vesicles. *Nanomedicine*. https://doi.org/10.2217/nnm-2019-0431

Schreiner, B., Wischhusen, J., Mitsdoerffer, M., Schneider, D., Bornemann, A., Melms, A., Tolosa, E., Weller, M., & Wiendl, H. (2003). Expression of the B7-related molecule ICOSL by human glioma cells in vitro and in vivo. *Glia*, *44*(3), 296–301. https://doi.org/10.1002/glia.10291

Sedgwick, A. J., Ghazanfari, N., Constantinescu, P., Mantamadiotis, T., & Barrow, A. D. (2020). The Role of NK Cells and Innate Lymphoid Cells in Brain Cancer. *Frontiers in Immunology*, *11*. https://www.frontiersin.org/article/10.3389/fimmu.2020.01549

Setti, M., Osti, D., Richichi, C., Ortensi, B., Del Bene, M., Fornasari, L., Beznoussenko, G., Mironov, A., Rappa, G., Cuomo, A., Faretta, M., Bonaldi, T., Lorico, A., & Pelicci, G. (2015). Extracellular vesicle-mediated transfer of CLIC1 protein is a novel mechanism for the regulation of glioblastoma growth. *Oncotarget*, *6*(31), 31413–31427. https://doi.org/10.18632/oncotarget.5105

Shen, R., Mo, Q., Schultz, N., Seshan, V. E., Olshen, A. B., Huse, J., Ladanyi, M., & Sander, C. (2012). Integrative subtype discovery in glioblastoma using iCluster. *PloS One*, *7*(4), e35236. https://doi.org/10.1371/journal.pone.0035236

Simpson, K. D., Templeton, D. J., & Cross, J. V. (2012). Macrophage migration inhibitory factor promotes tumor growth and metastasis by inducing myeloid-derived suppressor cells in

the tumor microenvironment. *Journal of Immunology (Baltimore, Md.: 1950)*, *189*(12), 5533–5540. https://doi.org/10.4049/jimmunol.1201161

Skog, J., Wurdinger, T., van Rijn, S., Meijer, D., Gainche, L., Sena-Esteves, M., Curry, W. T., Carter, R. S., Krichevsky, A. M., & Breakefield, X. O. (2008). Glioblastoma microvesicles transport RNA and protein that promote tumor growth and provide diagnostic biomarkers. *Nature Cell Biology*, *10*(12), 1470–1476. https://doi.org/10.1038/ncb1800

Sonabend, A. M., Rolle, C. E., & Lesniak, M. S. (2008). The Role of Regulatory T Cells in Malignant Glioma. *Anticancer Research*, *28*(2B), 1143–1150.

Spinelli, C., Montermini, L., Meehan, B., Brisson, A. R., Tan, S., Choi, D., Nakano, I., & Rak, J. (2018). Molecular subtypes and differentiation programmes of glioma stem cells as determinants of extracellular vesicle profiles and endothelial cell-stimulating activities. *Journal of Extracellular Vesicles*, *7*(1), 1490144. https://doi.org/10.1080/20013078.2018.1490144

Stranska, R., Gysbrechts, L., Wouters, J., Vermeersch, P., Bloch, K., Dierickx, D., Andrei, G., & Snoeck, R. (2018). Comparison of membrane affinity-based method with size-exclusion chromatography for isolation of exosome-like vesicles from human plasma. *Journal of Translational Medicine*, *16*(1), 1. https://doi.org/10.1186/s12967-017-1374-6

Stupp, R., Mason, W. P., van den Bent, M. J., Weller, M., Fisher, B., Taphoorn, M. J. B., Belanger, K., Brandes, A. A., Marosi, C., Bogdahn, U., Curschmann, J., Janzer, R. C., Ludwin, S. K., Gorlia, T., Allgeier, A., Lacombe, D., Cairncross, J. G., Eisenhauer, E., Mirimanoff, R. O., … National Cancer Institute of Canada Clinical Trials Group. (2005). Radiotherapy plus concomitant and adjuvant temozolomide for glioblastoma. *The New England Journal of Medicine*, *352*(10), 987–996. https://doi.org/10.1056/NEJMoa043330

Sugawa, N., Ekstrand, A. J., James, C. D., & Collins, V. P. (1990). Identical splicing of aberrant epidermal growth factor receptor transcripts from amplified rearranged genes in human glioblastomas. *Proceedings of the National Academy of Sciences of the United States of America*, *87*(21), 8602–8606. https://doi.org/10.1073/pnas.87.21.8602

Swann, J. B., & Smyth, M. J. (2007). Immune surveillance of tumors. *Journal of Clinical Investigation*, *117*(5), 1137–1146. https://doi.org/10.1172/JCI31405

Tambuyzer, B. R., Ponsaerts, P., & Nouwen, E. J. (2009). Microglia: Gatekeepers of central nervous system immunology. *Journal of Leukocyte Biology*, *85*(3), 352–370. https://doi.org/10.1189/jlb.0608385

Tankov, S., & Walker, P. R. (2021). Glioma-Derived Extracellular Vesicles – Far More Than Local Mediators. *Frontiers in Immunology*, *12*. https://www.frontiersin.org/article/10.3389/fimmu.2021.679954

Tchirkov, A., Rolhion, C., Bertrand, S., Doré, J.-F., Dubost, J.-J., & Verrelle, P. (2001). IL-6 gene amplification and expression in human glioblastomas. *British Journal of Cancer*, *85*(4), 518–522. https://doi.org/10.1054/bjoc.2001.1942

Teng, M. W. L., Vesely, M. D., Duret, H., McLaughlin, N., Towne, J. E., Schreiber, R. D., & Smyth, M. J. (2012). Opposing roles for IL-23 and IL-12 in maintaining occult cancer in an equilibrium state. *Cancer Research*, *72*(16), 3987–3996. https://doi.org/10.1158/0008-5472.CAN-12-1337

Teo, W.-Y., Sekar, K., Seshachalam, P., Shen, J., Chow, W.-Y., Lau, C. C., Yang, H., Park, J., Kang, S.-G., Li, X., Nam, D.-H., & Hui, K. M. (2019). Relevance of a TCGA-derived Glioblastoma Subtype Gene-Classifier among Patient Populations. *Scientific Reports*, *9*(1), 7442. https://doi.org/10.1038/s41598-019-43173-y

Terabe, M., Park, J. M., & Berzofsky, J. A. (2004). Role of IL-13 in regulation of anti-tumor immunity and tumor growth. *Cancer Immunology, Immunotherapy: CII*, *53*(2), 79–85. https://doi.org/10.1007/s00262-003-0445-0

Thakkar, J. P., Dolecek, T. A., Horbinski, C., Ostrom, Q. T., Lightner, D. D., Barnholtz-Sloan, J. S., & Villano, J. L. (2014). Epidemiologic and Molecular Prognostic Review of Glioblastoma. *Cancer Epidemiology, Biomarkers & Prevention : A Publication of the American Association for Cancer Research, Cosponsored by the American Society of Preventive Oncology*, *23*(10), 1985–1996. https://doi.org/10.1158/1055-9965.EPI-14-0275

Thiem, A., Hesbacher, S., Kneitz, H., di Primio, T., Heppt, M. V., Hermanns, H. M., Goebeler, M., Meierjohann, S., Houben, R., & Schrama, D. (2019). IFN-gamma-induced PD-L1 expression in melanoma depends on p53 expression. *Journal of Experimental & Clinical Cancer Research*, *38*(1), 397. https://doi.org/10.1186/s13046-019-1403-9

Treps, L., Perret, R., Edmond, S., Ricard, D., & Gavard, J. (2017). Glioblastoma stem-like cells secrete the pro-angiogenic VEGF-A factor in extracellular vesicles. *Journal of Extracellular Vesicles*, *6*(1), 1359479. https://doi.org/10.1080/20013078.2017.1359479

Tseng, D., Volkmer, J.-P., Willingham, S. B., Contreras-Trujillo, H., Fathman, J. W., Fernhoff, N. B., Seita, J., Inlay, M. A., Weiskopf, K., Miyanishi, M., & Weissman, I. L. (2013). Anti-CD47 antibody–mediated phagocytosis of cancer by macrophages primes an effective antitumor T-cell response. *Proceedings of the National Academy of Sciences*, *110*(27), 11103–11108. https://doi.org/10.1073/pnas.1305569110

Vahedi, G., Kanno, Y., Sartorelli, V., & O'Shea, J. J. (2013). Transcription factors and CD4 T cells seeking identity: Masters, minions, setters and spikers. *Immunology*, *139*(3), 294–298. https://doi.org/10.1111/imm.12113

Valdor, R., García-Bernal, D., Bueno, C., Ródenas, M., Moraleda, J. M., Macian, F., & Martínez, S. (2017). Glioblastoma progression is assisted by induction of immunosuppressive function of pericytes through interaction with tumor cells. *Oncotarget*, *8*(40), 68614–68626. https://doi.org/10.18632/oncotarget.19804

Vergauwen, G., Dhondt, B., Van Deun, J., De Smedt, E., Berx, G., Timmerman, E., Gevaert, K., Miinalainen, I., Cocquyt, V., Braems, G., Van den Broecke, R., Denys, H., De Wever, O., & Hendrix, A. (2017). Confounding factors of ultrafiltration and protein analysis in extracellular vesicle research. *Scientific Reports*, *7*(1), 2704. https://doi.org/10.1038/s41598-017-02599-y

Verhaak, R. G. W., Hoadley, K. A., Purdom, E., Wang, V., Qi, Y., Wilkerson, M. D., Miller, C. R., Ding, L., Golub, T., Mesirov, J. P., Alexe, G., Lawrence, M., O'Kelly, M., Tamayo, P., Weir, B. A., Gabrie, S., Winckler, W., Gupta, S., Jakkula, L., … Hayes, D. N. (2010). An integrated genomic analysis identifies clinically relevant subtypes of glioblastoma characterized by abnormalities in PDGFRA, IDH1, EGFR and NF1. *Cancer Cell*, *17*(1), 98. https://doi.org/10.1016/j.ccr.2009.12.020

Wainwright, D. A., Sengupta, S., Han, Y., Ulasov, I. V., & Lesniak, M. S. (2010). The Presence of IL-17A and T Helper 17 Cells in Experimental Mouse Brain Tumors and Human Glioma. *PLOS ONE*, *5*(10), e15390. https://doi.org/10.1371/journal.pone.0015390

Wallmann, T., Zhang, X.-M., Wallerius, M., Bolin, S., Joly, A.-L., Sobocki, C., Leiss, L., Jiang, Y., Bergh, J., Holland, E. C., Enger, P. Ø., Andersson, J., Swartling, F. J., Miletic, H., Uhrbom, L., Harris, R. A., & Rolny, C. (2018). Microglia Induce PDGFRB Expression in Glioma Cells to Enhance Their Migratory Capacity. *IScience*, *9*, 71–83. https://doi.org/10.1016/j.isci.2018.10.011

Wang, M., Cai, Y., Peng, Y., Xu, B., Hui, W., & Jiang, Y. (2020). Exosomal LGALS9 in the cerebrospinal fluid of glioblastoma patients suppressed dendritic cell antigen presentation and cytotoxic T-cell immunity. *Cell Death & Disease*, *11*(10), Article 10. https://doi.org/10.1038/s41419-020-03042-3

Wang, M., Jia, J., Cui, Y., Peng, Y., & Jiang, Y. (2021). CD73-positive extracellular vesicles promote glioblastoma immunosuppression by inhibiting T-cell clonal expansion. *Cell Death & Disease*, *12*(11), Article 11. https://doi.org/10.1038/s41419-021-04359-3

Wang, Q., Hu, B., Hu, X., Kim, H., Squatrito, M., Scarpace, L., deCarvalho, A. C., Lyu, S., Li, P., Li, Y., Barthel, F., Cho, H. J., Lin, Y.-H., Satani, N., Martinez-Ledesma, E., Zheng, S., Chang, E., Sauvé, C.-E. G., Olar, A., … Verhaak, R. G. W. (2017). Tumor evolution of glioma intrinsic gene expression subtype associates with immunological changes in the microenvironment. *Cancer Cell*, *32*(1), 42-56.e6. https://doi.org/10.1016/j.ccell.2017.06.003

Wei, J., Wu, A., Kong, L.-Y., Wang, Y., Fuller, G., Fokt, I., Melillo, G., Priebe, W., & Heimberger, A. B. (2011). Hypoxia Potentiates Glioma-Mediated Immunosuppression. *PLOS ONE*, *6*(1), e16195. https://doi.org/10.1371/journal.pone.0016195

Wei, Q., Singh, O., Ekinci, C., Gill, J., Li, M., Mamatjan, Y., Karimi, S., Bunda, S., Mansouri, S., Aldape, K., & Zadeh, G. (2021). TNFα secreted by glioma associated macrophages promotes endothelial activation and resistance against anti-angiogenic therapy. *Acta Neuropathologica Communications*, *9*(1), 67. https://doi.org/10.1186/s40478-021-01163-0

Westendorf, A. M., Skibbe, K., Adamczyk, A., Buer, J., Geffers, R., Hansen, W., Pastille, E., & Jendrossek, V. (2017). Hypoxia Enhances Immunosuppression by Inhibiting CD4+ Effector T Cell Function and Promoting Treg Activity. *Cellular Physiology and Biochemistry: International Journal of Experimental Cellular Physiology, Biochemistry, and Pharmacology*, *41*(4), 1271–1284. https://doi.org/10.1159/000464429

Wilson, T. A., Karajannis, M. A., & Harter, D. H. (2014). Glioblastoma multiforme: State of the art and future therapeutics. *Surgical Neurology International*, *5*, 64. https://doi.org/10.4103/2152-7806.132138

Wójtowicz, A., & Wietecha-Posłuszny, R. (2019). DESI-MS analysis of human fluids and tissues for forensic applications. *Applied Physics A*, *125*(5), 312. https://doi.org/10.1007/s00339-019-2564-2

Wu, A., Wei, J., Kong, L.-Y., Wang, Y., Priebe, W., Qiao, W., Sawaya, R., & Heimberger, A. B. (2010). Glioma cancer stem cells induce immunosuppressive macrophages/microglia. *Neuro-Oncology*, *12*(11), 1113–1125. https://doi.org/10.1093/neuonc/noq082

Wu, X., Peng, M., Huang, B., Zhang, H., Wang, H., Huang, B., Xue, Z., Zhang, L., Da, Y., Yang, D., Yao, Z., & Zhang, R. (2013). Immune microenvironment profiles of tumor immune equilibrium and immune escape states of mouse sarcoma. *Cancer Letters*, *340*(1), 124–133. https://doi.org/10.1016/j.canlet.2013.07.038

Xu, Y., Chen, L., Xu, B., Xiong, Y., Yang, M., Rui, X., Shi, L., Wu, C., Lu, B., & Jiang, J. (2017). Higher Numbers of T-Bet+ Tumor-Infiltrating Lymphocytes Associate with Better Survival in Human Epithelial Ovarian Cancer. *Cellular Physiology and Biochemistry*, *41*(2), 475–483. https://doi.org/10.1159/000456600

Xue, H., Yuan, G., Guo, X., Liu, Q., Zhang, J., Gao, X., Guo, X., Xu, S., Li, T., Shao, Q., Yan, S., & Li, G. (2016). A novel tumor-promoting mechanism of IL6 and the therapeutic efficacy of tocilizumab: Hypoxia-induced IL6 is a potent autophagy initiator in glioblastoma via the p-STAT3-MIR155-3p-CREBRF pathway. *Autophagy*, *12*(7), 1129–1152. https://doi.org/10.1080/15548627.2016.1178446

Yan, X., Orentas, R. J., & Johnson, B. D. (2006). Tumor-derived macrophage migration inhibitory factor (MIF) inhibits T lymphocyte activation. *Cytokine*, *33*(4), 188–198. https://doi.org/10.1016/j.cyto.2006.01.006

Yáñez-Mó, M., Siljander, P. R.-M., Andreu, Z., Zavec, A. B., Borràs, F. E., Buzas, E. I., Buzas, K., Casal, E., Cappello, F., Carvalho, J., Colás, E., Silva, A. C., Fais, S., Falcon-Perez, J. M., Ghobrial, I. M., Giebel, B., Gimona, M., Graner, M., Gursel, I., … De Wever, O. (2015). Biological properties of extracellular vesicles and their physiological functions. *Journal of Extracellular Vesicles*, *4*, 10.3402/jev.v4.27066. https://doi.org/10.3402/jev.v4.27066

Yang, I., Han, S. J., Kaur, G., Crane, C., & Parsa, A. T. (2010). The role of microglia in central nervous system immunity and glioma immunology. *Journal of Clinical Neuroscience: Official Journal of the Neurosurgical Society of Australasia*, *17*(1), 6–10. https://doi.org/10.1016/j.jocn.2009.05.006

Yang, J., Yao, Y., Tong, L., Zhu, Z., Wang, L., & Yang, J. (2021). CD47 is highly expressed in gliomas and targeting CD47 is a promising therapeutic strategy. *European Journal of Inflammation*, *19*, 20587392211000900. https://doi.org/10.1177/20587392211000899

Yao, M., Li, S., Wu, X., Diao, S., Zhang, G., He, H., Bian, L., & Lu, Y. (2018). Cellular origin of glioblastoma and its implication in precision therapy. *Cellular & Molecular Immunology*, *15*(8), 737–739. https://doi.org/10.1038/cmi.2017.159

Yekula, A., Yekula, A., Muralidharan, K., Kang, K., Carter, B. S., & Balaj, L. (2020). Extracellular Vesicles in Glioblastoma Tumor Microenvironment. *Frontiers in Immunology*, *10*, 3137. https://doi.org/10.3389/fimmu.2019.03137

Yu, M. W., & Quail, D. F. (2021). Immunotherapy for Glioblastoma: Current Progress and Challenges. *Frontiers in Immunology*, *12*. https://www.frontiersin.org/article/10.3389/fimmu.2021.676301

Yuana, Y., Sturk, A., & Nieuwland, R. (2013). Extracellular vesicles in physiological and pathological conditions. *Blood Reviews*, *27*(1), 31–39. https://doi.org/10.1016/j.blre.2012.12.002

Zhang, H.-P., Wu, Y., Liu, J., Jiang, J., Geng, X.-R., Yang, G., Mo, L., Liu, Z.-Q., Liu, Z.-G., & Yang, P.-C. (2013). TSP1-producing B cells show immune regulatory property and suppress allergy-related mucosal inflammation. *Scientific Reports*, *3*, 3345. https://doi.org/10.1038/srep03345

Zhang, J., Stevens, M. F. G., & Bradshaw, T. D. (2012). Temozolomide: Mechanisms of action, repair and resistance. *Current Molecular Pharmacology*, *5*(1), 102–114. https://doi.org/10.2174/1874467211205010102

Zhang, P., Xia, Q., Liu, L., Li, S., & Dong, L. (2020). Current Opinion on Molecular Characterization for GBM Classification in Guiding Clinical Diagnosis, Prognosis, and Therapy. *Frontiers in Molecular Biosciences*, *7*, 241. https://doi.org/10.3389/fmolb.2020.562798

Zhang, W., Zhong, W., Wang, B., Yang, J., Yang, J., Yu, Z., Qin, Z., Shi, A., Xu, W., Zheng, C., Schuchter, L. M., Karakousis, G. C., Mitchell, T. C., Amaravadi, R., Herlyn, M., Dong, H., Gimotty, P. A., Daaboul, G., Xu, X., & Guo, W. (2022). ICAM-1-mediated adhesion is a prerequisite for exosome-induced T cell suppression. *Developmental Cell*, *57*(3), 329-343.e7. https://doi.org/10.1016/j.devcel.2022.01.002

Zhang, Y., Dube, C., Gibert, M., Cruickshanks, N., Wang, B., Coughlan, M., Yang, Y., Setiady, I., Deveau, C., Saoud, K., Grello, C., Oxford, M., Yuan, F., & Abounader, R. (2018). The p53 Pathway in Glioblastoma. *Cancers*, *10*(9), 297. https://doi.org/10.3390/cancers10090297

Zhang, Y., Luo, Y., Qin, S.-L., Mu, Y.-F., Qi, Y., Yu, M.-H., & Zhong, M. (2016). The clinical impact of ICOS signal in colorectal cancer patients. *Oncoimmunology*, *5*(5), e1141857. https://doi.org/10.1080/2162402X.2016.1141857

Zhao, H., Yang, L., Baddour, J., Achreja, A., Bernard, V., Moss, T., Marini, J. C., Tudawe, T., Seviour, E. G., San Lucas, F. A., Alvarez, H., Gupta, S., Maiti, S. N., Cooper, L., Peehl, D., Ram, P. T., Maitra, A., & Nagrath, D. (2016). Tumor microenvironment derived exosomes pleiotropically modulate cancer cell metabolism. *ELife*, *5*, e10250. https://doi.org/10.7554/eLife.10250

Zhu, V. F., Yang, J., LeBrun, D. G., & Li, M. (2012). Understanding the role of cytokines in Glioblastoma Multiforme pathogenesis. *Cancer Letters*, *316*(2), 139–150. https://doi.org/10.1016/j.canlet.2011.11.001

Zou, J.-P., Morford, L. A., Chougnet, C., Dix, A. R., Brooks, A. G., Torres, N., Shuman, J. D., Coligan, J. E., Brooks, W. H., Roszman, T. L., & Shearer, G. M. (1999). Human Glioma-Induced Immunosuppression Involves Soluble Factor(s) That Alters Monocyte Cytokine Profile and Surface Markers. *The Journal of Immunology*, *162*(8), 4882–4892.

Cancer Research UK. Brain, other CNS and intracranial tumours incidence statistics. Retrieved from: http://www.cancerresearchuk.org/health-professional/cancer-statistics/statistics-by-cancer-type/brain-other-cns-and-intracranial-tumours/incidence#ref-0

APPENDIX 1: SUPPLEMENTARY EXPERIMENTS

S1.1. Effect of candidate proteins on T cell surface markers

In order to evaluate the effect of each candidate protein on T cell activation and exhaustion status, TIM-3, PD-1 and ICOS molecules expression was examined. Since no effect was reported at the ¼ dose of each protein according to our previous findings (Chapter 3.3.9), further experiments performed with Full and Half dose protein treatment.

ICAM-1 was added at concentrations of 1 μg/ml and 0.5 μg/ml to the isolated from peripheral blood CD4+ T cells. The cell surface TIM-3, PD-1 and ICOS were expressed by a smaller absolute amount of cells, after ICAM-1 treatment, but the expression levels per cell was equal to/or borderline higher than the control CD4+ T cells.

Similar results were reported after treating cells with CD47 at 10 μg/ml Full dose and 5 μg/ml Half dose or THBS1 at 2 μg/ml and 1 μg/ml, respectively. The cell counts expressing TIM-3, PD-1 and ICOS markers were slightly decreased in each case, but the cells were expressing the same level of markers on their surface as in the control.

MIF was the only candidate from the soluble protein fraction chosen as a potential T cell inhibitory mediator. Exposure of CD4+ T cells to MIF Full dose (500 ng/ml) and Half dose (250 ng/ml) had no effect on TIM-3 expression. PD-1 expression was slightly reduced, as a response to Full dose treatment, whilst the opposite was observed to the activation marker ICOS that demonstrated higher levels of expression at ICAM-1-Full dose treatment.

Figure 40 summarises and compares the effect of the highest doses used from each of the candidate proteins on the surface markers of CD4+ T cells. No proteins had significant effect or caused clear phenotype skewing. THBS1 inhibited the activation molecule ICOS and increased PD-1 exhaustion

marker expression, but more experiments are needed to be performed to confirm any observations and apply statistical analysis.

A. i.

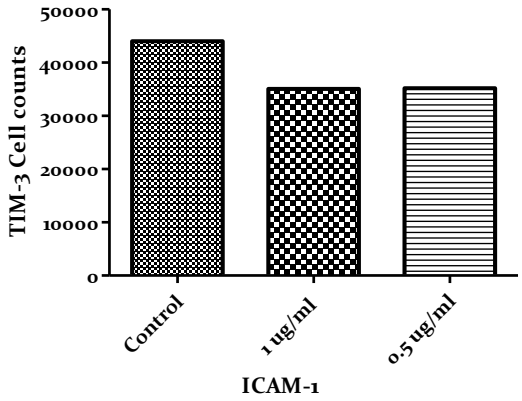
TIM-3 Cell counts
50000
40000
30000
20000
10000
0
Control
1 ug/ml
0.5 ug/ml
ICAM-1

ii.

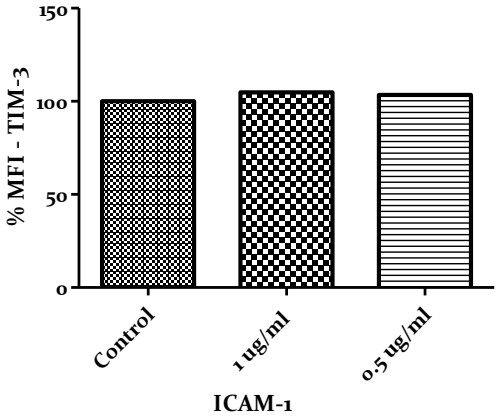
% MFI - TIM-3
150
100
50
0
Control
1 ug/ml
0.5 ug/ml
ICAM-1

iii.

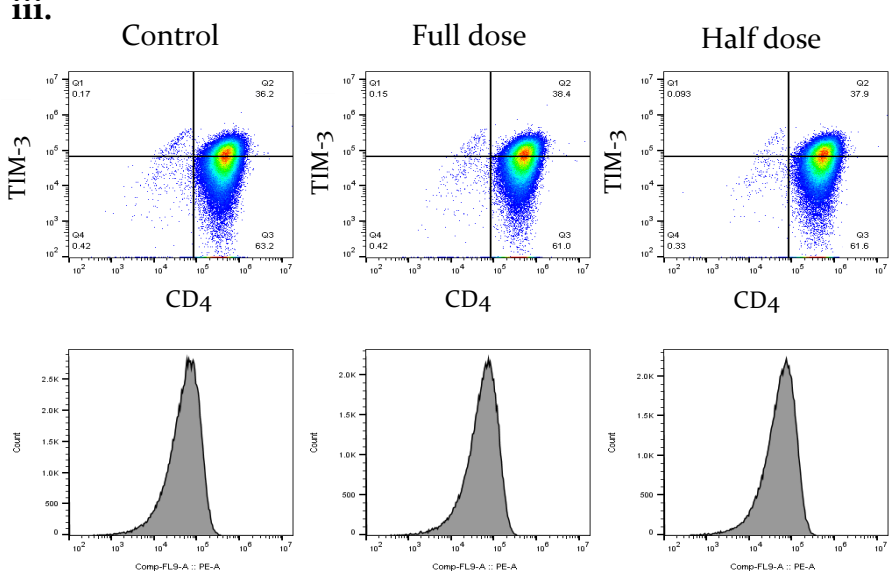
Control
Full dose
Half dose
TIM-3
CD4
Q1 0.17
Q2 36.2
Q4 0.42
Q3 63.2
Q1 0.15
Q2 38.4
Q4 0.42
Q3 61.0
Q1 0.093
Q2 37.9
Q4 0.33
Q3 61.6
Count
Comp-FL9-A :: PE-A

B. i.

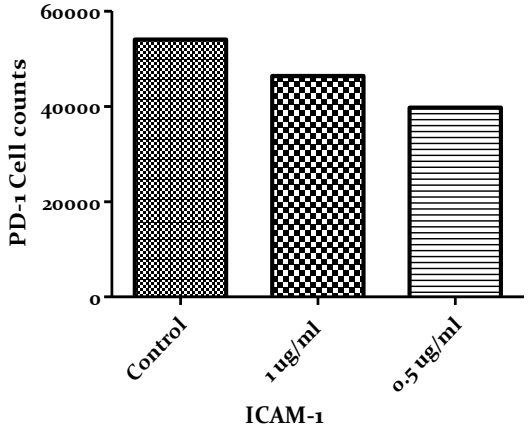
60000
40000
20000
0
PD-1 Cell counts
Control
1 ug/ml
0.5 ug/ml
ICAM-1

ii.

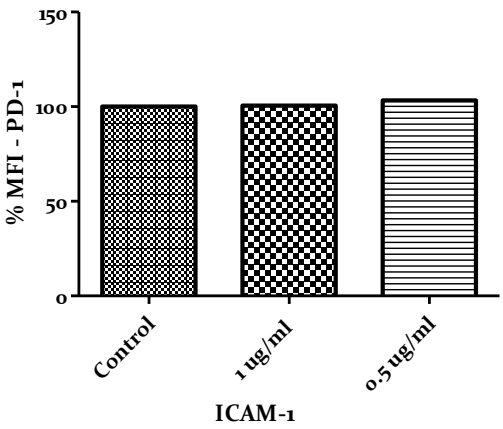
150
100
50
0
% MFI - PD-1
Control
1 ug/ml
0.5 ug/ml
ICAM-1

iii.

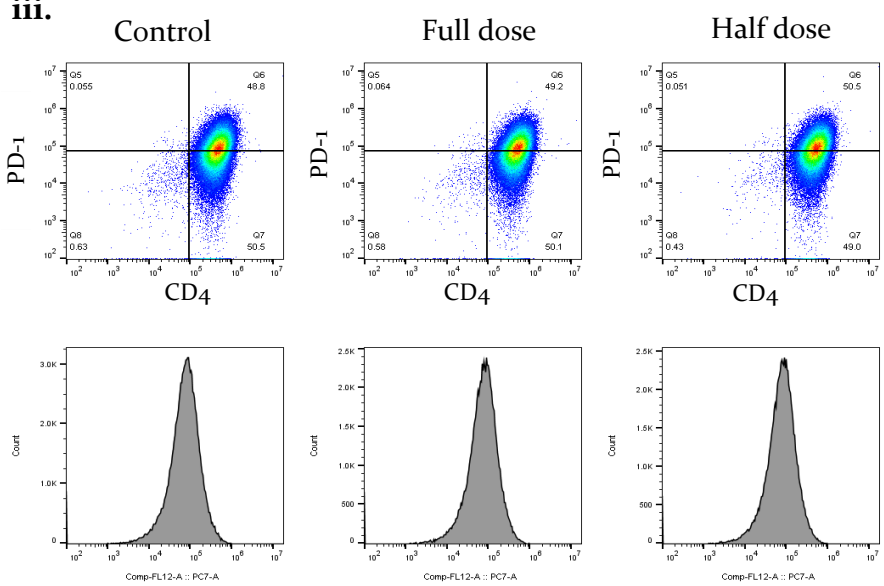
Control
Full dose
Half dose
PD-1
CD4
Q5 0.055
Q6 48.8
Q8 0.63
Q7 50.5
Q5 0.064
Q6 49.2
Q8 0.58
Q7 50.1
Q5 0.051
Q6 50.5
Q8 0.43
Q7 49.0
Count
Comp-FL12-A :: PC7-A

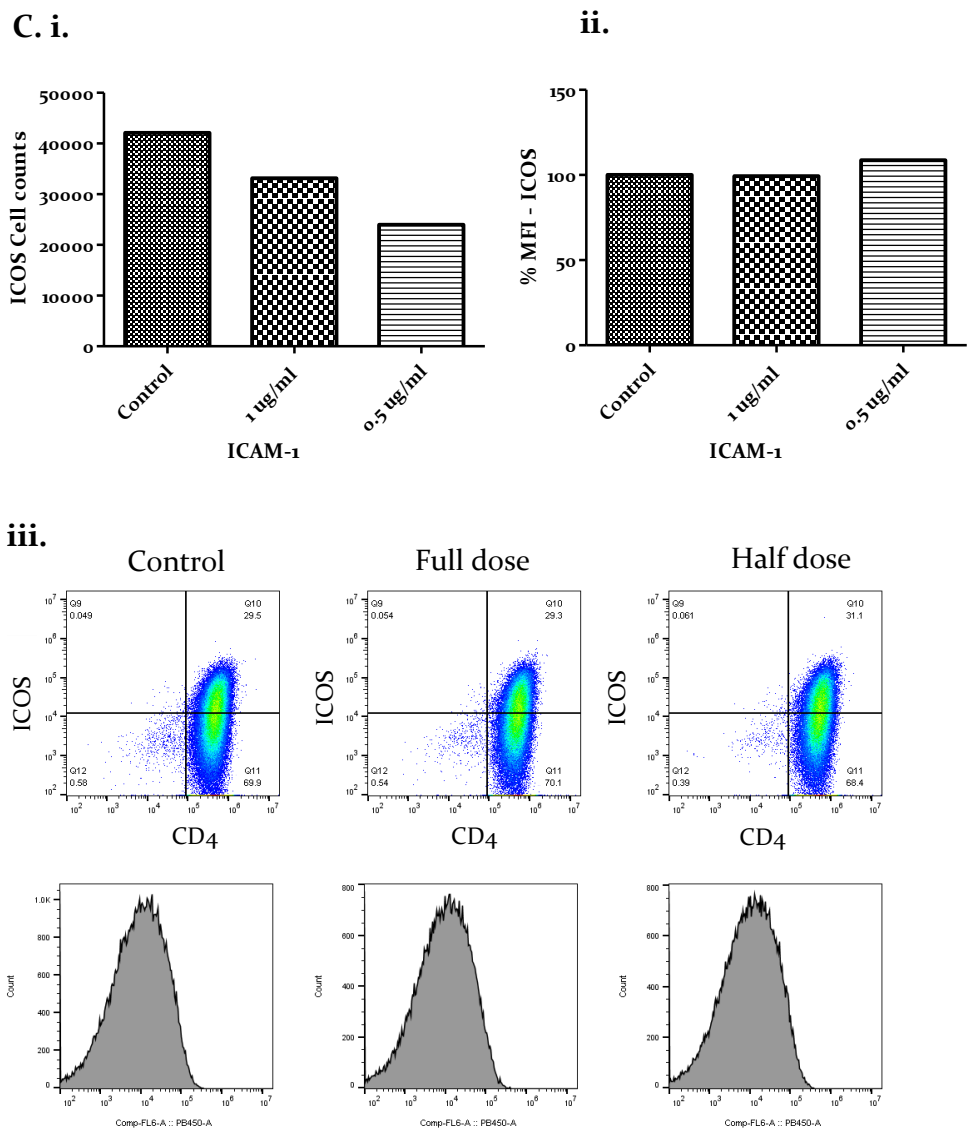

Figure 40. The effect of ICAM-1 on CD4+ cell surface marker expression.

CD4+ T cells were cultured with 1 μg/ml and 0.5 μg/ml ICAM-1 for 5 days. Then, cells were harvested and stained for surface (A) TIM-3, (B) PD-1 and (C) ICOS combined with CD4. (A.i- C.i) Graphs show changes in the number of cells producing the specific markers.(A.ii-C.ii) Representative graphs of the MFI level of expression of each marker over ICAM-1 titration. (A.iii-C.iii) Representative dot plots show surface expression for CD4+ T cells, when cultured alone (left panel), or in the presence of different concentrations of ICAM-1. Data is representative of one experiment (n=1).

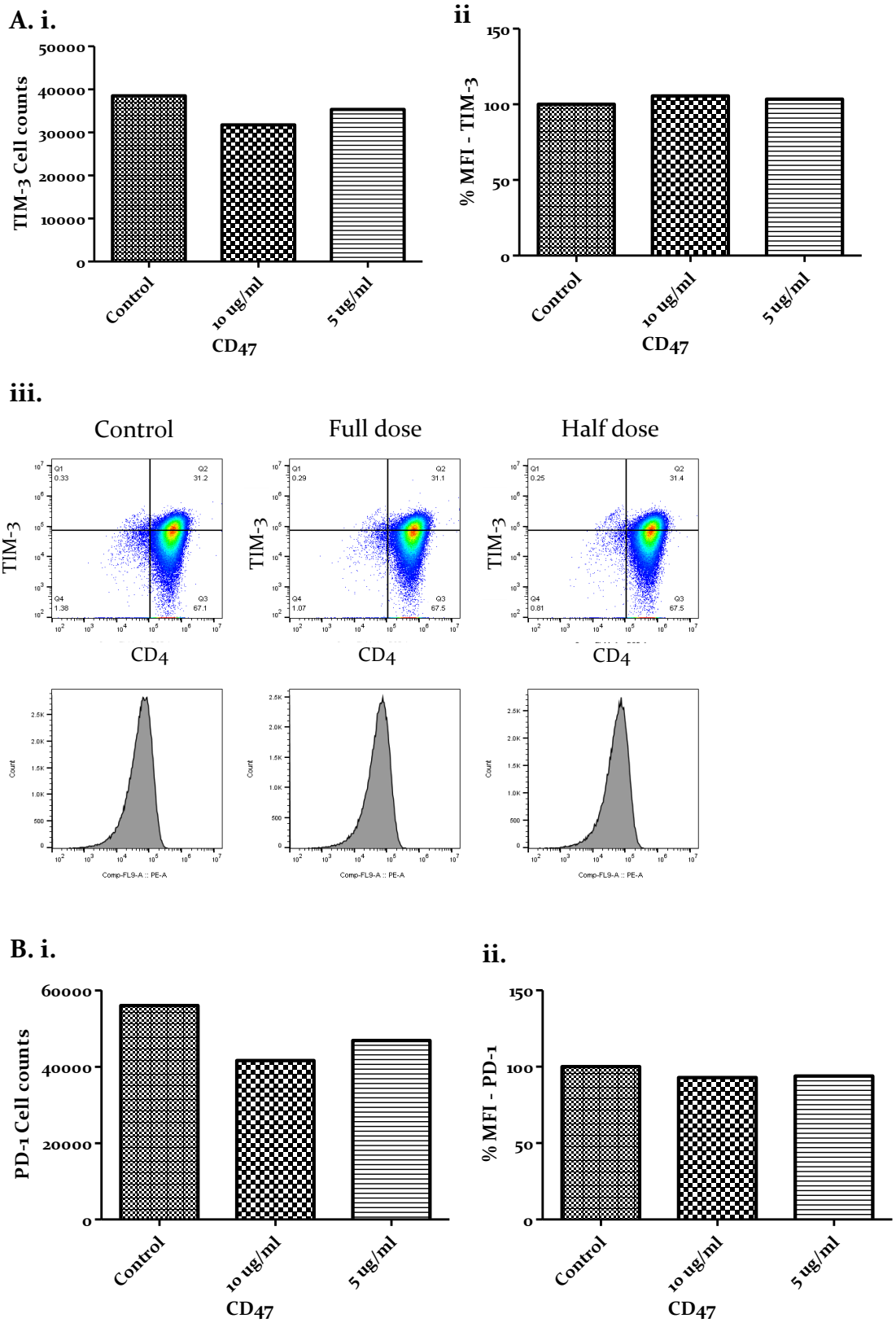
A. i.
TIM-3 Cell counts
50000
40000
30000
20000
10000
0
Control
10 ug/ml
5 ug/ml
CD47
ii
% MFI - TIM-3
150
100
50
0
Control
10 ug/ml
5 ug/ml
CD47
iii.
Control
Full dose
Half dose
TIM-3
CD4
Q1 0.33
Q2 31.2
Q4 1.38
Q3 67.1
Q1 0.29
Q2 31.1
Q4 1.07
Q3 67.5
Q1 0.25
Q2 31.4
Q4 0.81
Q3 67.5
Count
Comp-FL9-A :: PE-A
B. i.
PD-1 Cell counts
60000
40000
20000
0
Control
10 ug/ml
5 ug/ml
CD47
ii.
% MFI - PD-1
150
100
50
0
Control
10 ug/ml
5 ug/ml
CD47

iii.

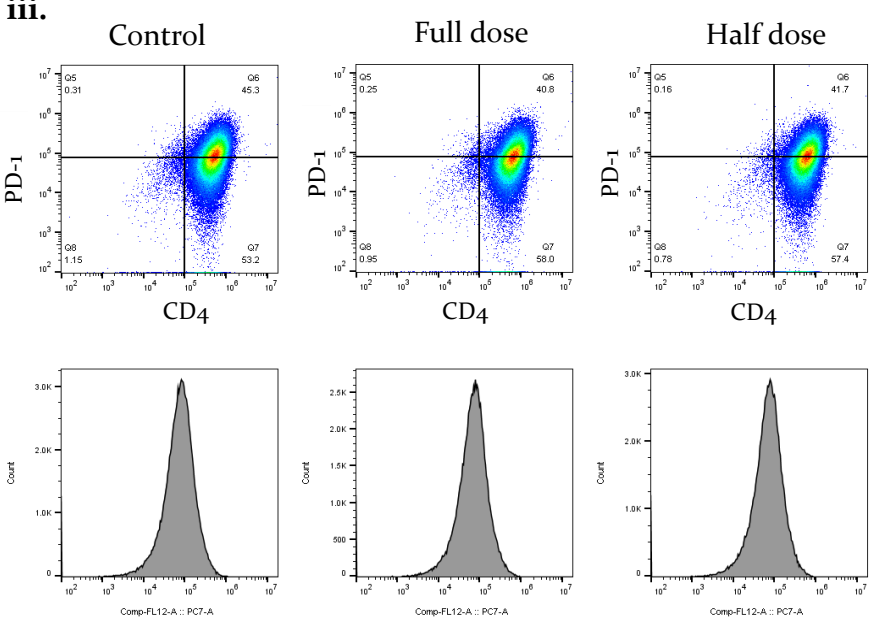
Control
Full dose
Half dose
PD-1
CD4
Q5 0.31
Q6 45.3
Q8 1.15
Q7 53.2
Q5 0.25
Q6 40.8
Q8 0.95
Q7 58.0
Q5 0.16
Q6 41.7
Q8 0.78
Q7 57.4
Count
Comp-FL12-A :: PC7-A

C. i.

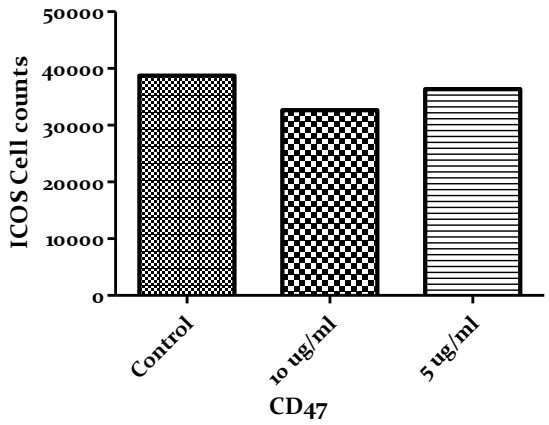
ICOS Cell counts
50000
40000
30000
20000
10000
0
Control
10 ug/ml
5 ug/ml
CD47

ii.

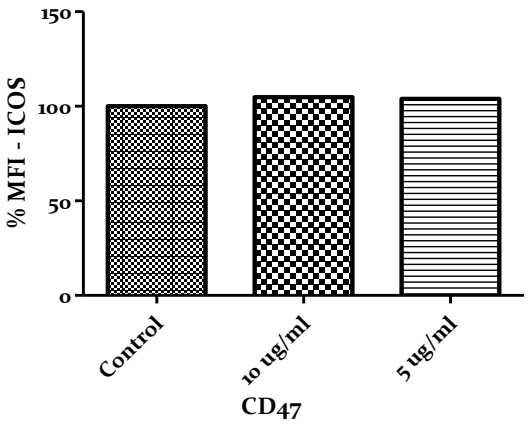
% MFI - ICOS
150
100
50
0
Control
10 ug/ml
5 ug/ml
CD47

iii.

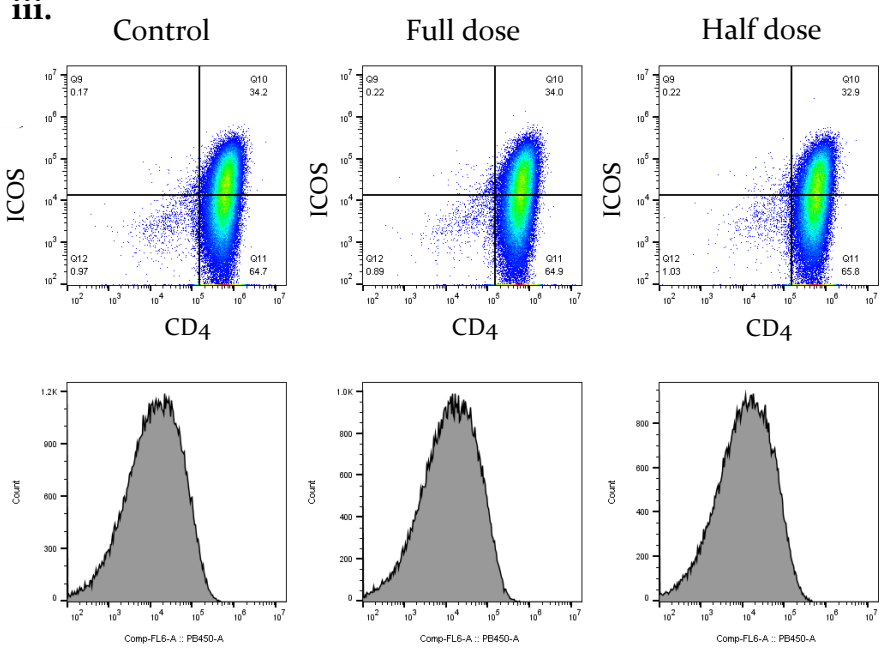

Figure 41. The effect of CD47 on CD4+ cell surface marker expression.

CD4+ T cells were cultured with 10μg/ml and 5 μg/ml CD47 in the presence of 5 x 10^4 CD3/CD28 Human T-activator Dynabeads. After 5 days cells were stained for surface (A) TIM-3, (B) PD-1 and (C) ICOS antibodies with also anti-human CD4.

(A.i- C.i) Graphs show the effect of CD47 in the number of cells expressing each surface marker. (A.ii-C.ii) Representative graphs of the MFI of each marker over CD47 titration. (A.iii-C.iii) Representative dot plots show surface expression of the indicated markers on CD4+ T cells, when cultured alone (left panel), or in the presence of different concentrations of CD47. Data is representative of one experiment (n=1).

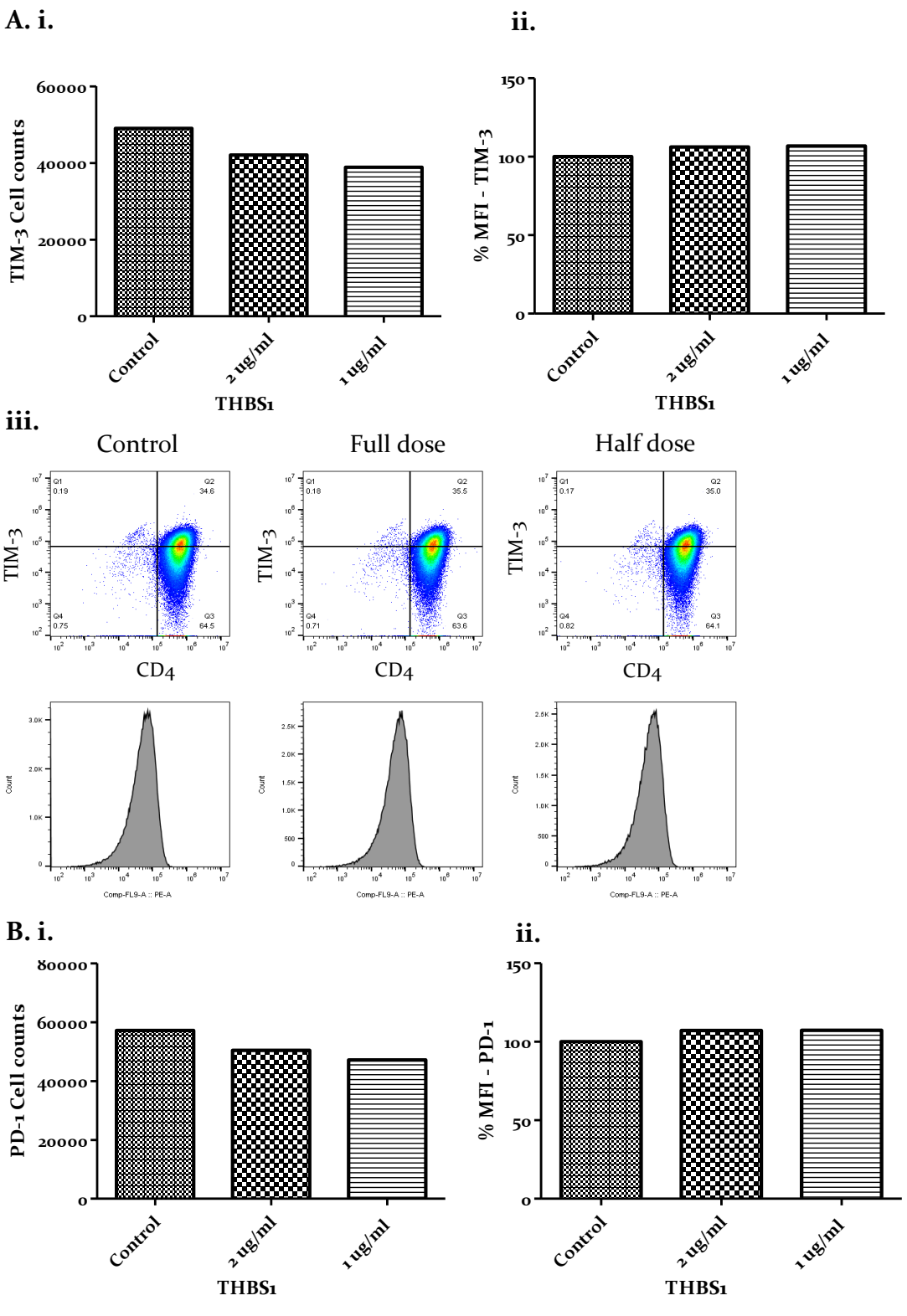
A. i.
ii.
TIM-3 Cell counts
% MFI - TIM-3
Control
2 ug/ml
1 ug/ml
THBS1
iii.
Control
Full dose
Half dose
TIM-3
CD4
Count
Comp-FL9-A :: PE-A
B. i.
ii.
PD-1 Cell counts
% MFI - PD-1

iii.

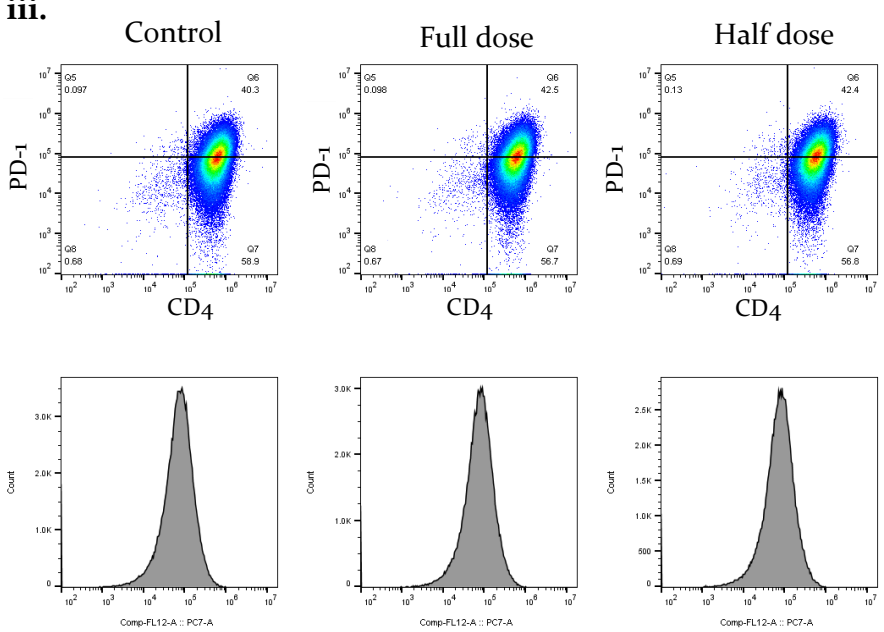
Control
Full dose
Half dose
PD-1
CD4
Q5 0.097
Q6 40.3
Q8 0.68
Q7 58.9
Q5 0.098
Q6 42.5
Q8 0.67
Q7 56.7
Q5 0.13
Q6 42.4
Q8 0.69
Q7 56.8
Count
Comp-FL12-A :: PC7-A

C. i.

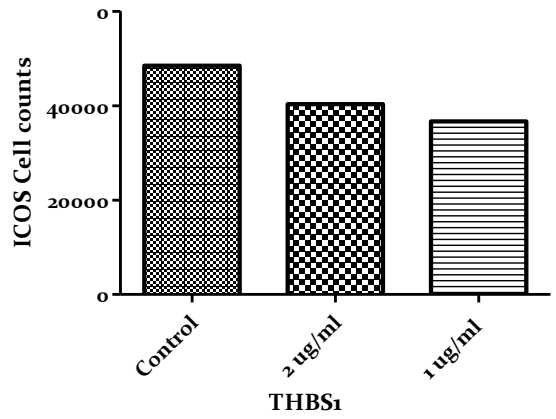
ICOS Cell counts
0
40000
20000
0
Control
2 ug/ml
1 ug/ml
THBS1

ii.

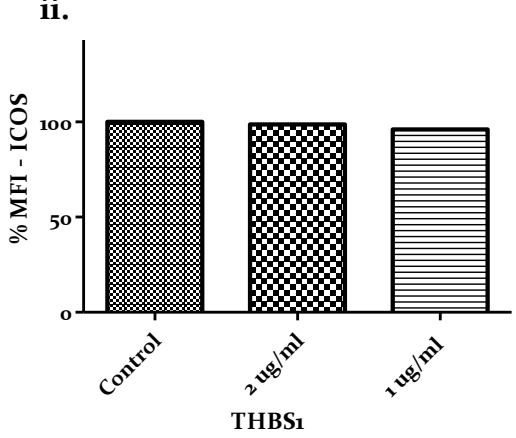
% MFI - ICOS
100
50
0
Control
2 ug/ml
1 ug/ml
THBS1

iii.

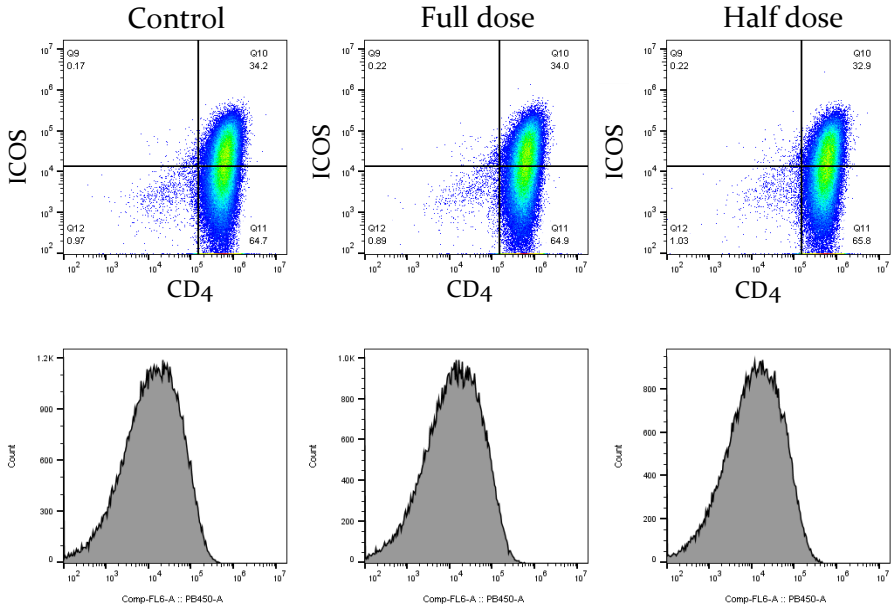

Figure 42. The effect of THBS1 on CD4+ cell surface marker expression.

CD4+ T cells were cultured at a density of 2.5x10⁴ per well with 2 μg/ml and 1 μg/ml THBS1 in the presence of 5 x 10⁴ CD3/CD28 Human T-activator Dynabeads. After 5 days, cells were stained for surface (A) TIM-3, (B) PD-1, (C) ICOS and CD4 antibodies and the response was assessed by flow cytometry.

(A.i- C.i) Graphs show the change in cell numbers producing the specific markers.(A.ii-C.ii) Graphs show the maximum fluorescence intensity of each marker over THBS1 titration. (A.iii-C.iii) Representative dot plots show the markers' expression on CD4+ cells, when seeded alone (left panel), or with different concentrations of THBS1.

Data is representative of one experiment (n=1). The data analysis was performed with FlowJo and GraphPad Prism.

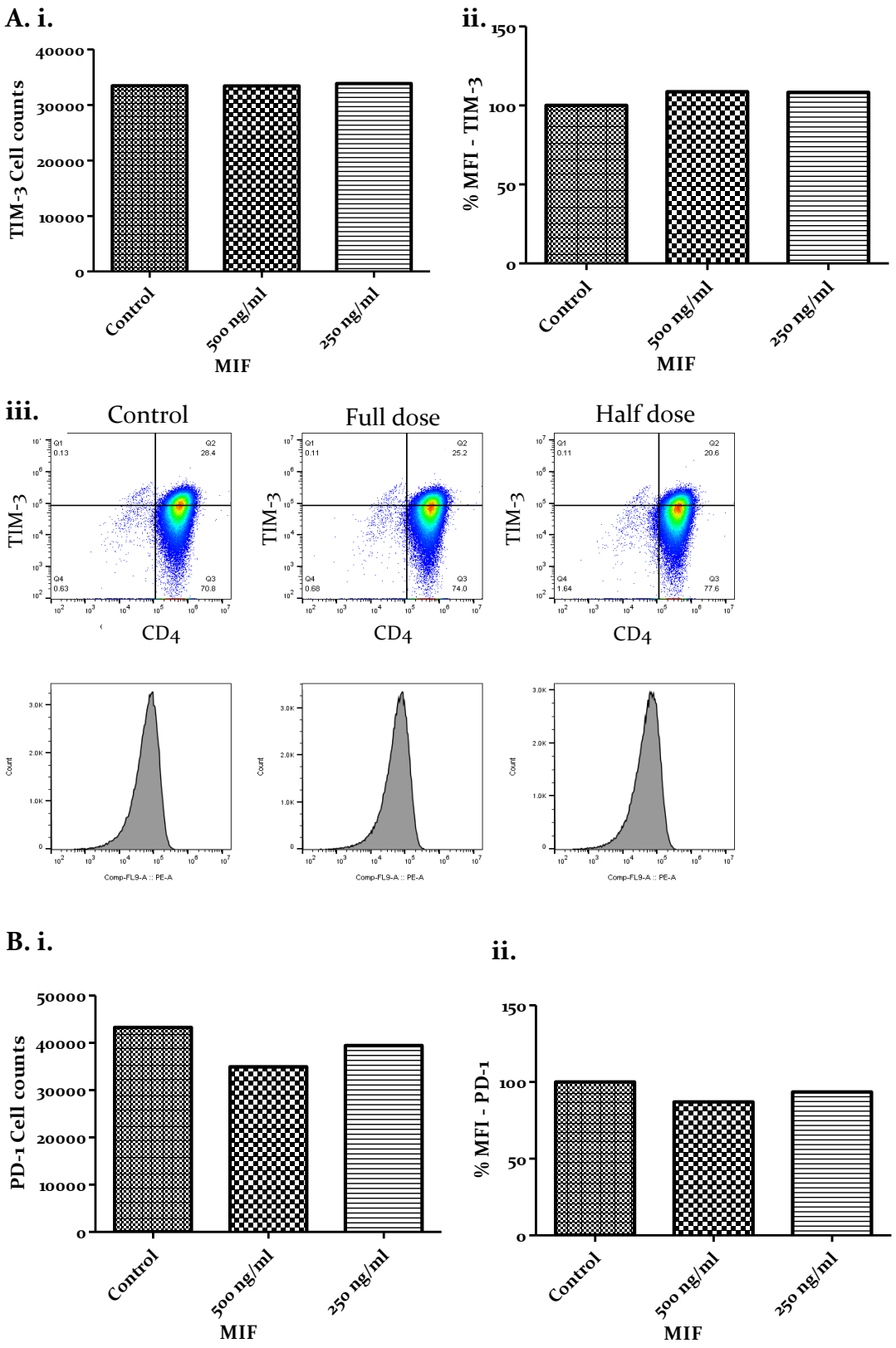
A. i.
TIM-3 Cell counts
40000
30000
20000
10000
0
Control
500 ng/ml
250 ng/ml
MIF
ii.
% MFI - TIM-3
150
100
50
0
Control
500 ng/ml
250 ng/ml
MIF
iii.
Control
Full dose
Half dose
TIM-3
CD4
Q1 0.13
Q2 28.4
Q4 0.63
Q3 70.8
Q1 0.11
Q2 25.2
Q4 0.68
Q3 74.0
Q1 0.11
Q2 20.6
Q4 1.64
Q3 77.6
Count
Comp-FL9-A :: PE-A
B. i.
PD-1 Cell counts
50000
40000
30000
20000
10000
0
Control
500 ng/ml
250 ng/ml
MIF
ii.
% MFI - PD-1
150
100
50
0
Control
500 ng/ml
250 ng/ml
MIF

iii.

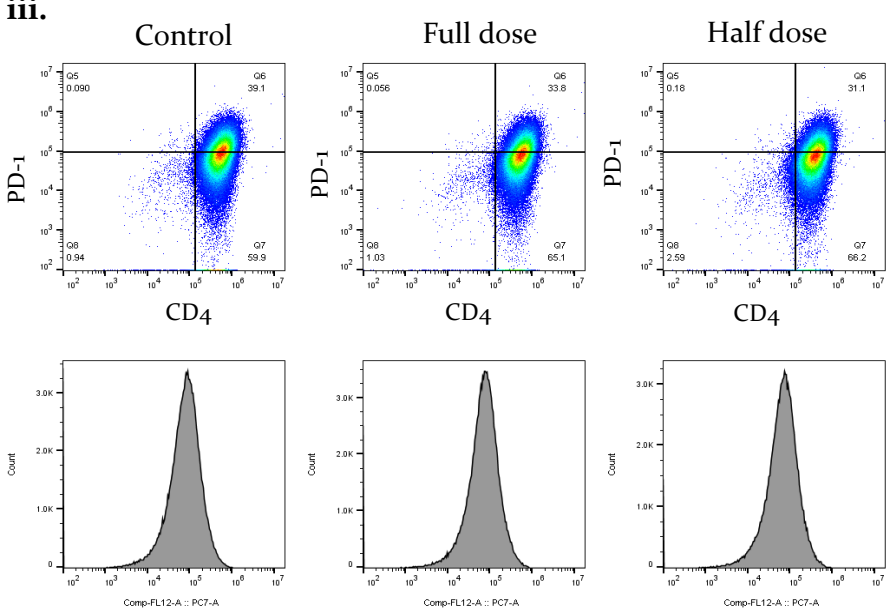
Control
Full dose
Half dose
PD-1
CD4
Q5 0.090
Q6 39.1
Q8 0.94
Q7 59.9
Q5 0.056
Q6 33.8
Q8 1.03
Q7 65.1
Q5 0.18
Q6 31.1
Q8 2.59
Q7 66.2
Count
Comp-FL12-A :: PC7-A

C. i.

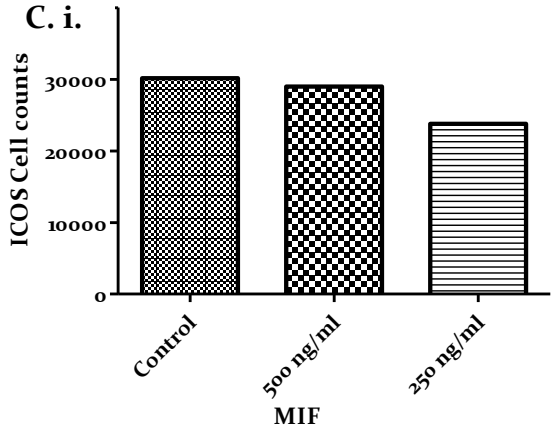
ICOS Cell counts
30000
20000
10000
0
Control
500 ng/ml
250 ng/ml
MIF

ii.

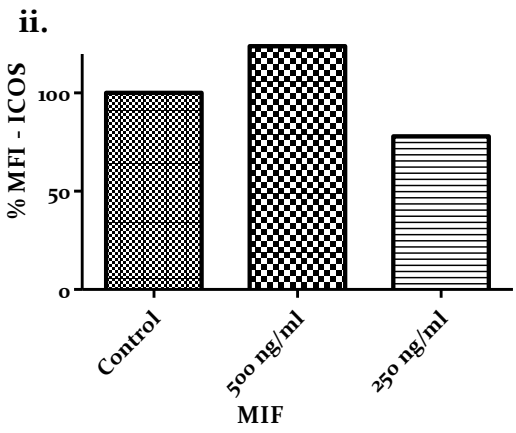
% MFI - ICOS
100
50
0
Control
500 ng/ml
250 ng/ml
MIF

iii.

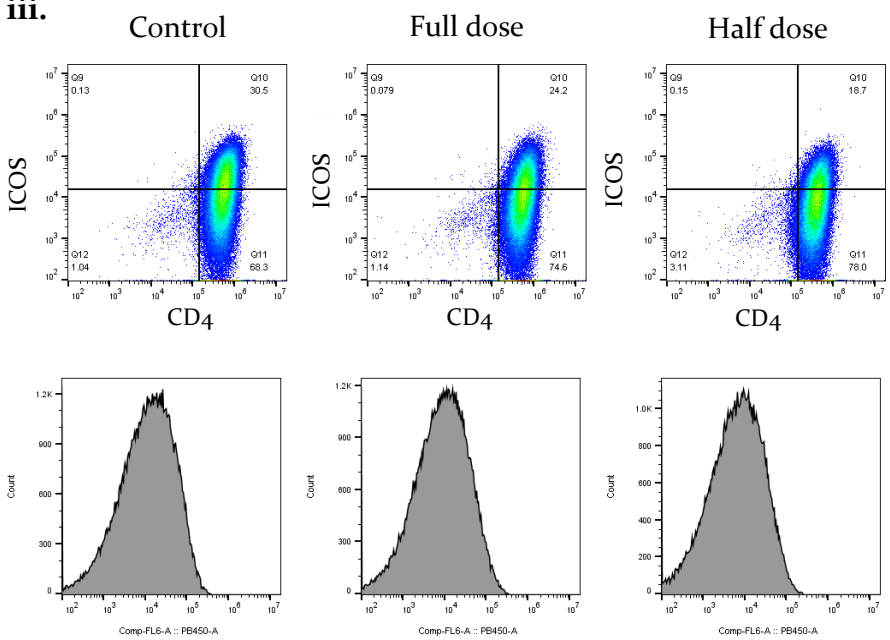

Figure 43. The effect of MIF on CD4+ cell surface marker expression.

Isolated CD4+ T cells from peripheral blood of a human healthy donor were cultured with 250 ng/ml and 500 ng/ml MIF in the presence of 5 x 10^4 CD3/CD28 Human T-activator Dynabeads. After 5 days, cells were stained for surface (A) TIM-3, (B) PD-1, (C) ICOS and CD4 antibodies. (A.i- C.i) Graphs show the effect of MIF in the number of cells expressing each surface marker. (A.ii-C.ii) Representative graphs of the MFI of each marker over MIF titration.

(A.iii-C.iii) Representative dot plots show surface expression of the indicated markers on CD4+ cells, when cultured alone (left panel), or in the presence of different concentrations of MIF. Data is representative of 2 experiments (n=2).

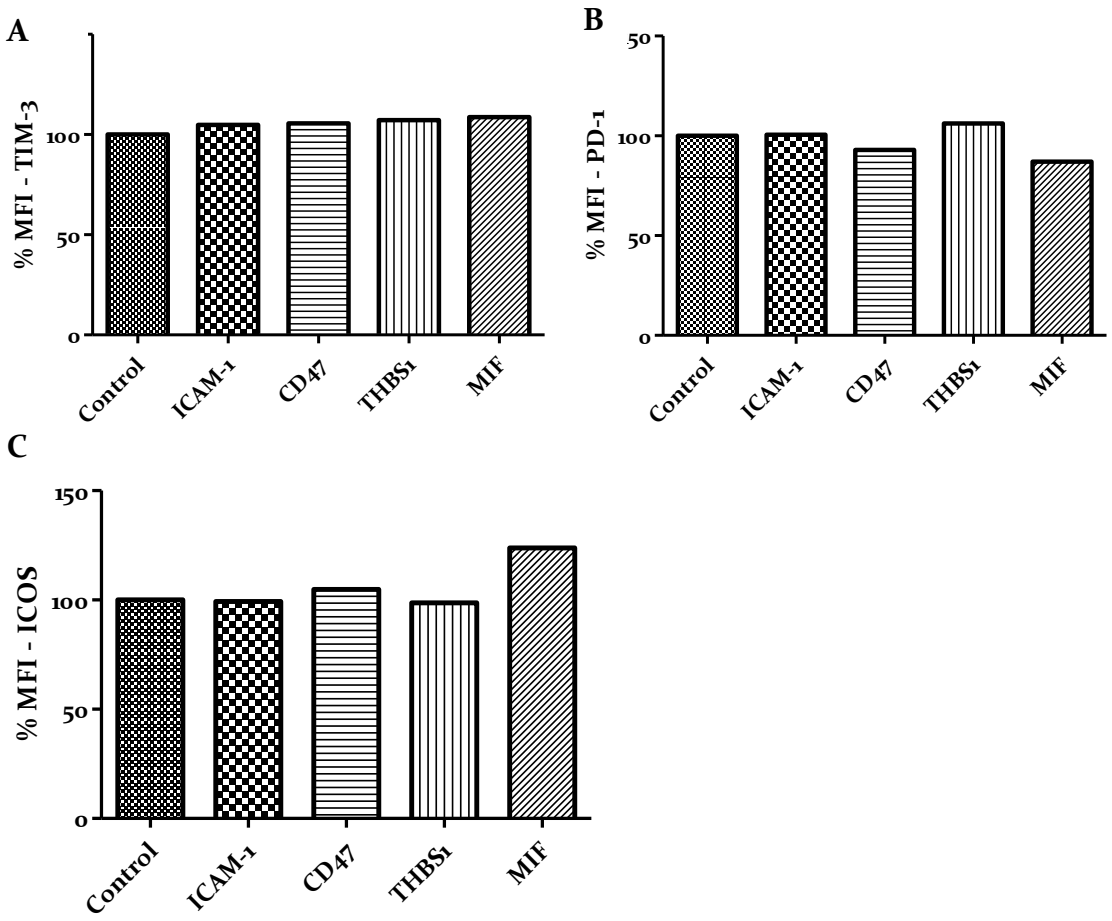

Figure 44. Comparison of the surface markers' expression after treatment with the highest indicated concentrations for each protein.

CD4+ T cells isolated from peripheral blood were cultured with 1 μg/ml ICAM-1, 10 μg/ml CD47, 2 μg/ml THBS1 or 500 ng/ml MIF in the presence of CD3/CD28 Human T-activator Dynabeads (1:2 ratio). After 5 days, cells were stained for surface (A) TIM-3, (B) PD-1, (C) ICOS and CD4 antibodies. (A- C) Graphs show the effect of the candidate proteins in Maximum Fluorescence Intensity as a percentage relative to the control where there was protein addition. Data is representative of 1 experiments (n=1).

S1.2. Effect of candidate immunosuppressive proteins on T cell cytokine production

The candidate proteins were assessed for their ability to suppress CD4+ T cells by shifting their cytokine release profile towards immunosuppression.

ICAM-1 did not cause any significant change in the secretion levels of the panel of cytokines examined (Fig. 47). Interestingly, CD47 addition to seeded CD4+ T cells resulted in a small decrease of 20% in the production of IL-21, TNFα and FNγ, but had no effect on TGFβ, IL-17 or IL-13 (Figure 46). Moreover, THBS1 slightly reduced secretion of TGFβ, IL-21, IFNγ and IL-13 in Half dose, but the expression levels were equal to the control, when Full dose was added on the CD4+ T cells (Fig. 47A-i,ii,iv,vi). TNFα, also, showed a decrease in production of approximately 20% as a response to Half dose THBS1 (Fig. 47-A.iii). IL-17, in contrast was increased by 6% at the same dosage (Fig. 47A-v). Treatment with MIF had no effect in the expression levels of TGFβ, IL-21, IL-17 and IL-13 in any of the doses. However, CD4+ T cells TNFα productions was increased by 13%,after treatment with MIF in both doses (Fig. 48A-iii), whilst IFNγ production was reduced by 20% when 250 ng/ml of MIF was added to the culture (Fig.48A-iv).

The graph in Figure 49, depicts a comparison of the effect that Full doses of the proteins have on the CD4+ T cell cytokine panel. Among the proteins, CD47 downregulated the production of pro-inflammatory cytokines in T cells, but the experiments need to be repeated to evaluate these preliminary results.

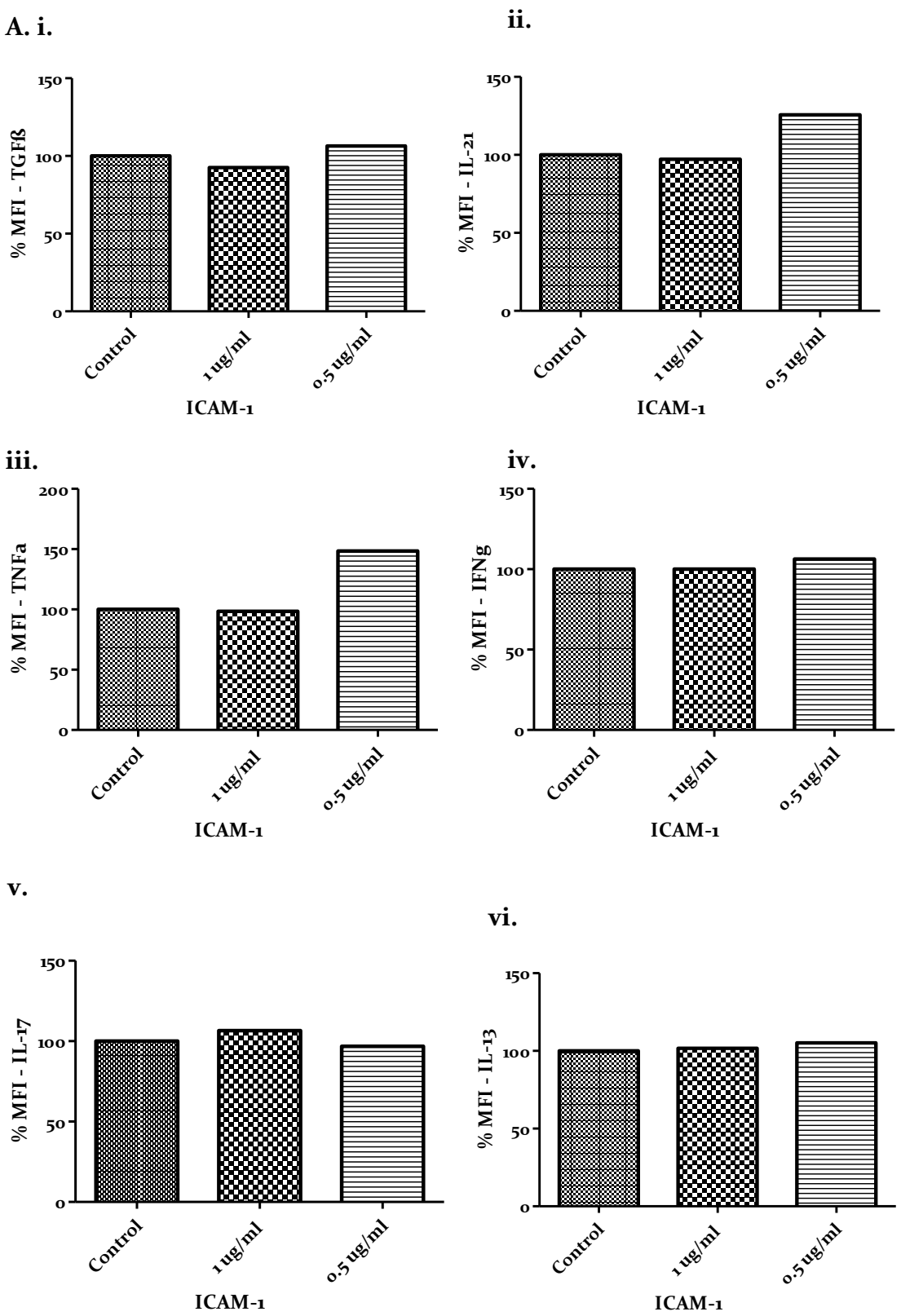
A. i.
% MFI - TGFß
150
100
50
0
Control
1 ug/ml
0.5 ug/ml
ICAM-1
ii.
% MFI - IL-21
150
100
50
0
Control
1 ug/ml
0.5 ug/ml
ICAM-1
iii.
% MFI - TNFa
200
150
100
50
0
Control
1 ug/ml
0.5 ug/ml
ICAM-1
iv.
% MFI - IFNg
150
100
50
0
Control
1 ug/ml
0.5 ug/ml
ICAM-1
v.
% MFI - IL-17
150
100
50
0
Control
1 ug/ml
0.5 ug/ml
ICAM-1
vi.
% MFI - IL-13
150
100
50
0
Control
1 ug/ml
0.5 ug/ml
ICAM-1

B. i.

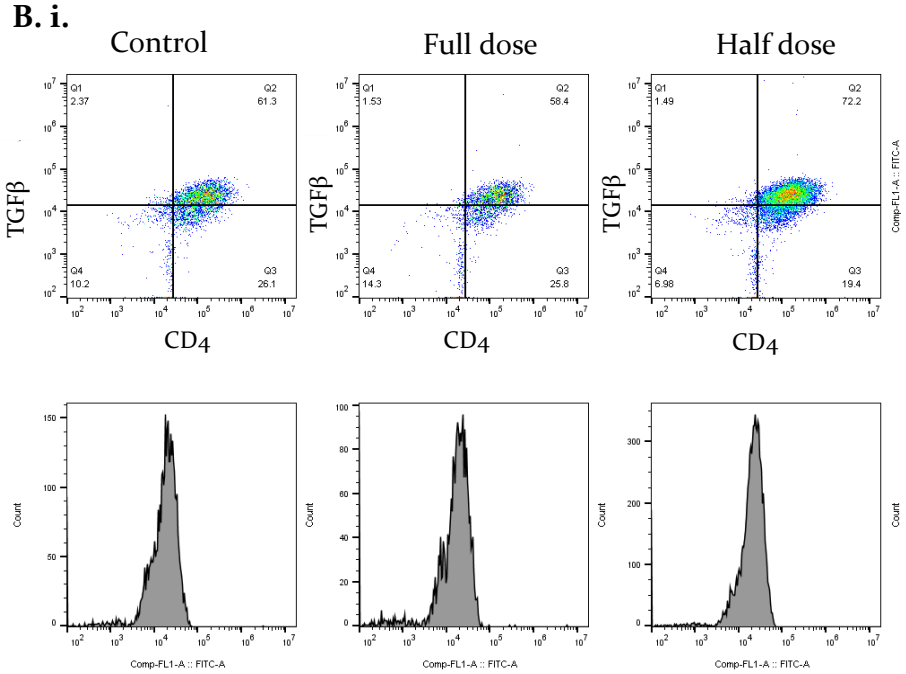
Control
Full dose
Half dose
TGFβ
CD4
Q1 2.37
Q2 61.3
Q4 10.2
Q3 26.1
Q1 1.53
Q2 58.4
Q4 14.3
Q3 25.8
Q1 1.49
Q2 72.2
Q4 6.98
Q3 19.4
Count
Comp-FL1-A :: FITC-A

ii.

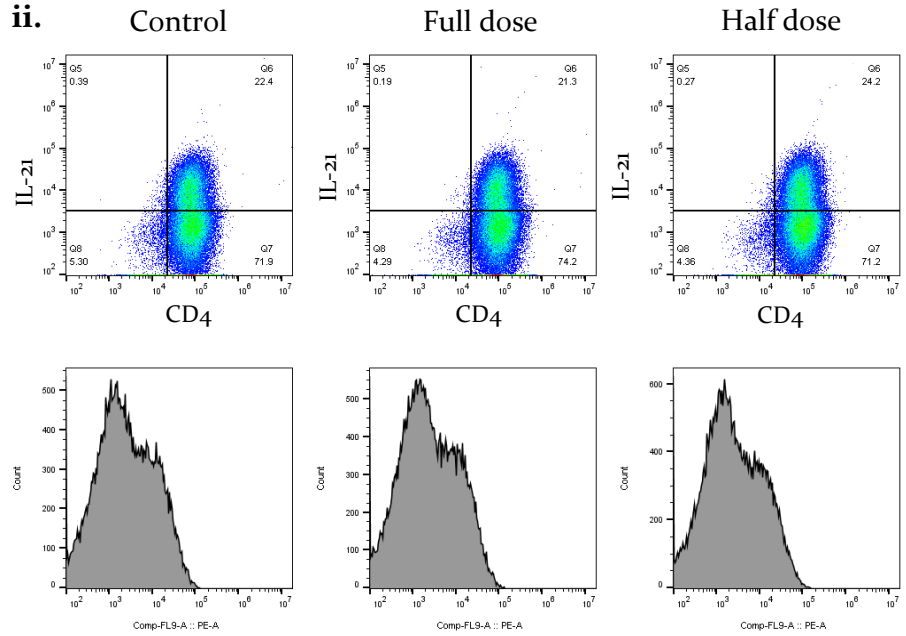
Control
Full dose
Half dose
IL-21
CD4
Q5 0.39
Q6 22.4
Q8 5.30
Q7 71.9
Q5 0.19
Q6 21.3
Q8 4.29
Q7 74.2
Q5 0.27
Q6 24.2
Q8 4.36
Q7 71.2
Count
Comp-FL9-A :: PE-A

iii.

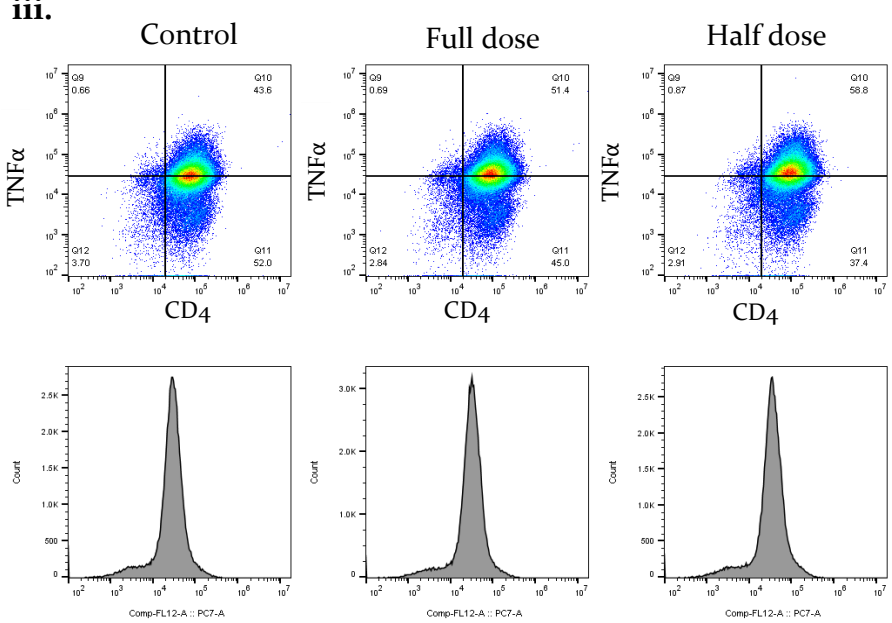
Control
Full dose
Half dose
TNFα
CD4
Q9 0.66
Q10 43.6
Q12 3.70
Q11 52.0
Q9 0.69
Q10 51.4
Q12 2.84
Q11 45.0
Q9 0.87
Q10 58.8
Q12 2.91
Q11 37.4
Count
Comp-FL12-A :: PC7-A

iv.

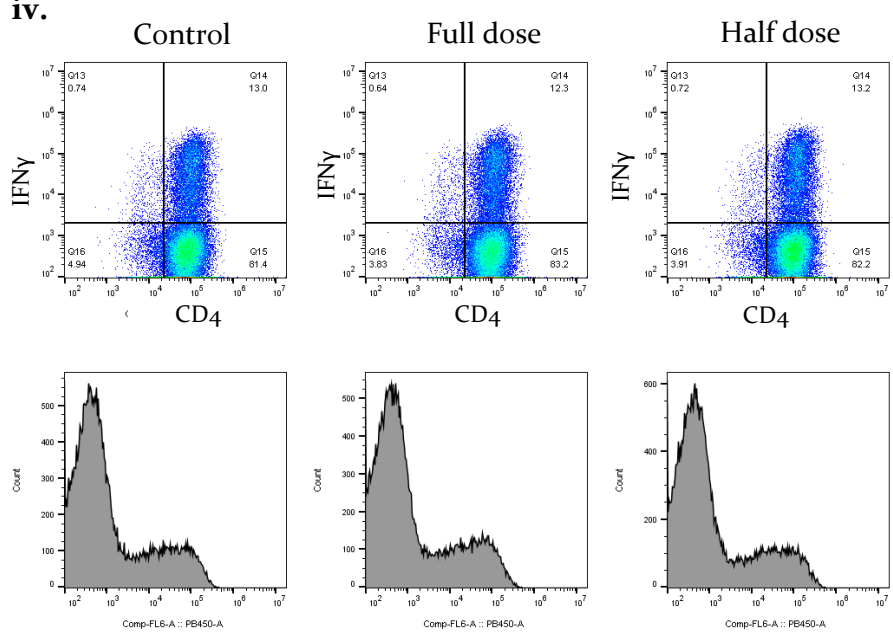
Control
Full dose
Half dose
IFNγ
CD4
Q13 0.74
Q14 13.0
Q16 4.94
Q15 81.4
Q13 0.64
Q14 12.3
Q16 3.83
Q15 83.2
Q13 0.72
Q14 13.2
Q16 3.91
Q15 82.2
Count
Comp-FL6-A :: PB450-A

v.

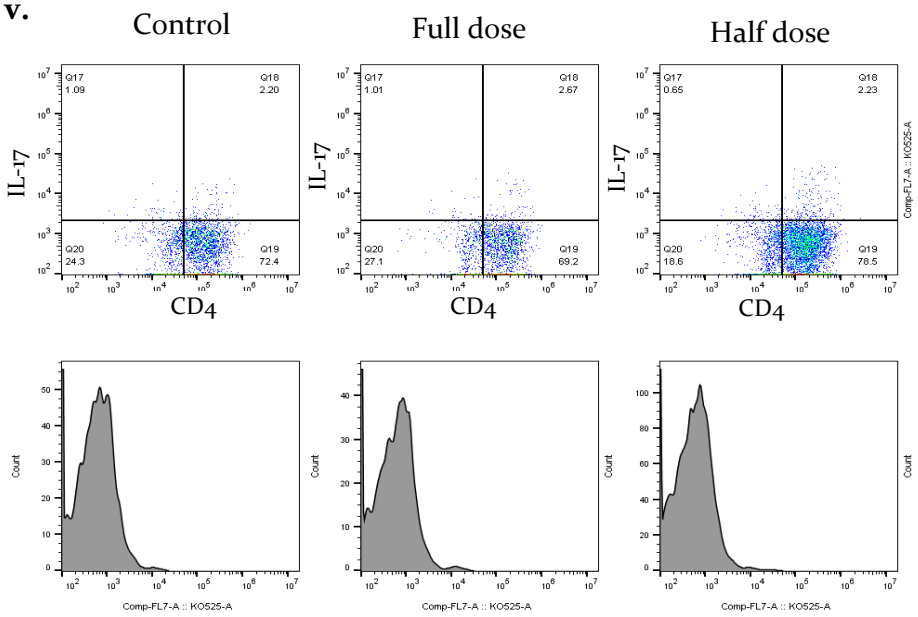
Control
Full dose
Half dose
IL-17
CD4
Q17 1.09
Q18 2.20
Q20 24.3
Q19 72.4
Q17 1.01
Q18 2.67
Q20 27.1
Q19 69.2
Q17 0.65
Q18 2.23
Q20 18.6
Q19 78.5
Count
Comp-FL7-A :: KO525-A

vi.

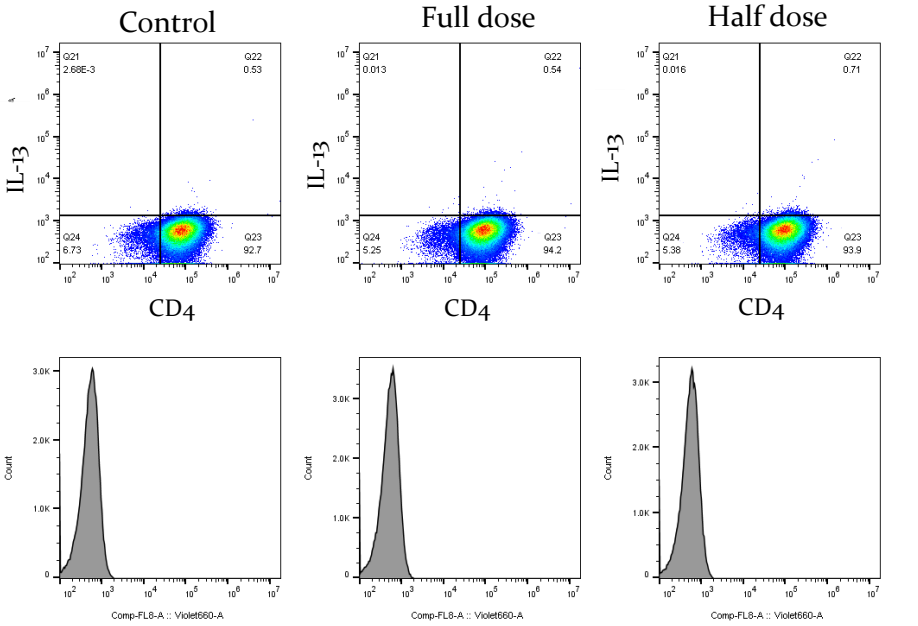
Control
Full dose
Half dose
IL-13
CD4
Q21 2.68E-3
Q22 0.53
Q24 6.73
Q23 92.7
Q21 0.013
Q22 0.54
Q24 5.25
Q23 94.2
Q21 0.016
Q22 0.71
Q24 5.38
Q23 93.9
Count
Comp-FL8-A :: Violet660-A

Figure 45. The effect of ICAM-1 on T cell cytokine production.

CD4+ isolated T cells from peripheral blood if a human healthy donor were cultured with 1 μg/ml and 0.5 μg/ml ICAM-1 in the presence of CD3/CD28 Dynabeads. After 4 days cells were re-stimulated and stained for intracellular (i) TGFβ, (ii) IL-21, (iii) TNFα, (iv) IFNγ, (v) IL-17 and (vi) IL-13 cytokines and cell surface CD4 antibody.

(A.i-vi) Graphs show the change in Maximum Fluorescence Intensity of each cytokine over the exposure to two concentrations of ICAM-1, as a percentage relative to the MFI detected in the control condition where no ICAM-1 was added on the cells.

(B.i-vi) Representative dot plots show the cytokine expression of CD4+ T cells when cultured alone (left panel), or in the presence of ICAM-1. Data is representative of 2 experiments and acquired with flow cytometry. Analysis was performed with FlowJo software and GraphPad Prism.

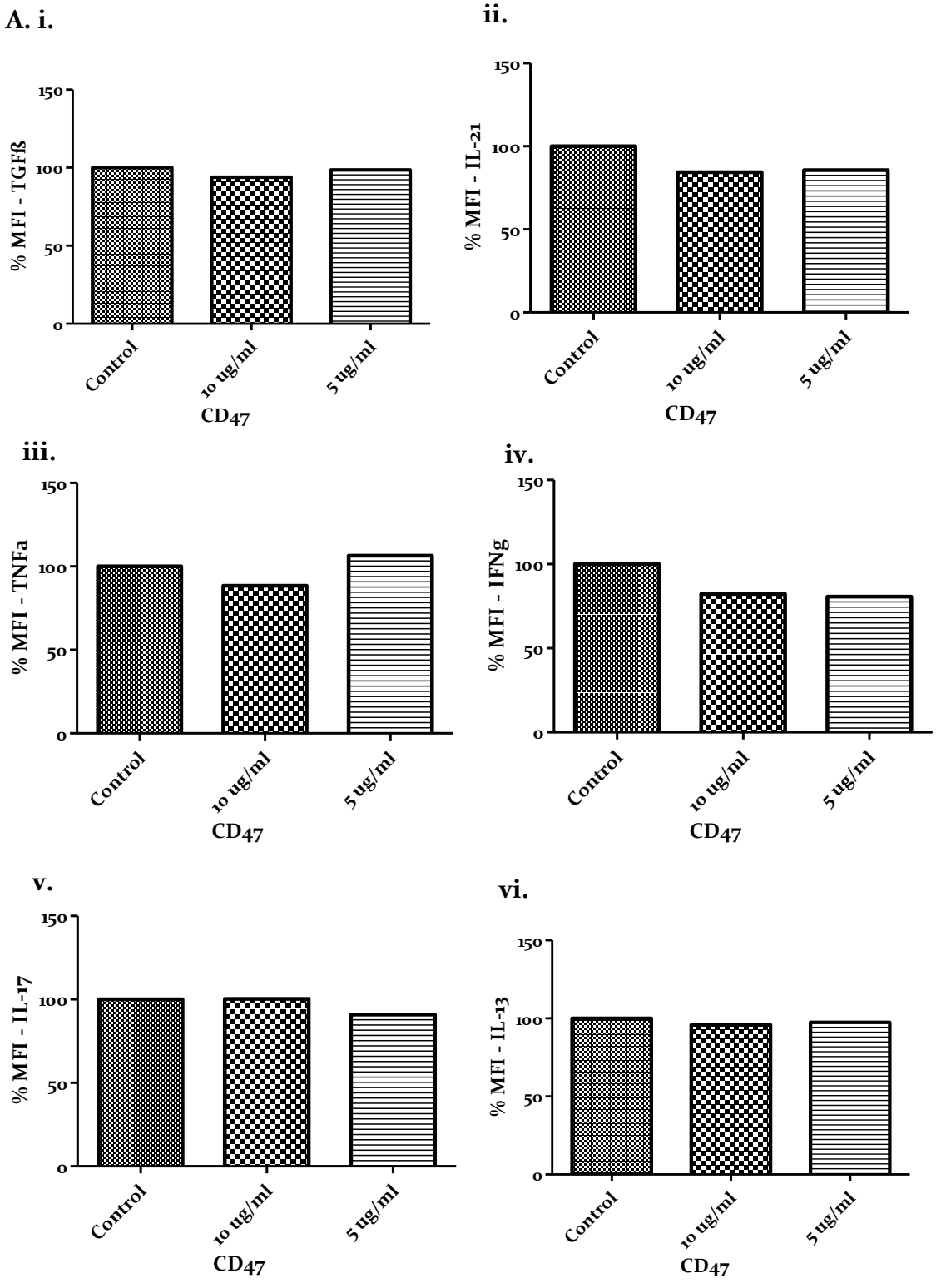
A. i.
% MFI - TGFß
150
100
50
0
Control
10 ug/ml
5 ug/ml
CD47
ii.
% MFI - IL-21
150
100
50
0
Control
10 ug/ml
5 ug/ml
CD47
iii.
% MFI - TNFa
150
100
50
0
Control
10 ug/ml
5 ug/ml
CD47
iv.
% MFI - IFNg
150
100
50
0
Control
10 ug/ml
5 ug/ml
CD47
v.
% MFI - IL-17
150
100
50
0
Control
10 ug/ml
5 ug/ml
CD47
vi.
% MFI - IL-13
150
100
50
0
Control
10 ug/ml
5 ug/ml
CD47

B. i.

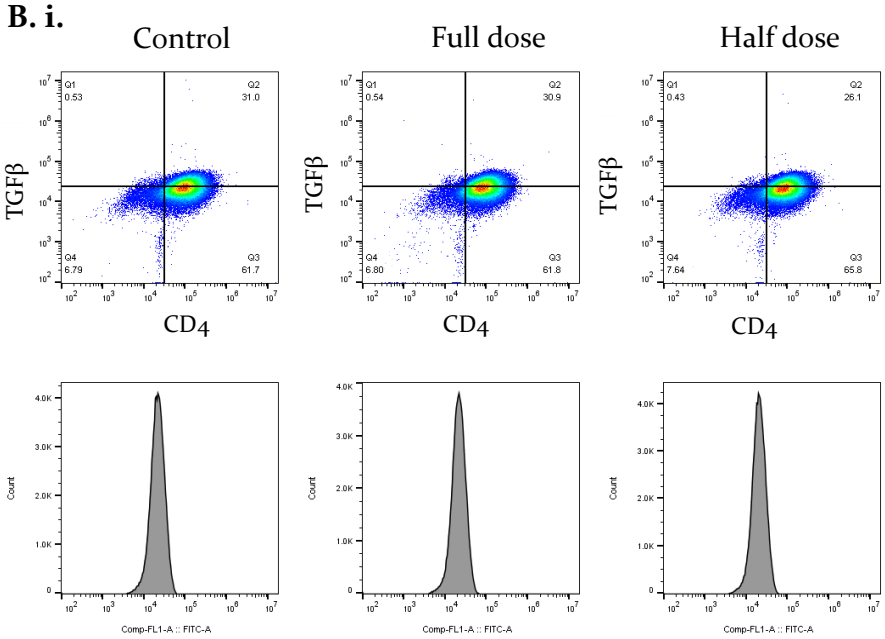
Control
Full dose
Half dose
TGFβ
CD4
Q1 0.53
Q2 31.0
Q4 6.79
Q3 61.7
Q1 0.54
Q2 30.9
Q4 6.80
Q3 61.8
Q1 0.43
Q2 26.1
Q4 7.64
Q3 65.8
Count
Comp-FL1-A :: FITC-A

ii.

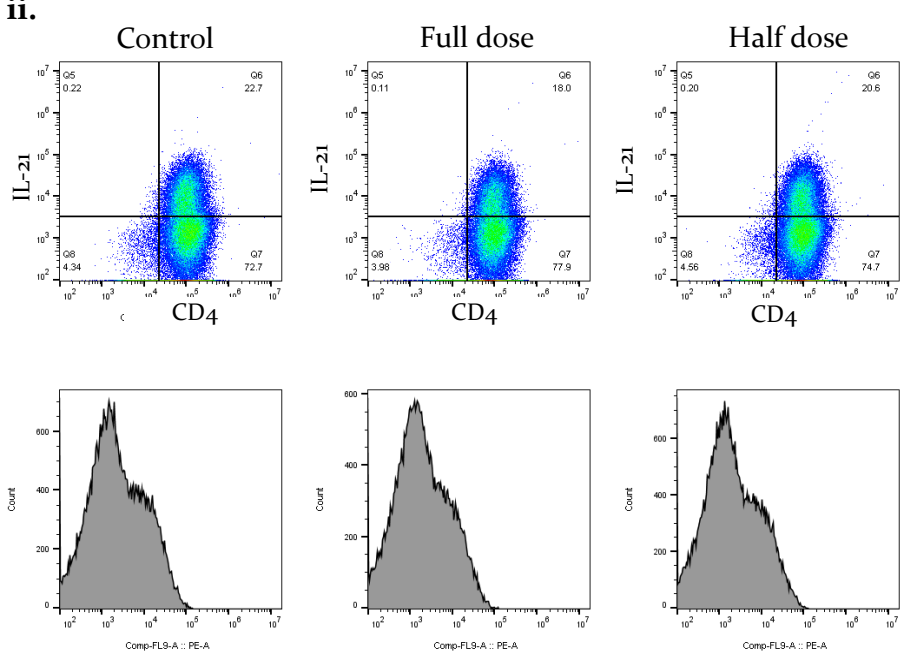
Control
Full dose
Half dose
IL-21
CD4
Q5 0.22
Q6 22.7
Q8 4.34
Q7 72.7
Q5 0.11
Q6 18.0
Q8 3.98
Q7 77.9
Q5 0.20
Q6 20.6
Q8 4.56
Q7 74.7
Count
Comp-FL9-A :: PE-A

iii.

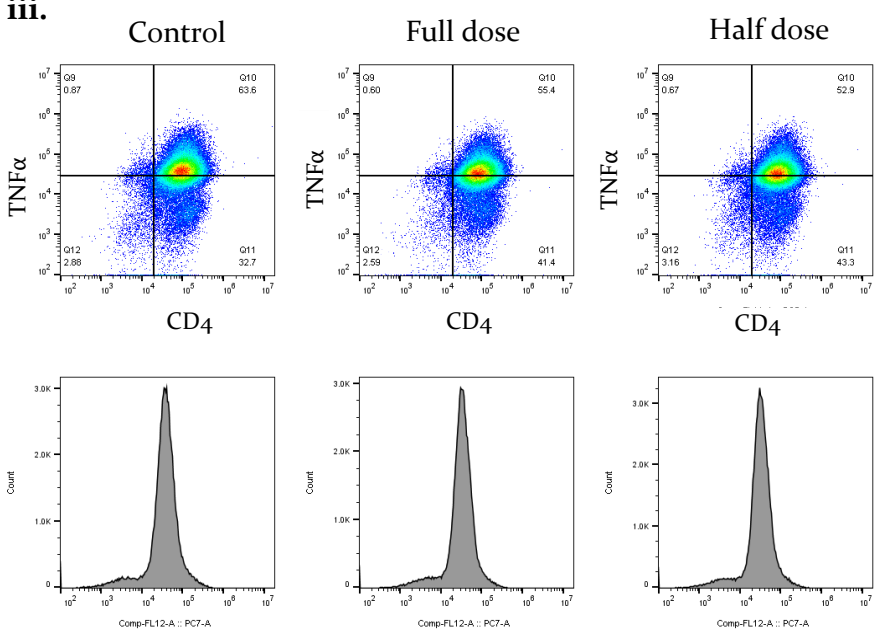
Control
Full dose
Half dose
TNFα
CD4
Q9 0.87
Q10 63.6
Q12 2.88
Q11 32.7
Q9 0.60
Q10 55.4
Q12 2.59
Q11 41.4
Q9 0.67
Q10 52.9
Q12 3.16
Q11 43.3
Count
Comp-FL12-A :: PC7-A

iv.

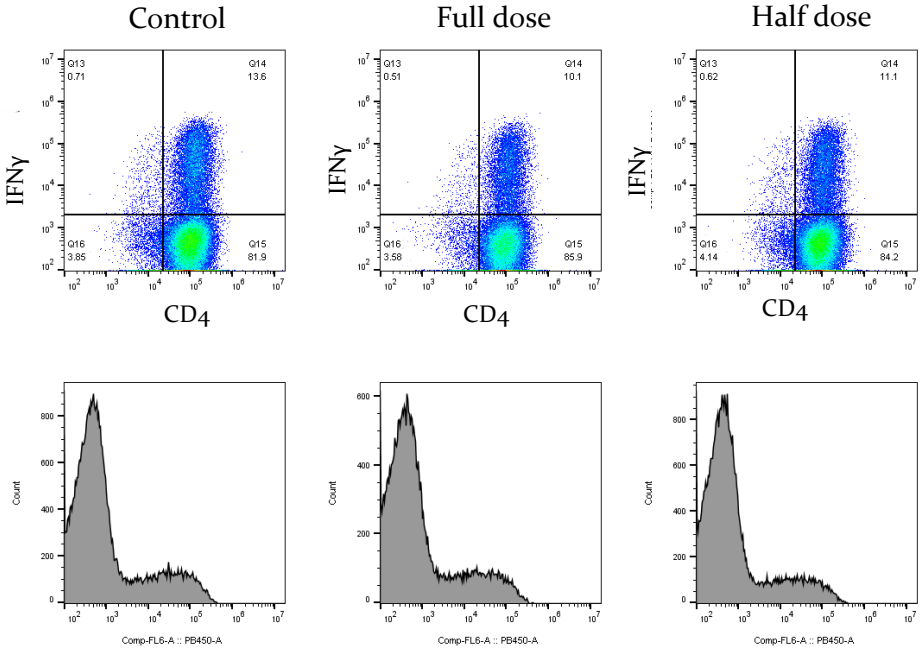
Control
Full dose
Half dose
IFNγ
CD4
Q13 0.71
Q14 13.6
Q16 3.85
Q15 81.9
Q13 0.51
Q14 10.1
Q16 3.58
Q15 85.9
Q13 0.62
Q14 11.1
Q16 4.14
Q15 84.2
Count
Comp-FL6-A :: PB450-A

v.

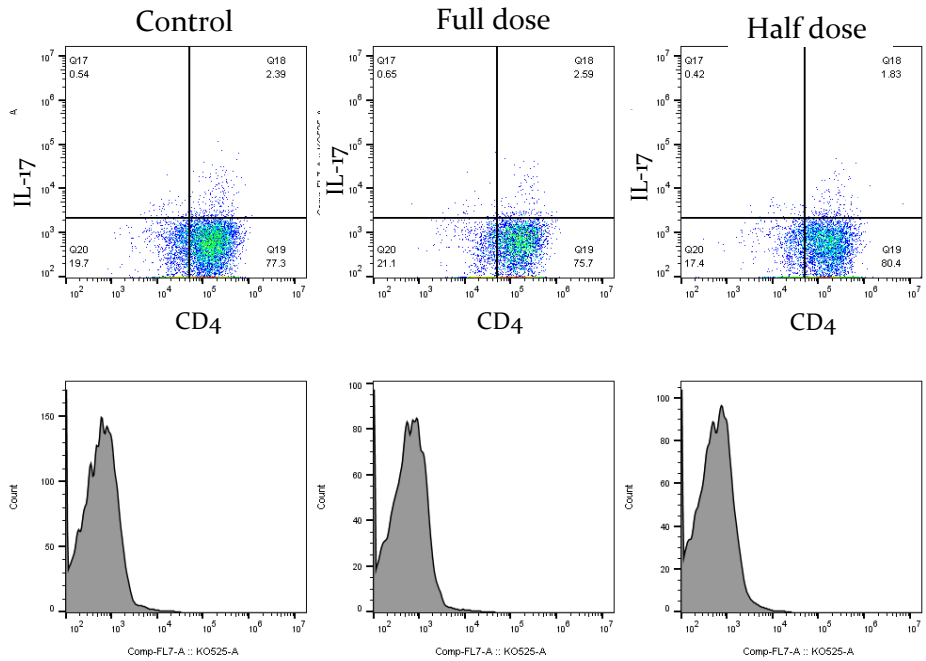
Control
Full dose
Half dose
IL-17
CD4
Q17 0.54
Q18 2.39
Q20 19.7
Q19 77.3
Q17 0.65
Q18 2.59
Q20 21.1
Q19 75.7
Q17 0.42
Q18 1.83
Q20 17.4
Q19 80.4
Count
Comp-FL7-A :: KO525-A

vi.

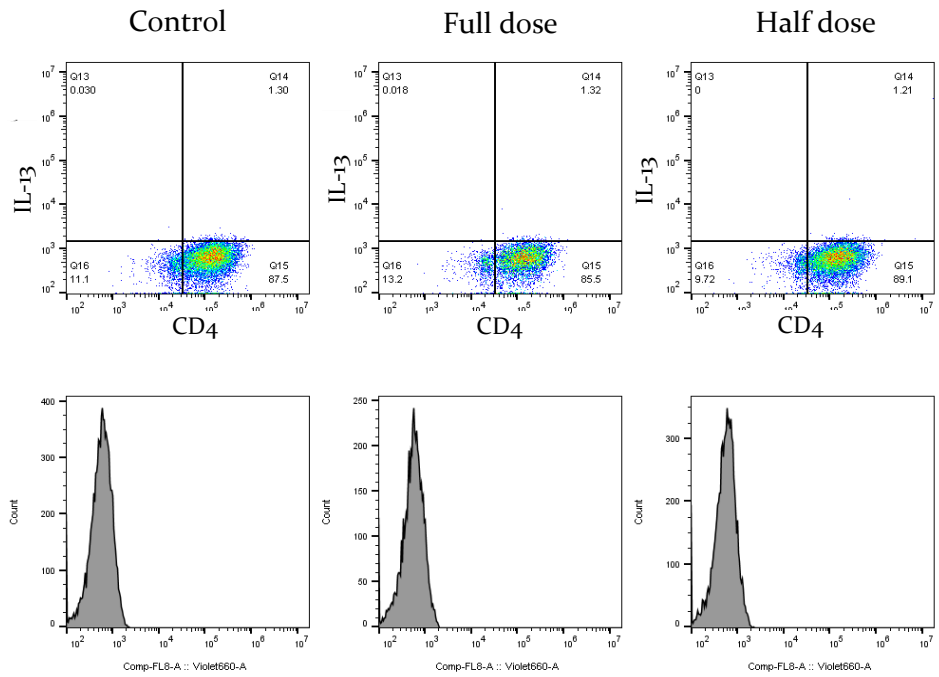
Control
Full dose
Half dose
IL-13
CD4
Q13 0.030
Q14 1.30
Q16 11.1
Q15 87.5
Q13 0.018
Q14 1.32
Q16 13.2
Q15 85.5
Q13 0
Q14 1.21
Q16 9.72
Q15 89.1
Count
Comp-FL8-A :: Violet660-A

Figure 46. The effect of CD47 on CD4+ cytokine production.

CD4+ T cells were cultured with 10 μg/ml and 5 μg/ml CD47 in the presence of 5 x 10^4 CD3/CD28 Human T-activator Dynabeads. After, 4 days cells were re-stimulated and stained for intracellular (i) TGFβ, (ii) IL-21, (iii) TNFα, (iv) IFNγ, (v) IL-17 and (vi) IL-13 cytokines and cell surface CD4 antibody.

(A.i-vi) Graphs show the change in Maximum Fluorescence Intensity of each cytokine over the exposure to two concentrations of CD47, as a percentage relative to the MFI detected in the control condition where no CD47 was added on the cells.

(B.i-vi) Representative dot plots show the cytokine expression of CD4+ T cells when cultured alone (left panel), or in the presence of CD47. Data is representative of 2 experiments and acquired with flow cytometry. Analysis was performed with FlowJo software and GraphPad Prism.

.

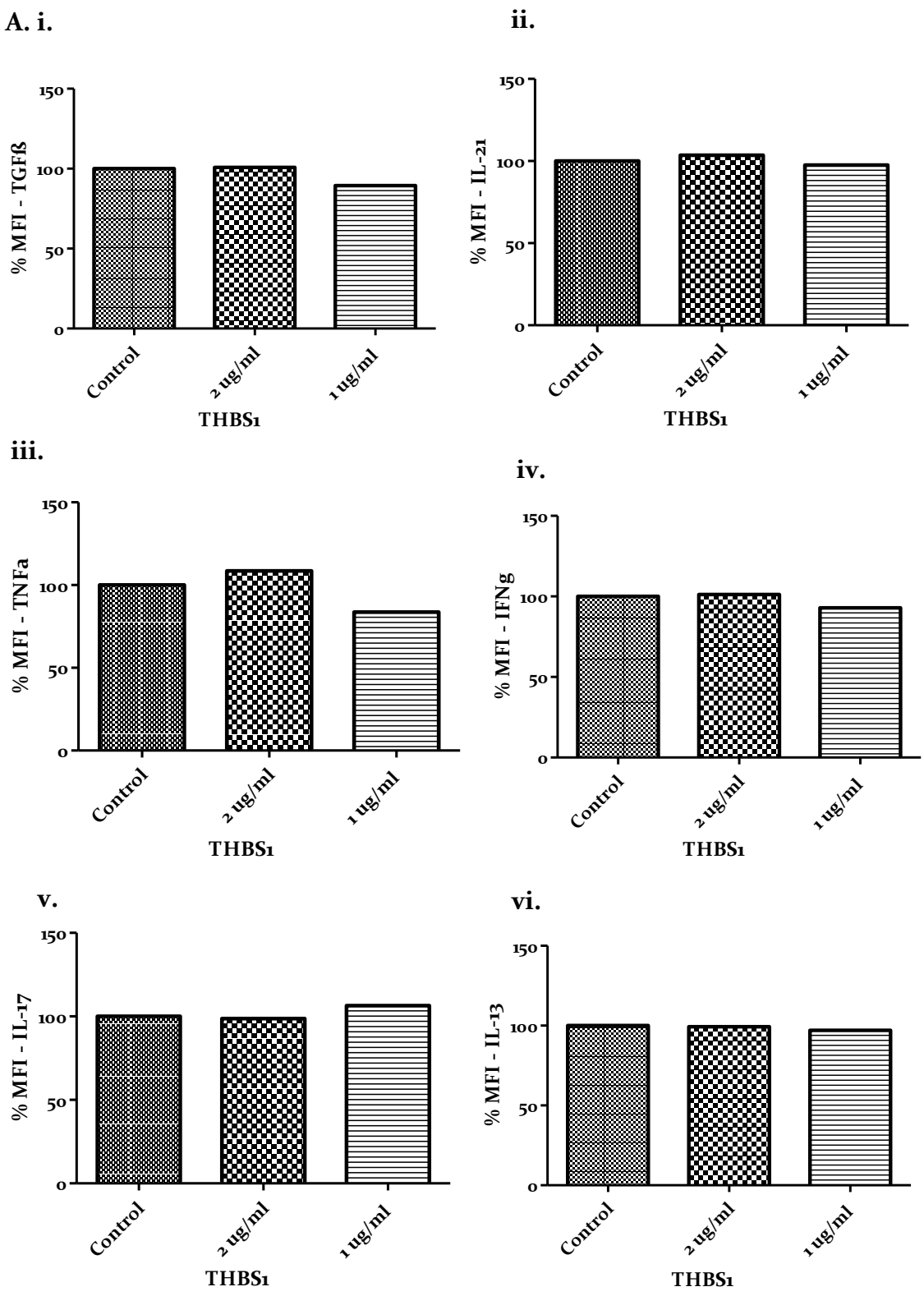
A. i.
% MFI - TGFß
150
100
50
0
Control
2 ug/ml
1 ug/ml
THBS1
ii.
% MFI - IL-21
150
100
50
0
Control
2 ug/ml
1 ug/ml
THBS1
iii.
% MFI - TNFa
150
100
50
0
Control
2 ug/ml
1 ug/ml
THBS1
iv.
% MFI - IFNg
150
100
50
0
Control
2 ug/ml
1 ug/ml
THBS1
v.
% MFI - IL-17
150
100
50
0
Control
2 ug/ml
1 ug/ml
THBS1
vi.
% MFI - IL-13
150
100
50
0
Control
2 ug/ml
1 ug/ml
THBS1

B. i.

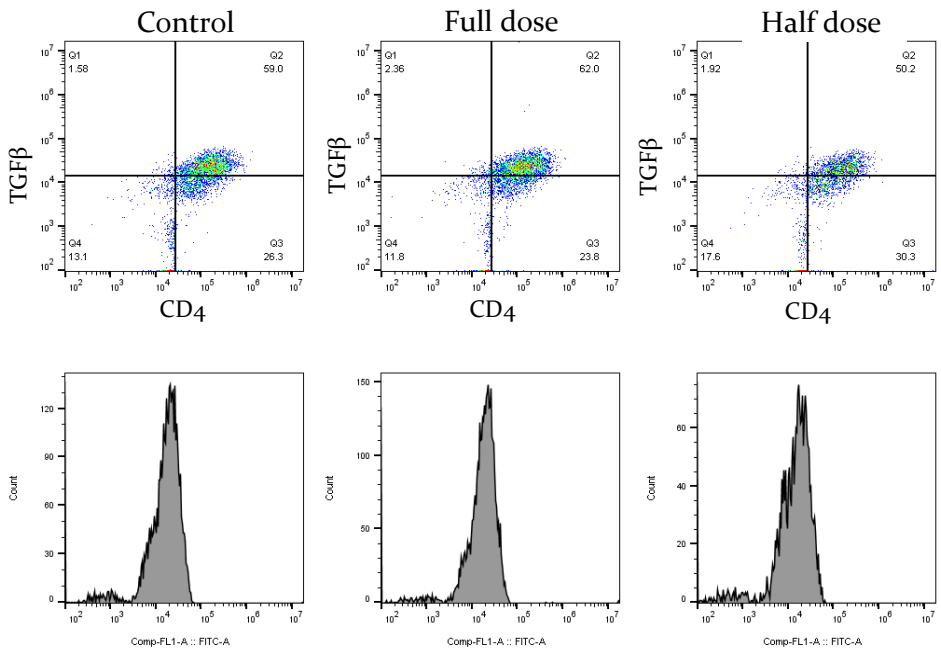
Control
Full dose
Half dose
TGFβ
CD4
Q1 1.58
Q2 59.0
Q4 13.1
Q3 26.3
Q1 2.36
Q2 62.0
Q4 11.8
Q3 23.8
Q1 1.92
Q2 50.2
Q4 17.6
Q3 30.3
Count
Comp-FL1-A :: FITC-A

ii.

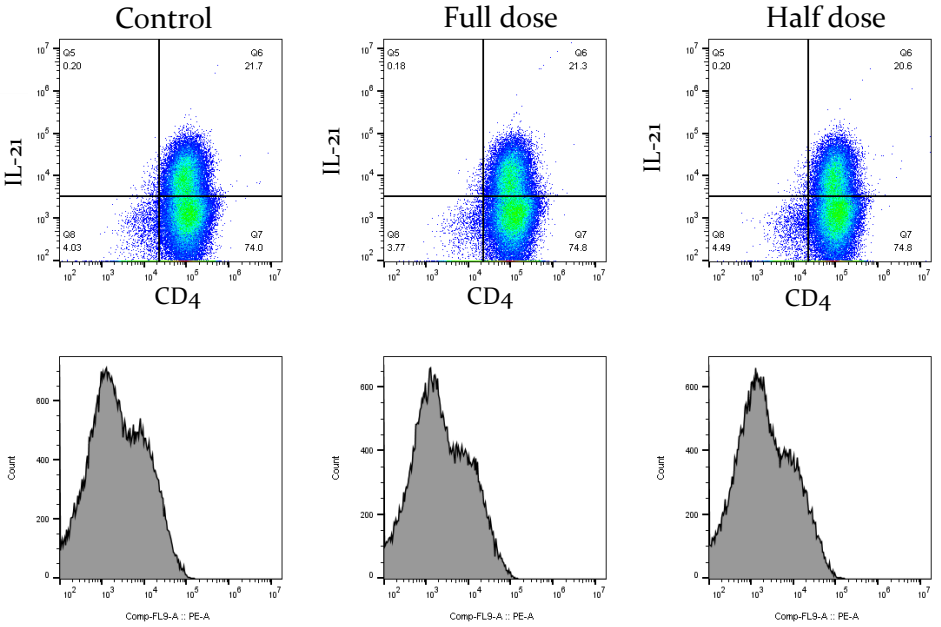
Control
Full dose
Half dose
IL-21
CD4
Q5 0.20
Q6 21.7
Q8 4.03
Q7 74.0
Q5 0.18
Q6 21.3
Q8 3.77
Q7 74.8
Q5 0.20
Q6 20.6
Q8 4.49
Q7 74.8
Count
Comp-FL9-A :: PE-A

iii.

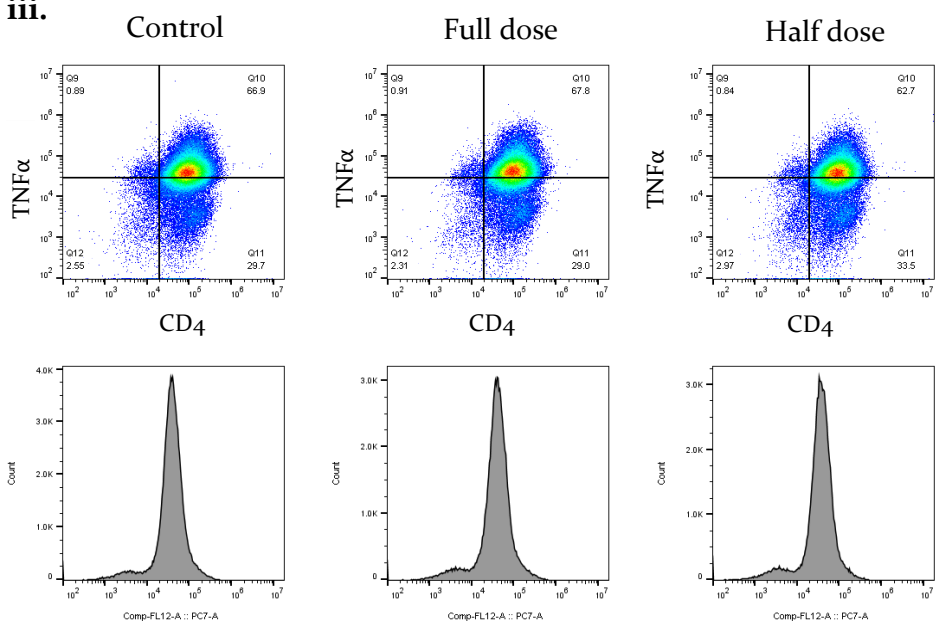
Control
Full dose
Half dose
TNFα
CD4
Q9 0.89
Q10 66.9
Q12 2.55
Q11 29.7
Q9 0.91
Q10 67.8
Q12 2.31
Q11 29.0
Q9 0.84
Q10 62.7
Q12 2.97
Q11 33.5
Count
Comp-FL12-A :: PC7-A

iv.

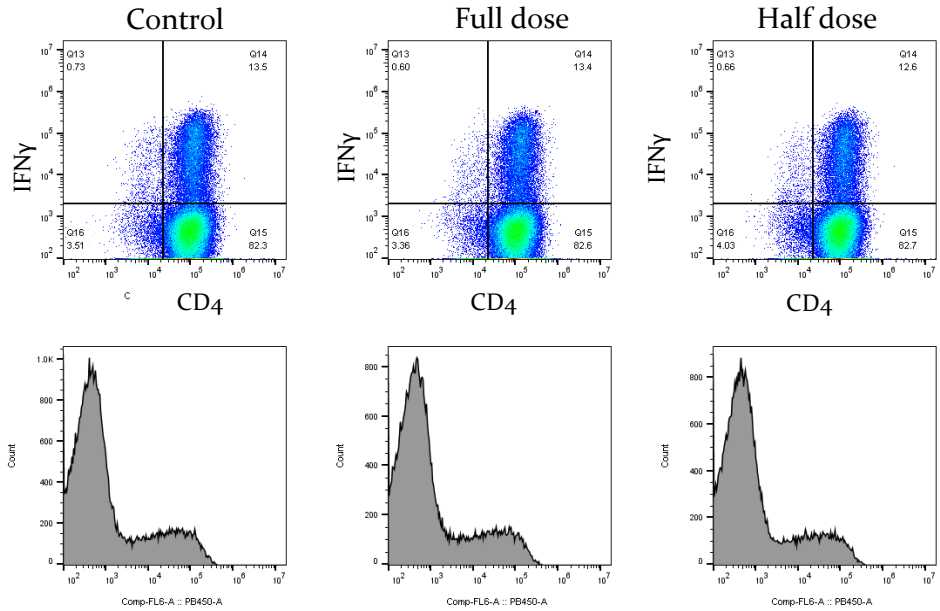
Control
Full dose
Half dose
IFNγ
CD4
Q13 0.73
Q14 13.5
Q16 3.51
Q15 82.3
Q13 0.60
Q14 13.4
Q16 3.36
Q15 82.6
Q13 0.66
Q14 12.6
Q16 4.03
Q15 82.7
Count
Comp-FL6-A :: PB450-A

v.

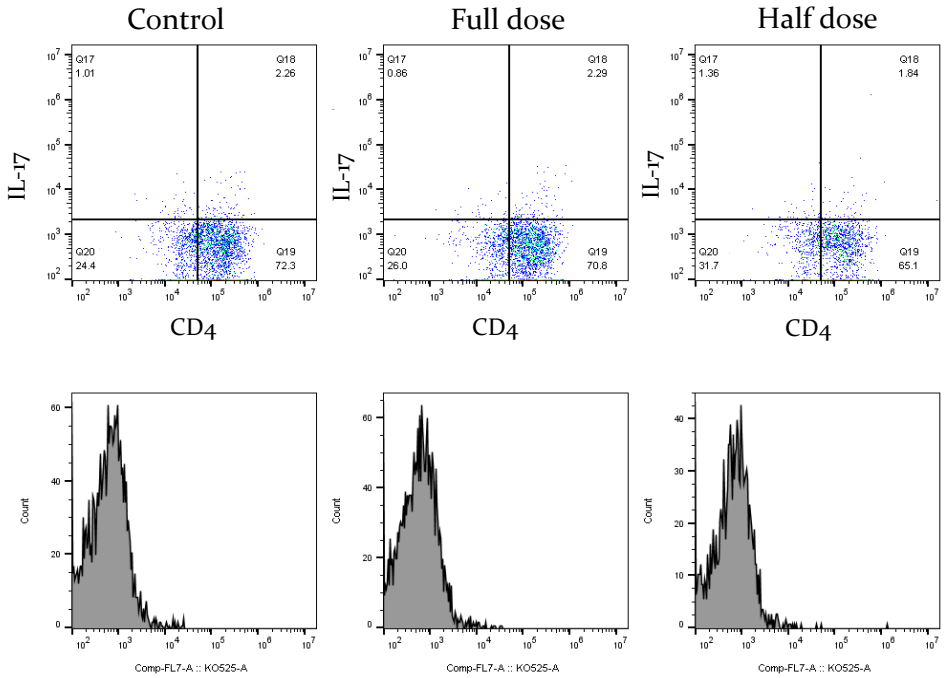
Control
Full dose
Half dose
IL-17
CD4
Q17 1.01
Q18 2.26
Q20 24.4
Q19 72.3
Q17 0.86
Q18 2.29
Q20 26.0
Q19 70.8
Q17 1.36
Q18 1.84
Q20 31.7
Q19 65.1
Count
Comp-FL7-A :: KO525-A

vi.

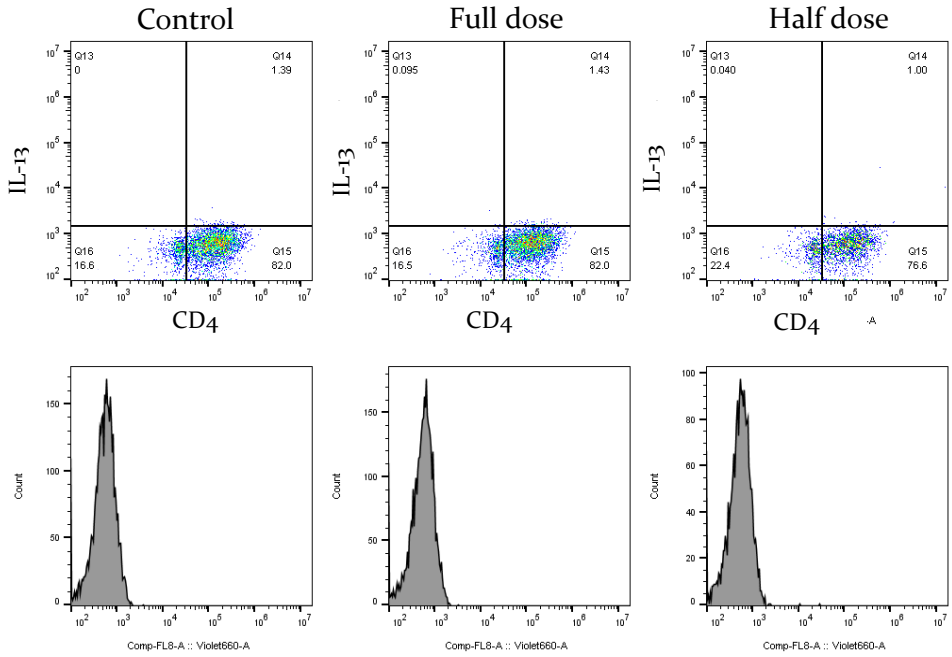
Control
Full dose
Half dose
IL-13
CD4
Q13 0
Q14 1.39
Q16 16.6
Q15 82.0
Q13 0.095
Q14 1.43
Q16 16.5
Q15 82.0
Q13 0.040
Q14 1.00
Q16 22.4
Q15 76.6
Count
Comp-FL8-A :: Violet660-A

Figure 47. The effect of THBS1 on CD4+ -mediated cytokine secretion.

CD4+ T cells were cultured at a density of $2.5x10^4$ cells/well with 2 μg/ml and 1 μg/ml THBS1 in the presence of $5x10^4$ CD3/CD28 Human T-activator Dynabeads. After, 4 days cells were re-stimulated and stained for intracellular (i) TGFβ, (ii) IL-21, (iii) TNFα, (iv) IFNγ, (v) IL-17 and (vi) IL-13 cytokines and cell surface CD4 antibody.

(A.i-vi) Graphs show the change in Maximum Fluorescence Intensity of each cytokine over the exposure to two concentrations of THBS1, as a percentage relative to the MFI detected in the control condition where no THBS1 was added on the cells.

(B.i-vi) Representative dot plots show the cytokine expression of CD4+ T cells when cultured alone (left panel), or in the presence of THBS1. Data is representative of 2 experiments and acquired with flow cytometry. Analysis was performed with FlowJo software and GraphPad Prism.

.

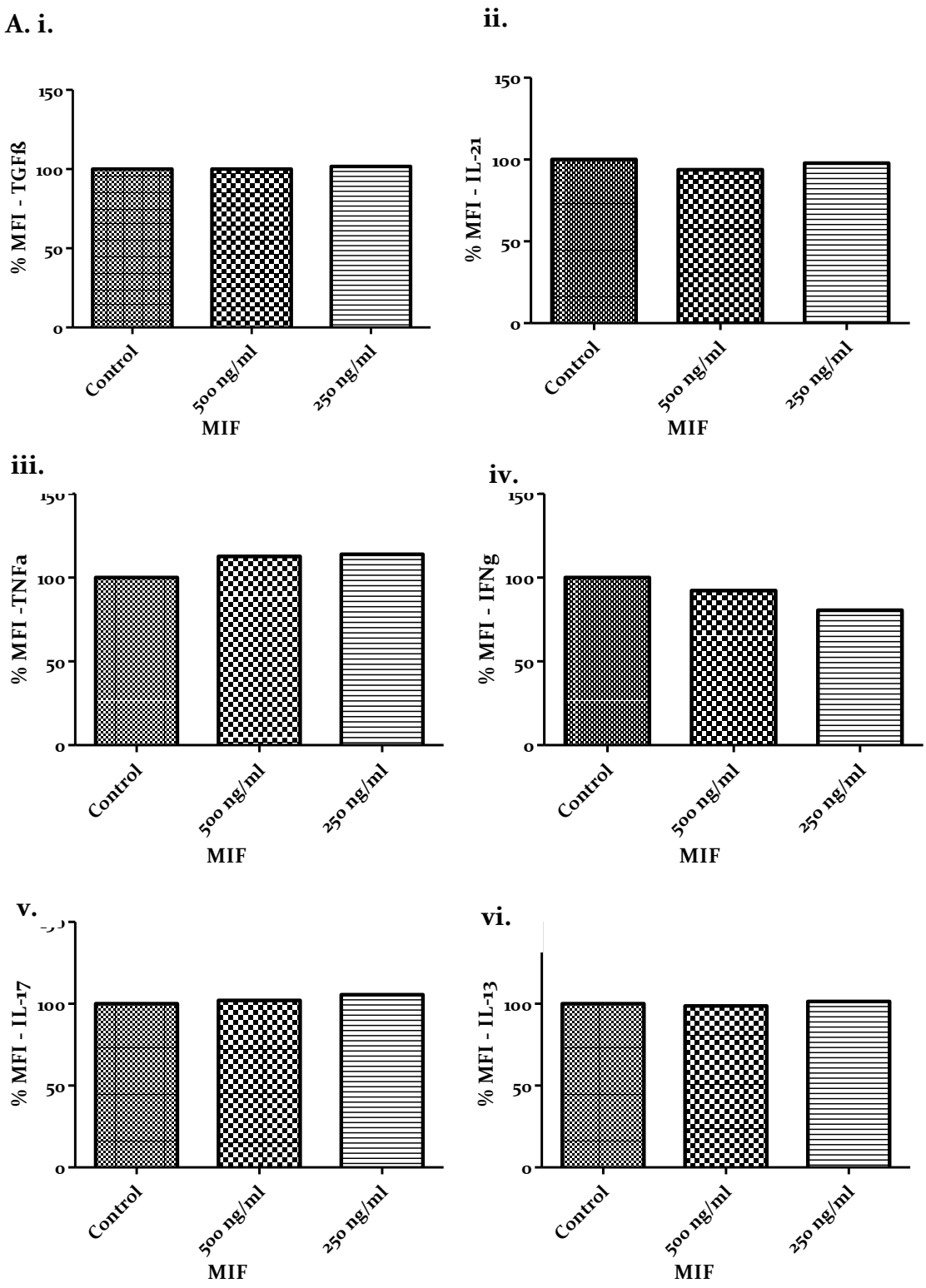
A. i.
% MFI - TGFß
150
100
50
0
Control
500 ng/ml
250 ng/ml
MIF
ii.
% MFI - IL-21
150
100
50
0
Control
500 ng/ml
250 ng/ml
MIF
iii.
% MFI -TNFa
150
100
50
0
Control
500 ng/ml
250 ng/ml
MIF
iv.
% MFI - IFNg
150
100
50
0
Control
500 ng/ml
250 ng/ml
MIF
v.
% MFI - IL-17
100
50
0
Control
500 ng/ml
250 ng/ml
MIF
vi.
% MFI - IL-13
100
50
0
Control
500 ng/ml
250 ng/ml
MIF

B. i.

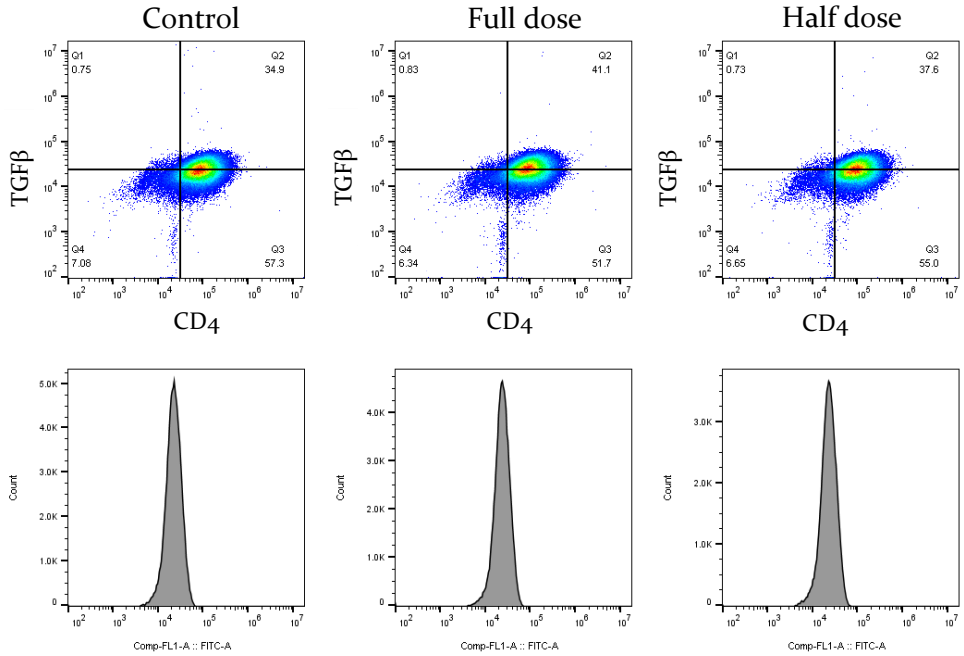
Control
Full dose
Half dose
TGFβ
CD4
Q1 0.75
Q2 34.9
Q4 7.08
Q3 57.3
Q1 0.83
Q2 41.1
Q4 6.34
Q3 51.7
Q1 0.73
Q2 37.6
Q4 6.65
Q3 55.0
Count
Comp-FL1-A :: FITC-A

ii.

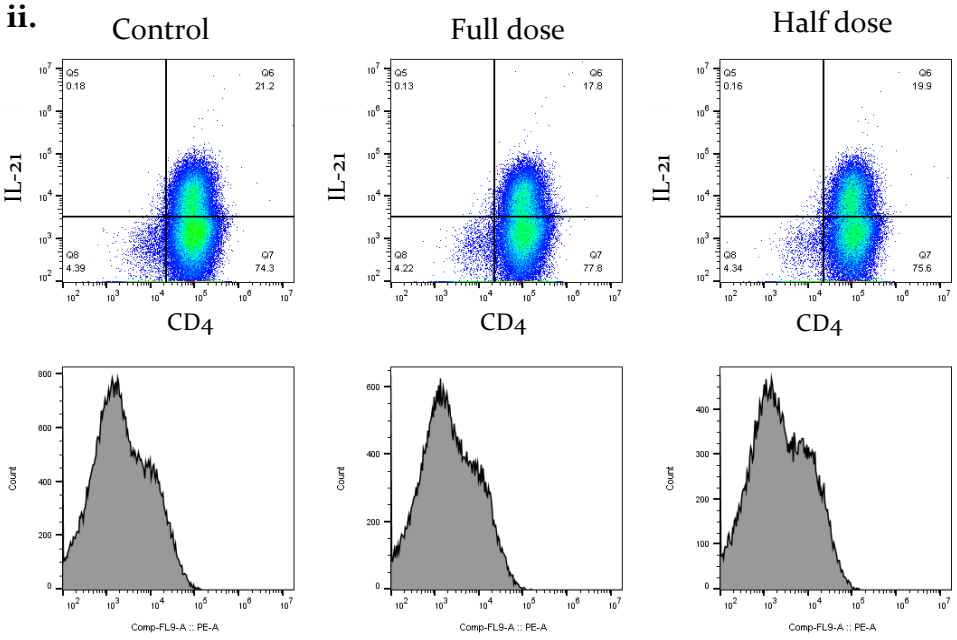
Control
Full dose
Half dose
IL-21
CD4
Q5 0.18
Q6 21.2
Q8 4.39
Q7 74.3
Q5 0.13
Q6 17.8
Q8 4.22
Q7 77.8
Q5 0.16
Q6 19.9
Q8 4.34
Q7 75.6
Count
Comp-FL9-A :: PE-A

iii.

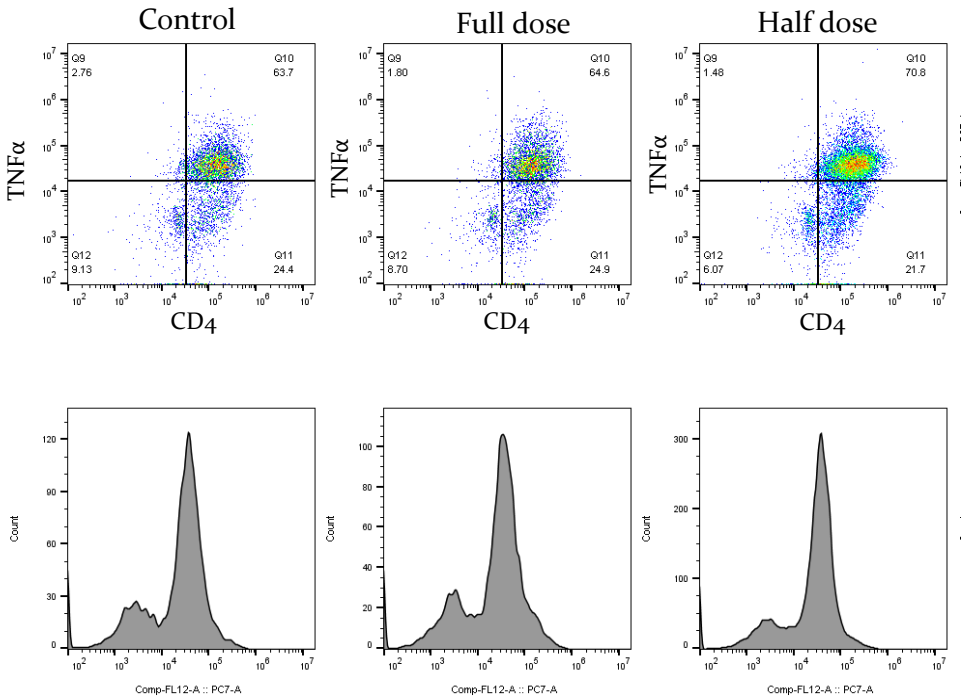
Control
Full dose
Half dose
TNFα
CD4
Q9 2.76
Q10 63.7
Q12 9.13
Q11 24.4
Q9 1.80
Q10 64.6
Q12 8.70
Q11 24.9
Q9 1.48
Q10 70.8
Q12 6.07
Q11 21.7
Count
Comp-FL12-A :: PC7-A

iv.

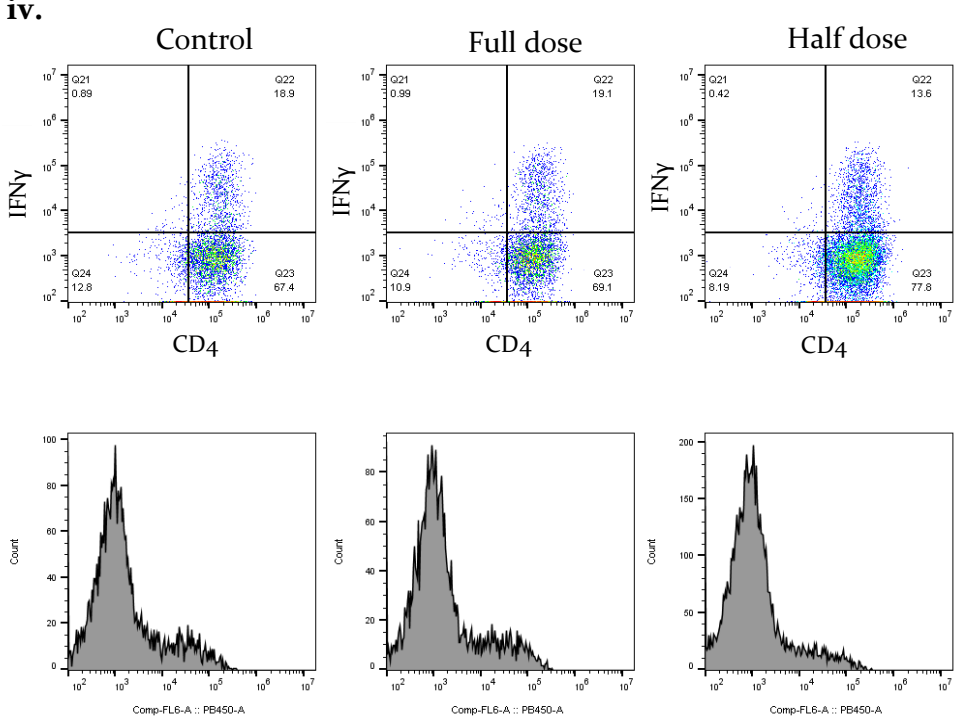
Control
Full dose
Half dose
IFNγ
CD4
Q21 0.89
Q22 18.9
Q24 12.8
Q23 67.4
Q21 0.99
Q22 19.1
Q24 10.9
Q23 69.1
Q21 0.42
Q22 13.6
Q24 8.19
Q23 77.8
Count
Comp-FL6-A :: PB450-A

v.

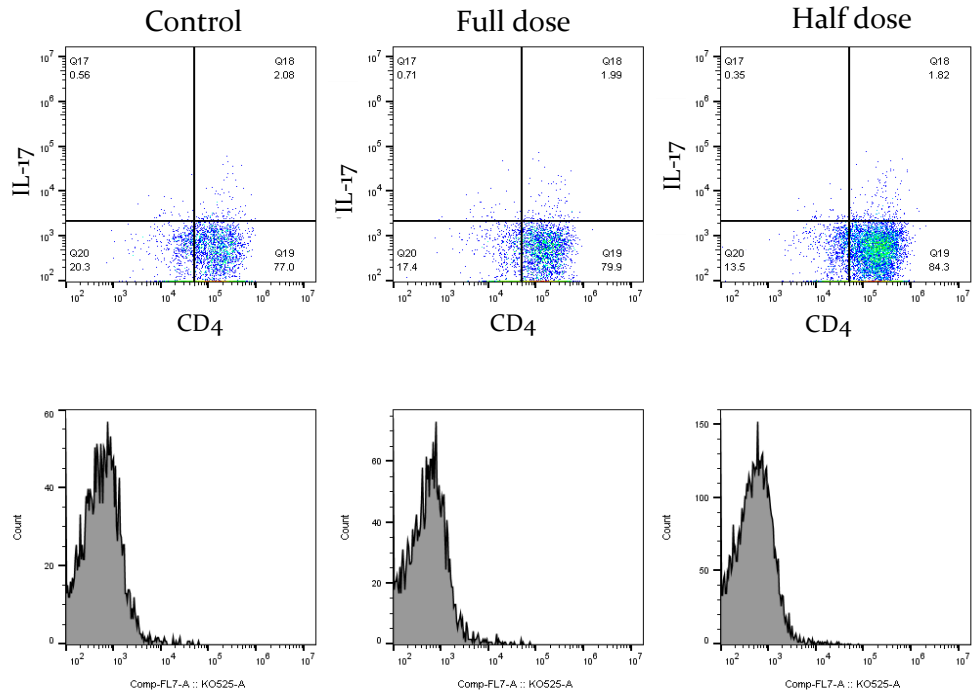
Control
Full dose
Half dose
IL-17
CD4
Q17 0.56
Q18 2.08
Q20 20.3
Q19 77.0
Q17 0.71
Q18 1.99
Q20 17.4
Q19 79.9
Q17 0.35
Q18 1.82
Q20 13.5
Q19 84.3
Count
Comp-FL7-A :: KO525-A

iv.

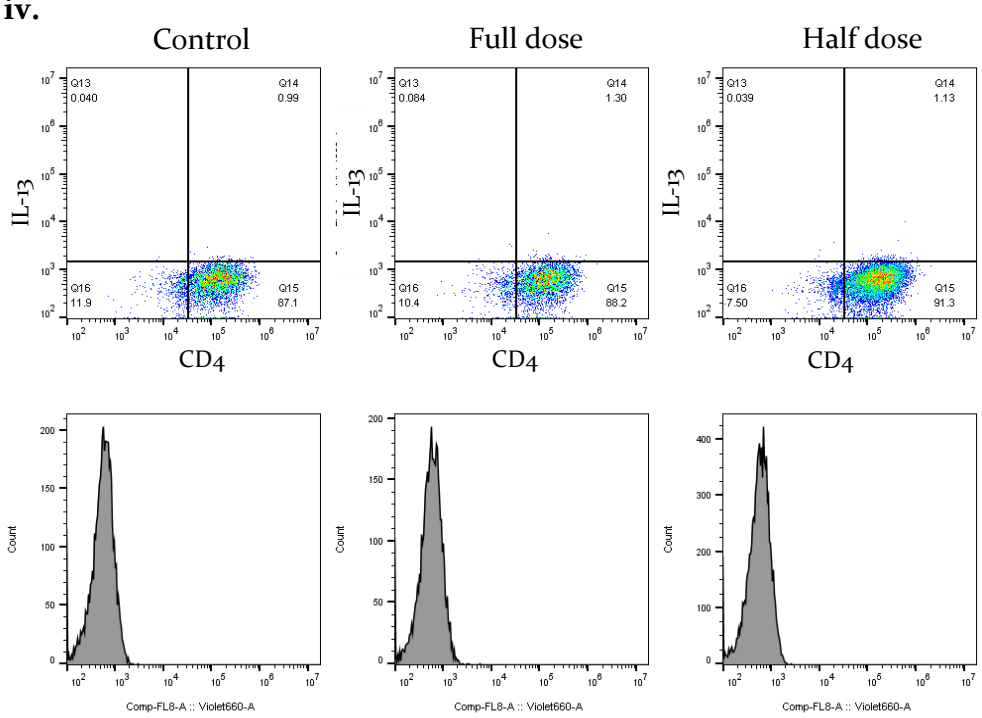
Control
Full dose
Half dose
IL-13
CD4
Q13 0.040
Q14 0.99
Q16 11.9
Q15 87.1
Q13 0.084
Q14 1.30
Q16 10.4
Q15 88.2
Q13 0.039
Q14 1.13
Q16 7.50
Q15 91.3
Count
Comp-FL8-A :: Violet660-A

Figure 48.The effect of MIF on T cell cytokine production.

CD4+ T cells isolated from peripheral blood of healthy human donor were seeded with 250 ng/ml and 500 ng/ml MIF and CD3/CD28 Human T-activator Dynabeads in a ration 1:2 for 5 days. Then, cells were re-stimulated and stained with (i) TGFβ, (ii) IL-21, (iii) TNFα, (iv) IFNγ, (v) IL-17 and (vi) IL-13 antibodies and cell surface anti-human CD4.

(A.i-vi) Graphs show the MFI for specific cytokines produced by the T cells, after being exposed to different concentrations of MIF. Maximum fluorescence intensity is presented in a percentage format compared to the MFI detected in the control condition where no MIF was added on the cells.

(B.i-vi) Representative dot plots show each cytokine production by T cells when cultured alone (left panel) and after treatment with concentrations of MIF. Data is representative of 2 experiments and acquired with flow cytometry. Analysis was performed with FlowJo software and GraphPad Prism.

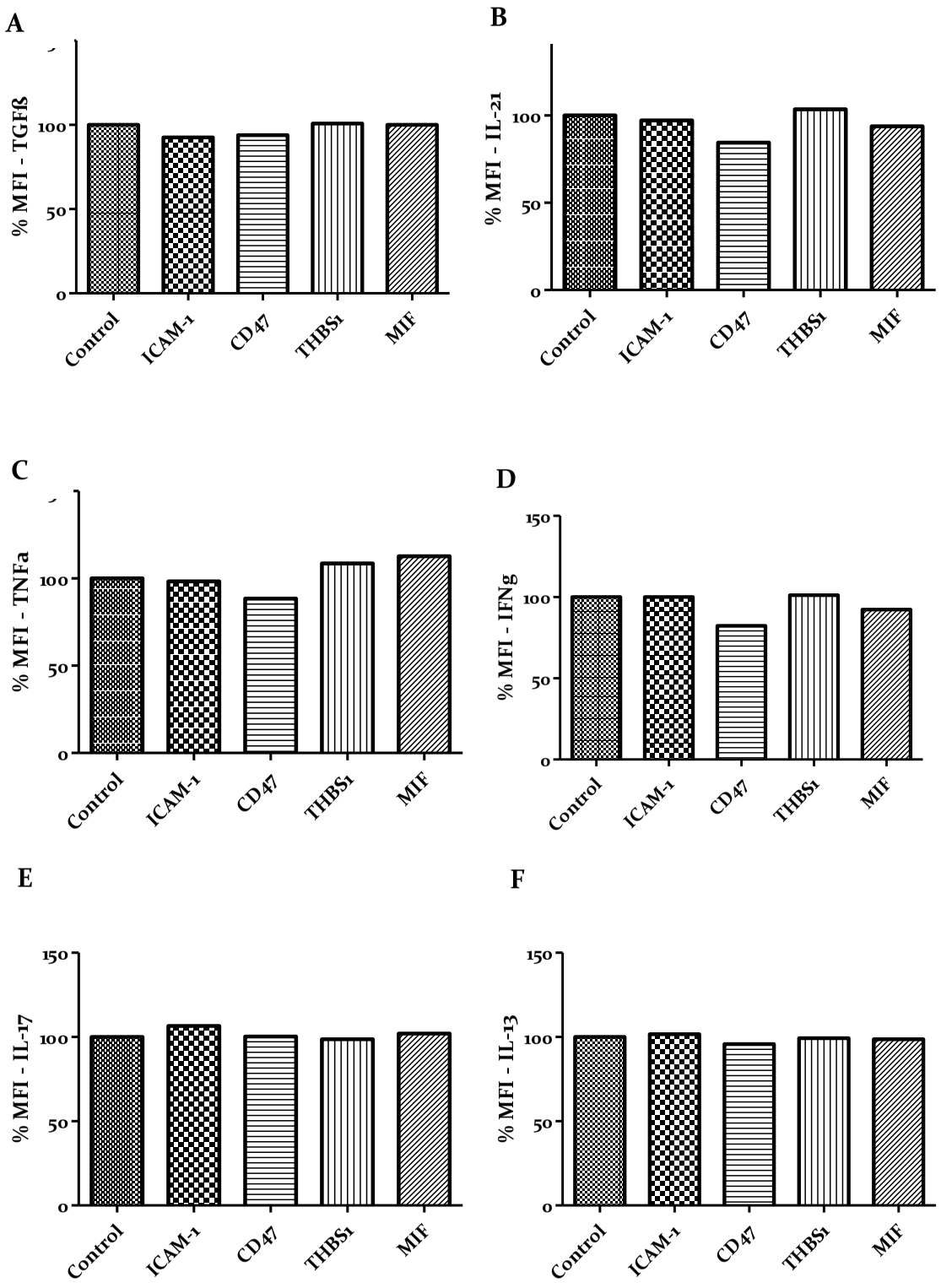
A
% MFI - TGFß
100
50
0
Control
ICAM-1
CD47
THBS1
MIF
B
% MFI - IL-21
100
50
0
Control
ICAM-1
CD47
THBS1
MIF
C
% MFI - TNFa
100
50
0
Control
ICAM-1
CD47
THBS1
MIF
D
% MFI - IFNg
150
100
50
0
Control
ICAM-1
CD47
THBS1
MIF
E
% MFI - IL-17
150
100
50
0
Control
ICAM-1
CD47
THBS1
MIF
F
% MFI - IL-13
150
100
50
0
Control
ICAM-1
CD47
THBS1
MIF

Figure 49. Comparison of the cytokine production after treatment with the highest indicated concentrations for each protein.

CD4+ T cells were seeded with CD3/CD28 Human T-activator Dynabeads (in 1:2 ratio) and treated with 1 μg/ml ICAM-1, 10 μg/ml CD47, 2 μg/ml THBS1 or 500 ng/ml MIF for 4 days. The cells were re-stimulated and stained for stained with (A) TGFβ, (B) IL-21, (C) TNFα, (D) IFNγ, (E) IL-17 and (F) IL-13 antibodies and the cell surface anti-human CD4.

(A- F) Graphs show the effect of the candidate proteins in Maximum Fluorescence Intensity as a percentage relative to the control where there was protein addition.

Data is representative of one experiment (n=1).

S1.3. Tregs inhibit T cell Viability in *in vitro* assays.

CD4+CD25+ Tregs express the forkhead transcription factor FoxP3, which regulates their function as suppressor cells (Fontenot et al., 2005) and it can be used as a specific subset biomarker. Both *in vitro* and *in vivo* studies have shown the Treg-mediated immunesuppression. Depletion of those cells has led to autoimmune diseases occurrence, but a number of cancer cases, including GBM tumours, it resulted in the restoration of anti-tumour immunity (Sakaguchi et al., 2009 ; El Andaloussi & Lesniak., 2006; Fecci et al., 2006). Tregs are highly represented in GBM tumour microenvironment and inhibit effector T cell activity by decreasing interleukin IL-2 and IFNγ production (Fecci et al., 2006).

Since Tregs are present in the GBM tumour microenvironment, the effect of them on T cells combined with concentrated EVs/soluble factors was aimed to be addressed. For this reason, an effective Treg isolation and suppression assay needed to be established first.

Here, the efficiency of isolating conventional T cells and Tregs was tested using the Human CD4+CD127lowCD25+ Regulatory T cell Isolation Kit from peripheral blood of healthy donor. Isolated cells were tested for their purity based on FoxP3 expression using flow cytometry (Figure 50). FoxP3 expression was observed in CD4+CD25+ Treg subset and the purification level was 87.7%, whilst a low portion of conventional T cell was expressing FoxP3. The Tconv cells were cultured at a density of 2.5×10^4 per well and the capacity of CD3/CD28 Dynabeads to activate T cells was tested at a 1:1, 1:5 and 1:10 ratios (Beads:Tconv) (Figure 51).

Furthermore, the efficiency of Tregs in suppressing Tconv cells was examined in different ratios with the 1:1 being the highest one. The cells were incubated for 6 days. Then, the cells were harvested, stained with antibodies against CD4 and FoxP3 and analysed by flow cytometry. Raw cell counts are depicted first (Figure 51-A). In 1:1 Beads:Tconv cells ratio, cell counts were persistently

high and no suppression was observed with the Treg titration. In 1:5 Beads to Tconv ratio, cells were activated in the absence of Tregs. When Tregs were added into the culture, the Tconv cells were suppressed in a dose-dependent manner, whilst in 1:10 Beads to T cells, T cells were not activated in the condition with no Tregs.

In Figure 51-B, Counts are presented as a percentage relative to the cell count of Tconv in absence of Tregs. Cells cultured in 1:1 Beads to Tconv did not show suppression by Tregs at any of the ratios added. In the Bead to Tconv ratio 1:5, Tregs were more suppressive for the Tconv cells when added in ascending ratios. In detail, Tconv cells were reduced with a final % maximum response of 47.63% when Tregs added in a ratio 1:1, but the significance importance of the experiment is not known, since it was performed once. The relative response of Tconv in 1:1 Beads to Tconv ratio, since they were not activated in the first place.

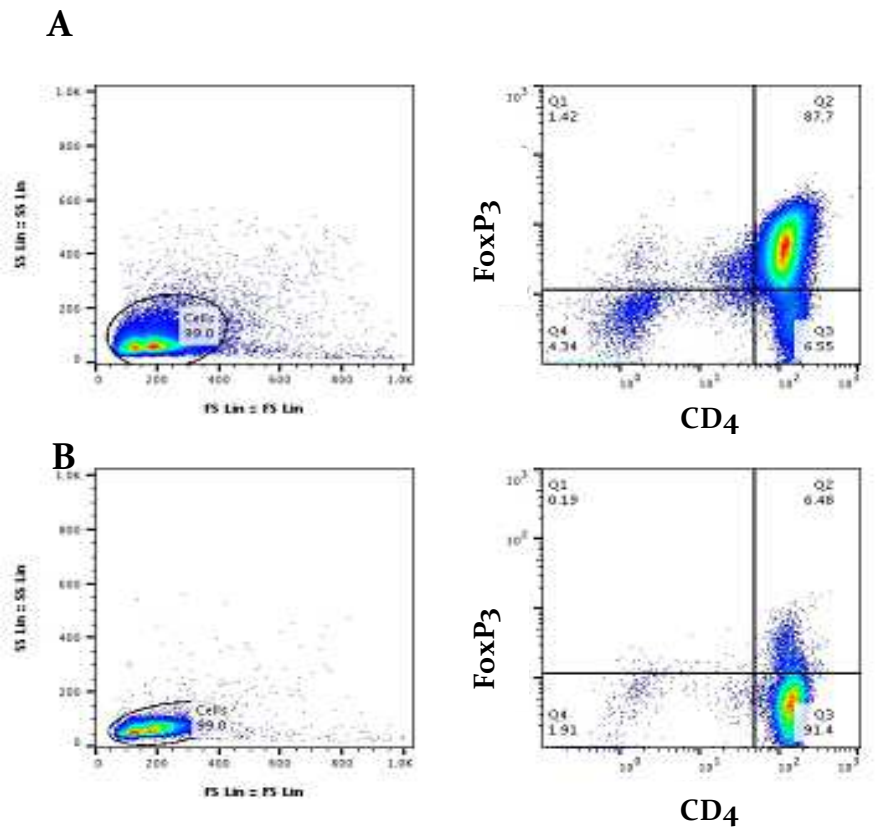

Figure 50. Regulatory T cells purity.

(A) Tregs and **(B)** conventional T cells were isolated from peripheral blood of a healthy donor. The two subpopulations were treated with anti-human CD_4 and $FoxP_3$ mAb and analysed by flow cytometry.

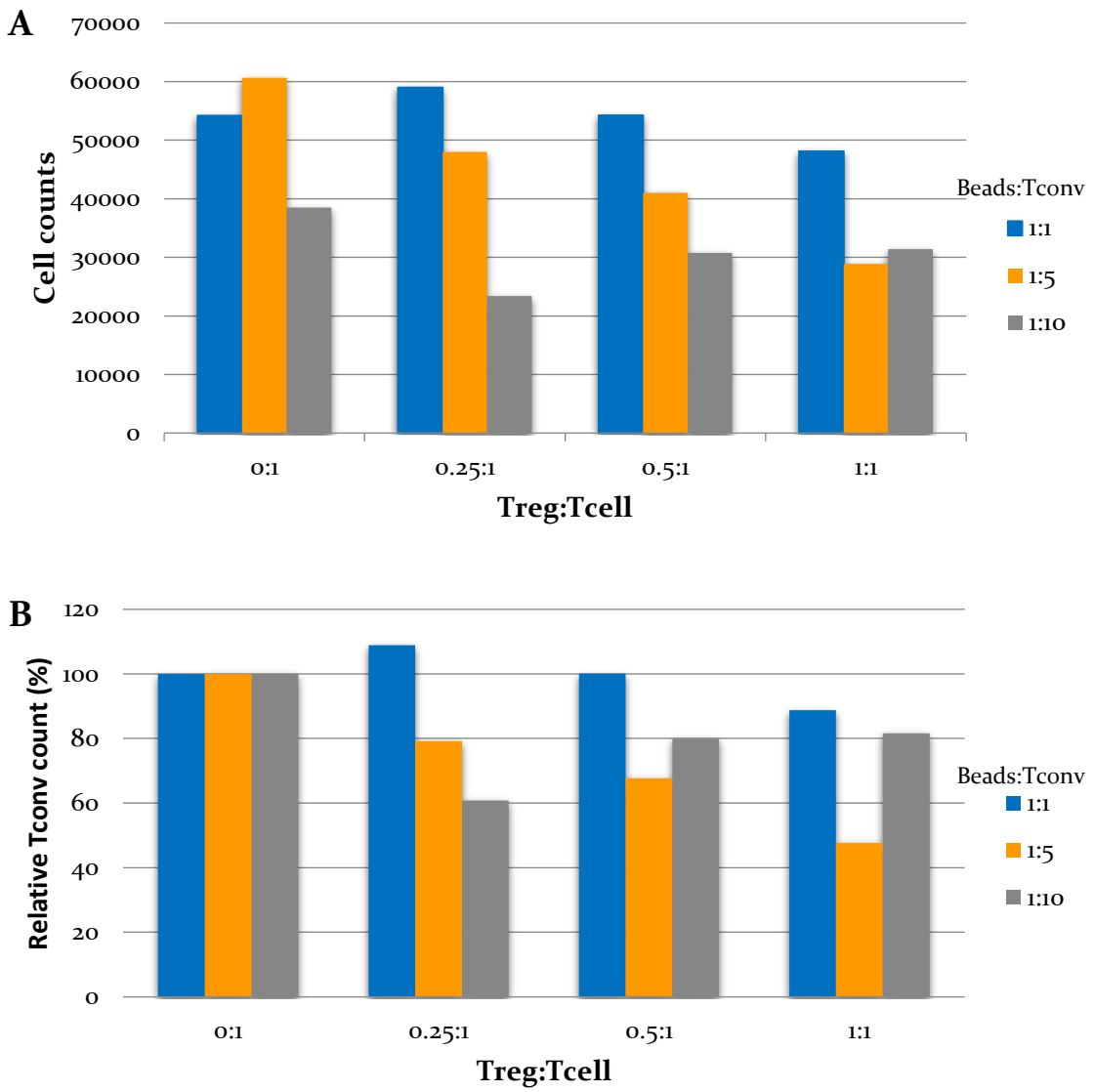

Figure 51. Treg suppression assay.

Tconv cells are plated at a density of 2.5 x 10^4 cells/well in a 96-well plate. CD3/CD28 dynabeads are added in ratios 1:1, 1:5 and 1:10 (Beads:Tconv). Tregs are pipetted in ratios 0.25:1, 0.5:1 and 1:1 Treg to Tconv. Tconv cells cultured with dynabeads in the absence of Tregs are used as control. After 6days cells were harvested and stained with anti-human CD-4 and FoxP3 mAb. Analysis performed by flow cytometry. **(A)** Graph shows cell counts for CD4+Foxp3- Tconv. **(B)** Counts are presented as a percentage, relative to Tconv counts with no Treg addition. Data is representative of one experiment (N=1). No statistical analysis was available for N<3.

APPENDIX 2: PROTOCOLS

S2.1 EasySep™ Human CD4+CD127lowCD25+ Regulatory T cell Isolation

Isolated Tconv from blood cone and stimulated with Dynabeads Human T-Activator CD3/CD28 (Gibco by Thermo Fisher Scientific, USA) were assessed against different numbers of Isolated Tregs in order to estimate the T cell suppression after 6 days.

Isolated peripheral blood was pipetted carefully on the top of the Histopaque and centrifuged at 400g for 30 minutes at room. PBMCs were transferred in a fresh falcon tube. PBS was added up to a volume of 20 mL and centrifuged at 250g for 10 minutes. After the supernatant was removed, 10 mL ACK Lysis Buffer was added for 5 minutes at room temperature and centrifuged at 400 x g for 5 minutes. Then, the PBMCs were re-suspended in 20 mL PBS with 2% RPMI (P2). The cells were calculated.

CD4+CD127lowCD25+ regulatory T cells isolation Kit (StemCell) was used to purify Tregs and conventional T cells from the peripheral blood mononuclear cells (PBMCs) that obtained before. A cell density of 50,000,000 cells/mL are transferred in a 15 mL tube and 50 µL/mL of the CD25 Positive Selection Cocktail is added to the sample. The mixture was re-suspended and left at the room temperature for 5 minutes. Releasable Rapidspheres (30 µL/mL) and 50 µL/mL of CD4 T cell Enrichment Cocktail were added to the sample to positively isolate CD4+/-CD25+ cells over immunomagnetic selection. (CD4+/-CD25- cells are collected in a different falcon tube to be used later).

S2.1.1. Treg isolation

Release buffer (100 µL/mL) is added to remove the magnetic particles from the CD25+ cells. Moreover, the sample is mixed with CD127high Depletion Cocktail in a concentration 50 µL/mL

and Dextran Rapidspheres (10 µL/mL) were also added. The CD127low cells are negatively isolated and constitute the Treg population.

S2.1.2. Human CD4+CD25- Responder T cell Enrichment

In the second population of cells collected (CD4+/-CD25- cells), Dextran RapidSpheres are added and the CD4+CD25- Responder T cell are isolated over positive selection using the magnet. These are the T conventional cells.

S2.2 Treg suppression assay

Tconv are plated in a 96-well plate at 2.5 x 10^4 cells per well. Dynabeads Human T-Activator CD3/CD28 (Gibco, Thermo Fisher Scientific, UK) were added in 1:1, 1:5 and 1:10 Beads to Tconv cells ratio. Next, Tregs are plated at a Treg to Tconv ratio of 0:1, 0.2.5:1, 0.5:1 and 1:1. All wells should be topped up to 200 µL final volume with C10 (Fig.52). The cells were placed into the incubator for 5 days.

The cells were harvested and stained with 2µl CD4 PE-Cy7 (Invitrogen by Thermo Fisher Scientific, USA) and 2 µl CD25 (eBioscience, UK) mAb. The cells were analysed by CytoFLEX S Flow Cytometer (Beckman Coulter, Germany) and FlowJo software.

S2.3 Treg purity

The procedure followed for the Treg isolation is the same as above using the Human CD4+CD127lowCD25+ Regulatory T cell Isolation Kit. From the Treg subset, a suspension of 100,000

cells is calculated and added in a flow tube (12 x 75 mm FACS tube, VWR International, USA) and topped up to 1 mL with C10.

The step was repeated for the Tconv cells. The cells were fixed/permeabilised and stained with 2 µL CD4 and 5 µL FoxP3 antibodies (BD Biosciences, USA) for 30 minutes and analysed using the CytoFLEX S Flow Cytometer and FlowJo software.

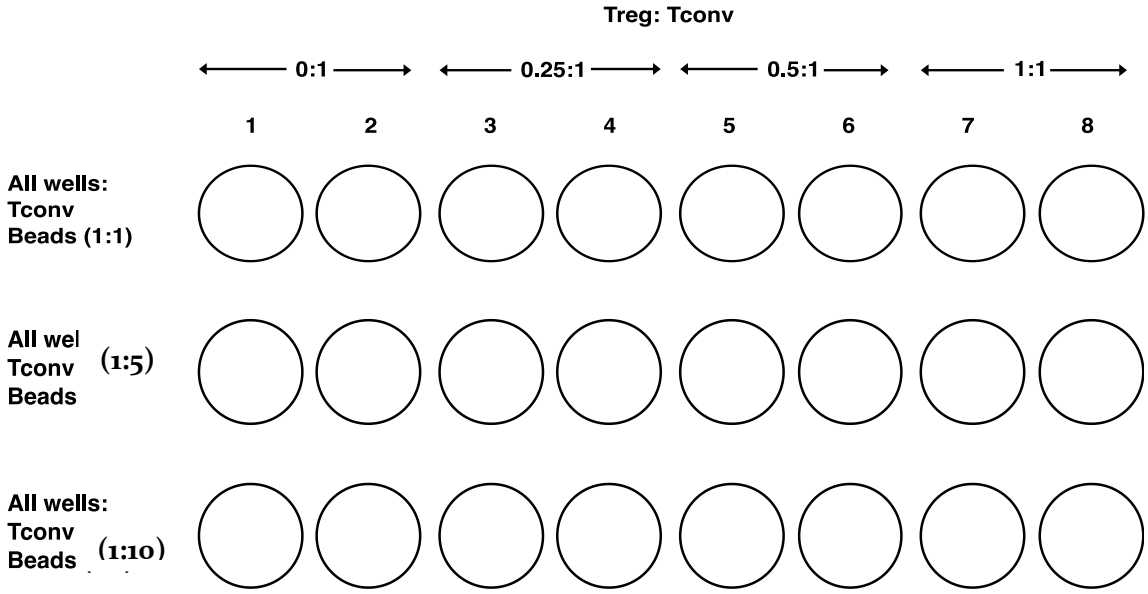

Figure 52. Representation of the Treg suppression assay experiment.

A number of 2.5 x 10^4 Tconv cells were plated. Beads and Tregs were added in the ratios shown above in solutions of 50 µL/well.

APPENDIX 3: SCIENTIFIC APPENDIX

Table 6. Proteomic analysis of the EV fractions from GBM patients

Accession	Description
1433B_HUMAN	14-3-3 protein beta/alpha
1433E_HUMAN	14-3-3 protein epsilon
1433F_HUMAN	14-3-3 protein eta
1433G_HUMAN	14-3-3 protein gamma
1433S_HUMAN	14-3-3 protein sigma
1433T_HUMAN	14-3-3 protein theta
1433Z_HUMAN	14-3-3 protein zeta/delta
2A5D_HUMAN	Serine/threonine-protein phosphatase 2A 56 kDa regulatory subunit delta isoform
2AAA_HUMAN	Serine/threonine-protein phosphatase 2A 65 kDa regulatory subunit A alpha isoform
2ABA_HUMAN	Serine/threonine-protein phosphatase 2A 55 kDa regulatory subunit B alpha isoform
4F2_HUMAN	4F2 cell-surface antigen heavy chain
5NTD_HUMAN	5'-nucleotidase
6PGD_HUMAN	6-phosphogluconate dehydrogenase, decarboxylating
A1AG1_HUMAN	Alpha-1-acid glycoprotein 1
A1AT_HUMAN	Alpha-1-antitrypsin
A1BG_HUMAN	Alpha-1B-glycoprotein
A2MG_HUMAN	Alpha-2-macroglobulin
A4_HUMAN	Amyloid-beta precursor protein
AACT_HUMAN	Alpha-1-antichymotrypsin
AATC_HUMAN	Aspartate aminotransferase, cytoplasmic
AATM_HUMAN	Aspartate aminotransferase, mitochondrial
AB12B_HUMAN	Protein ABHD12B
ABCA4_HUMAN	Retinal-specific phospholipid-transporting ATPase ABCA4
ABCA7_HUMAN	Phospholipid-transporting ATPase ABCA7
ABCAD_HUMAN	ATP-binding cassette sub-family A member 13
ABD12_HUMAN	Lysophosphatidylserine lipase ABHD12
ABHD8_HUMAN	Protein ABHD8
ACBP_HUMAN	Acyl-CoA-binding protein
ACLY_HUMAN	ATP-citrate synthase
ACON_HUMAN	Aconitate hydratase, mitochondrial
ACPH_HUMAN	Acylamino-acid-releasing enzyme
ACSL6_HUMAN	Long-chain-fatty-acid--CoA ligase 6
ACTA_HUMAN	Actin, aortic smooth muscle
ACTB_HUMAN	Actin, cytoplasmic 1

ACTBL_HUMAN	Beta-actin-like protein 2
ACTL9_HUMAN	Actin-like protein 9
ACTN1_HUMAN	Alpha-actinin-1
ACTN4_HUMAN	Alpha-actinin-4
ACTZ_HUMAN	Alpha-centractin
ADA10_HUMAN	Disintegrin and metalloproteinase domain-containing protein 10
ADA1D_HUMAN	Alpha-1D adrenergic receptor
ADDB_HUMAN	Beta-adducin
ADIPO_HUMAN	Adiponectin
ADT1_HUMAN	ADP/ATP translocase 1
ADT2_HUMAN	ADP/ATP translocase 2
ADT3_HUMAN	ADP/ATP translocase 3
AEDO_HUMAN	2-aminoethanethiol dioxygenase
AGRIN_HUMAN	Agrin
AINX_HUMAN	Alpha-internexin
AK1A1_HUMAN	Aldo-keto reductase family 1 member A1
AKA12_HUMAN	A-kinase anchor protein 12
AKAP9_HUMAN	A-kinase anchor protein 9
AKT1_HUMAN	RAC-alpha serine/threonine-protein kinase
AL1A1_HUMAN	Retinal dehydrogenase 1
AL1L1_HUMAN	Cytosolic 10-formyltetrahydrofolate dehydrogenase
AL3A2_HUMAN	Aldehyde dehydrogenase family 3 member A2
AL4A1_HUMAN	Delta-1-pyrroline-5-carboxylate dehydrogenase, mitochondrial
AL5AP_HUMAN	Arachidonate 5-lipoxygenase-activating protein
AL7A1_HUMAN	Alpha-aminoadipic semialdehyde dehydrogenase
AL9A1_HUMAN	4-trimethylaminobutyraldehyde dehydrogenase
ALBU_HUMAN	Albumin
ALDH2_HUMAN	Aldehyde dehydrogenase, mitochondrial
ALDOA_HUMAN	Fructose-bisphosphate aldolase A
ALDOC_HUMAN	Fructose-bisphosphate aldolase C
ALDR_HUMAN	Aldo-keto reductase family 1 member B1
ALG6_HUMAN	Dolichyl pyrophosphate Man9GlcNAc2 alpha-1,3-glucosyltransferase
ALS2_HUMAN	Alsin
AMN1_HUMAN	Protein AMN1 homolog
AMPD2_HUMAN	AMP deaminase 2
AMPL_HUMAN	Cytosol aminopeptidase
AMRP_HUMAN	Alpha-2-macroglobulin receptor-associated protein
ANAG_HUMAN	Alpha-N-acetylglucosaminidase
ANGT_HUMAN	Angiotensinogen
ANK1_HUMAN	Ankyrin-1
ANK2_HUMAN	Ankyrin-2

ANK3_HUMAN	Ankyrin-3
ANKF1_HUMAN	Ankyrin repeat and fibronectin type-III domain-containing protein 1
ANM5_HUMAN	Protein arginine N-methyltransferase 5
ANO6_HUMAN	Anoctamin-6
ANT3_HUMAN	Antithrombin-III
ANX11_HUMAN	Annexin A11
ANXA1_HUMAN	Annexin A1
ANXA2_HUMAN	Annexin A2
ANXA3_HUMAN	Annexin A3
ANXA4_HUMAN	Annexin A4
ANXA5_HUMAN	Annexin A5
ANXA6_HUMAN	Annexin A6
ANXA7_HUMAN	Annexin A7
AOFB_HUMAN	Amine oxidase [flavin-containing] B
AP1B1_HUMAN	AP-1 complex subunit beta-1
AP1G1_HUMAN	AP-1 complex subunit gamma-1
AP2A1_HUMAN	AP-2 complex subunit alpha-1
AP2A2_HUMAN	AP-2 complex subunit alpha-2
AP2B1_HUMAN	AP-2 complex subunit beta
AP2D_HUMAN	Transcription factor AP-2-delta
AP2M1_HUMAN	AP-2 complex subunit mu
AP2S1_HUMAN	AP-2 complex subunit sigma
APLP1_HUMAN	Amyloid-like protein 1
APMAP_HUMAN	Adipocyte plasma membrane-associated protein
APOA_HUMAN	Apolipoprotein(a)
APOA1_HUMAN	Apolipoprotein A-I
APOA2_HUMAN	Apolipoprotein A-II
APOA4_HUMAN	Apolipoprotein A-IV
APOB_HUMAN	Apolipoprotein B-100
APOC3_HUMAN	Apolipoprotein C-III
APOD_HUMAN	Apolipoprotein D
APOE_HUMAN	Apolipoprotein E
APOH_HUMAN	Beta-2-glycoprotein 1
APOM_HUMAN	Apolipoprotein M
AQP1_HUMAN	Aquaporin-1
AQP4_HUMAN	Aquaporin-4
AR6P1_HUMAN	ADP-ribosylation factor-like protein 6-interacting protein 1
ARC1A_HUMAN	Actin-related protein 2/3 complex subunit 1A
ARF1_HUMAN	ADP-ribosylation factor 1
ARF4_HUMAN	ADP-ribosylation factor 4
ARL8B_HUMAN	ADP-ribosylation factor-like protein 8B

ARP2_HUMAN	Actin-related protein 2
ARP3_HUMAN	Actin-related protein 3
ARPC2_HUMAN	Actin-related protein 2/3 complex subunit 2
ARPC3_HUMAN	Actin-related protein 2/3 complex subunit 3
ARPC4_HUMAN	Actin-related protein 2/3 complex subunit 4
ARSF_HUMAN	Arylsulfatase F
ASAH1_HUMAN	Acid ceramidase
ASB6_HUMAN	Ankyrin repeat and SOCS box protein 6
ASML_HUMAN	Probable bifunctional dTTP/UTP pyrophosphatase/methyltransferase protein
ASPM_HUMAN	Abnormal spindle-like microcephaly-associated protein
AT131_HUMAN	Endoplasmic reticulum transmembrane helix translocase
AT1A1_HUMAN	Sodium/potassium-transporting ATPase subunit alpha-1
AT1A2_HUMAN	Sodium/potassium-transporting ATPase subunit alpha-2
AT1A3_HUMAN	Sodium/potassium-transporting ATPase subunit alpha-3
AT1B1_HUMAN	Sodium/potassium-transporting ATPase subunit beta-1
AT1B2_HUMAN	Sodium/potassium-transporting ATPase subunit beta-2
AT1B3_HUMAN	Sodium/potassium-transporting ATPase subunit beta-3
AT2A2_HUMAN	Sarcoplasmic/endoplasmic reticulum calcium ATPase 2
AT2B1_HUMAN	Plasma membrane calcium-transporting ATPase 1
AT2B2_HUMAN	Plasma membrane calcium-transporting ATPase 2
AT2B4_HUMAN	Plasma membrane calcium-transporting ATPase 4
AT8A1_HUMAN	Phospholipid-transporting ATPase IA
ATD2B_HUMAN	ATPase family AAA domain-containing protein 2B
ATLA1_HUMAN	Atlastin-1
ATLA3_HUMAN	Atlastin-3
ATP5H_HUMAN	ATP synthase subunit d, mitochondrial
ATP5I_HUMAN	ATP synthase subunit e, mitochondrial
ATP5L_HUMAN	ATP synthase subunit g, mitochondrial
ATP6_HUMAN	ATP synthase subunit a
ATPA_HUMAN	ATP synthase subunit alpha, mitochondrial
ATPB_HUMAN	ATP synthase subunit beta, mitochondrial
ATPG_HUMAN	ATP synthase subunit gamma, mitochondrial
ATPO_HUMAN	ATP synthase subunit O, mitochondrial
ATRN_HUMAN	Attractin
ATRX_HUMAN	Transcriptional regulator ATRX
ATS12_HUMAN	A disintegrin and metalloproteinase with thrombospondin motifs 12
B2MG_HUMAN	Beta-2-microglobulin
B3AT_HUMAN	Band 3 anion transport protein
B3GLT_HUMAN	Beta-1,3-glucosyltransferase
BAF_HUMAN	Barrier-to-autointegration factor
BAP31_HUMAN	B-cell receptor-associated protein 31

BASI_HUMAN	Basigin
BASP1_HUMAN	Brain acid soluble protein 1
BAZ1A_HUMAN	Bromodomain adjacent to zinc finger domain protein 1A
BBIP1_HUMAN	BBSome-interacting protein 1
BCAS1_HUMAN	Breast carcinoma-amplified sequence 1
BDH2_HUMAN	3-hydroxybutyrate dehydrogenase type 2
BHE40_HUMAN	Class E basic helix-loop-helix protein 40
BI2L1_HUMAN	Brain-specific angiogenesis inhibitor 1-associated protein 2-like protein 1
BIN1_HUMAN	Myc box-dependent-interacting protein 1
BIP_HUMAN	Endoplasmic reticulum chaperone BiP
BLMH_HUMAN	Bleomycin hydrolase
BLVRB_HUMAN	Flavin reductase (NADPH)
BPI_HUMAN	Bactericidal permeability-increasing protein
BRD8_HUMAN	Bromodomain-containing protein 8
BRI3B_HUMAN	BRI3-binding protein
BST1_HUMAN	ADP-ribosyl cyclase/cyclic ADP-ribose hydrolase 2
BTAF1_HUMAN	TATA-binding protein-associated factor 172
BTBDH_HUMAN	BTB/POZ domain-containing protein 17
C1QA_HUMAN	Complement C1q subcomponent subunit A
C1QB_HUMAN	Complement C1q subcomponent subunit B
C1QC_HUMAN	Complement C1q subcomponent subunit C
C1R_HUMAN	Complement C1r subcomponent
C1S_HUMAN	Complement C1s subcomponent
C1TM_HUMAN	Monofunctional C1-tetrahydrofolate synthase, mitochondrial
C4BPA_HUMAN	C4b-binding protein alpha chain
CA2D3_HUMAN	Voltage-dependent calcium channel subunit alpha-2/delta-3
CAC1C_HUMAN	Voltage-dependent L-type calcium channel subunit alpha-1C
CAD15_HUMAN	Cadherin-15
CAD24_HUMAN	Cadherin-24
CADH2_HUMAN	Cadherin-2
CADM2_HUMAN	Cell adhesion molecule 2
CADM3_HUMAN	Cell adhesion molecule 3
CADM4_HUMAN	Cell adhesion molecule 4
CAH1_HUMAN	Carbonic anhydrase 1
CAH2_HUMAN	Carbonic anhydrase 2
CALL5_HUMAN	Calmodulin-like protein 5
CALM1_HUMAN	Calmodulin-1
CALR_HUMAN	Calreticulin
CALU_HUMAN	Calumenin
CALX_HUMAN	Calnexin
CAN1_HUMAN	Calpain-1 catalytic subunit

CAN2_HUMAN	Calpain-2 catalytic subunit
CAN5_HUMAN	Calpain-5
CAND1_HUMAN	Cullin-associated NEDD8-dissociated protein 1
CAP1_HUMAN	Adenylyl cyclase-associated protein 1
CAP2_HUMAN	Adenylyl cyclase-associated protein 2
CAP7_HUMAN	Azurocidin
CAPG_HUMAN	Macrophage-capping protein
CAPZB_HUMAN	F-actin-capping protein subunit beta
CAR10_HUMAN	Caspase recruitment domain-containing protein 10
CASPE_HUMAN	Caspase-14
CATA_HUMAN	Catalase
CATD_HUMAN	Cathepsin D
CATG_HUMAN	Cathepsin G
CAV1_HUMAN	Caveolin-1
CAYP1_HUMAN	Calcyphosin
CAZA1_HUMAN	F-actin-capping protein subunit alpha-1
CBG_HUMAN	Corticosteroid-binding globulin
CBPC3_HUMAN	Cytosolic carboxypeptidase 3
CBPE_HUMAN	Carboxypeptidase E
CBPM_HUMAN	Carboxypeptidase M
CBR1_HUMAN	Carbonyl reductase [NADPH] 1
CC127_HUMAN	Coiled-coil domain-containing protein 127
CC148_HUMAN	Coiled-coil domain-containing protein 148
CC167_HUMAN	Coiled-coil domain-containing protein 167
CCAR2_HUMAN	Cell cycle and apoptosis regulator protein 2
CCD47_HUMAN	Coiled-coil domain-containing protein 47
CCD71_HUMAN	Coiled-coil domain-containing protein 71
CD109_HUMAN	CD109 antigen
CD14_HUMAN	Monocyte differentiation antigen CD14
CD276_HUMAN	CD276 antigen
CD36_HUMAN	Platelet glycoprotein 4
CD38_HUMAN	ADP-ribosyl cyclase/cyclic ADP-ribose hydrolase 1
CD44_HUMAN	CD44 antigen
CD47_HUMAN	Leukocyte surface antigen CD47
CD63_HUMAN	CD63 antigen
CD81_HUMAN	CD81 antigen
CD82_HUMAN	CD82 antigen
CD9_HUMAN	CD9 antigen
CD99_HUMAN	CD99 antigen
CDC42_HUMAN	Cell division control protein 42 homolog
CDIPT_HUMAN	CDP-diacylglycerol--inositol 3-phosphatidyltransferase

CDK14_HUMAN	Cyclin-dependent kinase 14
CDS2_HUMAN	Phosphatidate cytidylyltransferase 2
CDSN_HUMAN	Corneodesmosin
CDT1_HUMAN	DNA replication factor Cdt1
CEND_HUMAN	Cell cycle exit and neuronal differentiation protein 1
CENPP_HUMAN	Centromere protein P
CERKL_HUMAN	Ceramide kinase-like protein
CERS1_HUMAN	Ceramide synthase 1
CERS2_HUMAN	Ceramide synthase 2
CERU_HUMAN	Ceruloplasmin
CFAB_HUMAN	Complement factor B
CFAH_HUMAN	Complement factor H
CFTR_HUMAN	Cystic fibrosis transmembrane conductance regulator
CGT_HUMAN	2-hydroxyacylsphingosine 1-beta-galactosyltransferase
CH10_HUMAN	10 kDa heat shock protein, mitochondrial
CH3L1_HUMAN	Chitinase-3-like protein 1
CH60_HUMAN	60 kDa heat shock protein, mitochondrial
CHD1_HUMAN	Chromodomain-helicase-DNA-binding protein 1
CHIC2_HUMAN	Cysteine-rich hydrophobic domain-containing protein 2
CHID1_HUMAN	Chitinase domain-containing protein 1
CHM2A_HUMAN	Charged multivesicular body protein 2a
CHM4B_HUMAN	Charged multivesicular body protein 4b
CHST8_HUMAN	Carbohydrate sulfotransferase 8
CI014_HUMAN	Putative uncharacterized protein encoded by LINC00032
CILK1_HUMAN	Serine/threonine-protein kinase ICK
CISY_HUMAN	Citrate synthase, mitochondrial
CKAP4_HUMAN	Cytoskeleton-associated protein 4
CLAP1_HUMAN	CLIP-associating protein 1
CLCA_HUMAN	Clathrin light chain A
CLCB_HUMAN	Clathrin light chain B
CLH1_HUMAN	Clathrin heavy chain 1
CLIC1_HUMAN	Chloride intracellular channel protein 1
CLIC4_HUMAN	Chloride intracellular channel protein 4
CLPP_HUMAN	ATP-dependent Clp protease proteolytic subunit, mitochondrial
CLPT1_HUMAN	Cleft lip and palate transmembrane protein 1
CLPX_HUMAN	ATP-dependent Clp protease ATP-binding subunit clpX-like, mitochondrial
CLUS_HUMAN	Clusterin
CMC1_HUMAN	Calcium-binding mitochondrial carrier protein Aralar1
CMC2_HUMAN	Calcium-binding mitochondrial carrier protein Aralar2
CN37_HUMAN	2',3'-cyclic-nucleotide 3'-phosphodiesterase
CNDP1_HUMAN	Beta-Ala-His dipeptidase

CNDP2_HUMAN	Cytosolic non-specific dipeptidase
CNGA2_HUMAN	Cyclic nucleotide-gated olfactory channel
CNTN1_HUMAN	Contactin-1
CO1A1_HUMAN	Collagen alpha-1(I) chain
CO1A2_HUMAN	Collagen alpha-2(I) chain
CO3_HUMAN	Complement C3
CO3A1_HUMAN	Collagen alpha-1(III) chain
CO4A_HUMAN	Complement C4-A
CO4A2_HUMAN	Collagen alpha-2(IV) chain
CO5_HUMAN	Complement C5
CO6A1_HUMAN	Collagen alpha-1(VI) chain
CO8A_HUMAN	Complement component C8 alpha chain
CO8G_HUMAN	Complement component C8 gamma chain
CO9_HUMAN	Complement component C9
COEA1_HUMAN	Collagen alpha-1(XIV) chain
COF1_HUMAN	Cofilin-1
COMD4_HUMAN	COMM domain-containing protein 4
COMP_HUMAN	Cartilage oligomeric matrix protein
COMT_HUMAN	Catechol O-methyltransferase
COPA_HUMAN	Coatomer subunit alpha
COPG2_HUMAN	Coatomer subunit gamma-2
COSA1_HUMAN	Collagen alpha-1(XXVIII) chain
COX2_HUMAN	Cytochrome c oxidase subunit 2
COX5A_HUMAN	Cytochrome c oxidase subunit 5A, mitochondrial
CP11A_HUMAN	Cholesterol side-chain cleavage enzyme, mitochondrial
CP2U1_HUMAN	Cytochrome P450 2U1
CPN2_HUMAN	Carboxypeptidase N subunit 2
CPNE1_HUMAN	Copine-1
CPNE2_HUMAN	Copine-2
CPNE3_HUMAN	Copine-3
CPNS1_HUMAN	Calpain small subunit 1
CPSF5_HUMAN	Cleavage and polyadenylation specificity factor subunit 5
CREB5_HUMAN	Cyclic AMP-responsive element-binding protein 5
CROCC_HUMAN	Rootletin
CRYAB_HUMAN	Alpha-crystallin B chain
CRYM_HUMAN	Ketimine reductase mu-crystallin
CSK21_HUMAN	Casein kinase II subunit alpha
CSK2B_HUMAN	Casein kinase II subunit beta
CSKP_HUMAN	Peripheral plasma membrane protein CASK
CSN1_HUMAN	COP9 signalosome complex subunit 1
CSN2_HUMAN	COP9 signalosome complex subunit 2

CSN3_HUMAN	COP9 signalosome complex subunit 3
CSN4_HUMAN	COP9 signalosome complex subunit 4
CSN5_HUMAN	COP9 signalosome complex subunit 5
CSN8_HUMAN	COP9 signalosome complex subunit 8
CSPG2_HUMAN	Versican core protein
CSPG4_HUMAN	Chondroitin sulfate proteoglycan 4
CTCFL_HUMAN	Transcriptional repressor CTCFL
CTL1_HUMAN	Choline transporter-like protein 1
CTL2_HUMAN	Choline transporter-like protein 2
CTNA1_HUMAN	Catenin alpha-1
CTNA2_HUMAN	Catenin alpha-2
CTNB1_HUMAN	Catenin beta-1
CTND2_HUMAN	Catenin delta-2
CTRO_HUMAN	Citron Rho-interacting kinase
CUL1_HUMAN	Cullin-1
CXA1_HUMAN	Gap junction alpha-1 protein
CY1_HUMAN	Cytochrome c1, heme protein, mitochondrial
CY24A_HUMAN	Cytochrome b-245 light chain
CYB5B_HUMAN	Cytochrome b5 type B
CYBR1_HUMAN	Cytochrome b reductase 1
CYFP1_HUMAN	Cytoplasmic FMR1-interacting protein 1
CYFP2_HUMAN	Cytoplasmic FMR1-interacting protein 2
CYRIB_HUMAN	CYFIP-related Rac1 interactor B
CYTA_HUMAN	Cystatin-A
D19L3_HUMAN	Probable C-mannosyltransferase DPY19L3
DC1I1_HUMAN	Cytoplasmic dynein 1 intermediate chain 1
DC1I2_HUMAN	Cytoplasmic dynein 1 intermediate chain 2
DC1L2_HUMAN	Cytoplasmic dynein 1 light intermediate chain 2
DCD_HUMAN	Dermcidin
DCOR_HUMAN	Ornithine decarboxylase
DCTN1_HUMAN	Dynactin subunit 1
DCTN2_HUMAN	Dynactin subunit 2
DDAH1_HUMAN	N(G),N(G)-dimethylarginine dimethylaminohydrolase 1
DDAH2_HUMAN	N(G),N(G)-dimethylarginine dimethylaminohydrolase 2
DDB1_HUMAN	DNA damage-binding protein 1
DDX60_HUMAN	Probable ATP-dependent RNA helicase DDX60
DEAF1_HUMAN	Deformed epidermal autoregulatory factor 1 homolog
DESM_HUMAN	Desmin
DESP_HUMAN	Desmoplakin
DGKQ_HUMAN	Diacylglycerol kinase theta
DHB11_HUMAN	Estradiol 17-beta-dehydrogenase 11

DHB12_HUMAN	Very-long-chain 3-oxoacyl-CoA reductase
DHB4_HUMAN	Peroxisomal multifunctional enzyme type 2
DHE3_HUMAN	Glutamate dehydrogenase 1, mitochondrial
DHPR_HUMAN	Dihydropteridine reductase
DHX29_HUMAN	ATP-dependent RNA helicase DHX29
DHX30_HUMAN	ATP-dependent RNA helicase DHX30
DJB11_HUMAN	DnaJ homolog subfamily B member 11
DJB13_HUMAN	DnaJ homolog subfamily B member 13
DJB14_HUMAN	DnaJ homolog subfamily B member 14
DJC10_HUMAN	DnaJ homolog subfamily C member 10
DLDH_HUMAN	Dihydrolipoyl dehydrogenase, mitochondrial
DNJ5B_HUMAN	DnaJ homolog subfamily C member 5B
DNJA2_HUMAN	DnaJ homolog subfamily A member 2
DNM1L_HUMAN	Dynamin-1-like protein
DNPEP_HUMAN	Aspartyl aminopeptidase
DNSL1_HUMAN	Deoxyribonuclease-1-like 1
DOCK5_HUMAN	Dedicator of cytokinesis protein 5
DPB1_HUMAN	HLA class II histocompatibility antigen, DP beta 1 chain
DPM1_HUMAN	Dolichol-phosphate mannosyltransferase subunit 1
DPOLB_HUMAN	DNA polymerase beta
DPYL2_HUMAN	Dihydropyrimidinase-related protein 2
DPYL3_HUMAN	Dihydropyrimidinase-related protein 3
DPYL5_HUMAN	Dihydropyrimidinase-related protein 5
DRC6_HUMAN	Dynein regulatory complex subunit 6
DSC1_HUMAN	Desmocollin-1
DYH2_HUMAN	Dynein heavy chain 2, axonemal
DYH5_HUMAN	Dynein heavy chain 5, axonemal
DYH9_HUMAN	Dynein heavy chain 9, axonemal
DYHC1_HUMAN	Cytoplasmic dynein 1 heavy chain 1
DYN1_HUMAN	Dynamin-1
E41L2_HUMAN	Band 4.1-like protein 2
E41LA_HUMAN	Band 4.1-like protein 4A
EAA1_HUMAN	Excitatory amino acid transporter 1
EAA2_HUMAN	Excitatory amino acid transporter 2
ECH1_HUMAN	Delta(3,5)-Delta(2,4)-dienoyl-CoA isomerase, mitochondrial
ECHA_HUMAN	Trifunctional enzyme subunit alpha, mitochondrial
ECHB_HUMAN	Trifunctional enzyme subunit beta, mitochondrial
ECI1_HUMAN	Enoyl-CoA delta isomerase 1, mitochondrial
EDIL3_HUMAN	EGF-like repeat and discoidin I-like domain-containing protein 3
EEA1_HUMAN	Early endosome antigen 1
EF1A1_HUMAN	Elongation factor 1-alpha 1

EF1B_HUMAN	Elongation factor 1-beta
EF1D_HUMAN	Elongation factor 1-delta
EF1G_HUMAN	Elongation factor 1-gamma
EF2_HUMAN	Elongation factor 2
EGFR_HUMAN	Epidermal growth factor receptor
EID2_HUMAN	EP300-interacting inhibitor of differentiation 2
EIF3A_HUMAN	Eukaryotic translation initiation factor 3 subunit A
EIF3B_HUMAN	Eukaryotic translation initiation factor 3 subunit B
EIF3E_HUMAN	Eukaryotic translation initiation factor 3 subunit E
EIF3F_HUMAN	Eukaryotic translation initiation factor 3 subunit F
EIF3I_HUMAN	Eukaryotic translation initiation factor 3 subunit I
EIF3L_HUMAN	Eukaryotic translation initiation factor 3 subunit L
EIF3M_HUMAN	Eukaryotic translation initiation factor 3 subunit M
EIFCL_HUMAN	Eukaryotic translation initiation factor 3 subunit C-like protein
ELMO2_HUMAN	Engulfment and cell motility protein 2
ELNE_HUMAN	Neutrophil elastase
EM55_HUMAN	55 kDa erythrocyte membrane protein
EMARD_HUMAN	Endoplasmic reticulum membrane-associated RNA degradation protein
EMC1_HUMAN	ER membrane protein complex subunit 1
EMC2_HUMAN	ER membrane protein complex subunit 2
EMC3_HUMAN	ER membrane protein complex subunit 3
EMC4_HUMAN	ER membrane protein complex subunit 4
EMC7_HUMAN	ER membrane protein complex subunit 7
EMP3_HUMAN	Epithelial membrane protein 3
ENDD1_HUMAN	Endonuclease domain-containing 1 protein
ENOA_HUMAN	Alpha-enolase
ENOG_HUMAN	Gamma-enolase
ENPL_HUMAN	Endoplasmin
ENPP6_HUMAN	Glycerophosphocholine cholinephosphodiesterase ENPP6
ENTP2_HUMAN	Ectonucleoside triphosphate diphosphohydrolase 2
EPB41_HUMAN	Protein 4.1
EPB42_HUMAN	Protein 4.2
EPDR1_HUMAN	Mammalian ependymin-related protein 1
EPHA1_HUMAN	Ephrin type-A receptor 1
EPM2A_HUMAN	Laforin
ERAP1_HUMAN	Endoplasmic reticulum aminopeptidase 1
ERC2_HUMAN	ERC protein 2
ERLEC_HUMAN	Endoplasmic reticulum lectin 1
ERLN2_HUMAN	Erlin-2
ERO1A_HUMAN	ERO1-like protein alpha
ERP29_HUMAN	Endoplasmic reticulum resident protein 29

ES8L3_HUMAN	Epidermal growth factor receptor kinase substrate 8-like protein 3
ESYT1_HUMAN	Extended synaptotagmin-1
ETFA_HUMAN	Electron transfer flavoprotein subunit alpha, mitochondrial
EZRI_HUMAN	Ezrin
F10A1_HUMAN	Hsc70-interacting protein
F13A_HUMAN	Coagulation factor XIII A chain
FA5_HUMAN	Coagulation factor V
FABP7_HUMAN	Fatty acid-binding protein, brain
FACE1_HUMAN	CAAX prenyl protease 1 homolog
FAM3C_HUMAN	Protein FAM3C
FARP1_HUMAN	FERM, ARHGEF and pleckstrin domain-containing protein 1
FAS_HUMAN	Fatty acid synthase
FBLN1_HUMAN	Fibulin-1
FBX2_HUMAN	F-box only protein 2
FBXL7_HUMAN	F-box/LRR-repeat protein 7
FCGBP_HUMAN	IgGFc-binding protein
FCGRN_HUMAN	IgG receptor FcRn large subunit p51
FERM2_HUMAN	Fermitin family homolog 2
FETA_HUMAN	Alpha-fetoprotein
FGF1_HUMAN	Fibroblast growth factor 1
FGFR3_HUMAN	Fibroblast growth factor receptor 3
FHL1_HUMAN	Four and a half LIM domains protein 1
FIBA_HUMAN	Fibrinogen alpha chain
FIBB_HUMAN	Fibrinogen beta chain
FIBG_HUMAN	Fibrinogen gamma chain
FILA2_HUMAN	Filaggrin-2
FINC_HUMAN	Fibronectin
FKB10_HUMAN	Peptidyl-prolyl cis-trans isomerase FKBP10
FKBP2_HUMAN	Peptidyl-prolyl cis-trans isomerase FKBP2
FKBP8_HUMAN	Peptidyl-prolyl cis-trans isomerase FKBP8
FLNA_HUMAN	Filamin-A
FLNB_HUMAN	Filamin-B
FLNC_HUMAN	Filamin-C
FLOT1_HUMAN	Flotillin-1
FLOT2_HUMAN	Flotillin-2
FN3K_HUMAN	Fructosamine-3-kinase
FND3A_HUMAN	Fibronectin type-III domain-containing protein 3A
FNTA_HUMAN	Protein farnesyltransferase/geranylgeranyltransferase type-1 subunit alpha
FP100_HUMAN	Fanconi anemia core complex-associated protein 100
FPRP_HUMAN	Prostaglandin F2 receptor negative regulator
FR1L4_HUMAN	Fer-1-like protein 4

FRIH_HUMAN	Ferritin heavy chain
FRIL_HUMAN	Ferritin light chain
FRY_HUMAN	Protein furry homolog
FRYL_HUMAN	Protein furry homolog-like
FS2P1_HUMAN	Putative fatty acid desaturase 2-like protein FADS2B
FSCN1_HUMAN	Fascin
FUMH_HUMAN	Fumarate hydratase, mitochondrial
FXR1_HUMAN	Fragile X mental retardation syndrome-related protein 1
FXYD6_HUMAN	FXYD domain-containing ion transport regulator 6
G37L1_HUMAN	G-protein coupled receptor 37-like 1
G3P_HUMAN	Glyceraldehyde-3-phosphate dehydrogenase
G6PE_HUMAN	GDH/6PGL endoplasmic bifunctional protein
G6PI_HUMAN	Glucose-6-phosphate isomerase
GABT_HUMAN	4-aminobutyrate aminotransferase, mitochondrial
GALT8_HUMAN	Probable polypeptide N-acetylgalactosaminyltransferase 8
GANAB_HUMAN	Neutral alpha-glucosidase AB
GAPR1_HUMAN	Golgi-associated plant pathogenesis-related protein 1
GBB1_HUMAN	Guanine nucleotide-binding protein G(I)/G(S)/G(T) subunit beta-1
GBG12_HUMAN	Guanine nucleotide-binding protein G(I)/G(S)/G(O) subunit gamma-12
GCC2_HUMAN	GRIP and coiled-coil domain-containing protein 2
GCN1_HUMAN	eIF-2-alpha kinase activator GCN1
GCP6_HUMAN	Gamma-tubulin complex component 6
GDIA_HUMAN	Rab GDP dissociation inhibitor alpha
GDIB_HUMAN	Rab GDP dissociation inhibitor beta
GDIR1_HUMAN	Rho GDP-dissociation inhibitor 1
GELS_HUMAN	Gelsolin
GFAP_HUMAN	Glial fibrillary acidic protein
GG6L1_HUMAN	Golgin subfamily A member 6-like protein 1
GGA2_HUMAN	ADP-ribosylation factor-binding protein GGA2
GGT5_HUMAN	Glutathione hydrolase 5 proenzyme
GLE1_HUMAN	Nucleoporin GLE1
GLNA_HUMAN	Glutamine synthetase
GLOD4_HUMAN	Glyoxalase domain-containing protein 4
GLPA_HUMAN	Glycophorin-A
GLPC_HUMAN	Glycophorin-C
GLPK_HUMAN	Glycerol kinase
GLU2B_HUMAN	Glucosidase 2 subunit beta
GLYM_HUMAN	Serine hydroxymethyltransferase, mitochondrial
GMDS_HUMAN	GDP-mannose 4,6 dehydratase
GNA11_HUMAN	Guanine nucleotide-binding protein subunit alpha-11
GNA13_HUMAN	Guanine nucleotide-binding protein subunit alpha-13

GNAI1_HUMAN	Guanine nucleotide-binding protein G(i) subunit alpha-1
GNAI2_HUMAN	Guanine nucleotide-binding protein G(i) subunit alpha-2
GNAI3_HUMAN	Guanine nucleotide-binding protein G(i) subunit alpha-3
GNAO_HUMAN	Guanine nucleotide-binding protein G(o) subunit alpha
GNAQ_HUMAN	Guanine nucleotide-binding protein G(q) subunit alpha
GNAS1_HUMAN	Guanine nucleotide-binding protein G(s) subunit alpha isoforms XLas
GNPI1_HUMAN	Glucosamine-6-phosphate isomerase 1
GOGA4_HUMAN	Golgin subfamily A member 4
GOLI4_HUMAN	Golgi integral membrane protein 4
GOT1B_HUMAN	Vesicle transport protein GOT1B
GP143_HUMAN	G-protein coupled receptor 143
GP1BA_HUMAN	Platelet glycoprotein Ib alpha chain
GPC1_HUMAN	Glypican-1
GPC3_HUMAN	Glypican-3
GPC5B_HUMAN	G-protein coupled receptor family C group 5 member B
GPDM_HUMAN	Glycerol-3-phosphate dehydrogenase, mitochondrial
GPM6A_HUMAN	Neuronal membrane glycoprotein M6-a
GPM6B_HUMAN	Neuronal membrane glycoprotein M6-b
GPNMB_HUMAN	Transmembrane glycoprotein NMB
GRAN_HUMAN	Grancalcin
GRHPR_HUMAN	Glyoxylate reductase/hydroxypyruvate reductase
GRP75_HUMAN	Stress-70 protein, mitochondrial
GSHB_HUMAN	Glutathione synthetase
GSHR_HUMAN	Glutathione reductase, mitochondrial
GSLG1_HUMAN	Golgi apparatus protein 1
GSTM3_HUMAN	Glutathione S-transferase Mu 3
GSTP1_HUMAN	Glutathione S-transferase P
GTPBA_HUMAN	GTP-binding protein 10
GTR1_HUMAN	Solute carrier family 2, facilitated glucose transporter member 1
GTR10_HUMAN	Solute carrier family 2, facilitated glucose transporter member 10
GTR14_HUMAN	Solute carrier family 2, facilitated glucose transporter member 14
GTR3_HUMAN	Solute carrier family 2, facilitated glucose transporter member 3
GTR5_HUMAN	Solute carrier family 2, facilitated glucose transporter member 5
GUAD_HUMAN	Guanine deaminase
GYS1_HUMAN	Glycogen [starch] synthase, muscle
H12_HUMAN	Histone H1.2
H15_HUMAN	Histone H1.5
H2A1B_HUMAN	Histone H2A type 1-B/E
H2A2A_HUMAN	Histone H2A type 2-A
H2AY_HUMAN	Core histone macro-H2A.1
H2B1A_HUMAN	Histone H2B type 1-A

H2B1B_HUMAN	Histone H2B type 1-B
H31_HUMAN	Histone H3.1
H31T_HUMAN	Histone H3.1t
H4_HUMAN	Histone H4
H90B2_HUMAN	Putative heat shock protein HSP 90-beta 2
HACD3_HUMAN	Very-long-chain (3R)-3-hydroxyacyl-CoA dehydratase 3
HACL2_HUMAN	2-hydroxyacyl-CoA lyase 2
HARS1_HUMAN	Histidine--tRNA ligase, cytoplasmic
HBA_HUMAN	Hemoglobin subunit alpha
HBB_HUMAN	Hemoglobin subunit beta
HBD_HUMAN	Hemoglobin subunit delta
HBG1_HUMAN	Hemoglobin subunit gamma-1
HCDH_HUMAN	Hydroxyacyl-coenzyme A dehydrogenase, mitochondrial
HDHD2_HUMAN	Haloacid dehalogenase-like hydrolase domain-containing protein 2
HEBP1_HUMAN	Heme-binding protein 1
HECAM_HUMAN	Hepatocyte cell adhesion molecule
HECD3_HUMAN	E3 ubiquitin-protein ligase HECTD3
HELZ_HUMAN	Probable helicase with zinc finger domain
HEM2_HUMAN	Delta-aminolevulinic acid dehydratase
HEMO_HUMAN	Hemopexin
HEP2_HUMAN	Heparin cofactor 2
HERC2_HUMAN	E3 ubiquitin-protein ligase HERC2
HLAA_HUMAN	HLA class I histocompatibility antigen, A alpha chain
HLAB_HUMAN	HLA class I histocompatibility antigen, B alpha chain
HLAC_HUMAN	HLA class I histocompatibility antigen, C alpha chain
HM13_HUMAN	Minor histocompatibility antigen H13
HMCES_HUMAN	Abasic site processing protein HMCES
HMGB1_HUMAN	High mobility group protein B1
HMOX2_HUMAN	Heme oxygenase 2
HNRPC_HUMAN	Heterogeneous nuclear ribonucleoproteins C1/C2
HNRPD_HUMAN	Heterogeneous nuclear ribonucleoprotein D0
HNRPQ_HUMAN	Heterogeneous nuclear ribonucleoprotein Q
HNRPR_HUMAN	Heterogeneous nuclear ribonucleoprotein R
HORN_HUMAN	Hornerin
HPLN1_HUMAN	Hyaluronan and proteoglycan link protein 1
HPLN2_HUMAN	Hyaluronan and proteoglycan link protein 2
HPRT_HUMAN	Hypoxanthine-guanine phosphoribosyltransferase
HPT_HUMAN	Haptoglobin
HPTR_HUMAN	Haptoglobin-related protein
HRG_HUMAN	Histidine-rich glycoprotein
HS105_HUMAN	Heat shock protein 105 kDa

HS12A_HUMAN	Heat shock 70 kDa protein 12A
HS2ST_HUMAN	Heparan sulfate 2-O-sulfotransferase 1
HS71A_HUMAN	Heat shock 70 kDa protein 1A
HS90A_HUMAN	Heat shock protein HSP 90-alpha
HS90B_HUMAN	Heat shock protein HSP 90-beta
HSP13_HUMAN	Heat shock 70 kDa protein 13
HSP72_HUMAN	Heat shock-related 70 kDa protein 2
HSP74_HUMAN	Heat shock 70 kDa protein 4
HSP7C_HUMAN	Heat shock cognate 71 kDa protein
HSPB1_HUMAN	Heat shock protein beta-1
HTRA1_HUMAN	Serine protease HTRA1
HV315_HUMAN	Immunoglobulin heavy variable 3-15
HV323_HUMAN	Immunoglobulin heavy variable 3-23
HV374_HUMAN	Immunoglobulin heavy variable 3-74
HV601_HUMAN	Immunoglobulin heavy variable 6-1
HXK1_HUMAN	Hexokinase-1
HYAS1_HUMAN	Hyaluronan synthase 1
HYEP_HUMAN	Epoxide hydrolase 1
HYOU1_HUMAN	Hypoxia up-regulated protein 1
IC1_HUMAN	Plasma protease C1 inhibitor
ICAM1_HUMAN	Intercellular adhesion molecule 1
IDHC_HUMAN	Isocitrate dehydrogenase [NADP] cytoplasmic
IF172_HUMAN	Intraflagellar transport protein 172 homolog
IF2A_HUMAN	Eukaryotic translation initiation factor 2 subunit 1
IF2B3_HUMAN	Insulin-like growth factor 2 mRNA-binding protein 3
IF4A2_HUMAN	Eukaryotic initiation factor 4A-II
IFIT2_HUMAN	Interferon-induced protein with tetratricopeptide repeats 2
IFT74_HUMAN	Intraflagellar transport protein 74 homolog
IGA2_HUMAN	Immunoglobulin alpha-2 heavy chain
IGG1_HUMAN	Immunoglobulin gamma-1 heavy chain
IGHA1_HUMAN	Immunoglobulin heavy constant alpha 1
IGHG2_HUMAN	Immunoglobulin heavy constant gamma 2
IGHG3_HUMAN	Immunoglobulin heavy constant gamma 3
IGHG4_HUMAN	Immunoglobulin heavy constant gamma 4
IGHM_HUMAN	Immunoglobulin heavy constant mu
IGJ_HUMAN	Immunoglobulin J chain
IGKC_HUMAN	Immunoglobulin kappa constant
IGL1_HUMAN	Immunoglobulin lambda-1 light chain
IGLC2_HUMAN	Immunoglobulin lambda constant 2
IGSF3_HUMAN	Immunoglobulin superfamily member 3
IGSF8_HUMAN	Immunoglobulin superfamily member 8

IKBL1_HUMAN	NF-kappa-B inhibitor-like protein 1
ILEU_HUMAN	Leukocyte elastase inhibitor
ILF2_HUMAN	Interleukin enhancer-binding factor 2
IMB1_HUMAN	Importin subunit beta-1
INADL_HUMAN	InaD-like protein
INF2_HUMAN	Inverted formin-2
INT4_HUMAN	Integrator complex subunit 4
IQCM_HUMAN	IQ domain-containing protein M
IQCN_HUMAN	IQ domain-containing protein N
IQGA1_HUMAN	Ras GTPase-activating-like protein IQGAP1
ITA2_HUMAN	Integrin alpha-2
ITA2B_HUMAN	Integrin alpha-IIb
ITA3_HUMAN	Integrin alpha-3
ITA6_HUMAN	Integrin alpha-6
ITA7_HUMAN	Integrin alpha-7
ITAM_HUMAN	Integrin alpha-M
ITAV_HUMAN	Integrin alpha-V
ITB1_HUMAN	Integrin beta-1
ITB2_HUMAN	Integrin beta-2
ITB3_HUMAN	Integrin beta-3
ITB4_HUMAN	Integrin beta-4
ITB8_HUMAN	Integrin beta-8
ITCH_HUMAN	E3 ubiquitin-protein ligase Itchy homolog
ITIH1_HUMAN	Inter-alpha-trypsin inhibitor heavy chain H1
ITIH2_HUMAN	Inter-alpha-trypsin inhibitor heavy chain H2
ITIH3_HUMAN	Inter-alpha-trypsin inhibitor heavy chain H3
ITIH4_HUMAN	Inter-alpha-trypsin inhibitor heavy chain H4
IWS1_HUMAN	Protein IWS1 homolog
IZUM1_HUMAN	Izumo sperm-egg fusion protein 1
JAK1_HUMAN	Tyrosine-protein kinase JAK1
JAM2_HUMAN	Junctional adhesion molecule B
JPH3_HUMAN	Junctophilin-3
KAD1_HUMAN	Adenylate kinase isoenzyme 1
KAP2_HUMAN	cAMP-dependent protein kinase type II-alpha regulatory subunit
KAP3_HUMAN	cAMP-dependent protein kinase type II-beta regulatory subunit
KCC2A_HUMAN	Calcium/calmodulin-dependent protein kinase type II subunit alpha
KCC2D_HUMAN	Calcium/calmodulin-dependent protein kinase type II subunit delta
KCD12_HUMAN	BTB/POZ domain-containing protein KCTD12
KCRB_HUMAN	Creatine kinase B-type
KIF19_HUMAN	Kinesin-like protein KIF19
KLD7A_HUMAN	Kelch domain-containing protein 7A

KNG1_HUMAN	Kininogen-1
KPBB_HUMAN	Phosphorylase b kinase regulatory subunit beta
KPCA_HUMAN	Protein kinase C alpha type
KPYM_HUMAN	Pyruvate kinase PKM
KTN1_HUMAN	Kinectin
KV108_HUMAN	Immunoglobulin kappa variable 1-8
KV401_HUMAN	Immunoglobulin kappa variable 4-1
KVD20_HUMAN	Immunoglobulin kappa variable 3D-20
KVD28_HUMAN	Immunoglobulin kappa variable 2D-28
LAMA2_HUMAN	Laminin subunit alpha-2
LAMA4_HUMAN	Laminin subunit alpha-4
LAMB1_HUMAN	Laminin subunit beta-1
LAMB2_HUMAN	Laminin subunit beta-2
LAMC1_HUMAN	Laminin subunit gamma-1
LAMP1_HUMAN	Lysosome-associated membrane glycoprotein 1
LAMP2_HUMAN	Lysosome-associated membrane glycoprotein 2
LDHA_HUMAN	L-lactate dehydrogenase A chain
LDHB_HUMAN	L-lactate dehydrogenase B chain
LEG1_HUMAN	Galectin-1
LEG3_HUMAN	Galectin-3
LEG8_HUMAN	Galectin-8
LEMD2_HUMAN	LEM domain-containing protein 2
LFG3_HUMAN	Protein lifeguard 3
LG3BP_HUMAN	Galectin-3-binding protein
LHPP_HUMAN	Phospholysine phosphohistidine inorganic pyrophosphate phosphatase
LITD1_HUMAN	LINE-1 type transposase domain-containing protein 1
LMAN1_HUMAN	Protein ERGIC-53
LMAN2_HUMAN	Vesicular integral-membrane protein VIP36
LMNA_HUMAN	Prelamin-A/C
LMNB1_HUMAN	Lamin-B1
LMNB2_HUMAN	Lamin-B2
LNP_HUMAN	Endoplasmic reticulum junction formation protein lunapark
LORF2_HUMAN	LINE-1 retrotransposable element ORF2 protein
LOX12_HUMAN	Polyunsaturated fatty acid lipoxygenase ALOX12
LRC41_HUMAN	Leucine-rich repeat-containing protein 41
LRP1_HUMAN	Prolow-density lipoprotein receptor-related protein 1
LRRD1_HUMAN	Leucine-rich repeat and death domain-containing protein 1
LRRF1_HUMAN	Leucine-rich repeat flightless-interacting protein 1
LSAMP_HUMAN	Limbic system-associated membrane protein
LSS_HUMAN	Lanosterol synthase
LV316_HUMAN	Immunoglobulin lambda variable 3-16

LV39_HUMAN	Immunoglobulin lambda variable 3-9
LYOX_HUMAN	Protein-lysine 6-oxidase
M2OM_HUMAN	Mitochondrial 2-oxoglutarate/malate carrier protein
MA7D1_HUMAN	MAP7 domain-containing protein 1
MACF1_HUMAN	Microtubule-actin cross-linking factor 1, isoforms 1/2/3/5
MAG_HUMAN	Myelin-associated glycoprotein
MALD2_HUMAN	MARVEL domain-containing protein 2
MAOM_HUMAN	NAD-dependent malic enzyme, mitochondrial
MAOX_HUMAN	NADP-dependent malic enzyme
MAP1A_HUMAN	Microtubule-associated protein 1A
MAP1B_HUMAN	Microtubule-associated protein 1B
MAP4_HUMAN	Microtubule-associated protein 4
MARCS_HUMAN	Myristoylated alanine-rich C-kinase substrate
MBP_HUMAN	Myelin basic protein
MCAT_HUMAN	Mitochondrial carnitine/acylcarnitine carrier protein
MCM10_HUMAN	Protein MCM10 homolog
MDHC_HUMAN	Malate dehydrogenase, cytoplasmic
MDHM_HUMAN	Malate dehydrogenase, mitochondrial
MDN1_HUMAN	Midasin
MED23_HUMAN	Mediator of RNA polymerase II transcription subunit 23
MESD_HUMAN	LRP chaperone MESD
MEST_HUMAN	Mesoderm-specific transcript homolog protein
MET25_HUMAN	Methyltransferase-like protein 25
MET7A_HUMAN	Methyltransferase-like protein 7A
MET7B_HUMAN	Methyltransferase-like protein 7B
MFGM_HUMAN	Lactadherin
MFRP_HUMAN	Membrane frizzled-related protein
MFS10_HUMAN	Major facilitator superfamily domain-containing protein 10
MGAP_HUMAN	MAX gene-associated protein
MGLL_HUMAN	Monoglyceride lipase
MGST1_HUMAN	Microsomal glutathione S-transferase 1
MGST2_HUMAN	Microsomal glutathione S-transferase 2
MIC60_HUMAN	MICOS complex subunit MIC60
MIF_HUMAN	Macrophage migration inhibitory factor
MISP_HUMAN	Mitotic interactor and substrate of PLK1
MKS1_HUMAN	Meckel syndrome type 1 protein
ML12A_HUMAN	Myosin regulatory light chain 12A
MLC1_HUMAN	Membrane protein MLC1
MLEC_HUMAN	Malectin
MLP3A_HUMAN	Microtubule-associated proteins 1A/1B light chain 3A
MMP2_HUMAN	72 kDa type IV collagenase

MNAR1_HUMAN	Major intrinsically disordered Notch2-binding receptor 1
MO4L2_HUMAN	Mortality factor 4-like protein 2
MOES_HUMAN	Moesin
MOGS_HUMAN	Mannosyl-oligosaccharide glucosidase
MORC1_HUMAN	MORC family CW-type zinc finger protein 1
MOT1_HUMAN	Monocarboxylate transporter 1
MOT8_HUMAN	Monocarboxylate transporter 8
MOXD1_HUMAN	DBH-like monooxygenase protein 1
MPCP_HUMAN	Phosphate carrier protein, mitochondrial
MPRD_HUMAN	Cation-dependent mannose-6-phosphate receptor
MPU1_HUMAN	Mannose-P-dolichol utilization defect 1 protein
MRCKA_HUMAN	Serine/threonine-protein kinase MRCK alpha
MRGX2_HUMAN	Mas-related G-protein coupled receptor member X2
MRM1_HUMAN	rRNA methyltransferase 1, mitochondrial
MRP_HUMAN	MARCKS-related protein
MRP2_HUMAN	Canalicular multispecific organic anion transporter 1
MTAP2_HUMAN	Microtubule-associated protein 2
MTCH2_HUMAN	Mitochondrial carrier homolog 2
MTMR7_HUMAN	Myotubularin-related protein 7
MTMR9_HUMAN	Myotubularin-related protein 9
MUC18_HUMAN	Cell surface glycoprotein MUC18
MVP_HUMAN	Major vault protein
MXRA7_HUMAN	Matrix-remodeling-associated protein 7
MYADM_HUMAN	Myeloid-associated differentiation marker
MYCN_HUMAN	N-myc proto-oncogene protein
MYDGF_HUMAN	Myeloid-derived growth factor
MYH10_HUMAN	Myosin-10
MYH9_HUMAN	Myosin-9
MYL1_HUMAN	Myosin light chain 1/3, skeletal muscle isoform
MYL6_HUMAN	Myosin light polypeptide 6
MYL6B_HUMAN	Myosin light chain 6B
MYO1F_HUMAN	Unconventional myosin-If
MYO5C_HUMAN	Unconventional myosin-Vc
MYO6_HUMAN	Unconventional myosin-VI
MYOM3_HUMAN	Myomesin-3
MYP2_HUMAN	Myelin P2 protein
MYPR_HUMAN	Myelin proteolipid protein
NAGK_HUMAN	N-acetyl-D-glucosamine kinase
NAMPT_HUMAN	Nicotinamide phosphoribosyltransferase
NB5R3_HUMAN	NADH-cytochrome b5 reductase 3
NBPFA_HUMAN	Neuroblastoma breakpoint family member 10

NCAM1_HUMAN	Neural cell adhesion molecule 1
NCAM2_HUMAN	Neural cell adhesion molecule 2
NCAN_HUMAN	Neurocan core protein
NCEH1_HUMAN	Neutral cholesterol ester hydrolase 1
NCHL1_HUMAN	Neural cell adhesion molecule L1-like protein
NCPR_HUMAN	NADPH--cytochrome P450 reductase
NDKA_HUMAN	Nucleoside diphosphate kinase A
NDRG1_HUMAN	Protein NDRG1
NDRG2_HUMAN	Protein NDRG2
NDRG4_HUMAN	Protein NDRG4
NDUBA_HUMAN	NADH dehydrogenase [ubiquinone] 1 beta subcomplex subunit 10
NDUBB_HUMAN	NADH dehydrogenase [ubiquinone] 1 beta subcomplex subunit 11, mitochondrial
NDUS1_HUMAN	NADH-ubiquinone oxidoreductase 75 kDa subunit, mitochondrial
NDUS3_HUMAN	NADH dehydrogenase [ubiquinone] iron-sulfur protein 3, mitochondrial
NDUV2_HUMAN	NADH dehydrogenase [ubiquinone] flavoprotein 2, mitochondrial
NEBU_HUMAN	Nebulin
NEK10_HUMAN	Serine/threonine-protein kinase Nek10
NENF_HUMAN	Neudesin
NEST_HUMAN	Nestin
NEUL4_HUMAN	Neuralized-like protein 4
NEUM_HUMAN	Neuromodulin
NFASC_HUMAN	Neurofascin
NFH_HUMAN	Neurofilament heavy polypeptide
NFL_HUMAN	Neurofilament light polypeptide
NFM_HUMAN	Neurofilament medium polypeptide
NHRF1_HUMAN	Na(+)/H(+) exchange regulatory cofactor NHE-RF1
NHSL2_HUMAN	NHS-like protein 2
NICA_HUMAN	Nicastrin
NID1_HUMAN	Nidogen-1
NID2_HUMAN	Nidogen-2
NINL_HUMAN	Ninein-like protein
NIPS1_HUMAN	Protein NipSnap homolog 1
NIPS2_HUMAN	Protein NipSnap homolog 2
NLRP6_HUMAN	NACHT, LRR and PYD domains-containing protein 6
NNRD_HUMAN	ATP-dependent (S)-NAD(P)H-hydrate dehydratase
NNRE_HUMAN	NAD(P)H-hydrate epimerase
NNTM_HUMAN	NAD(P) transhydrogenase, mitochondrial
NOMO1_HUMAN	Nodal modulator 1
NOTC3_HUMAN	Neurogenic locus notch homolog protein 3
NP1L1_HUMAN	Nucleosome assembly protein 1-like 1
NP1L4_HUMAN	Nucleosome assembly protein 1-like 4

NPM_HUMAN	Nucleophosmin
NPTN_HUMAN	Neuroplastin
NPTX1_HUMAN	Neuronal pentraxin-1
NRCAM_HUMAN	Neuronal cell adhesion molecule
NRSN1_HUMAN	Neurensin-1
NRX3A_HUMAN	Neurexin-3
NSUN4_HUMAN	5-methylcytosine rRNA methyltransferase NSUN4
NUCB1_HUMAN	Nucleobindin-1
NUCL_HUMAN	Nucleolin
NUMA1_HUMAN	Nuclear mitotic apparatus protein 1
NUP54_HUMAN	Nucleoporin p54
ODAD1_HUMAN	Outer dynein arm-docking complex subunit 1
ODO2_HUMAN	Dihydrolipoyllysine-residue succinyltransferase component of 2-oxoglutarate dehydrogenase complex, mitochondrial
OFD1_HUMAN	Oral-facial-digital syndrome 1 protein
OFUT1_HUMAN	GDP-fucose protein O-fucosyltransferase 1
OLA1_HUMAN	Obg-like ATPase 1
OMGP_HUMAN	Oligodendrocyte-myelin glycoprotein
OPCM_HUMAN	Opioid-binding protein/cell adhesion molecule
OR1K1_HUMAN	Olfactory receptor 1K1
OR1M1_HUMAN	Olfactory receptor 1M1
OR8H2_HUMAN	Olfactory receptor 8H2
ORC6_HUMAN	Origin recognition complex subunit 6
OST48_HUMAN	Dolichyl-diphosphooligosaccharide--protein glycosyltransferase 48 kDa subunit
OSTP_HUMAN	Osteopontin
P20D1_HUMAN	N-fatty-acyl-amino acid synthase/hydrolase PM20D1
P2Y12_HUMAN	P2Y purinoceptor 12
P4HA1_HUMAN	Prolyl 4-hydroxylase subunit alpha-1
PA1B2_HUMAN	Platelet-activating factor acetylhydrolase IB subunit alpha2
PA1B3_HUMAN	Platelet-activating factor acetylhydrolase IB subunit alpha1
PABP1_HUMAN	Polyadenylate-binding protein 1
PABP4_HUMAN	Polyadenylate-binding protein 4
PACN1_HUMAN	Protein kinase C and casein kinase substrate in neurons protein 1
PACR_HUMAN	Pituitary adenylate cyclase-activating polypeptide type I receptor1
PADI2_HUMAN	Protein-arginine deiminase type-2
PAI1_HUMAN	Plasminogen activator inhibitor 1
PALB2_HUMAN	Partner and localizer of BRCA2
PAPOG_HUMAN	Poly(A) polymerase gamma
PAR14_HUMAN	Protein mono-ADP-ribosyltransferase PARP14
PAR6G_HUMAN	Partitioning defective 6 homolog gamma
PARK7_HUMAN	Parkinson disease protein 7
PARP1_HUMAN	Poly [ADP-ribose] polymerase 1

PAX5_HUMAN	Paired box protein Pax-5
PCLO_HUMAN	Protein piccolo
PCNT_HUMAN	Pericentrin
PCOC1_HUMAN	Procollagen C-endopeptidase enhancer 1
PCP_HUMAN	Lysosomal Pro-X carboxypeptidase
PCYOX_HUMAN	Prenylcysteine oxidase 1
PCYXL_HUMAN	Prenylcysteine oxidase-like
PDCD6_HUMAN	Programmed cell death protein 6
PDE4D_HUMAN	cAMP-specific 3',5'-cyclic phosphodiesterase 4D
PDE6C_HUMAN	Cone cGMP-specific 3',5'-cyclic phosphodiesterase subunit alpha'
PDIA1_HUMAN	Protein disulfide-isomerase
PDIA3_HUMAN	Protein disulfide-isomerase A3
PDIA4_HUMAN	Protein disulfide-isomerase A4
PDIA6_HUMAN	Protein disulfide-isomerase A6
PDLI3_HUMAN	PDZ and LIM domain protein 3
PDXK_HUMAN	Pyridoxal kinase
PEBP1_HUMAN	Phosphatidylethanolamine-binding protein 1
PECR_HUMAN	Peroxisomal trans-2-enoyl-CoA reductase
PEDF_HUMAN	Pigment epithelium-derived factor
PERM_HUMAN	Myeloperoxidase
PEX1_HUMAN	Peroxisome biogenesis factor 1
PFKAL_HUMAN	ATP-dependent 6-phosphofructokinase, liver type
PFKAM_HUMAN	ATP-dependent 6-phosphofructokinase, muscle type
PFKAP_HUMAN	ATP-dependent 6-phosphofructokinase, platelet type
PGAM1_HUMAN	Phosphoglycerate mutase 1
PGBM_HUMAN	Basement membrane-specific heparan sulfate proteoglycan core protein
PGCA_HUMAN	Aggrecan core protein
PGCB_HUMAN	Brevican core protein
PGH1_HUMAN	Prostaglandin G/H synthase 1
PGK1_HUMAN	Phosphoglycerate kinase 1
PGM1_HUMAN	Phosphoglucomutase-1
PGRC1_HUMAN	Membrane-associated progesterone receptor component 1
PGRC2_HUMAN	Membrane-associated progesterone receptor component 2
PGS1_HUMAN	Biglycan
PGS2_HUMAN	Decorin
PHAR1_HUMAN	Phosphatase and actin regulator 1
PHAR3_HUMAN	Phosphatase and actin regulator 3
PHB_HUMAN	Prohibitin
PHB2_HUMAN	Prohibitin-2
PHKG2_HUMAN	Phosphorylase b kinase gamma catalytic chain, liver/testis isoform
PI42A_HUMAN	Phosphatidylinositol 5-phosphate 4-kinase type-2 alpha

PI42C_HUMAN	Phosphatidylinositol 5-phosphate 4-kinase type-2 gamma
PIGS_HUMAN	GPI transamidase component PIG-S
PIGT_HUMAN	GPI transamidase component PIG-T
PIGU_HUMAN	Phosphatidylinositol glycan anchor biosynthesis class U protein
PLAK_HUMAN	Junction plakoglobin
PLCA_HUMAN	1-acyl-sn-glycerol-3-phosphate acyltransferase alpha
PLCC_HUMAN	1-acyl-sn-glycerol-3-phosphate acyltransferase gamma
PLCD1_HUMAN	1-phosphatidylinositol 4,5-bisphosphate phosphodiesterase delta-1
PLCG1_HUMAN	1-phosphatidylinositol 4,5-bisphosphate phosphodiesterase gamma-1
PLEC_HUMAN	Plectin
PLK1_HUMAN	Serine/threonine-protein kinase PLK1
PLLP_HUMAN	Plasmolipin
PLM_HUMAN	Phospholemman
PLMN_HUMAN	Plasminogen
PLOD1_HUMAN	Procollagen-lysine,2-oxoglutarate 5-dioxygenase 1
PLP2_HUMAN	Proteolipid protein 2
PLPP3_HUMAN	Phospholipid phosphatase 3
PLPR5_HUMAN	Phospholipid phosphatase-related protein type 5
PLS1_HUMAN	Phospholipid scramblase 1
PLS3_HUMAN	Phospholipid scramblase 3
PLSL_HUMAN	Plastin-2
PLTP_HUMAN	Phospholipid transfer protein
PNPH_HUMAN	Purine nucleoside phosphorylase
PODXL_HUMAN	Podocalyxin
PON1_HUMAN	Serum paraoxonase/arylesterase 1
PON2_HUMAN	Serum paraoxonase/arylesterase 2
POSTN_HUMAN	Periostin
PP1B_HUMAN	Serine/threonine-protein phosphatase PP1-beta catalytic subunit
PP1R7_HUMAN	Protein phosphatase 1 regulatory subunit 7
PP2AA_HUMAN	Serine/threonine-protein phosphatase 2A catalytic subunit alpha isoform
PP2BA_HUMAN	Serine/threonine-protein phosphatase 2B catalytic subunit alpha isoform
PPAL_HUMAN	Lysosomal acid phosphatase
PPAP_HUMAN	Prostatic acid phosphatase
PPBT_HUMAN	Alkaline phosphatase, tissue-nonspecific isozyme
PPIA_HUMAN	Peptidyl-prolyl cis-trans isomerase A
PPIB_HUMAN	Peptidyl-prolyl cis-trans isomerase B
PPM1J_HUMAN	Protein phosphatase 1J
PPT1_HUMAN	Palmitoyl-protein thioesterase 1
PRAF2_HUMAN	PRA1 family protein 2
PRAF3_HUMAN	PRA1 family protein 3
PRDX1_HUMAN	Peroxiredoxin-1

PRDX2_HUMAN	Peroxiredoxin-2
PRDX4_HUMAN	Peroxiredoxin-4
PRDX6_HUMAN	Peroxiredoxin-6
PRKDC_HUMAN	DNA-dependent protein kinase catalytic subunit
PROF1_HUMAN	Profilin-1
PROL4_HUMAN	Proline-rich protein 4
PROS_HUMAN	Vitamin K-dependent protein S
PRS23_HUMAN	Serine protease 23
PRS6A_HUMAN	26S proteasome regulatory subunit 6A
PRS7_HUMAN	26S proteasome regulatory subunit 7
PRS8_HUMAN	26S proteasome regulatory subunit 8
PRSR2_HUMAN	Proline and serine-rich protein 2
PSA_HUMAN	Puromycin-sensitive aminopeptidase
PSA1_HUMAN	Proteasome subunit alpha type-1
PSA2_HUMAN	Proteasome subunit alpha type-2
PSA3_HUMAN	Proteasome subunit alpha type-3
PSA4_HUMAN	Proteasome subunit alpha type-4
PSA5_HUMAN	Proteasome subunit alpha type-5
PSA6_HUMAN	Proteasome subunit alpha type-6
PSA7_HUMAN	Proteasome subunit alpha type-7
PSB1_HUMAN	Proteasome subunit beta type-1
PSB2_HUMAN	Proteasome subunit beta type-2
PSB3_HUMAN	Proteasome subunit beta type-3
PSB4_HUMAN	Proteasome subunit beta type-4
PSB5_HUMAN	Proteasome subunit beta type-5
PSB6_HUMAN	Proteasome subunit beta type-6
PSB7_HUMAN	Proteasome subunit beta type-7
PSB8_HUMAN	Proteasome subunit beta type-8
PSB9_HUMAN	Proteasome subunit beta type-9
PSD11_HUMAN	26S proteasome non-ATPase regulatory subunit 11
PSD12_HUMAN	26S proteasome non-ATPase regulatory subunit 12
PSDE_HUMAN	26S proteasome non-ATPase regulatory subunit 14
PSF3_HUMAN	DNA replication complex GINS protein PSF3
PSMD2_HUMAN	26S proteasome non-ATPase regulatory subunit 2
PSMD3_HUMAN	26S proteasome non-ATPase regulatory subunit 3
PSMD6_HUMAN	26S proteasome non-ATPase regulatory subunit 6
PSMD7_HUMAN	26S proteasome non-ATPase regulatory subunit 7
PSMD8_HUMAN	26S proteasome non-ATPase regulatory subunit 8
PSME2_HUMAN	Proteasome activator complex subunit 2
PTEN_HUMAN	Phosphatidylinositol 3,4,5-trisphosphate 3-phosphatase and dual-specificity protein phosphatase PTEN
PTGDS_HUMAN	Prostaglandin-H2 D-isomerase

PTPRE_HUMAN	Receptor-type tyrosine-protein phosphatase epsilon
PTPRZ_HUMAN	Receptor-type tyrosine-protein phosphatase zeta
PTX3_HUMAN	Pentraxin-related protein PTX3
PUR6_HUMAN	Multifunctional protein ADE2
PUR9_HUMAN	Bifunctional purine biosynthesis protein ATIC
PURA_HUMAN	Transcriptional activator protein Pur-alpha
PURB_HUMAN	Transcriptional activator protein Pur-beta
PVR_HUMAN	Poliovirus receptor
PXDC2_HUMAN	Plexin domain-containing protein 2
PXL2A_HUMAN	Peroxiredoxin-like 2A
PYGB_HUMAN	Glycogen phosphorylase, brain form
QCR2_HUMAN	Cytochrome b-c1 complex subunit 2, mitochondrial
R10B1_HUMAN	Radial spoke head 10 homolog B
RAB10_HUMAN	Ras-related protein Rab-10
RAB1B_HUMAN	Ras-related protein Rab-1B
RAB21_HUMAN	Ras-related protein Rab-21
RAB2A_HUMAN	Ras-related protein Rab-2A
RAB35_HUMAN	Ras-related protein Rab-35
RAB3A_HUMAN	Ras-related protein Rab-3A
RAB4A_HUMAN	Ras-related protein Rab-4A
RAB5A_HUMAN	Ras-related protein Rab-5A
RAB5B_HUMAN	Ras-related protein Rab-5B
RAB5C_HUMAN	Ras-related protein Rab-5C
RAB6A_HUMAN	Ras-related protein Rab-6A
RAB6B_HUMAN	Ras-related protein Rab-6B
RAB7A_HUMAN	Ras-related protein Rab-7a
RAB8B_HUMAN	Ras-related protein Rab-8B
RAC1_HUMAN	Ras-related C3 botulinum toxin substrate 1
RADI_HUMAN	Radixin
RAE1_HUMAN	Rab proteins geranylgeranyltransferase component A 1
RALA_HUMAN	Ras-related protein Ral-A
RAN_HUMAN	GTP-binding nuclear protein Ran
RAP1A_HUMAN	Ras-related protein Rap-1A
RAP2B_HUMAN	Ras-related protein Rap-2b
RARA_HUMAN	Retinoic acid receptor alpha
RASA1_HUMAN	Ras GTPase-activating protein 1
RASH_HUMAN	GTPase HRas
RASM_HUMAN	Ras-related protein M-Ras
RB11A_HUMAN	Ras-related protein Rab-11A
RBPMS_HUMAN	RNA-binding protein with multiple splicing
RCN1_HUMAN	Reticulocalbin-1

RCN2_HUMAN	Reticulocalbin-2
RCOR3_HUMAN	REST corepressor 3
RD23A_HUMAN	UV excision repair protein RAD23 homolog A
REEP5_HUMAN	Receptor expression-enhancing protein 5
REEP6_HUMAN	Receptor expression-enhancing protein 6
RELN_HUMAN	Reelin
RER1_HUMAN	Protein RER1
RETR2_HUMAN	Reticulophagy regulator 2
RETR3_HUMAN	Reticulophagy regulator 3
RFA1_HUMAN	Replication protein A 70 kDa DNA-binding subunit
RFA2_HUMAN	Replication protein A 32 kDa subunit
RFNG_HUMAN	Beta-1,3-N-acetylglucosaminyltransferase radical fringe
RHAG_HUMAN	Ammonium transporter Rh type A
RHCE_HUMAN	Blood group Rh(CE) polypeptide
RHEB_HUMAN	GTP-binding protein Rheb
RHOA_HUMAN	Transforming protein RhoA
RHOG_HUMAN	Rho-related GTP-binding protein RhoG
RL10A_HUMAN	60S ribosomal protein L10a
RL12_HUMAN	60S ribosomal protein L12
RL14_HUMAN	60S ribosomal protein L14
RL18_HUMAN	60S ribosomal protein L18
RL34_HUMAN	60S ribosomal protein L34
RL4_HUMAN	60S ribosomal protein L4
RL6_HUMAN	60S ribosomal protein L6
RL7_HUMAN	60S ribosomal protein L7
RL7A_HUMAN	60S ribosomal protein L7a
RLA0_HUMAN	60S acidic ribosomal protein P0
RLA2_HUMAN	60S acidic ribosomal protein P2
RM47_HUMAN	39S ribosomal protein L47, mitochondrial
RNPC3_HUMAN	RNA-binding region-containing protein 3
RO60_HUMAN	60 kDa SS-A/Ro ribonucleoprotein
ROA3_HUMAN	Heterogeneous nuclear ribonucleoprotein A3
RP3A_HUMAN	Rabphilin-3A
RPN1_HUMAN	Dolichyl-diphosphooligosaccharide--protein glycosyltransferase subunit 1
RPN2_HUMAN	Dolichyl-diphosphooligosaccharide--protein glycosyltransferase subunit 2
RRBP1_HUMAN	Ribosome-binding protein 1
RS10_HUMAN	40S ribosomal protein S10
RS16_HUMAN	40S ribosomal protein S16
RS18_HUMAN	40S ribosomal protein S18
RS19_HUMAN	40S ribosomal protein S19
RS2_HUMAN	40S ribosomal protein S2

RS23_HUMAN	40S ribosomal protein S23
RS27A_HUMAN	Ubiquitin-40S ribosomal protein S27a
RS5_HUMAN	40S ribosomal protein S5
RS7_HUMAN	40S ribosomal protein S7
RSMB_HUMAN	Small nuclear ribonucleoprotein-associated proteins B and B'
RSPH9_HUMAN	Radial spoke head protein 9 homolog
RSSA_HUMAN	40S ribosomal protein SA
RT18C_HUMAN	28S ribosomal protein S18c, mitochondrial
RTN1_HUMAN	Reticulon-1
RTN3_HUMAN	Reticulon-3
RTN4_HUMAN	Reticulon-4
RUSF1_HUMAN	RUS family member 1
RUVB1_HUMAN	RuvB-like 1
RUVB2_HUMAN	RuvB-like 2
RUXE_HUMAN	Small nuclear ribonucleoprotein E
RUXF_HUMAN	Small nuclear ribonucleoprotein F
S10A6_HUMAN	Protein S100-A6
S10A7_HUMAN	Protein S100-A7
S10A8_HUMAN	Protein S100-A8
S10A9_HUMAN	Protein S100-A9
S10AB_HUMAN	Protein S100-A11
S1A7A_HUMAN	Protein S100-A7A
S29A1_HUMAN	Equilibrative nucleoside transporter 1
S35F6_HUMAN	Solute carrier family 35 member F6
S38A3_HUMAN	Sodium-coupled neutral amino acid transporter 3
S39A7_HUMAN	Zinc transporter SLC39A7
S39AE_HUMAN	Metal cation symporter ZIP14
S4A4_HUMAN	Electrogenic sodium bicarbonate cotransporter 1
S61A1_HUMAN	Protein transport protein Sec61 subunit alpha isoform 1
S6A11_HUMAN	Sodium- and chloride-dependent GABA transporter 3
S6A17_HUMAN	Sodium-dependent neutral amino acid transporter SLC6A17
SAA1_HUMAN	Serum amyloid A-1 protein
SAA4_HUMAN	Serum amyloid A-4 protein
SAC1_HUMAN	Phosphatidylinositol-3-phosphatase SAC1
SACS_HUMAN	Sacsin
SAHH_HUMAN	Adenosylhomocysteinase
SAHH2_HUMAN	S-adenosylhomocysteine hydrolase-like protein 1
SAHH3_HUMAN	Adenosylhomocysteinase 3
SALL2_HUMAN	Sal-like protein 2
SAMP_HUMAN	Serum amyloid P-component
SAP_HUMAN	Prosaposin

SATT_HUMAN	Neutral amino acid transporter A
SBP1_HUMAN	Methanethiol oxidase
SC22B_HUMAN	Vesicle-trafficking protein SEC22b
SC23A_HUMAN	Protein transport protein Sec23A
SC61G_HUMAN	Protein transport protein Sec61 subunit gamma
SC6A9_HUMAN	Sodium- and chloride-dependent glycine transporter 1
SCAM1_HUMAN	Secretory carrier-associated membrane protein 1
SCAM3_HUMAN	Secretory carrier-associated membrane protein 3
SCD5_HUMAN	Stearoyl-CoA desaturase 5
SCFD2_HUMAN	Sec1 family domain-containing protein 2
SCG3_HUMAN	Secretogranin-3
SCND3_HUMAN	SCAN domain-containing protein 3
SCPDL_HUMAN	Saccharopine dehydrogenase-like oxidoreductase
SCRB2_HUMAN	Lysosome membrane protein 2
SCRN1_HUMAN	Secernin-1
SDCB1_HUMAN	Syntenin-1
SDHA_HUMAN	Succinate dehydrogenase [ubiquinone] flavoprotein subunit, mitochondrial
SDHB_HUMAN	Succinate dehydrogenase [ubiquinone] iron-sulfur subunit, mitochondrial
SEC62_HUMAN	Translocation protein SEC62
SEP11_HUMAN	Septin-11
SEPT2_HUMAN	Septin-2
SEPT3_HUMAN	Neuronal-specific septin-3
SEPT4_HUMAN	Septin-4
SEPT6_HUMAN	Septin-6
SEPT7_HUMAN	Septin-7
SEPT8_HUMAN	Septin-8
SEPT9_HUMAN	Septin-9
SERA_HUMAN	D-3-phosphoglycerate dehydrogenase
SERC_HUMAN	Phosphoserine aminotransferase
SERPH_HUMAN	Serpin H1
SETLP_HUMAN	Protein SETSIP
SF3B3_HUMAN	Splicing factor 3B subunit 3
SFPQ_HUMAN	Splicing factor, proline- and glutamine-rich
SFXN1_HUMAN	Sideroflexin-1
SFXN3_HUMAN	Sideroflexin-3
SHPS1_HUMAN	Tyrosine-protein phosphatase non-receptor type substrate 1
SIG16_HUMAN	Sialic acid-binding Ig-like lectin 16
SIR2_HUMAN	NAD-dependent protein deacetylase sirtuin-2
SIRBL_HUMAN	Signal-regulatory protein beta-1 isoform 3
SKOR1_HUMAN	SKI family transcriptional corepressor 1
SLIT3_HUMAN	Slit homolog 3 protein

SLK_HUMAN	STE20-like serine/threonine-protein kinase
SMD3_HUMAN	Small nuclear ribonucleoprotein Sm D3
SMYD2_HUMAN	N-lysine methyltransferase SMYD2
SNAA_HUMAN	Alpha-soluble NSF attachment protein
SNAG_HUMAN	Gamma-soluble NSF attachment protein
SNG1_HUMAN	Synaptogyrin-1
SNG3_HUMAN	Synaptogyrin-3
SNP25_HUMAN	Synaptosomal-associated protein 25
SNPC5_HUMAN	snRNA-activating protein complex subunit 5
SNPH_HUMAN	Syntaphilin
SODC_HUMAN	Superoxide dismutase [Cu-Zn]
SODM_HUMAN	Superoxide dismutase [Mn], mitochondrial
SORCN_HUMAN	Sorcin
SP16H_HUMAN	FACT complex subunit SPT16
SPB12_HUMAN	Serpin B12
SPB3_HUMAN	Serpin B3
SPB6_HUMAN	Serpin B6
SPCS2_HUMAN	Signal peptidase complex subunit 2
SPKAP_HUMAN	A-kinase anchor protein SPHKAP
SPP2A_HUMAN	Signal peptide peptidase-like 2A
SPRC_HUMAN	SPARC
SPRL1_HUMAN	SPARC-like protein 1
SPRY7_HUMAN	SPRY domain-containing protein 7
SPTA1_HUMAN	Spectrin alpha chain, erythrocytic 1
SPTB1_HUMAN	Spectrin beta chain, erythrocytic
SPTB2_HUMAN	Spectrin beta chain, non-erythrocytic 1
SPTN1_HUMAN	Spectrin alpha chain, non-erythrocytic 1
SPTN5_HUMAN	Spectrin beta chain, non-erythrocytic 5
SPYA_HUMAN	Serine--pyruvate aminotransferase
SQOR_HUMAN	Sulfide:quinone oxidoreductase, mitochondrial
SRS11_HUMAN	Serine/arginine-rich splicing factor 11
SRSF1_HUMAN	Serine/arginine-rich splicing factor 1
SRSF2_HUMAN	Serine/arginine-rich splicing factor 2
SRSF6_HUMAN	Serine/arginine-rich splicing factor 6
SSBP_HUMAN	Single-stranded DNA-binding protein, mitochondrial
SSDH_HUMAN	Succinate-semialdehyde dehydrogenase, mitochondrial
SSRG_HUMAN	Translocon-associated protein subunit gamma
SSRP1_HUMAN	FACT complex subunit SSRP1
STAM1_HUMAN	Signal transducing adapter molecule 1
STAR9_HUMAN	StAR-related lipid transfer protein 9
STIM1_HUMAN	Stromal interaction molecule 1

STML1_HUMAN	Stomatin-like protein 1
STML2_HUMAN	Stomatin-like protein 2, mitochondrial
STOM_HUMAN	Stomatin
STRP2_HUMAN	Striatin-interacting protein 2
STT3A_HUMAN	Dolichyl-diphosphooligosaccharide--protein glycosyltransferase subunit STT3A
STX12_HUMAN	Syntaxin-12
STX1B_HUMAN	Syntaxin-1B
STX4_HUMAN	Syntaxin-4
STX7_HUMAN	Syntaxin-7
STXB1_HUMAN	Syntaxin-binding protein 1
STXB3_HUMAN	Syntaxin-binding protein 3
SUCA_HUMAN	Succinate--CoA ligase [ADP/GDP-forming] subunit alpha, mitochondrial
SUMF2_HUMAN	Inactive C-alpha-formylglycine-generating enzyme 2
SURF4_HUMAN	Surfeit locus protein 4
SUSD3_HUMAN	Sushi domain-containing protein 3
SV2A_HUMAN	Synaptic vesicle glycoprotein 2A
SYAC_HUMAN	Alanine--tRNA ligase, cytoplasmic
SYCM_HUMAN	Probable cysteine--tRNA ligase, mitochondrial
SYGP1_HUMAN	Ras/Rap GTPase-activating protein SynGAP
SYN1_HUMAN	Synapsin-1
SYNE1_HUMAN	Nesprin-1
SYNEM_HUMAN	Synemin
SYPH_HUMAN	Synaptophysin
SYSC_HUMAN	Serine--tRNA ligase, cytoplasmic
SYSM_HUMAN	Serine--tRNA ligase, mitochondrial
SYT1_HUMAN	Synaptotagmin-1
SYWC_HUMAN	Tryptophan--tRNA ligase, cytoplasmic
TAGL2_HUMAN	Transgelin-2
TALDO_HUMAN	Transaldolase
TAP1_HUMAN	Antigen peptide transporter 1
TAP2_HUMAN	Antigen peptide transporter 2
TAU_HUMAN	Microtubule-associated protein tau
TBA1A_HUMAN	Tubulin alpha-1A chain
TBA4A_HUMAN	Tubulin alpha-4A chain
TBB2A_HUMAN	Tubulin beta-2A chain
TBB2B_HUMAN	Tubulin beta-2B chain
TBB3_HUMAN	Tubulin beta-3 chain
TBB4A_HUMAN	Tubulin beta-4A chain
TBB4B_HUMAN	Tubulin beta-4B chain
TBB5_HUMAN	Tubulin beta chain
TBC9B_HUMAN	TBC1 domain family member 9B

TBCK_HUMAN	TBC domain-containing protein kinase-like protein
TBX2_HUMAN	T-box transcription factor TBX2
TCP4_HUMAN	Activated RNA polymerase II transcriptional coactivator p15
TCPD_HUMAN	T-complex protein 1 subunit delta
TCPE_HUMAN	T-complex protein 1 subunit epsilon
TCPG_HUMAN	T-complex protein 1 subunit gamma
TCPH_HUMAN	T-complex protein 1 subunit eta
TCPQ_HUMAN	T-complex protein 1 subunit theta
TCPZ_HUMAN	T-complex protein 1 subunit zeta
TECR_HUMAN	Very-long-chain enoyl-CoA reductase
TENA_HUMAN	Tenascin
TENR_HUMAN	Tenascin-R
TERA_HUMAN	Transitional endoplasmic reticulum ATPase
TFG_HUMAN	Protein TFG
TFR1_HUMAN	Transferrin receptor protein 1
TGON2_HUMAN	Trans-Golgi network integral membrane protein 2
THAS_HUMAN	Thromboxane-A synthase
THBG_HUMAN	Thyroxine-binding globulin
THEM6_HUMAN	Protein THEM6
THIL_HUMAN	Acetyl-CoA acetyltransferase, mitochondrial
THRB_HUMAN	Prothrombin
THY1_HUMAN	Thy-1 membrane glycoprotein
TITIN_HUMAN	Titin
TKT_HUMAN	Transketolase
TLE6_HUMAN	Transducin-like enhancer protein 6
TLN1_HUMAN	Talin-1
TM109_HUMAN	Transmembrane protein 109
TM205_HUMAN	Transmembrane protein 205
TM245_HUMAN	Transmembrane protein 245
TM9S2_HUMAN	Transmembrane 9 superfamily member 2
TMC5_HUMAN	Transmembrane channel-like protein 5
TMED2_HUMAN	Transmembrane emp24 domain-containing protein 2
TMED9_HUMAN	Transmembrane emp24 domain-containing protein 9
TMEDA_HUMAN	Transmembrane emp24 domain-containing protein 10
TMF1_HUMAN	TATA element modulatory factor
TMM33_HUMAN	Transmembrane protein 33
TMM43_HUMAN	Transmembrane protein 43
TMOD2_HUMAN	Tropomodulin-2
TMX1_HUMAN	Thioredoxin-related transmembrane protein 1
TMX3_HUMAN	Protein disulfide-isomerase TMX3
TNIP2_HUMAN	TNFAIP3-interacting protein 2

TOIP1_HUMAN	Torsin-1A-interacting protein 1
TOIP2_HUMAN	Torsin-1A-interacting protein 2
TOM70_HUMAN	Mitochondrial import receptor subunit TOM70
TOP1_HUMAN	DNA topoisomerase 1
TPD52_HUMAN	Tumor protein D52
TPIS_HUMAN	Triosephosphate isomerase
TPM3_HUMAN	Tropomyosin alpha-3 chain
TPM4_HUMAN	Tropomyosin alpha-4 chain
TPP1_HUMAN	Tripeptidyl-peptidase 1
TPPC5_HUMAN	Trafficking protein particle complex subunit 5
TPPC8_HUMAN	Trafficking protein particle complex subunit 8
TPPP_HUMAN	Tubulin polymerization-promoting protein
TPPP3_HUMAN	Tubulin polymerization-promoting protein family member 3
TPR_HUMAN	Nucleoprotein TPR
TPTE_HUMAN	Putative tyrosine-protein phosphatase TPTE
TRFE_HUMAN	Serotransferrin
TRFL_HUMAN	Lactotransferrin
TRI10_HUMAN	Tripartite motif-containing protein 10
TRIPB_HUMAN	Thyroid receptor-interacting protein 11
TRPM5_HUMAN	Transient receptor potential cation channel subfamily M member 5
TRY3_HUMAN	Trypsin-3
TSN3_HUMAN	Tetraspanin-3
TSN4_HUMAN	Tetraspanin-4
TSN6_HUMAN	Tetraspanin-6
TSN7_HUMAN	Tetraspanin-7
TSNAX_HUMAN	Translin-associated protein X
TSP1_HUMAN	Thrombospondin-1
TTC24_HUMAN	Tetratricopeptide repeat protein 24
TTHY_HUMAN	Transthyretin
TTLL8_HUMAN	Protein monoglycylase TTLL8
TTYH1_HUMAN	Protein tweety homolog 1
TWF2_HUMAN	Twinfilin-2
TXND5_HUMAN	Thioredoxin domain-containing protein 5
TXTP_HUMAN	Tricarboxylate transport protein, mitochondrial
TYPH_HUMAN	Thymidine phosphorylase
UBA1_HUMAN	Ubiquitin-like modifier-activating enzyme 1
UBR2_HUMAN	E3 ubiquitin-protein ligase UBR2
UCHL1_HUMAN	Ubiquitin carboxyl-terminal hydrolase isozyme L1
UCRI_HUMAN	Cytochrome b-c1 complex subunit Rieske, mitochondrial
UGGG1_HUMAN	UDP-glucose:glycoprotein glucosyltransferase 1
UGPA_HUMAN	UTP--glucose-1-phosphate uridylyltransferase

ULK2_HUMAN	Serine/threonine-protein kinase ULK2
UN45B_HUMAN	Protein unc-45 homolog B
UT1_HUMAN	Urea transporter 1
VA0D1_HUMAN	V-type proton ATPase subunit d 1
VAMP1_HUMAN	Vesicle-associated membrane protein 1
VAMP2_HUMAN	Vesicle-associated membrane protein 2
VAPA_HUMAN	Vesicle-associated membrane protein-associated protein A
VAS1_HUMAN	V-type proton ATPase subunit S1
VAT1_HUMAN	Synaptic vesicle membrane protein VAT-1 homolog
VATA_HUMAN	V-type proton ATPase catalytic subunit A
VATB2_HUMAN	V-type proton ATPase subunit B, brain isoform
VATE1_HUMAN	V-type proton ATPase subunit E 1
VATH_HUMAN	V-type proton ATPase subunit H
VATL_HUMAN	V-type proton ATPase 16 kDa proteolipid subunit
VDAC1_HUMAN	Voltage-dependent anion-selective channel protein 1
VDAC2_HUMAN	Voltage-dependent anion-selective channel protein 2
VIME_HUMAN	Vimentin
VINC_HUMAN	Vinculin
VISL1_HUMAN	Visinin-like protein 1
VP13D_HUMAN	Vacuolar protein sorting-associated protein 13D
VP33A_HUMAN	Vacuolar protein sorting-associated protein 33A
VPP1_HUMAN	V-type proton ATPase 116 kDa subunit a1
VPS16_HUMAN	Vacuolar protein sorting-associated protein 16 homolog
VPS29_HUMAN	Vacuolar protein sorting-associated protein 29
VPS35_HUMAN	Vacuolar protein sorting-associated protein 35
VPS45_HUMAN	Vacuolar protein sorting-associated protein 45
VTDB_HUMAN	Vitamin D-binding protein
VTNC_HUMAN	Vitronectin
VWA8_HUMAN	von Willebrand factor A domain-containing protein 8
VWF_HUMAN	von Willebrand factor
WDR1_HUMAN	WD repeat-containing protein 1
WDR48_HUMAN	WD repeat-containing protein 48
WFS1_HUMAN	Wolframin
WNT7A_HUMAN	Protein Wnt-7a
XPO2_HUMAN	Exportin-2
XPP1_HUMAN	Xaa-Pro aminopeptidase 1
XRCC5_HUMAN	X-ray repair cross-complementing protein 5
XRCC6_HUMAN	X-ray repair cross-complementing protein 6
YB035_HUMAN	Putative uncharacterized protein FLJ33534
YBOX1_HUMAN	Y-box-binding protein 1
YIF1B_HUMAN	Protein YIF1B

YIPF6_HUMAN	Protein YIPF6
ZBT21_HUMAN	Zinc finger and BTB domain-containing protein 21
ZDH17_HUMAN	Palmitoyltransferase ZDHHC17
ZER1_HUMAN	Protein zer-1 homolog
ZN521_HUMAN	Zinc finger protein 521
ZN671_HUMAN	Zinc finger protein 671
ZN846_HUMAN	Zinc finger protein 846
ZNF44_HUMAN	Zinc finger protein 44
ZSWM6_HUMAN	Zinc finger SWIM domain-containing protein 6
ZSWM9_HUMAN	Uncharacterized protein ZSWIM9